3D Printed Denture Materials: Key Aspects of their Physico-Mechanical and Biological Properties

A thesis submitted to the University of Manchester for the degree of

Doctor of Philosophy

in the Faculty of Biology, Medicine and Health

2023

Ahmed T Altarazi

School of Medical Sciences

Division of Dentistry

Table of Contents

Word Count: 63,688

List of Figures

List of Tables

List of Abbreviations, Symbols and Units

PO	Printing orientation
CT	Curing time
PMMA	Polymethyl methacrylate
MMA	Methyl methacrylate
CQ	Camphorquinone
PPM	Part per million
SEM	Scanning electron microscope
EDX	Energy Dispersive X-ray
FTIR	Fourier Transform Infrared Spectroscopy
ISO	International Organization for Standardization
3D	Three-dimensional
SLA	Stereolithography
STL	Standard Tessellation Language
C=C	Carbon double bond
C=O	Carbon oxygen double bond
MPa	Megapascal
°C	Centigrade
h	Hour
min	minute
nm	Nanometer
µm	Micrometer
mm	Millimeter
wt%	Percentage content by weight
cm^{-1}	Wavelength unit
ml	Millilitre
g	Gram
mg	Milligram
$\mu g/mm^3$	Microgram per cubic millimetre
N	Newton
a_{iN}	Charpy impact strength
CAD/CAM	Computer aided design/ computer aided manufacturing
UV	Ultraviolet
DC	Degree of conversion

ND	NextDent
FL	Formlabs
HC	Heat-cured
NPs	Nanoparticles
TiO_2	Titanium dioxide
SiO_2	Silicon dioxide
ZrO_2	Zirconia oxide
AB	AlamarBlue
LDH	Lactate dehydrogenase
HGF	Human gingival fibroblasts
HBSS	Hank’s balanced salt solution
ROS	Reactive oxygen species

Abstract

Problem statement: The advent of 3D-printing technology has brought a revolution in the field of dentistry, offering a quick, reliable, and economical method for fabricating various dental appliances, including denture bases. Nevertheless, the mechanical and physical properties of 3D-printed denture base materials tend to be relatively poor compared to conventional denture base materials. On the other hand, the printing parameters such as printing orientation, layer thickness, light wavelength, curing time etc. can affect the properties of the printed resin. Furthermore, the denture base materials are prone to attract micro-organism resulting in oral diseases like denture stomatitis. To counter this, metal or metal oxide nanoparticles were incorporated into the denture base materials to create an innovative nanocomposite material that displays enhanced physical, mechanical and biological characteristics.

Aim: This research aimed to optimise the printing parameters, and to develop a novel denture base nanocomposite material by infusing varying concentrations of TiO_2 nanoparticles with 3D-printed denture base resin. The study also intended to evaluate their mechanical, physical, and biological properties, and to investigate the effect of hydrolytic ageing in artificial saliva on the mechanical properties.

Methods: Initially, various printing parameters were examined to ascertain the ideal print settings encompassing different printing orientations (0°, 45°, 90°) and different curing times (20, 30, 50 min) in relation to the unmodified 3D-printed denture base resin (NextDent).

Following this, the optimal printing parameters were applied to evaluate the physical and mechanical properties of the unmodified 3D-printed denture base resin in terms of degree of polymerisation, sorption, solubility, flexural strength, flexural modulus, Vickers hardness, Martens hardness, and impact strength to compare the 3D-printed resins (NextDent® and Formlabs®) with conventional heat-cured resin (Schottlander®) as a control. The specimens were subsequently exposed to hydrolytic ageing in artificial saliva for a three-month duration. After this period, the mechanical properties were re-examined to assess the effect of ageing.

Next, the 3D-printed resin (NextDent®) was reinforced with different concentrations (0.10, 0.25, 0.50, and 0.75 wt.%) of silanated TiO_2 nanoparticles. The resultant nanocomposite materials were then characterised in terms of degree of conversion, sorption/solubility, Vickers

hardness, Martens hardness, flexural strength/modulus, impact strength, antifungal properties, cytotoxicity, and biocompatibility. These properties were compared with the unmodified 3D-printed resin (NextDent®) and conventional heat-cured resin (Schottlander®) materials as controls. Following exposure to artificial saliva ageing, the nanocomposites were re-evaluated in terms of the mechanical properties. The fractured surface was also analysed using an optical and scanning electron microscopes.

Results: The results showed that 90° printing orientation produced significantly higher values of flexural strength, Vickers hardness, and water sorption compared to a 0° orientation ($p < 0.05$). However, alterations in the post-curing time did not result in significant variations in the properties tested ($p > 0.05$). Notwithstanding, a post-curing time of 30 minutes yielded marginally improved characteristics compared to 20 min, with no detectable difference observed with 50 min.

After establishing the optimal printing parameters and using them to compare 3D-printed materials with conventional heat-cured resin, the data demonstrated that 3D-printed resins had significantly higher sorption values than the control ($p < 0.05$). Higher solubility was also evident, although the difference was not statistically significant ($p > 0.05$). There were no significant differences in Vickers and Martens hardness, or impact strength, among the materials tested. However, the 3D-printed materials exhibited significantly greater flexural strength values (88-94 MPa) compared to the heat-cured material (73 MPa) ($p < 0.05$). The degree of conversion of 3D-printed resins were lower than that of the control group, but this variation was not statistically significant ($p > 0.05$). The 3D-printed materials also contained a significantly higher filler content compared to the control ($p < 0.05$). Additionally, three months of artificial saliva ageing had a significant effect on the Vickers hardness for all groups tested, and the Martens hardness of the heat-cured control group only ($p < 0.05$). However, it did not significantly affect the mechanical properties ($p > 0.05$).

The integration of TiO_2 nanoparticles (NPs) into 3D-printed resin significantly improved flexural strength/modulus, impact strength, Vickers hardness, and DC ($p < 0.05$), and marginally enhanced Martens hardness ($p > 0.05$) compared to the unmodified resin. Sorption values showed no significant enhancements ($p > 0.05$), while solubility reduced significantly ($p < 0.05$). The addition of 0.10 wt.% NPs yielded the best performance among the different concentrations of the nanocomposite groups. Although ageing slightly diminished the materials' performance, the overall trend remained the same. Scanning electron microscope

images revealed a homogeneous dispersion of the nanoparticles at lower concentrations (0.10 and 0.25 wt.%), but disclosed agglomeration at higher concentrations (0.50 and 0.75 wt.%).

As for the biological properties, 3D-printed denture base resin reinforced with TiO_2 NPs up to a concentration of 0.5 wt.% demonstrated statistically significant anti-fungal properties against *Candida albicans* ($p<0.05$), without any cytotoxic effect on human gingival fibroblasts. Nevertheless, a concentration of 0.75 wt.% exhibited a minor, and statistically insignificant reduction ($p>0.05$) in the number of fungal colonies. The optimal concentration of TiO_2 NPs for achieving a balance between anti-fungal properties and compatibility was found to be 0.25 wt.%.

Significance: 3D-printed unmodified resins for denture base have shown to be a viable substitute for traditional heat-cured materials in prosthetic dentistry, as they exhibited mechanical, physical, and surface properties that meet the established standards. The newly created nanocomposite material demonstrated further improved mechanical, physical, and also antimicrobial properties, effectively limiting fungal growth and thus reducing the incidence of denture stomatitis.

Declaration

I declare that no portion of the work referred to in the thesis has been submitted in support of an application for another degree or qualification of this or any other university or other institute of learning.

Copyright Statement

Acknowledgements

I would like to sincerely thank my supervisors, Professor Hugh Devlin, Professor Nick Silikas, and Dr. Julfikar Haider, for their invaluable guidance, unwavering encouragement, and boundless patience. Their scientific perspectives, vast experience, and insightful input have greatly enriched my research. I am particularly grateful for their kindness and support during the challenging times, especially in the initial two years of my PhD journey, as well as the countless hours we spent in meetings, building my knowledge and experience together.

I would like to express my sincere appreciation to the Faculty of Science and Engineering at Manchester Metropolitan University. I am thankful to Mr. Michael Green for his invaluable assistance with mechanical testing, and to Dr. Hayley Andrews for her expert guidance in SEM imaging and EDX analysis. Additionally, I am grateful to Dr. Evgeny Kushnerev and Professor Andrew Mcbain for their guidance and support through all the biological experiments, and to Professor. Reza Roudsari for his clinical supervision. Last but not least, I would like to thank my postgraduate colleagues, Hamad Algamaiah, who inspired me to strive for publication, Kawther Bukhari and her husband Asim for their unwavering support and camaraderie throughout our entire academic journey. Their presence as both colleagues and neighbours has been a true blessing.

To all those who have contributed to my studies in any capacity, I am deeply thankful. The list of people deserving appreciation is extensive, and I am grateful for each and every contribution.

Last but not least, it is my great pleasure to thank the Ministry of Higher Education of Saudi Arabia for providing the financial support throughout my PhD study.

Dedication

I would like to dedicate this thesis to numerous people who have had a major impact on my life and contributed to the achievement of my academic goals.

First, I would like to dedicate my work to my beloved wife, Shayma. From the very beginning, you embraced my pursuit of knowledge with open arms, understanding the countless hours I spent away from home. You provided me with full support during the challenging circumstances that could have been reasons for not completing my academic journey. You have sacrificed your own precious time, putting your aspirations on hold, to ensure that I could fully devote myself to achieving my goals. As I conclude this chapter of my academic journey, I want to express my deepest gratitude to you, my partner, my best friend, and my soulmate.

Furthermore, I would like to dedicate this work to my beautiful, amazing daughters, Maria and Layla. They were the torch that gave us the energy throughout our days. Although the disability that Layla had at birth made her quiet, it did not prevent her from being a constant source of joy. We have had wonderful memories as a family during my academic journey.

Finally, I would also like to dedicate this work to my father, mother, brothers and sisters, and my close friends. Thank you for supporting and encouraging me during my studies.

The Author

In 2013, I graduated from the School of Dentistry of King Abdulaziz University, Jeddah, Saudi Arabia, with a Bachelor degree in Dental medicine and Surgery. I later progressed to work as a teaching assistant in the Dentistry School of Taibah University. In 2016, I was awarded a scholarship from the Ministry of Higher Education in Saudi Arabia to pursue my postgraduate studies, and I subsequently secured a place as a master's student in the Dental Materials Science Department of The University of Sheffield, UK. After completing the master's degree in 2017, I started my PhD study on Dental Materials and Technology at The University of Manchester, UK.

Publications-Conference

I have presented different aspects of my research at the following conferences/meetings:

1. Title: Studying the Effect of Curing Time on the Properties of 3D Printed Denture Base Material

- Poster at British Society for Oral and Dental Research (BSODR) Annual Scientific Meeting 2021, University of Birmingham, Birmingham, UK

2. Title: Assessing the physical and mechanical properties of 3D printed acrylic material for denture base application

- Presentation at PGR Show case event at School of Dentistry University of Manchester in July (2022). Awarded a certificate of Best Postgraduate Research Student Oral Presentation.

Publications - International Journal

1. Altarazi A, et al: Assessing the physical and mechanical properties of 3D printed acrylic material for denture base application. Dent Mater 2022;38:1841-1854

doi.org/10.1016/j.dental.2022.09.006

2. Altarazi A, et al. 3D Printed Denture Base Material: Effect of Incorporating TiO_2 Nanoparticles and Artificial Ageing on the Physical and Mechanical Properties

doi.org/10.1016/j.dental.2023.10.005

3. 3D-Printed Nanocomposite Denture Base Resin: The Effect of incorporating TiO_2 Nanoparticles on the Growth of Candida albicans

doi.org/10.1111/jopr.13784

Publications - International Journal submitted/under preparation

1- Current Progress in the Development of Resin Materials with Nanofillers for 3D Printing of Denture Base – to be submitted to Polymer Journal MDPI.
2- Effect of Artificial Ageing on the Physical and Mechanical Properties of 3D-printed Denture Base Materials – to be submitted to Polymer Journal MDPI.

Rationale of thesis format

This thesis is structured in a journal format, where four studies are presented as individual chapters in a format suitable for publication in peer-reviewed journals. The Introduction, Materials and methods, Aims and objectives, and Discussion chapters, however, follow the conventional thesis format. It's worth noting that, in line with the University's thesis presentation guidelines, there may be some overlapping information across sections of the thesis due to its alternative format. One paper (Chapter 4) has been published, and two others have been submitted for publication and under review (Chapter 6 and Chapter 7). Two papers are now in process for publication (Chapter 1 and Chapter 5). This structure aided the author in developing proficiency and experience in crafting content in a journal-style format. The supervisors made valuable contributions to the thesis by engaging in discussions and providing feedback on drafts of each chapter.

Chapter 1: General Introduction and Literature Review

Ahmed Altarazi, Julfikar Haider, Abdulaziz Alhotan, Nick Silikas, Hugh Devlin

To be submitted to Polymers Journal MDPI as a review

1.1. INTRODUCTION

Many people worldwide have missing teeth, and a significant number of them use partial or complete dentures, crowns, bridges, or even implant-retained prostheses. Edentulism, the condition of having lost all natural teeth, exhibits notable variation in prevalence across different countries. In the United States, recent research by Slade et al. (Slade et al., 2014) revealed a prevalence of 4.9% among adults aged 15 and above. Canada, on the other hand, displayed an overall rate of 6.4% in 2010, with significant disparities between provinces ranging from 14% in Quebec to 5% in the Northwest Regions. Brazil exhibited regional differences, with more industrialized and affluent areas reporting lower rates. Peltzer et al.'s (Peltzer et al., 2014) cross-country study included China, Ghana, India, Mexico, Russia, and South Africa, uncovering varying rates of edentulism. India recorded the highest prevalence at 16.3%, followed by China at 9%, Mexico at 21.7%, Russia at 18%, and South Africa at 8.5%. Notably, Ghana had the lowest prevalence at 3%. European studies reflected changing trends over time, with Sweden reporting a decrease in prevalence from 19% in 1975 to 3% in 1997 among individuals aged 25–74. Switzerland's 5.7% rate of complete edentulism, as identified by Zitzmann et al. (Zitzmann et al., 2001), demonstrated age-related patterns, with a significant rate among those aged 65 to 74. A more recent study in Indonesia by Pengpid and Peltzer in 2018 (Pengpid and Peltzer, 2018) reported an overall prevalence of 7.2%, rising sharply to 29.8% among individuals aged 80 and older. These findings underscore the diverse factors influencing edentulism rates, including socioeconomic conditions, healthcare access, and regional disparities (Al-Rafee, 2020). To maintain functionality, appearance, and oral health, these individuals may wish to replace their missing teeth. The method of replacement depends on the specific clinical situation presented to the dental professional. When patients prefer or have no option other than wearing dentures, it is a must to learn about the materials used for their dental prostheses and whether these materials possess the necessary qualities for that purpose. This could involve the materials used for both the denture base and the artificial teeth. The denture base resin is the component of the denture that sits on the supporting tissues, and it is the part to which the artificial teeth are attached (McCabe and Walls, 2013).

The concept of prosthetic tooth replacement is not a recent development; records of dental prosthesis construction date back to as early as 2500 BC in Egypt, where the use of artificial teeth in dentures has been documented. Over the centuries, teeth have been extracted from the deceased or acquired from impoverished individuals who were compelled to sell them. Besides

human teeth, animal teeth, such as those from hippopotamuses or elephant ivory, were also employed. These teeth were then trimmed and shaped to fit the specific requirements before being used (Johnson, 1959). Early dental prostheses were crafted from naturally available materials, such as ivory, bone, and wood (Elshereksi et al., 2014). Archaeologists have also discovered other examples of removable prostheses. A complete upper and lower denture made from ox femur, dating back to around 1500 BC, was found in Switzerland. These dentures were created using two bone arch-shaped templates joined at the posterior edge to form a "hinge." However, it appears that these prostheses were designed more for aesthetic purposes than functionality (Michael D Murray and Brian W Darvell, 1993). The Etruscans (circa 700 BC) also produced partial dentures using bones and ivory, which were then fastened to the remaining teeth with gold wires and bands (Anusavice et al., 2012).

In the late 18th century, the first porcelain complete denture was developed. While porcelain offered low solubility and low water absorption, it also had the disadvantages of being brittle and hard to grind (Elshereksi et al., 2014). The quality of porcelain dentures did not improve until the mid-19th century when commercial manufacturing led to increased competition among companies, driving them to create teeth with natural shades and translucency (Johnson, 1959). Around this time, vulcanite, a type of vulcanized rubber, was introduced for denture base production. Although these dark-red bases were more cost-effective, they were challenging to colour and raised hygiene concerns due to saliva absorption (Elshereksi et al., 2014).

Taggert made a significant advancement in 1907 by developing a technique for producing cast inlays. The development of cast alloys later enabled their use in prostheses during the 20th century. Various metals and alloys are now available for removable, all-metal, and metal-ceramic dentures, as well as for inlays, onlays, crowns, and frameworks (Anusavice et al., 2012).

In 1937, Dr. Walter Wright introduced polymethyl methacrylate (PMMA) as a denture base material (Jacob John et al., 2001). Although storage, packing, and curing methods initially posed challenges, dentists enthusiastically adopted the material. Within a decade, 98% of denture bases incorporated PMMA (Elshereksi et al., 2014; J. John et al., 2001; Johnson, 1959).

1.2. POLYMETHYL METHACRYLATE AS ACRYLIC RESIN DENTURE BASE MATERIAL

PMMA, also known as acrylic resin, has been the most extensively documented and utilised material in prosthetic dentistry since 1937 (Ayad et al., 2008). It is employed in the fabrication of dentures and teeth, offering significant advantages over other materials, such as chemical stability in the oral environment, satisfactory aesthetics, and precise fit. Additionally, PMMA is relatively easy to produce and process in the laboratory, and it is clinically adaptable for manipulation, adjustment, and repair. Moreover, it necessitates only relatively inexpensive processing equipment (Ahmed and Ebrahim, 2014). The mechanical and physical properties of acrylic resins (PMMA) surpass those of polystyrene resin, nylon, epoxy resin, and polypropylene. However, acrylic resins typically exhibit low strength and are prone to fracturing (Alhareb and Ahmad, 2011). Figure 1.1 represents different areas related to acrylic resin materials for denture bases.

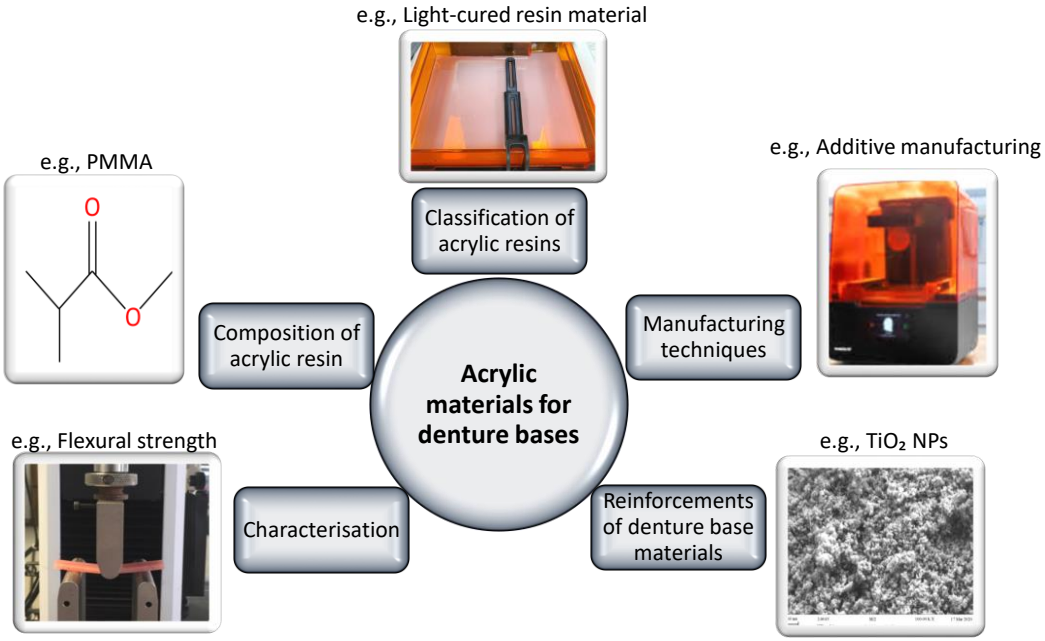

Figure 1.1. Areas related to acrylic materials for denture bases

1.3. CLASSIFICATION OF ACRYLIC RESIN DENTURE BASE MATERIALS

Denture base acrylic resins can be categorized based on various curing methods. These primarily involve the application of heat, chemical reactions (self-curing), light exposure, or the use of microwave energy for the curing process (Ferracane, 2001).

1.3.1. Heat-cured polymethylmethacrylate

The most prevalent curing method for PMMA is heat-polymerisation, typically employing a heated water bath (Bural et al., 2011). There are two suggested heat-polymerisation approaches. The first is an extended process, in which products are kept at a consistent temperature of 60-70ºC for 6-9 hours. The second method concludes the gradual heating with a boiling phase for either 30 minutes (short-term) or an hour (long-term) (Bural et al., 2011; Honorez et al., 1989). Heat-curing PMMA results in a stronger denture base material than those cured by light or chemical methods, offering additional advantages such as better colour stability and reduced residual monomer levels (Elshereksi et al., 2014)

1.3.2. Self-cured polymethylmethacrylate

This curing method is also known as autopolymerisation, cold cure, or chemical cure. Although it shares the same chemical composition as heat-cured acrylic, the powder component contains polymer beads with lower molecular weight compared to those in heat-cured PMMA. Furthermore, it necessitates chemical polymerisation initiated by amine molecules. This method provides a shorter curing time and is suitable for repairs or immediate denture fabrication. However, drawbacks include higher residual monomer levels, resulting in lower strength, polymerisation shrinkage, and reduced colour stability compared to heat-cured acrylic resins. Due to these issues, it is widely acknowledged that acrylic dentures created through heat-polymerisation possess superior mechanical, chemical, and physical properties compared to those made by chemical polymerisation (Ferracane, 2001; Noort and Barbour, 2013).

1.3.3. Microwave polymethylmethacrylate

The first documented use of microwave energy for curing denture base materials dates back to Nishii in 1968. Later, Kimura pioneered the rapid curing of polymethyl methacrylate using this technique (S. Singh et al., 2013). Microwave polymerisation involves inducing molecular movement within an electromagnetic field, which promotes intermolecular collisions and generates heat energy that the resin absorbs (Spartalis et al., 2015). This curing method offers a shorter and cleaner process, yielding a denture base that adapts well to the dental cast (Ferracane, 2001). Despite these benefits, however, microwave curing has received limited clinical acceptance (Spartalis et al., 2015).

1.3.4. Light-cured acrylic resin

Light-cured denture base resins, which first entered the market in the 1980s, are free of methyl methacrylate monomer and serve as an alternative to heat and self-cured PMMA. Researchers initially reported the light-activated urethane dimethacrylate (UDMA) denture base polymer, known as Triad (Ali et al., 2008). This light-activated system exhibited low bacterial adherence, easy manipulation and processing, and was well-accepted and tolerated by patients. Additionally, it could bond with other denture base resins, making it suitable for repairing or adjusting existing dentures. However, the system's application was limited due to its brittleness and low impact resistance. Consequently, numerous studies have been conducted to develop new light- and heat-activated denture base materials. Recent research has demonstrated that the impact and flexural strengths of these newer light- and heat-cured materials are favourable and higher than those of older light-cured acrylic denture base materials (Ali et al., 2008).

1.4. COMPOSITION OF ACRYLIC RESIN

1.4.1. Heat-cured acrylic resin material

Heat-cured acrylic resin is the preferred material used in the construction of denture bases (Salim et al., 1992). It's been noted that nearly 98% of all denture bases are made with this heat-cured resin, given its hardness and resilience, which are sufficient to keep the teeth in contact during chewing. The heat-cured denture base resin should fulfil all the necessary material property requirements to create an ideal dental prosthesis (Elshereksi et al., 2014). Heat-cured denture base resin is produced from PMMA powder (Figure 1.2a) and methyl methacrylate (MMA) monomer (Figure 1.2b). This blend is commonly referred to as conventional heat-cured denture base resin (Bonsor and Pearson, 2012). The powder is made up of tiny spheres and exhibits a granular texture in some products. This powder readily dissolves in the liquid monomer and, for resins that are heat-processed, has an average particle size of roughly 150μm. Furthermore, elements such as initiators/accelerators, stabilisers, and pigments are also present (Bonsor and Pearson, 2012).

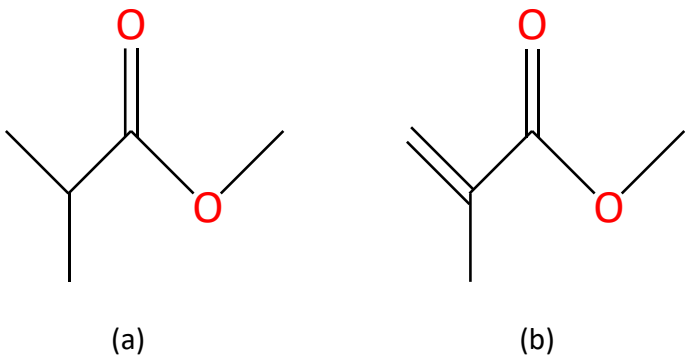

Figure 1.2. Chemical structure of: (a) PMMA, (b) MMA (Bonsor and Pearson, 2012)

1.4.2. Light-cured acrylic resin material

Light-cured resins are composed of three main component; the organic phase, the inorganic phase, and the coupling agent.

1.4.2.1. The organic phase

Also known as the resin matrix, and the matrices most commonly utilised are founded on methacrylate chemistry, particularly dimethacrylates based monomers like Bis-GMA, EBPDMA, UDMA, TEGDMA, and D3MA (Figure 1.3)(Moszner and Salz, 2001). Non-dimethacrylates based monomers are less commonly used as matrices, and they include Ormocers and Siloranes (Cavalcante et al., 2011; Ilie and Hickel, 2011).

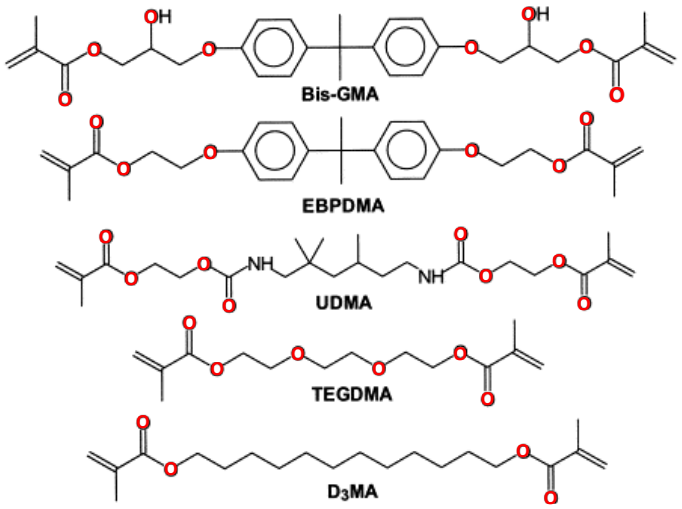

Figure 1.3. Chemical structure of frequently used dimethacrylate based monomers (Moszner and Salz, 2001)

1.4.2.2. The inorganic phase or filler

The majority of advancements in commercial resin composites over the past several decades have been refinements to the filler system. Characteristics such as filler morphology, size, orientation, distribution, and volume within the matrix all exert influence on the composite's properties. The integration of inorganic filler particles into the organic matrix enables a reduction in monomer content and boosts the physical and mechanical properties of the resulting resin composite (CHUNG and Greener, 1990). Incorporating fillers in light-cured resin lends rigidity, strength, dimensional stability, minimises polymerisation shrinkage, enhances colour, optical attributes, handling properties, wear resistance, inherent surface roughness and polishability (Ferracane, 1995; Powers and Sakaguchi, 2006). In recent years, the focus has been on optimising filler size and content (Powers and Sakaguchi, 2006). Traditional macro fillers (0.1 to 100 μm) have been replaced with significantly smaller particles, ranging from micro to nano size. As a result, alterations in filler size and morphology have improved the mechanical properties and aesthetics of composites in comparison to their traditional counterparts (Ferracane, 1995; Ilie and Hickel, 2009).

1.4.2.3. The coupling agent (organosilane)

Silane is a coupling agent that forms a chemical bond between the filler and the organic matrix. The organic matrix and the inorganic filler are distinct materials, which leads to potential issues

around compatibility and adhesion between them. The silane coupling agent serves as an adhesion promoter, chemically binding the two phases together and thereby enhancing the mechanical properties of the composite resin (Mohsen and Craig, 1995). The most commonly used silane in dental composites is 3-methacryloxypropyl-triethoxysilane (MPTMS) (Bowen, 1979). This bifunctional molecule has alkoxysilane groups (Si-OH) on one end that react with the filler to form oxane bonds (Si-O-CH_3). At the other end, it has methacrylate functional groups that copolymerise with resin monomers, forming carbon-carbon covalent bonds (Ferracane, 1995). This silane coupling layer is created by coating the inorganic fillers to enhance their wettability, then mixing them with the organic matrix to generate a composite material (Bowen, 1979). Without this layer, successful adhesion between the phases does not occur. Should adhesion fail, the composite restoration is susceptible to water absorption at the filler matrix interface, stress distribution between the filler and matrix is disrupted, and the filler particles may be easily dislodged (Dean, 2021).

Moreover, light-cured denture base resin also incorporates elements such as photoinitiators, stabilisers, and pigments. Light-cure composite systems utilise camphoroquinone (CQ) as the photoinitiator for polymerisation. An external blue light source, ranging between 400 – 550 nm, is absorbed by the CQ which then interacts with a co-initiator to generate free radicals, initiating the polymerisation process (Bowen, 1979). It is crucial to consider the concentration of CQ in the composite material, as its yellow colour can impact the aesthetic qualities, and the colour could absorb the light, subsequently affecting the depth of cure (Kwon et al., 2012). 1-phenyl-1,2-propanedione (PPD) can be introduced to the standard CQ-amine system. PPD, with an absorption maximum of 410 nm, results in polymers that are less yellow in colour and may reduce the shrinkage stress rate without altering the properties of the final material (Schneider et al., 2010; Stansbury, 2000). In a similar vein, triacylphosphine oxide (TPO) has absorption characteristics comparable to PPD. It exhibits high reactivity when exposed to a quartz–tungsten–halogen (QTH) light (Kwon et al., 2012; Stansbury, 2000). Another variant of photoinitiator systems includes Ivocerin. It is a germanium-based initiator with an absorption range close to that of CQ and higher than TPO. It has been reported to exhibit greater curing activity than CQ (Fugolin and Pfeifer, 2017; Moszner et al., 2008).

Polymerisation inhibitors are incorporated into the resin mixture to avert spontaneous polymerisation of matrix monomers under standard storage conditions. These inhibitors also impede uncontrolled photopolymerisation by ambient room light when atmospheric oxygen is

present. Phenols, such as 2,6-di-tert-butylmethylphenol (BHT) and hydroquinone monomethylether (MEHQ), are most commonly utilised for this role. They are introduced into the light-cured resin mixture in extremely low concentrations, reaching 100-200 parts per million (ppm) (Bowen, 1979; Klapdohr and Moszner, 2005).

UV stabilisers enhance the clinical colour consistency of the resin by reducing the impact of UV light on the matrix and averting its photodegradation, as this can lead to the composite darkening over time. The most frequently used UV stabilisers are 2-hydroxybenzophenones and 3-(2-hydroxyphenyl)-benzotriazols, present in quantities of 0.10 to 0.50% w/w (Klapdohr and Moszner, 2005).

The colour of the light-cured denture base resin holds significant importance. In order to cater to the growing aesthetic preferences of patients and dentists, pigments are incorporated into the resin. A range of differently coloured inorganic pigments are added to the mixture in proportions of 0.001 – 0.05% w/w. The most frequently utilised colours are yellow, black, white, and red (Klapdohr and Moszner, 2005).

1.5. DENTURE BASE MANUFACTURING TECHNIQUES

The most common methods for fabricating denture base resins are: (1) compression moulding technique, (2) injection moulding technique, and (3) computer aided design/ computer aided manufacturing (CAD/CAM) technology. The first two techniques are employed for manufacturing heat-cured resins in laboratories based on dental technicians' preferences or equipment availability. The injection moulding technique is faster than compression moulding and helps reduce polymerisation shrinkage and material porosity. However, it is a complex procedure that requires specialised flasks and equipment. Consequently, many dental technicians prefer the compression moulding technique (Eakle and Bastin, 2019). Figure 1.4 shows the conventional manufacturing steps for producing a heat-cured denture.

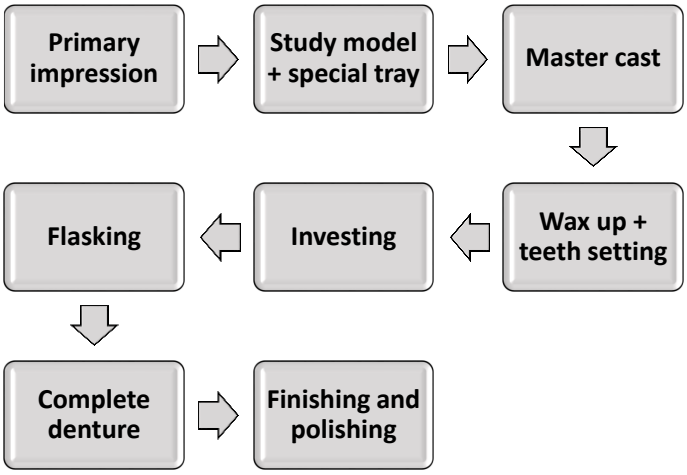

Figure 1.4. Steps needed for conventional fabrication of heat-cured denture base

1.6. CAD/CAM TECHNOLOGY

CAD/CAM, a relatively recent approach to denture fabrication, is becoming increasingly prevalent in dentistry (Alshaikh et al., 2022; Chebib et al., 2022; Goodacre et al., 2016; Rueggeberg, 2002; Tasaka et al., 2019). CAD/CAM dentures provide several advantages for both patients and clinicians (Al-Dwairi et al., 2019; Batisse and Nicolas, 2021; M. D. Murray and B. W. Darvell, 1993; Ring, 1985). These dentures can be created in some cases in just two appointments, significantly reducing clinical and patient time (Al-Dwairi et al., 2019; M. D. Murray and B. W. Darvell, 1993). Manufacturing companies digitally scan and store patient records (Goodacre et al., 2016; Rueggeberg, 2002). Consequently, there is no need for recasts or new clinical records if a patient loses or breaks their denture, enabling a quick production of an exact replacement prosthesis (Goodacre et al., 2016; Rueggeberg, 2002). Dentures can be fabricated using a subtractive (milling) or additive (3D-printing) methods (Batisse and Nicolas, 2021; Goodacre et al., 2016; Ring, 1985; Rueggeberg, 2002). The subtractive technique is currently the most frequently utilised method (Batisse and Nicolas, 2021; Ring, 1985).

Any CAD/CAM system comprises three essential components (Alshaikh et al., 2022; Batisse and Nicolas, 2021; Beuer et al., 2008; van Noort, 2012):

1. Data acquisition: This initial phase involves scanning the treatment site or stone model using a digitisation tool or scanner, capturing digital data that is then processed by a computer.
2. Data processing: CAD/CAM software generates the data set required for the intended prosthesis. The digital impressions are converted into a 3D computer model, and the dentist or dental technician designs restorations such as crowns, bridges, inlays, or onlays on the computer.

3. Manufacturing: The digital data is converted into the desired prosthetic. Once the prosthesis design is completed by the CAD, information is sent to the production unit, which is controlled by the CAM software. CAM milling involves subtractive manufacturing, where a block of material (e.g., ceramic, composite, or metal) is shaped based on the digital design, or 3D printing uses additive manufacturing, layering materials to build the restoration.

1.6.1. Subtractive manufacturing

The subtractive manufacturing (SM) method involves mechanically milling unwanted portions from a pre-polymerised resin block to create a complete denture. This process is controlled by a computer that directs the milling machine according to the desired design (Davidowitz and Kotick, 2011; van Noort, 2012), and it is typically used for producing simple restorations and crowns. Complete denture manufacturing using SM can proceed along two routes.

The first route involves taking a conventional impression of the edentulous area to create a stone model. A wax-up with teeth setting is then made, which is later digitised using a digital scanner and sent to the CAM machine. Finally, the CAM machine shapes the complete denture by cutting the resin material block.

The second route begins by taking a digital impression of the edentulous area, which is sent directly to the CAD software. The CAD software then designs the complete denture according to the clinician's or technician's specifications, serving as an alternative to the conventional impression combined with the wax-up and teeth setting steps. The complete denture design is then sent to the CAM machine as the final step in the denture manufacturing process (Bilgin et al., 2016; Rekow et al., 1991). Figure 1.5 illustrates SM steps for creating a complete denture.

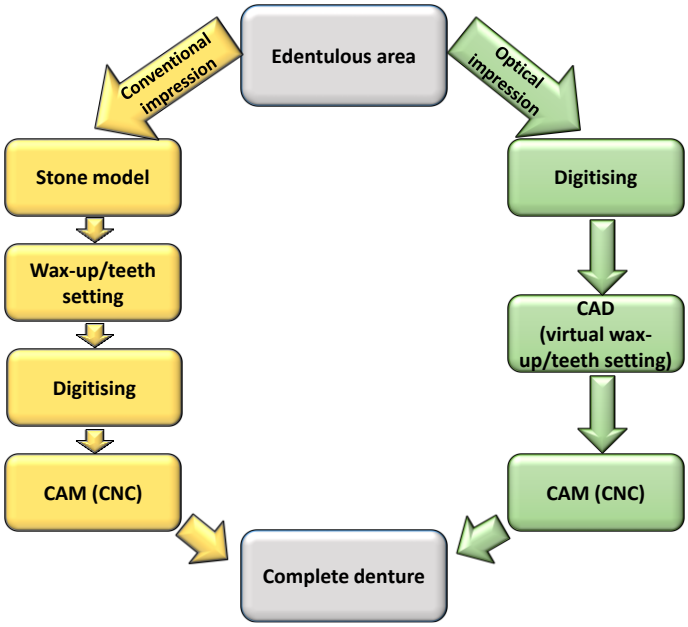

Figure 1.5. Steps for subtractive manufacturing of denture base

1.6.2. Additive manufacturing (rapid prototyping)

Additive manufacturing (AM), as opposed to SM, is typically used for creating complex restorations or prostheses. AM involves joining materials according to three-dimensional (3D) model data designed by CAD software to produce the desired shape. The CAD design is segmented into layers, which are then forwarded to the rapid prototyping machine. The final object is constructed layer by layer (Alghazzawi, 2016). Liquid polymer resin is commonly employed as the material for AM of dental objects, and curing is often necessary to achieve the required strength in the final product (Alghazzawi, 2016; J. W. Stansbury and M. J. Idacavage, 2016). AM presents a significant advantage by eliminating material waste associated with SM due to the precise layering following the shape provided by the CAD software (Dawood et al., 2015), and also can create the undercuts better than SM (Skordou et al., 2021). AM includes various techniques tailored to suit different materials and applications (Chia and Wu, 2015). Figure 1.6 illustrates the AM steps for fabricating a denture.

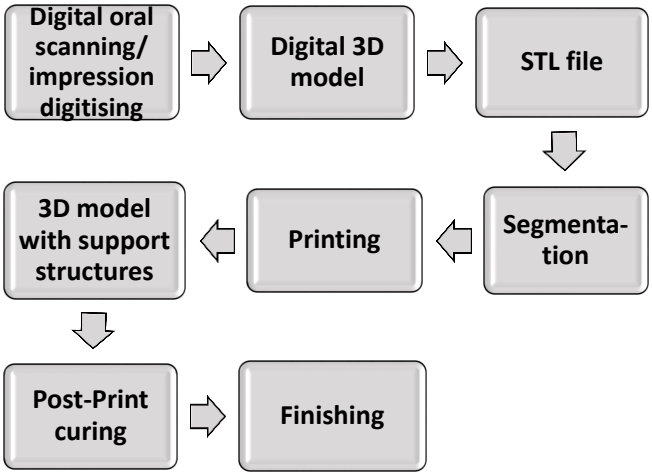

Figure 1.6. Steps needed for additive manufacturing of denture base.

1.6.3. Comparative analysis of fabrication methods

Comparing the CAD/CAM technique with the traditional method, the CAD/CAM approach generally offers advantages including user-friendliness, speed, time efficiency, and enhanced denture quality (Miyazaki and Hotta, 2011). It diminishes the clinician's chair time needed for denture fabrication and placement to 2-3 appointments, facilitates the provision of replacements using saved digital data, and lessens the workload for the technician (Cristache et al., 2020). Furthermore, it shows higher or similar overall precision in the dentures produced as compared to the traditional method (Lee et al., 2019; McLaughlin et al., 2019). Similar in vitro trueness and tissue surface adaptation have been observed for CAD/CAM mandibular denture bases made using both AM and SM techniques (Masri et al., 2020). Nonetheless, SM shows superior dimensional stability and mechanical properties as compared to AM, owing to the different polymerisation environments associated with each method (Prpic et al., 2020). The resin blocks in SM are pre-polymerised under high temperature and pressure, while in AM, the liquid resin is light-cured. This discrepancy can lead to the shrinkage of the final denture due to the presence of unreacted monomers in the AM process (Lin et al., 2019; Vallittu et al., 1995). The average adaptation discrepancy for the AM was reported to be slightly higher (0.08 mm) compared to the subtractive manufacturing (0.06 mm) (Masri et al., 2020). These unreacted monomers may also cause allergic reactions in patients or dental technicians who have a sensitivity to polymer resin products (Devlin and Watts, 1984). Generally, SM is preferred for small intraoral restorations as it yields a homogeneous end product with satisfactory accuracy. However, for larger, more complex prostheses such as denture bases or

facial prostheses, AM is more suitable due to its relatively superior accuracy (Abduo et al., 2014; Grande et al., 2022). Table 1.1 provides a comparison between CAD/CAM techniques and the conventional method across various aspects.

Table 1.1. A relative comparison between conventional and CAD/CAM methods for denture base manufacturing (Della Bona et al., 2021; van Noort, 2012)

Related factors	Conventional method	CAD/CAM	
Human errors	↑	↓	
Clinical visits	↑	↓	
Number of visits	↑	↓	
Digital archiving	N/A	↑	
Retention	↑	↑	
Patient-centred outcomes	↑	↑↑	
Mechanical properties	↓	↑	
Physical properties	↓	↑	
Accuracy of the fitted surface	↑	↑↑	
Dimensional stability	↓	SM	AM
		↑	↓
Shrinkage	↑	SM	AM
		↓	↑
Resin type	PMMA	SM	AM
		PMMA	Dimethacrylate based polymer
Total cost on the treatment	↓	↑	
Total cost in 10 years	↓	↓↓	
New training	↓	↑	

1.7. 3D PRINTING TECHNOLOGY IN DENTISTRY

The accuracy and reliability of 3D-printing have significantly improved in recent years, making it increasingly suitable for dental applications (Mubaraki et al., 2022; Tian et al., 2021a). Various dental products, including surgical guides, temporary crowns, denture bases, and

dental splints, have been produced using 3D-printing technology Figure 1.7 shows a downward scope for the application of 3D-printing in dental field (Rekow et al., 1991; Tahayeri et al., 2018).

This technology is based on photo-polymerisation, using a controlled light source to cure liquid resin into hardened plastic. During the printing process, the molecular components of the material form covalent bonds. At this stage, the material is not fully cured, and the layers are in a semi-reacted state called the green state (Schweiger et al., 2019). This state differs from the completely cured state in that the molecules on the surface have polymerisable groups that can form covalent bonds with the layer placed on top of it. As the next layer cures, the polymerisation process incorporates the previous layer and forms covalent bonds in the Z-axis, meaning that there are no differences in the chemical bonds in the X, Y, and Z-axes at the molecular level. Once the printing process is completed, the final product remains in the green state, and the mechanical properties are not set. As a result, a post-curing process is needed to finalise the polymerisation process (Chen et al., 2022; Shah et al., 2023). Table 1.2 and Table 1.3 display some of the commercially available 3D printers with their post-cure devices and technical parameters.

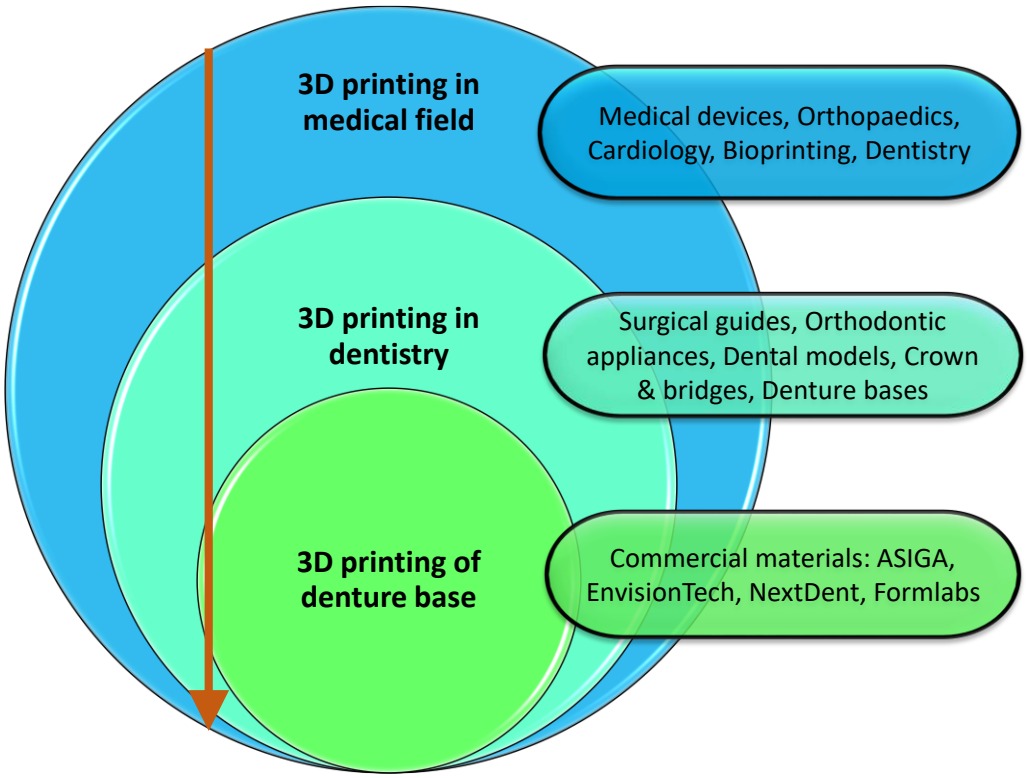

Figure 1.7. A downward scope for the applications of 3D printing

Table 1.2. 3D printers with their operating parameters

Printer commercial name	Formlabs Form2	NextDent 5100	EnvisionTEC one	ASIGA max UV
Printer technology	SLA	DLP	DLP	DLP
Light source	UV laser	LED light projector	LED light projector	LED light projector
Light source wavelength (nm)	405	405	385	385
Light source resolution (micron)	N/A (laser)	65	93	62
Laser power (mW)	250	n/a	n/a	n/a
Layer thickness (micron)	25-300	n/a	n/a	n/a

Table 1.3.. Post-cure boxes and their parameters

Company	Formlabs	NextDent	EnvisionTec
Number of light sources	13	12	36
LED power per light source (W)	39	18	n/a
LED wave length (nm)	405	300 - 550	390 - 420
Maximum temperature	80° C	60 - 80° C	70° C

The American division of the International Association for Testing Materials (ASTM) International Standard Organization created voluntary consensus-based technical standards for a diverse array of materials, products, systems, and services. The ASTM Committee F42 on AM technologies has identified seven AM categories: stereolithography (SLA) or digital light projection (DLP), material jetting (MJ) or polyjet printing (PP), material extrusion (ME) or fused deposition modelling (FDM), selective laser sintering (SLS) or selective laser melting (SLM), binder jetting, and direct energy deposition (Revilla-León and Özcan, 2019). The fundamental differences between these technologies concern the materials utilised and how the layers are constructed to generate the 3D object (J. W. Stansbury and M. J. Idacavage, 2016). SLA and DLP are the two primary 3D-printing technologies used in dental applications (Alghazzawi, 2016; Alshamrani et al., 2022; Mubaraki et al., 2022; Rekow et al., 1991; Tahayeri et al., 2018; Tian et al., 2021a).

1.7.1. Stereolithography technique (SLA)

SLA was invented by Chuck W. Hull, and during the same period, Prof. André filed a distinct patent for SLA technology in France (Hull, 1984). SLA represents an efficient means of creating complex shapes with high accuracy and precision; it is typically used to create resin-based items (Al-Dulaijan et al., 2022; J. W. Stansbury and M. J. Idacavage, 2016). The SLA comprises a photosensitive liquid resin reservoir, model build platform, and laser, which cures the resin (Mubaraki et al., 2022; Tian et al., 2021a). The build platform is immersed in liquid resin during the construction process, and ultra-violet (UV) laser is used to polymerise the resin. After polymerising each layer, the platform elevates by a distance corresponding to the layer's thickness, allowing the uncured resin to cover the previous layer. The process is repeated until the entire object is printed. In laser-based SLA 3D-printing, a UV laser is employed to outline the cross-sections of the object. The laser is focused using a series of lenses, and then it is reflected by a pair of motorized scanning mirrors, known as galvanometers. These scanning mirrors accurately direct the laser beam towards the reservoir of UV-sensitive resin, curing each layer in the process (Mubaraki et al., 2022; Tian et al., 2021a). The depth of cure is determined by the photoinitiator and irradiation exposure conditions (such as wavelength, power, and exposure time or speed), as well as any added dyes, pigments, or other UV absorbers, and this ultimately influences the z axis resolution (Infuehr et al., 2007; J. W. Stansbury and M. J. Idacavage, 2016). In general, the layer thickness in the SLA process relies on the standards set by the specific printer model. This thickness can range from 15 to 150 μm, with a surface roughness of approximately 35 to 40 μm Ra. The UV light wavelength required to polymerise the raw material also varies depending on the printer, typically falling within the range of 200 to 500 nm (Revilla-León and Özcan, 2019). One of the key benefits of SLA technology is its ability to print complex geometries. However, a primary limitation is the need for support structures during the manufacturing process. These support structures consume additional material and result in increased production and post-processing time (Petrovic et al., 2011).

1.7.2. Digital light projection technique (DLP)

Larry Hornbeck, from Texas Instruments, developed the technology for DLP in 1987 (Revilla-León and Özcan, 2019). DLP system shares similarities with SLA technology and is classified under the same AM category by the ASTM (Revilla-León and Özcan, 2019). In contrast to

SLA, DLP employs ultraviolet light (not a laser) to cure the liquid resin layer by layer. The digital micromirror device, a key component of DLP technology, is a rectangular array of mirrors that make up the microsystem (Al-Dulaijan et al., 2022; J. W. Stansbury and M. J. Idacavage, 2016). The resolution of the projected image is directly related to the number of mirrors, with each mirror representing one pixel or more. The angles of individual micromirrors can be adjusted (Mubaraki et al., 2022; Tian et al., 2021a). A single pixel of light from the light source is projected onto the printing surface after being reflected by the micromirror (Mubaraki et al., 2022; Tian et al., 2021a). DLP offers some advantages over traditional SLA, including faster layer fabrication, as it can print and cure an entire layer across the build plate within a few seconds. The use of DLP printing is anticipated to grow within the dental industry due to its accuracy and efficiency (Alghazzawi, 2016; Alshamrani et al., 2022; Mubaraki et al., 2022; Rekow et al., 1991; Tahayeri et al., 2018; Tian et al., 2021a). However, the lower power of the light source and the faster printing driven by commercial needs for speed rather than the quality is a concern. Figure 1.8 is a schematic diagram of the SLA and DLP manufacturing technologies.

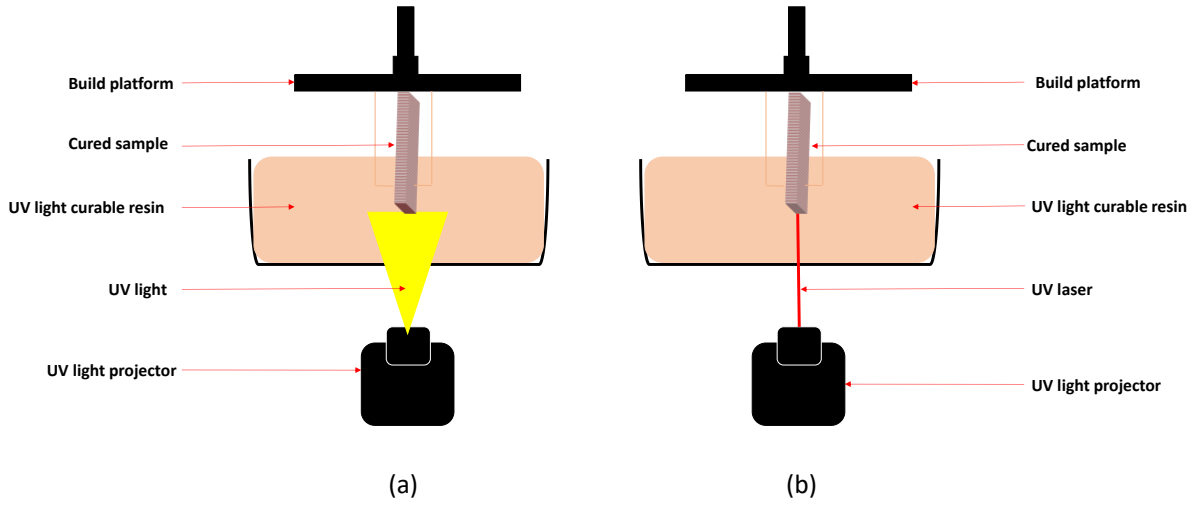

Figure 1.8. Schematic diagram of: (a) DLP, (b) SLA

1.7.3. Material jetting (MJ)

MJ technology, involves selectively jetting liquid resin from numerous nozzles and curing it with UV light (Jeffrey W Stansbury and Mike J Idacavage, 2016). The UV-curable polymers are applied only in areas specified by the virtual design. Since multiple print nozzles can be used, support materials are co-deposited alongside the primary material. Furthermore, this

method allows for different colours and building materials with varying properties to be used, including the creation of structures with spatially graded properties (Fahad et al., 2013; Singh, 2013).

1.7.4. Material extrusion (ME, FDM)

ME or Fused Deposition Modelling (FDM) was first developed by Scott Crump in the early 1990s and commercialised by Stratasys. The original patents have since expired, leading to numerous FDM brands entering the consumer market (van Noort, 2012). FDM involves extruding thermoplastic material through a nozzle, where it is heated and deposited layer by layer. The nozzle moves horizontally while a platform moves vertically after each new layer is deposited (Chia and Wu, 2015; Miller et al., 2010). Although many factors influence the final quality of an FDM-produced model, it has significant potential and viability when these factors are effectively controlled. FDM shares similarities with other 3D-printing processes, such as layer-by-layer construction, but it differs in that material is added through a nozzle under constant pressure and in a continuous stream. To achieve accurate results, this pressure must be maintained steadily and at a consistent speed. Material layers can be bonded using temperature control or chemical agents (Gibson et al., 2014). The nozzle depositing material always has a radius, as it is impossible to create a perfectly square nozzle, which impacts the final quality of the printed object (Chua et al., 2010). Compared to other processes, FDM offers lower accuracy and speed, and the final model's quality is limited by the material nozzle thickness. In applications requiring high tolerances, factors like gravity and surface tension must be considered. Typical layer thickness in FDM ranges from 0.178 to 0.356 mm (Revilla-León and Özcan, 2019).

1.7.5. Selective laser sintering (SLS, SLM)

Laser-based manufacturing of objects from powder involves two main processes: selective laser sintering and selective laser melting. These methods involve melting and layering powdered material with a laser to create the final product (Kruth et al., 2005; Torabi et al., 2015). "Selective Laser Sintering" (SLS) is the term used for processing polymers and ceramics, while "Selective Laser Melting" (SLM) or "Direct Metal Laser Sintering" are applied to the fabrication of metals and alloys (van Noort, 2012). SLS/SLM technology is highly suitable for use in dentistry, particularly in prosthetic dentistry, as it allows for a wide range of dental materials to be deployed in the fabrication of dental structures. These materials include

thermoplastic polymers, waxes, metals and alloys (such as titanium and its alloys, cobalt-chrome alloys, and stainless steel), ceramics, and thermoplastic composites. SLS can be employed to create maxillofacial prostheses, functional skeletons, and individual scaffolds for tissue engineering using polymers and composites. When processing metals and alloys using SLM, various products can be manufactured, including bulk and porous orthopaedic and dental implants, dental crowns, bridges, and frameworks for partial prostheses (Averyanova, 2012; Traini et al., 2008; van Noort, 2012). During the manufacturing process, numerous dental constructions can be fabricated on the machine table simultaneously, significantly increasing the productivity of this technology (Abou Tara et al., 2011; Kruth et al., 2005).

1.8. EFFECT OF PRINTING PARAMETERS

Accuracy is an important factor when assessing an object produced by AM. 3D-printed surgical guides were reported to have superior accuracy when placing the implant compared to conventional surgical guides (Bencharit et al., 2018). Other studies reported a 13% deviation of the 3D-printed object from the original design (Juneja et al., 2018), which was related to numerous factors, including the operator manipulation of the data, the printable material, and the printing process (Deeb et al., 2017; Matta et al., 2017). Some parameters in the printing process cannot be manipulated by the operator, such as the printing velocity and cure depth, while others can be adjusted, such as the printing orientation, printing wavelength, and the object's position on the build platform. Moreover, the after-printing process, including washing, cleaning, and final curing time and temperature, can also be manipulated. These pre- and post-processes affect not only the accuracy of the printed objects but also their mechanical properties (Alharbi et al., 2016; Vayrynen et al., 2016). Table 1.4 shows the parameters and their effect on the printed material.

Table 1.4. Different parameters and their effects on the printed dentures

Printing parameters	Effects
Printing orientations	• Horizontal orientation improves the flexural strength (Alharbi et al., 2016; Shim et al., 2020) and the compressive strength of interim 3D-printed dental restoration (Alharbi et al., 2016) • Vertical orientation improves the flexural strength of a 3D-printed surgical guide resin (Unkovskiy et al., 2018; Vayrynen et al., 2016) and the flexural modulus of a 3D-printed epoxy-based resin (Vayrynen et al., 2016) • Horizontal orientation improves the accuracy of a 3D-printed crown and bridge resin (Park et al., 2018)
Position on the build platform	• Printing on the middle of the build platform improves the accuracy of the print made of 3D-printed surgical guide resin (Unkovskiy et al., 2018)
Layer thickness	• Thinner layering improves the tensile and the impact strength (Chockalingam et al., 2006)

1.9. AVAILABLE DENTURE BASE MATERIALS FOR 3D-PRINTING

In response to the demand for denture base materials suitable for 3D-printing that offer superior physical, mechanical, thermal, and aesthetic properties, acrylic materials dominate the dental market. It is important to emphasise that the denture is printed from two different types of resin, denture base and denture teeth materials The 3D-printable acrylic materials are light-cured; some examples now available include 3D resins from Formlabs (USA), NextDent (Netherlands), ASIGA (Australia), and EnvisionTEC (USA). Other 3D-printable denture base materials are available that use LED light flashes and a specific type of gas for the post-curing process, rather than the combination of constant LED light and heat. These materials include FotoDent denture (Dreve), LC Denture (IMPRIMO), and Optiprint denture (dentona). Table 1.5 shows some commercially available 3D-printed acrylic materials with their properties for denture base manufacturing. However, 3D-printed materials generally have disadvantages that need addressing, such as reduced mechanical properties, including flexural and impact strength, and polymerisation shrinkage (Gad and Abualsaud, 2019). Therefore, acrylic materials should evolve using different technologies to improve the aforementioned properties. The literature indicates that the incorporation of reinforcing agents can yield new composite materials with improved mechanical, physical, or biological properties. In the dental field, many attempts have been made to improve 3D-printed resins by adding different types of fillers (Al-Harbi et al., 2019; Bacali et al., 2019; Chen et al., 2019; Cierech et al., 2018; Gad and Abualsaud, 2019; Gad et al., 2020; Gad et al., 2017), and the properties of the resulting composite material depend on the nature, shape, size, and distribution of the inorganic fillers.

Table 1.5. Denture base polymers for 3D printing and their parameters

Commercial name	Digital denture	Denture 3D+	Denture base II	DentureTEC	Denture
Company	Formlabs	NextDent	DENTCA	Saremco	Detax
Printing wavelength (nm)	405	405	385/405	385	385
Printing temperature (° C)	31	18 – 28	18 – 30	35	23 – 25
Post-cure time (minutes)	30	30	20 - 60	4000 flashes (N* gas)	2000 flashes (N* gas)
Post-cure temperature (° C)	80	60	> 60	Not needed	Not needed
Post-cure wavelength (nm)	405	300 – 550	320 – 405	320 – 500	320 – 500

**N: nitrogen gas*

1.10. REINFORCEMENTS OF DENTURE BASE MATERIALS FOR 3D-PRINTING

The application of 3D-printing for fabricating complete removable denture bases has gained popularity. Nevertheless, this technique still faces challenges concerning its mechanical and physical properties (Alifui-Segbaya et al., 2019; Lee, 2020). Research has shown that double bond conversion in 3D-printing is not as effective as in traditional PMMA resins (Alifui-Segbaya et al., 2019). Furthermore, 3D-printed denture base resin has lower flexural strength, elastic modulus, impact strength, and surface hardness compared to heat-polymerised resin (Gad et al., 2022c; Perea-Lowery et al., 2021b). Researchers have explored various methods to reinforce 3D-printed resin, with the use of nanoparticles (NPs) being one of the most promising strategies (Gad et al., 2017; Gad et al., 2016). Prior research has revealed that nanoscale reinforcing agents have contributed to the development of a new category of nanocomposites that display distinct physical and mechanical properties (Navidfar et al., 2016). In dentistry, the integration of nanosized fillers in PMMA has been extensively investigated to enhance dental materials properties (Chaijareenont et al., 2012). The resulting composite material's attributes are affected by the type, size, and shape of the additional NPs used in combination with the polymer matrix (Jordan et al., 2005). Table 1.6 shows the evolutions and the additions made to improve 3D-printed materials for complete denture manufacturing, and the properties of the resultant composite materials.

Table 1.6. Summary of information extracted from selected studies.

Reference	Added particles/ Weight percentage	3D printing technology	Characterisation	Specimen shape and size	Clinical significance
Totu et al. (TOTU et al., 2018; Totu et al., 2017)	TiO_2 (0.1 – 2.5 wt %) Particles size: 56 – 170 nm	DLP	Biological/Antimicrobial: Candida species: C. scotti Bacterial species: Staphylococcus aureus Cytotoxicity: fibroblasts	N/A	The denture made with this composite material can resist fungal growth.
			Microscopy: SEM, EDX		
			Chemical: FTIR		
Chen et al. (Shenggui Chen et al., 2018; Chen et al., 2019)	TiO_2 /PEEK (1 – 4 wt %) Particles size: 30 - 40 nm	SLA/DLP	Biological/Antimicrobial: Candida species: C. scotti; Bacterial species: E. coli, Staph aureus; Cytocompatibility/Cytotoxicity	N/A	The denture made with this composite material has better mechanical properties and can resist bacterial and fungal growth.
			Microscopy: SEM; TEM		
			Chemical: FTIR; XRD		
			Mechanical: Flexural strength and modulus; Impact strength	-64 x 10 x 3.3 mm	
Mangal et al. (Mangal et al., 2020a; Mangal et al., 2020b)	Nanodiamonds (0.1 wt %) Particles size: 4 - 255 nm	DLP	Biological/Antimicrobial: Bacterial species: Streptococcus mutans	-20 x 20 x 3.5 mm	3D printed specimens made with the composite material has better mechanical and physical quality compared to the unmodified material. Resistance to S. mutans is proven.
			Physical: Surface roughness; Accuracy; Water sorption and solubility, Hydrophilicity	-15 x 1 mm disk	
			Chemical: FTIR	N/A	
			Microscopy: SEM; TEM		
			Mechanical: Flexural strength and modulus; Impact strength; Hydrothermal fatigue; Surface microhardness	- 64 x 10 x 3.3 mm - 64 x 12.7 x 3.2 mm	
			Tribological: Wear resistance	N/A	
Chen et al. (S. Chen et al., 2018)	Cellulose nanocrystals (CNCs)- silver nanoparticles (AgNPs) (0.05, 0.1, 0.15, 0.2 and 0.25wt.%)	DLP	Biological/Antimicrobial: Bacterial species: Staphylococcus aureus, E. coli Cytocompatibility/Cytotoxicity: fibroblasts	N/A	Composite resin (CNCs-AgNPs 0.10-0.25wt%) exhibits strong antibacterial activity with no discernible cytotoxic impact. Due to the uniform distribution of AgNPs throughout the resin matrix, the group with CNCs-AgNPs of 0.10wt% exhibited the best mechanical qualities.
			Chemical: FTIR	-64 x 10 x 3.3 mm	
			Microscopy: TEM	N/A	
			Radiation: XPS		
			Mechanical: Flexural strength, elastic modulus and impact strength	64 x 10 x 3.3 mm	
Liao et al. (Liao et al., 2020)	P-6S-NP3 (1 – 3 wt %) Particles size: 3100 - 3500 nm	DLP	Biological/Antimicrobial: Bacterial species: Staphylococcus aureus, E. coli	64 mm × 10 mm × 3.3 mm	3D printed objects made with the composite material has better mechanical and physical quality compared to the original resin.
			Physical: Water contact angle		
			Chemical: FTIR; XRD		

	6S-NP3 (3 wt %) Particles size: up to 4100 nm		Microscopy: SEM Mechanical: Flexural strength and modulus; Impact strength		Resistance to S. aureus and E. coli is proven.
Duan et al. (Duan et al., 2020)	Thermochromic pigments (0.3 – 1.0 wt %) Particles size: 3 – 4 µm	SLA	Physical: Conversion rate; Colour change behaviour Chemical: FTIR Microscopy: SEM Mechanical: Tensile strength; Young's modulus; Elongation at break	-13 x 5 mm cylinder -Eiffel tower structure sample	Objects or appliances printed with this composite material have better mechanical properties and provides a thermosensor function to them
Alshaikh et al. (Alshaikh et al., 2022)	ZrO_2 nanoparticles (0.5 – 5.0wt. %) Particles size = 40 nm	DLP	Flexure strength and elastic modulus Impact strength Surface roughness and hardness	64 × 10 × 3.3 mm 50 × 6 × 4 mm 15 × 2 mm	The ZrO_2NPs supplement enhanced the 3D-printed resins' mechanical properties.
Gad et al. (Gad et al., 2022a)	Silicon dioxide nanoparticles (0.25wt.% and 0.50wt.%)	DLP	Flexural strength Impact strength	64 × 10 × 3.3 mm 50 × 6 × 4 mm	While the inclusion of Silicon dioxide nanoparticles did not result in any significant changes in the surface roughness, the result revealed an overall increase in the mechanical properties of the modified 3D-printed resin.
Aati et al (Aati et al., 2022b)	Ag/MSN (0.0 – 2.0 wt.%) Size = 3 nm	DLP	Biological/Antifungal: Fungal species: C. albicans Cytotoxicity: human oral fibroblasts Physical: Surface hardness, surface roughness, water sorption and solubility, FTIR Microscopy: TEM, AFM Mechanical: Flexural strength, fracture toughness	N/A -15 x 1 mm disc N/A -65 × 10 × 3.3 mm -39 × 8.0 × 4.0 mm	The addition of Ag/MSN significantly enhanced the mechanical and antimicrobial properties without showing adverse effect on human fibroblasts.
Khattar et al (Khattar et al., 2022)	ZrO_2 nanoparticles (0.5 – 5.0 wt.%) Size = 40 nm	DLP	Biological/Antifungal: Fungal species: C. albicans Physical: surface roughness	-15 x 2 mm	Incorporating ZrO_2 nanoparticles into 3D-printed resin at a low concentration (0.5wt.%) leads to a significant reduction in the adhesion of C. albicans without affecting the surface roughness of the printed material.
		DLP	Physical: Surface hardness, surface roughness	N/A	

Al-Douri et al (Al-Douri and Sadoon, 2023)	ZnO nanoparticles (2.0, 3.0, and 4.0 wt.%)		Mechanical: flexural strength	-64 × 10 × 3.3 mm	The addition of ZnO improved the flexural strength and decreased the surface roughness, while the surface hardness was not affected.

1.11. PROPERTIES OF ACRYLIC RESIN DENTURE BASE MATERIAL

1.11.1. Physical properties

1.11.1.1. Water sorption and solubility

Polymeric materials are inclined to absorb water over time due to the polar characteristics of the resin molecules (Vallittu et al., 1995). This water absorption can detrimentally impact the material's mechanical and physical attributes negatively, increasing surface roughness and leading to unpleasant odours, and could also cause dimensional stability issues (UMEMOTO and KURATA, 1997). The solubility of polymers signifies the quantity the un-polymerised monomer and other soluble substances within the polymer (Rahal et al., 2004b). As water infiltrates the resin matrix, it dissolves the unreacted monomer and triggers plasticisation, which consequently weakens the polymer (Malacarne et al., 2006a).

1.11.1.2. Surface roughness

Surface roughness can impact patient comfort, increase the likelihood of staining, and influence overall oral health (Gungor et al., 2014). It can also compromise the cleanliness of the denture base, as a rougher surface facilitates bacterial adherence. Once these bacteria adhere, they can be tough to remove using typical oral hygiene practices (Oliveira et al., 2008). This can precipitate plaque build-up, fungal infections, denture-induced stomatitis, angular cheilitis, and even tooth decay (Ozyilmaz and Akin, 2019). To prevent the attachment of these microorganisms, the surface roughness of polished dentures should be kept below 0.2 μm (Onwubu et al., 2018).

1.11.1.3. Colour stability

Colour consistency is crucial for the aesthetic appeal of denture bases, ensuring they blend seamlessly with the natural soft tissues in the mouth (Altıncı and Durkaya, 2016). Changes in colour can be intrinsic, stemming from alterations in the matrix as the material ages, or extrinsic, where the material is discoloured by food, beverages, smoking, or cleaning agents (Goiato et al., 2013). Other external factors that can influence the colour of the material include disinfectants and cleaning solutions, as well as temperature fluctuations caused by consumption of hot or cold food and drink (Altıncı and Durkaya, 2016; Goiato et al., 2013).

1.11.2. Mechanical properties

1.11.2.1. Flexural strength and modulus

Flexural strength, a crucial characteristic of polymeric materials, signifies a material's stiffness and fracture resistance (Jagger et al., 2002). It's defined as the peak stress a material can bear before snapping (Ferracane, 2001). The material's flexural strength is critical during the process of masticating with a denture base in the mouth. As compressive, tensile and shear strengths amalgamate, the denture base deforms under the significant load due to flexural and fatigue failure (J. John et al., 2001; Li et al., 2006). The three-point bend test is an appropriate method to assess the type of stress exerted on the prosthesis during chewing, and as such, it is employed to evaluate the flexural strength of denture base resin materials (Gungor et al., 2017). Various mechanical tests that chart a stress-strain curve can also be used to compute the material's modulus of elasticity (Ilie et al., 2017). This modulus signifies the material's stiffness, which is determined from the slope of the elastic region in the stress-strain curve (Anusavice et al., 2012).

1.11.2.2. Impact strength

The impact strength of denture base resin is described as "the energy needed to break a material under an impact force" (Anusavice et al., 2012). According to Machado and colleagues, impact strength quantifies the energy required to initiate and expand a crack within a material. Thus, it can represent the stress contact force needed to induce a fracture in a denture base under situations such as accidental dropping (Machado et al., 2012). The prevalent clinical failures of denture base resins stem from impact and fatigue failures, typically occurring on a denture's midline due to insufficient resistance to impact and bending (Thomas et al., 2015).

The Charpy and Izod impact tests are two methods to assess the impact strengths of denture base resins. In the Charpy test, a sample is positioned horizontally, supported at both ends, and hit in the middle with a weighted pendulum. Conversely, in the Izod impact test, a sample is held vertically, supported at one end and struck at the other (Faot et al., 2006). The Charpy method fractures the sample's centre with a swinging pendulum. It is then possible to compute the energy (in Joules) lost during the fracture by comparing the swing length after the impact to a free swing where no impact occurs (Anusavice et al., 2012).

1.11.2.3. Fracture toughness

The failure of denture base acrylic resin, primarily due to fractures within the oral environment, is a significant concern. An essential parameter for evaluating the suitability of dental polymers is their fracture toughness, which is defined as the material's capacity to resist crack propagation (Al-Haddad et al., 2014; Hamza et al., 2004). Al-Haddad et al. characterized fracture toughness as the "critical stress intensity factor (K_{IC})," providing insights into crack propagation, which is the primary cause of acrylic fractures (Al-Haddad et al., 2014). Several methods exist for assessing fracture toughness, with the three-point bend test, also known as the 'single-edge notched bend' (SENB) test, being a recommended approach. This test necessitates specific geometrical considerations to achieve a state of plane strain (Williams and Cawood, 1990).

1.11.2.4. Surface hardness

Hardness is a measure of a material's ability to resist indentation, cutting, scratching, and abrasion (Noort and Barbour, 2013). It's crucial for resins to have adequate hardness to withstand the forces exerted during chewing or denture cleaning (Ana Paula Farina et al., 2012). The typical way to evaluate a material's surface hardness involves using an indenter to create an indentation on the material's surface over a certain time, and then measuring the resulting indentation size. Different tests use different indenter shapes such as Vickers uses a pyramid, Rockwell uses a cone, and Brinell uses a ball (Figure 1.9) (Noort and Barbour, 2013).

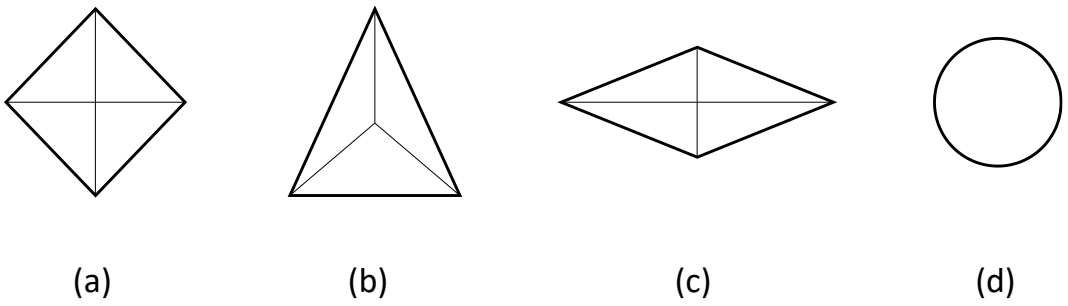

Figure 1.9. Shapes of different indenters: (a) Vickers, (b) Berkovich, (c) Knoop, (d) Brinell and Rockwell

1.11.2.5. Tensile bonding strength

Tensile strength represents the maximum amount of tensile stress that a material can tolerate before breaking (Combe et al., 1999). It plays a critical role in maintaining the structural soundness of dentures, preventing the denture teeth from detaching from the base. Factors such as extreme load,

insufficient polymerisation, fatigue, and substandard manufacturing can affect it (Matos et al., 2018). Tensile strength is determined by applying a continuous load in a tensile testing machine and then measuring the resulting stretch (Noort and Barbour, 2013).

1.11.2.6. Creep (viscoelastic behaviour)

Creep refers to the deformation that a material demonstrates under the influence of an applied load (Vaidyanathan and Vaidyanathan, 2001). This deformation can manifest under different types of loads, leading to two categories of creep: static and dynamic. Static creep occurs when the load is constant, while dynamic creep occurs under a periodic or cyclic load (El Hejazi and Watts, 1999). The viscoelastic properties of a dental restorative material can be assessed using a variety of methods such as indentation, three-point bending, and compression testing of a cylindrical specimen (Alrahlah et al., 2018; El Hejazi and Watts, 1999). Factors that impact the viscoelastic behaviour, or creep, include the chemical composition of the material, the degree of polymerisation, temperature and humidity, and the applied load (Al-Ahdal et al., 2015; Druck et al., 2015; Ruyter and Øysæd, 1987; Vaidyanathan and Vaidyanathan, 2001).

1.11.3. Biological properties

Biocompatibility, as defined by Jorge et al., refers to the acceptance (or rejection) of a synthetic material by the surrounding tissues and the body as a whole (Jorge et al., 2007). Denture resin is biocompatible and do not irritate or damage the oral mucosa. While the monomers are acknowledged to be toxic and irritating at high concentrations, after thorough heat polymerisation, the remaining monomer levels are minimal and pose no harm to the surrounding tissues. If the polymerisation process is carried out slowly at the right temperatures, residual monomer levels will be insignificant (Aati et al., 2022a; Jeon et al., 2022; Vasiliu et al., 2016).

In case of nanocomposite materials, nanoparticles, due to their capacity to infiltrate cellular membranes and organelles, may pose potential health risks (Bremer-Hoffmann et al., 2018). However, these nanoparticles are typically encapsulated within a matrix and have a reduced probability of escaping from dental materials (Rupf et al., 2015). Despite this, it is crucial to assess other potential routes of exposure, such as inhalation, ingestion, or direct contact with bodily tissues. The prevailing perception is that nanoparticles pose less risk, but this field necessitates further investigation (Rupf et al., 2015).

1.12. 3D-PRINTED NANOCOMPOSITE MATERIALS FOR DENTURE BASE APPLICATION

1.12.1. Physical characteristics

Nanodiamond (ND) particles, due to their round and nano-sized structure, have emerged as ideal fillers for developing composite materials, particularly in the realm of 3D-printed polymers (Karami et al., 2019). Researchers, such as Mangal et al. (Mangal et al., 2020a) have demonstrated the substantial advantages of using ND particles in modifying these polymers. Upon addition of ND particles, the material exhibited significant improvements in several physical properties, specifically surface hardness and roughness. These improvements, however, rely on the uniform dispersion of the ND particles within the polymer matrix (Mangal et al., 2019). Further exploring the impact of ND particles, Mangal et al. also investigated their effect on the wettability of the polymer. Wettability, a measure of how easily a liquid spreads on a surface, was found to decrease, indicated by a significant reduction in the contact angle between water and the nanocomposite material. This decreased wettability was accompanied by reduced water sorption and solubility. (Mangal et al., 2020a), Lastly, they discovered that the addition of ND particles resulted in a noteworthy improvement in surface wear resistance, particularly in an environment simulating toothbrush cleansing. This resistance extended to increased wear resilience against stainless steel and titanium surfaces, without significantly altering surface roughness. The exact improvements in wear resistance, hardness, and other properties, in terms of percentages, should be quantified in further studies to provide a more comprehensive understanding of the benefits of using ND particles in 3D-printed polymers (Mangal et al., 2019).

Additionally, Mangal et al. (Mangal et al., 2020b) evaluated the precision of 3D-printed specimens, both unmodified and those reinforced with nanoparticles, by referencing a CAD file. Utilising a digital scanner, they analysed each group of printed samples for congruity with the CAD reference. To quantify the degree of accuracy, they calculated the root-mean-square (RMS) values for the samples using a superimposition method. The findings showed minimal morphological alterations across the three groups, based on RMS values, and deviations from the CAD reference were contained within a range of ±200 µm.

Duan et al. introduced an additional layer of complexity to 3D-printed resin by incorporating silanated thermochromic pigments (Duan et al., 2020). Two pigment types, blue and pink, were utilized in this study. Observations indicated that the colouration of the enhanced material began

to fade when exposed to temperatures exceeding 31° C. Interestingly, these pigment additions did not disrupt the printing parameters of the resin material.

On the same manner, Aati et al investigated the effect of incorporating silver loaded mesoporous silica nanoparticles (Ag/MSN) on the physical properties on 3D-printed denture base resin (Aati et al., 2022b). Surface hardness displayed a linear improvement trend up to a 1.0 wt% addition, beyond which the surface hardness value started to decline significantly. This decrease was attributed to particle agglomeration at higher concentration levels. The assessment of composite material surface roughness revealed that, despite an increase in surface roughness, the results remained below the recommended threshold for surface roughness (≤200 nm). The degree of polymerisation was also examined, and although there was a declining trend in the value, it did not reach a significant level with an addition of 1.0 wt%. However, with a 2.0 wt.% addition, the measurement exhibited a significant decrease. This decrease was attributed to the dark coloration of the specimens due to nanoparticle aggregation, which could hinder the curing light from penetrating deeper layers. Water sorption and solubility were analysed, and the addition of Ag/MSN nanoparticles did not result in a significant difference in water sorption values. Conversely, a significant effect was observed in water solubility values, where the values decreased due to the entrapment of water molecules within the samples, resulting in some negative readings. Both water sorption and solubility values adhered to the standards outlined in ISO 10477.

Finally, the impacts of silicon dioxide (SiO_2) and zirconia oxide (ZrO_2) additives on the surface roughness of 3D-printed denture base resin were investigated by Gad et al. and Alshaikh et al (Alshaikh et al., 2022; Gad et al., 2022a) Their findings suggested no discernible alterations in surface roughness for nanocomposite materials compared to the unmodified variants. Contrary to their findings, Khattar et. al. (Khattar et al., 2022) reported a significant increase in the surface roughness after the addition of ZnO nanoparticles compared to the unmodified material. On the other hand, the surface hardness was significantly increased with the addition of SiO_2 nanoparticles, while the addition of ZrO_2 nanoparticles showed an insignificant increase in the value.

1.12.2. Mechanical characteristics

Chen et al. studied the mechanical properties of 3D-printed resin in conjunction with Titanium dioxide (TiO_2), and a composite of TiO_2 and Polyetheretherketone (PEEK) (Chen et al., 2019). Their findings indicated that the incorporation of 1.0 wt.% TiO_2 resulted in a rise in flexural strength and modulus, when compared to the control group. However, the inclusion of 2.0 wt%

TiO_2 led to complications during printing, such as flaking and over-solidification, ultimately causing the printing process to fail. This failure could be attributed to the aggregation of TiO_2 NPs within the polymer matrix. Additionally, an excessive quantity of TiO_2 NPs might have led to the over-absorption of ultraviolet light, potentially interfering with the curing process, thereby decreasing the mechanical properties of the nanocomposite material. To surmount these hurdles, PEEK microparticles were added to enhance the dispersion of TiO_2 NPs and boost the mechanical properties of the resultant composite material. This addition showed improvements in flexural strength, modulus, and impact strength, the latter of which saw significant enhancement.

In a similar vein, Mangal et al. examined the effects of ND and aminated-nanodiamond (A-ND) additives to the mechanical properties of 3D-printed denture base resin material (Mangal et al., 2020a; Mangal et al., 2020b). Both types of nanocomposite materials exhibited increases in flexural strength, modulus, and impact strength, with the A-ND composite material demonstrating significant enhancements relative to the control group and the ND nanocomposite group. The authors attributed the superior results of the A-ND nanocomposite group to stronger covalent bonds with the polymer matrix and better mono-dispersion of the nanoparticles, confirmed by transmission electron microscope observations, compared to the pure ND group.

Exploring a similar path, Duan et al. assessed the mechanical behaviour of 3D-printed resin combined with thermochromic pigments (Duan et al., 2020). They discovered a reduction in mechanical properties, including tensile strength, Young's modulus, and elongation at break, in comparison with pure 3D-printed material. This decline was ascribed to inadequate bonding between the thermochromic pigments and the 3D-printed resin, leading to material failure. To address this issue, they introduced a silane coupling agent, methacryloxypropyltrimethoxysilane (MPTMS). Consequently, some mechanical properties, such as Young's modulus and tensile strength, saw significant improvement, albeit at the cost of elongation at break (flexibility). The enhancement in mechanical properties was linked to a nearly 15% increase in the conversion rate in the silanated group compared to the un-silanated group, leading to stronger chemical bonds. However, any increase in the addition of silanated thermochromic pigments beyond the optimal level resulted in a decrease in tensile strength, with 1.0 wt% of the pigments resembling the pure material in value. Additionally, each increase of 0.2 wt% in filler weight led to a decrease of 20 MPa in Young's modulus.

On a similar note, Liao et al. (Liao et al., 2020) examined the impact of incorporating nano silver-loaded zirconium phosphate (P-6S-NP3) into 3D-printed resin material at varying concentrations. The addition of P-6S-NP3 was found to enhance the flexural strength, modulus, and impact

strength of the composite material, with the best flexural strength achieved at 2.0 wt% of P-6S-NP3. However, 6S-NP3 without surface treatment or grafting demonstrated weaker mechanical properties compared to the P-6S-NP3 groups and the control group. This was attributed to nanoparticle aggregation within the composite material, which easily flaked under stress. These findings underscored the crucial role of effective dispersion and compatibility of P-6S-NP3 within the composite material.

Chen et al. (S. Chen et al., 2018) examined several mechanical properties of 3D-printed denture base resin infused with silver nanoparticle-loaded cellulose nanocrystal (CNC-Ag NPs). Their findings demonstrated that flexural strength increased by 6% and 12% with the addition of 0.05 and 0.1 wt% CNC-Ag NPs respectively. The flexural strength plateaued with the addition of 0.15 and 0.20 wt%, and decreased when the concentration of fillers reached 0.25 wt%. The flexural modulus showed a minor increase with up to 0.20 wt% filler concentration, followed by a minor decrease with further additions. Meanwhile, the impact strength of the composite material was higher across all test groups compared to the pure material, with a significant increase observed at 0.05 and 0.1 wt% additions (48% and 73% respectively).

Simulating the oral environment, Mangal et al. (Mangal et al., 2020b) conducted a hydrothermal fatigue experiment involving multiple immersion cycles of their samples in water baths to accelerate the physiological ageing of the nanocomposite. Despite the expectation that the ageing effect would decrease the nanocomposite material's mechanical properties, the test groups displayed significantly superior flexural strength, elastic modulus, and modulus of resilience when compared to the control group.

Meanwhile, Gad et al. (Gad et al., 2022a) explored the effect of incorporating SiO_2 NPs on mechanical properties. They reported improvements in flexural strength, impact strength, and surface hardness of the nanocomposite material in comparison to the unmodified material, and advised adding less than 0.5 wt.% due to the low density of SiO_2 NPs relative to other metal oxides. In addition, they investigated the effect of the thermocycling ageing process on the unmodified and the nanocomposite material, noting a negative impact on most tested properties.

In the same vein, the impact of ZrO_2 NPs addition on mechanical properties has been studied (Alshaikh et al., 2022). Alshaikh et al. probed the effects of incorporating a range of 0.5 – 5.0 wt.% ZrO_2 NPs into 3D-printed denture base resin. Based on their results, they concluded that the additions improved flexural strength, elastic modulus, impact strength, and surface hardness of the nanocomposite material.

Similarly, Aati et. al. (Aati et al., 2022b) incorporated Ag/MSN nanoparticles to the 3D-printed resin, and they studied their effect on the flexural strength and the fracture toughness. They concluded that the flexural strength was decreasing with the addition of the nanoparticles, but this decrease was not significant, and the resultant nanocomposite was in compliance with the ISO 20795-1, 2013 (BS EN ISO, 2013). The authors interpret this as a limitation in the operation of 3D printers, where the initial curing time and intensity during layer formation are insufficient to activate the monomer and initiate bonding in the initial phase. Consequently, during the later stage of post-curing, the UV light primarily affects the nearest surface layer, enhancing its hardness, but it does not adequately reach the deeper internal structure. In contrast to flexural strength, the introduction of Ag/MSN nanoparticles led to a significant enhancement in the fracture toughness of 3D-printed resin. This increase was found to be significant in all the modified samples when compared to the control group. The existence of the Ag/MSN complex has impeded crack propagation, thus imparting an improved protective attribute to nanocomposites. These nanocomposites are constructed with an advanced capability to resist the spread of formed cracks.

Finally, Al-Douri et. al. (Al-Douri and Sadoon, 2023) reported a significant increase in the flexural strength of a 3D-printed resin after the addition of ZnO nanoparticles. This increase was noticed up to 3.0 wt.% addition of the nanoparticles. The increase observed in the experimental groups can be attributed to the role of nanoparticles as fillers that integrate into the resin matrix. This integration reduces gaps, spaces, and fractures within the resin material. Furthermore, the proper distribution of nanoparticles allows them to interpose between the linear chains of the polymer, resulting in reduced polymer chain mobility and an increase in flexural strength. However, it is worth noting that the addition of 4.0 wt.% ZnO nanoparticles led to a decrease in flexural strength, in contrast to lower concentrations. This decrease might be explained by a reduction in the load-bearing cross-sectional area of the polymer matrix. It is also possible that an excessive number of filler particles is causing stress concentration. One potential cause of this decrease could be incomplete resin wetting of the fillers. Moreover, ZnO may interfere with the integrity of the polymer matrix.

1.12.3. Biological characteristics

TiO_2 nanoparticles are have been proven known for their antimicrobial properties, largely due to the generation of cytotoxic oxygen radicals (Tsuji et al., 2016). Given its chemical stability, TiO_2 can decompose and oxidise both organic and inorganic compounds under certain conditions, making it an effective antimicrobial additive (L. S. Acosta-Torres et al., 2011). Totu et al. (Totu et al., 2017) discussed the benefits of employing TiO_2 with 3D printed acrylic resin in denture

bases, aiming to enhance the antifungal capabiliy of existing materials. As such, they pioneered the creation and investigation of a 3D-printed/TiO_2 nanocomposite material, enriched with superior properties for fabricating denture prostheses. This involved adding varying quantities of TiO_2 nanoparticles (0.2%, 0.4%, 0.6%, 1.0%, and 2.5%) to the 3D-printed resin. Fourier Transform Infrared Spectroscopy (FTIR) test results corroborated the successful interaction between the NPs and the polymer, particularly noticeable with the addition of 0.4 wt% TiO_2. The resultant 3D-printed/TiO_2 nanocomposite demonstrated potent antifungal properties, particularly against *Candida scotti*. Notably, the 3D-printed/TiO_2 nanocomposite completely inhibited the growth of Candida scotti, confirmed via the 2, 3, 5-Triphenyltetrazolium chloride (TTC) test. Additionally, the 3D-printed/TiO_2 nanocomposite exhibited remarkable antibacterial efficacy against *Staphylococcus aureus* and displayed no cytotoxic effects on human fibroblast cells.

Likewise, Chen et al. (Chen et al., 2019) assessed the antibacterial properties of 3D-printed/ TiO_2 nanocomposites and 3D-printed resin embedded with TiO_2/PEEK nanocomposites. The researchers tested the materials against *Staphylococcus aureus* and *Escherichia coli* strains, and both nanocomposites displayed robust antibacterial activity relative to the control group. A cytotoxicity evaluation using fibroblast cultures revealed an initial dip in survival rate, which was followed by a significant upturn in proliferation until day 7, with cell viability closely mirroring the control group. This suggests that the nanocomposite material exhibits commendable cytocompatibility and may potentially enhance cellular activities. Reinforcing this conclusion, cytocompatibility tests on dental pulp cells revealed superior survival rates in the groups containing TiO_2 compared to those without, underlining the cytocompatibility of TiO_2 nanoparticles.

Mengal et al (Mangal et al., 2020a) examined the resistance of a 3D-printed resin incorporating ND nanocomposite against *Streptococcus mutans* over a 48-hour period. Their findings revealed a statistically significant reduction in the biofilm formation of *Streptococcus mutans* in the nanocomposite material compared to the control group.

Liao et al (Liao et al., 2020) gauged the antibacterial efficacy of silver NPs added to 3D-printed resin, using *Streptococcus aureus* and *Escherichia coli* for their analysis. The P-6S-NP3 nanocomposite demonstrated superior antibacterial properties compared to both the unmodified 3D-printed resin and unmodified silver nanoparticle control groups, which exhibited no antibacterial effect. Interestingly, the nanocomposite material demonstrated a more potent antibacterial effect against *Escherichia coli* than *Streptococcus aureus*.

In a parallel study, Chen et al. (S. Chen et al., 2018) assessed the antibacterial impact of a 3D-printed/CNC-Ag composite material, using the same bacterial species over a 24-hour duration. They found a 50% reduction in bacterial concentration for both species with the addition of 0.05 wt% NPs compared to the control group (unmodified 3D-printed resin). For the other groups (0.1 – 0.25 wt%), the bacterial concentration dropped significantly for both species, implying an exceptional antibacterial effect. After 7 days, the nanocomposite material exhibited virtually no toxic effects on the L929 fibroblasts, comparable to the negative control group.

Aati. et al. (Aati et al., 2022b) studied the biocompatibility of the addition of Ag/MSN NPs into 3D-printed resin, as the ions release from the resin itself; in addition to the silver ion release was a concern. In general, all test specimens, including those with a 2.0 wt% content of Ag/MSN, exhibited cell viability exceeding 75%. Therefore, in accordance with ISO standard 10993-5 (BS EN ISO, 2009), it can be concluded that the modified 3D-printed resin is biocompatible and does not induce any significant cytotoxic effects. Moreover, they studied the effect of the nanoparticles on the growth and adhesion of *Candida albicans*, and they revealed that the Ag/MSN-modified 3D-printed resin has demonstrated a significant reduction in biofilm formation and adhesion, even after a 3-month aging period. This suggests that Ag/MSN nanoparticles has potential as an advanced antimicrobial material for long-term drug delivery and release.

Lastly, Khattar et. al. investigated the effect of incorporating ZrO_2 into 3D-printed resin. Their investigations revealed that the introduction of ZrO_2 nanoparticles was found to influence *Candida albicans* adhesion. Notably, the 0.5% ZrO_2 nanoparticles-infused 3D-printed resin group exhibited a significant reduction in *Candida. albicans* count when compared to both heat-polymerised PMMA and other 3D-printed resin groups. This decrease is likely attributable to the antibacterial properties of ZrO_2 nanoparticles, a characteristic established in prior research. The presence of specific ZrO_2 nanoparticles near *the Candida albicans* cell membrane on the resin's surface may contribute to its antifungal attributes. Nonetheless, elevated concentrations were associated with greater cell growth, possibly due to the clustering of ZrO_2 nanoparticles and the formation of clusters either within the resin matrix or on its surface. Conversely, the colony-forming unit (CFU) results indicated a minor reduction in *Candida albicans* adhesion with the incorporation of ZrO_2 NPs, but this reduction was not statistically significant.

Chapter 2: Aim and Objectives

2.1. AIM

The aim of this project was to create a nanocomposite acrylic resin material for 3D-printed denture base resin infused with varying concentrations of titanium dioxide nanoparticles (TiO_2 NPs) through characterisations of the material's mechanical, physical, and biological properties in comparison to both unmodified 3D-printed light cured resin and heat-cured PMMA denture base.

2.2. OBJECTIVES

1. To *investigate the effect of printing orientation and post-curing time* on the mechanical and physical properties of the unmodified 3D-printed denture base resin in terms of surface hardness, flexural strength, flexural modulus, sorption and solubility, and the degree of polymerisation.

2. To examine the *physical properties of the unmodified 3D-printed resin* using the established printing parameters in comparison to heat-cured PMMA including sorption and solubility, degree of conversion, and filler content.

3. To compare the *mechanical properties of the unmodified 3D-printed resin* using the established printing parameters to heat-cured PMMA including flexural strength, flexural modulus, impact strength, and surface hardness (Vickers and Martens) before and after hydrolytic aging in artificial saliva.

4. To characterise previously tested *mechanical and physical properties of the newly developed nanocomposite materials* with varying concentrations of TiO_2 NPs (0.1, 0.25, 0.50 and 0.75 wt.%) using the established printing parameters with and without hydrolytic aging in artificial saliva.

5. To assess the *biological properties of the new nanocomposite materials*, including its anti-fungal properties, cellular cytotoxicity, and cellular viability.

2.3. THESIS ORGANISATION

The organisation of the thesis is presented in Figure 2.1. The experimental chapters starting from Chapter 4 to Chapter 7, where the first three chapters deal with Introduction, Literature review and Aims and objectives.

To print a light cured resin, there are both controllable and uncontrollable parameters in the 3D printing and post-curing equipment. Uncontrollable settings include printer light wavelength and power, layer thickness, and post-curing light wavelength and power. Whereas, the controllable parameters involve printing orientation, post-curing time, and post-curing temperature. Therefore,

the controllable printing parameters must be optimised for a specific denture base resin material to achieve the most desired physical and mechanical properties. In the first part of the work (Chapter 4), printing orientation and post-curing time of NextDent resin material were optimised. Since the highest temperature was used in the post-curing set-up, hence the effects of the other two parameters on the printed sample were determined for subsequent use in fabricating TiO_2 nanoparticle (NP) reinforced NextDent resin. Flexural strength, flexural modulus, surface hardness, sorption and solubility, and degree of conversion were tested to identify the optimal printing orientation (0°, 45°, 90°) and optimal post-curing time (20, 30, 50 min).

After establishing these optimal settings, the NextDent specimens were printed to characterise the material's physical and mechanical properties (degree of conversion, sorption and solubility, surface hardness, flexural strength, flexural modulus, impact strength), comparing them with conventional heat-cured PMMA (control) and another 3D-printed denture base resin (Formlabs) in Chapter 5. The impact of hydrolytic aging in artificial saliva for three months on the properties of three materials was also evaluated. This can provide a baseline comparison between the two different 3D-printed denture base resins and the conventional denture base PMMA.

Subsequently, TiO_2 NPs were added to the NextDent 3D-printed material to create new nanocomposite materials at different concentrations (0.0, 0.10, 0.25, 0.50, 0.75 wt.%) using the established printing parameters (Chapter 4). The nanocomposites were characterised for the same mechanical and physical properties previously tested in Chapter 5 to find the suitable NPs concentration. Furthermore, hydrolytic ageing in artificial saliva was also conducted for three months and mechanical properties were characterised after ageing to ensure the suitability of the material in clinical set-up.

The newly developed denture base nanocomposites were also characterised for the biological properties (Chapter 7) such as cell cytotoxicity and cell viability in order ensure the new material is not posing any adverse effect on the human cells. TiO_2 NPs were added in the NextDent resin mainly due to their excellent antimicrobial activities, which have already been established by many previous studies. Therefore, the antifungal efficacy of the nanocomposites was evaluated against the popular oral microorganism *candida albicans.*

Finally, the conclusions are drawn in Chapter 8 with some future directions of the study.

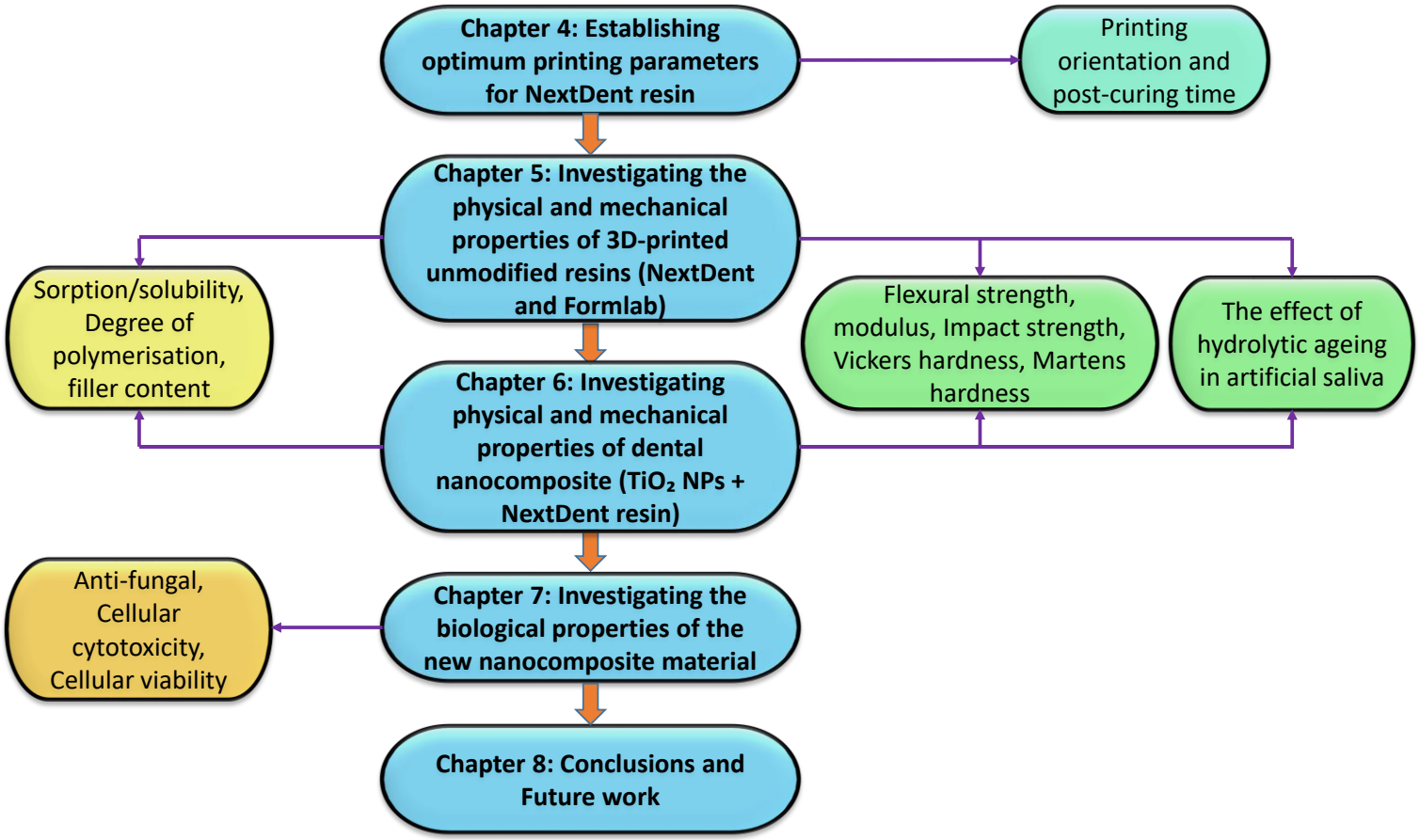

Figure 2.1. Presents details of chapters within the thesis

Chapter 3: Materials and Methods

3.1. INTRODUCTION

A variety of methods were utilised to accomplish the objectives of this project. Conventional methods were used to study the physical, mechanical, and biological characteristics. The strategies and methods implemented in each study are outlined in their respective chapters, though a more comprehensive explanation of the procedures is provided in this chapter.

3.2. RAW MATERIALS

The raw materials employed in this study to fulfil the research aims are specified in Table 3.1.

Table 3.1. Raw materials used in this research.

Material	Commercial name	Composition (wt.%)	Manufacturer
3D-printed denture base	Denture 3D+	- Ethoxylated bisphenol A dimethacrylate (≥75) - 7,7,9-trimethyl-4,13-dioxo-3,14-diazahexadecane-1,16-diyl bismethacrylate (10-20) - 2-hydroxyethyl methacrylate (5-10) - Silicon dioxide (5-10) - Titanium dioxide (<0.1)	NextDent, Soesterberg, Netherlands
3D-printed denture base	Digital denture	- Methacrylate monomer (40–60) - diurethane dimethacrylate (30–50) - propylidynetrimethyl trimethacrylate (5–10)	Formlabs, MA, USA
Heat-cured denture base	Pegasus Plus Denture Base	- Polymethylmethacrylate (>98)	Schottlander, Herts, England
Silanated Titanium dioxide nanoparticles	Silane-coated Titanium oxide nanoparticles	- Titanium dioxide nanoparticles, Rutile, Silane Coated (KH-550)(99.5)	Sky Spring Nano Materials, Inc., TX, USA

3.3. PREPARATION OF THE SPECIMENS

3.3.1. 3D-PRINTING AND POST-PRINTING PROCESSING

Formlabs Form 2 printer (Formlabs, Somerville, USA) that uses SLA technology with a 405 nm laser wavelength and 50 µm layer thickness, was equipped with a cartridge of liquid denture base resin. For any third party material, it had to be poured in the resin tray manually, and printed using the open mode system. Specimen designs were made using open source Tinkercad website and converted to STL format for compatibility with the printer's software. The software, Preform,

allowed the manipulation of the design's position whether vertical, horizontal, or at an angle. Automatic support structures were incorporated to sustain the specimen throughout the printing process. After printing, all specimens were taken off the build platform, stripped of support structures, and immersed in a Form Wash container (Formlabs, Somerville, USA) filled with 99.8% ethanol for 5 minutes for NextDent specimens, or 99.9% isopropyl alcohol (IPA) for 10 minutes for Formlabs specimens, to remove any surplus resin that was still on the surface of the specimen from the liquid resin pool without harming the printed components. The specimens were then air-dried for 10 minutes to remove any remaining alcohol. Lastly, to finalise the polymerisation process, the specimens were put in a UV light box (Formlabs, Somerville, USA), with a temperature setting of 60° C (NextDent) or 80° C (Formlabs), LED wavelength of 405 nm, and LED power of 39W. Figures 3.1 – 3.6 describe the process of specimens manufacturing using 3D-printing technology. Polishing of the specimens were undergone on the edges and faces of all specimens. The specimens were ground wet until smooth and flat using silicon carbide polishing papers at a grain size of approximately 30 µm (P500), 18 µm (P1000), and 15 µm (P1200).

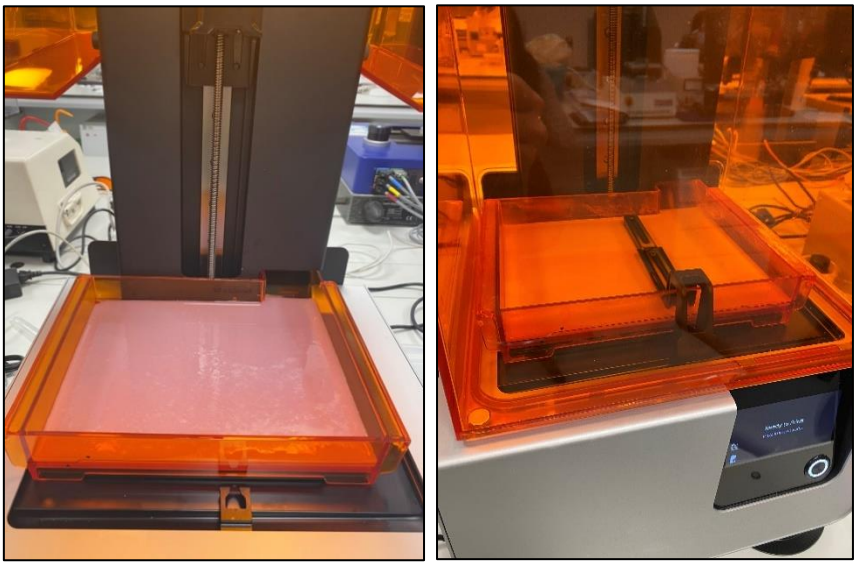

Figure 3.1. Resin material poured into the printer's resin tray

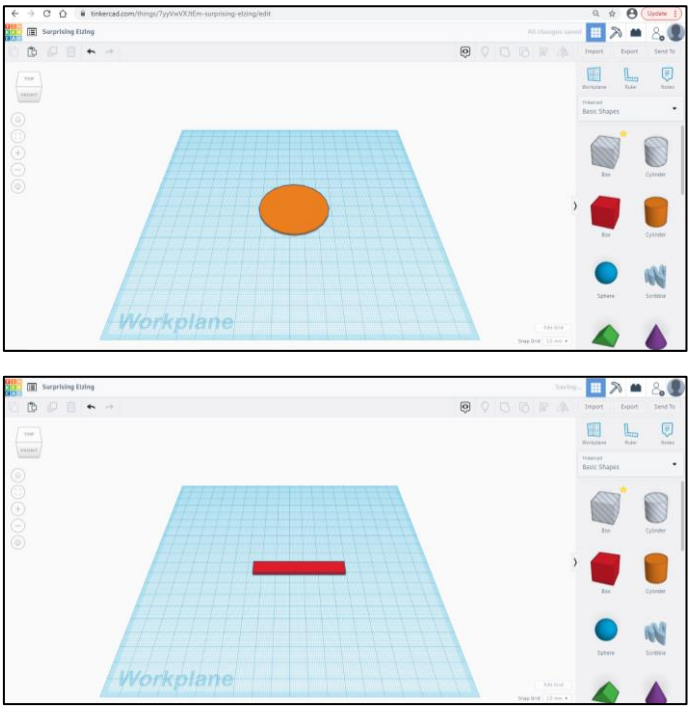

Figure 3.2. Designing the specimen in Tinkercad website

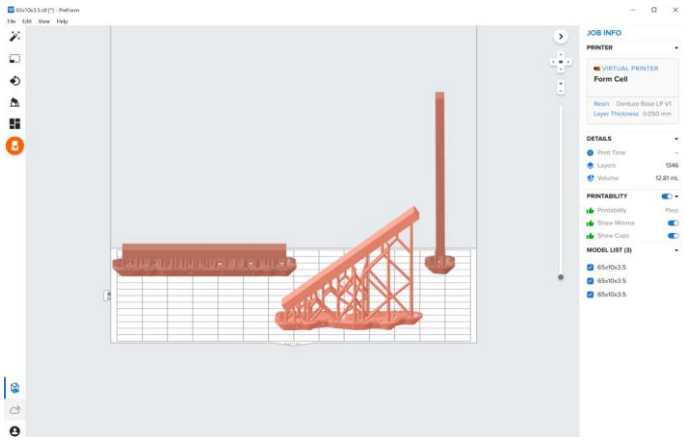

Figure 3.3. Manipulating the specimen via Preform software before printing

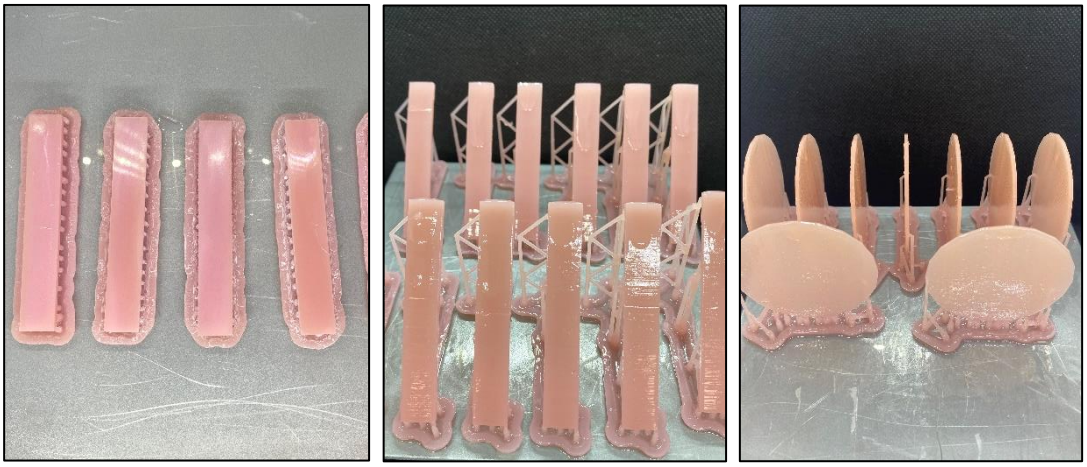

Figure 3.4. Specimens attached on the build platform after the printing process was finished.

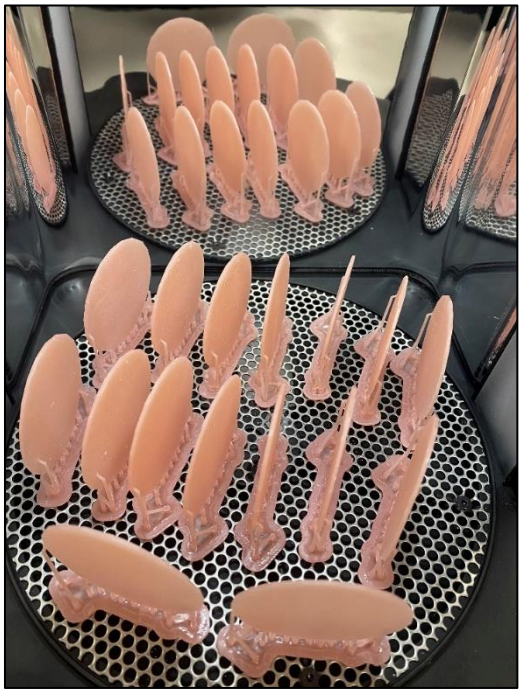

Figure 3.5. Specimen were placed in a UV light box for final polymerisation.

Figure 3.6. Polishing lapping machine

3.3.2. HEAT-CURED SPECIMENS

In line with the manufacturer's guidelines, the HC material's powder was blended into the liquid until a uniform mixture bearing a pliable, dough-like texture was achieved. This blend was then hand-loaded into a mould (Figure 3.7). Upon sealing the mould and situating it in a hydraulic press exerting a pressure of 15 MPa, surplus material was scraped off from the mould's periphery. The mould was subsequently submerged in a curing bath for a span of six hours to initiate polymerisation at a temperature of 80°C. Post this, it was taken out and permitted to gradually cool down for a half-hour at ambient temperature (23±1) prior to unsealing the mould to extract the specimens. A polishing machine (Interlab, Hull, UK) was thereafter utilised to trim, grind, and buff the specimens, employing pumice powder, emery paper, and a tungsten carbide bur.

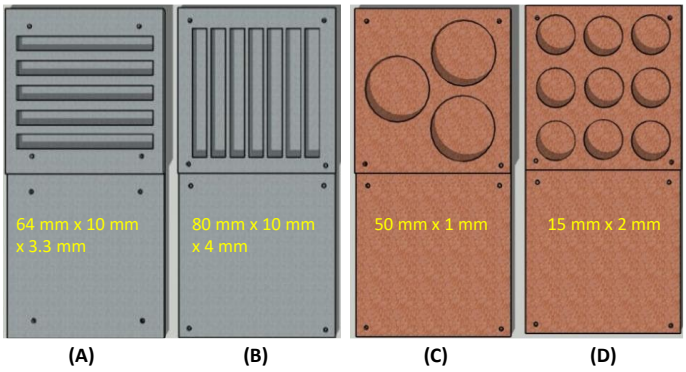

Figure 3.7. Design of four different moulds according to the type of tests undertaken, (A) flexural strength and modulus (B) impact strength (C) sorption and solubility (D) surface hardness.

3.4. CHARACTERISATION OF RAW MATERIALS

3.4.1. Characterisation of TiO_2 NPs and 3D-printed denture base resin

The dimensions and shape distribution of titanium dioxide nanoparticles (TiO_2 NPs) were assessed using a scanning electron microscope (SEM) (Carl Zeiss Ltd, 40 VP, Smart SEM, Cambridge, UK). SEM visualisation was carried out using a secondary electron detector at an acceleration voltage of 2.0 kV. An EDX analysis (Energy Dispersive X-ray) was employed to evaluate the elements present within the 3D-printed denture base resin and TiO_2 NPs powder. The filler particles were chosen at random and then loaded into the SEM/EDX for imaging, utilising the secondary electron detector at an acceleration voltage of 20.0 kV.

3.4.2. Assessment of silanised TiO_2 NPs

Fourier Transform Infrared spectroscopy (FTIR) was undertaken to identify the functional groups and the surface treatment within the TiO_2 NPs powder. The spectra were recorded within the wavelength range of 4000 to 400 cm^{-1} with a resolution of 4 cm^{-1}, averaging 32 scans using a Spotlight 200i FT-IR Microscope System (FTIR, Perkin-Elmer, Ohio, USA), all conducted at ambient temperature (23±1 °C). Figure 3.8 shows TiO_2 NPs that have undergone silane treatment on their surface, resulting in the development of hydrophobic properties in the NPs.

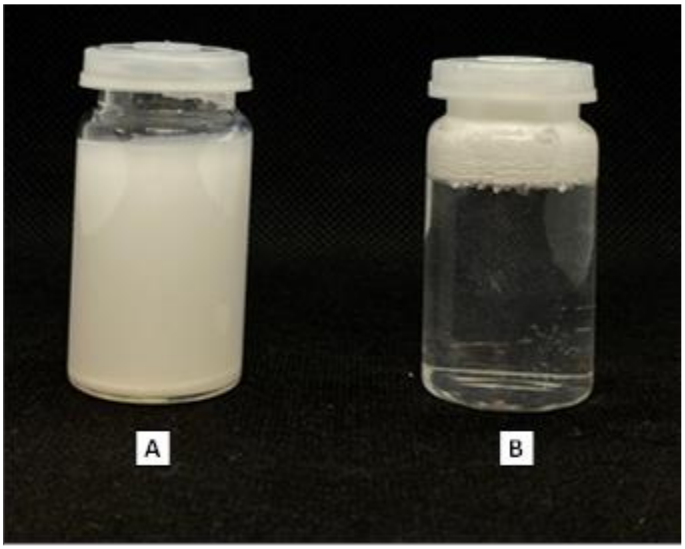

Figure 3.8. Photograph illustrating (a) non-treated TiO_2 NPs, (b) Silane treated TiO_2 NP

3.4.3. Selection of concentration of TiO_2 NPs with 3D-printed denture base resin-Pilot study

To ascertain the most fitting weight percentages of silanised TiO_2 NPs for this project, a pilot study was conducted with a various amounts of NPs concentrations that were based on previous studies from the literature (Totu et. al., 2017, Chen et. al., 2019). A 0.10, 0.25, 0.50, 0.75, 1.0, and 2.0 wt.% with 3D-printed denture base resin mixtures were used. The composition specifics of the specimen groups utilised in this pilot study are outlined in Table 3.2.

Thirty specimens of 3D-printed resin integrated with TiO_2 NPs at concentrations previously mentioned were created, with five specimens for each concentration as part of the pilot study to test flexural strength. The printing orientation was 0° and the post-curing time was 30 min. The dimensions of the specimens were fashioned to a standard size of 64 ± 1.0 mm × 10 ± 0.1 mm × 3.3 ± 0.1 mm. The flexural strength and modulus were analysed using a Zwick universal testing machine (Zwick/Roell Z020, Leominster, UK). The results of the pilot study measuring the flexural strength in the specimens are presented in Table 3.2.

Table 3.2. Weight percent of TiO_2 in combination with 3D-printed acrylic resin content of the specimen groups in the pilot study, with the mean (MPa) and standard deviation (SD) values of flexural strength and modulus for concentrations (0.0, 0.10, 0.25, 0.50, 0.75, 1.0, and 2.0 wt.% of TiO_2).

Composite material (3D printed liquid resin + TiO_2 NPs)	**3D printed liquid resin (g)**	**Added TiO_2 NPs (g)**	**Flexural strength (MPa) & SD**	**Flexural modulus (MPa) & SD**
0.0 wt.%	100.0	0.0	58.9 (6.6)	2571.0 (45.4)
0.10 wt.%	99.9	0.10	91.1 (8.5)	3139.6 (213.0)
0.25 wt.%	99.75	0.25	95.09 (8.6)	2858 (336.2)
0.50 wt.%	99.50	0.50	93.6 (6.4)	2765.1 (152.6)
0.75 wt.%	99.25	0.75	90.2 (13.5)	2728 (77.9)
1.00 wt.%	99.0	1.00	90.8 (10.1)	2995.0 (242.0)
2.00 wt.%	98.0	2.00	Failed to be printed	

Based on the findings from the pilot study, it was observed that the addition of 0.25 wt.% of TiO_2 NPs to the 3D-printed resin enhanced flexural strength the most. However, the addition of more than 0.50 wt.% NPs did not show any further enhancement, and the addition of 2.0 wt.% led to a failure in the printing process. Further, taking into account the data collected from relevant literature, a decision was made to utilise the following weight percentages to develop the new nanocomposite material: 0.0% (control), 0.10 wt.%, 0.25 wt.%, 0.50 wt.%, and 0.75 wt.%.

3.5. PREPARATION OF THE SPECIMENS

Within this project, the TiO_2 powder was weighed using an electronic scale (Ohaus Analytical plus, Ohaus Corporation, USA) accurate to 0.01 mg, based on the data presented in Table 3.2. To ensure a homogenous mixture devoid of any powder particle clustering, the TiO_2 NPs powder was gradually introduced into the liquid resin, followed by blending with a speed mixer operating at 2000 rpm for a duration of five minutes. Due to the elevated concentration of NPs, the 0.50 wt.% and 0.75wt.% groups necessitated two stages of mixing: initially, half the volume of powder was amalgamated with the liquid resin, followed by the addition of the remaining half. The composite material was subsequently poured into the tray of the 3D-printer to commence the printing process. Figure 3.9 illustrates the process of mixing TiO_2 NPs powder with 3D-printed liquid resin.

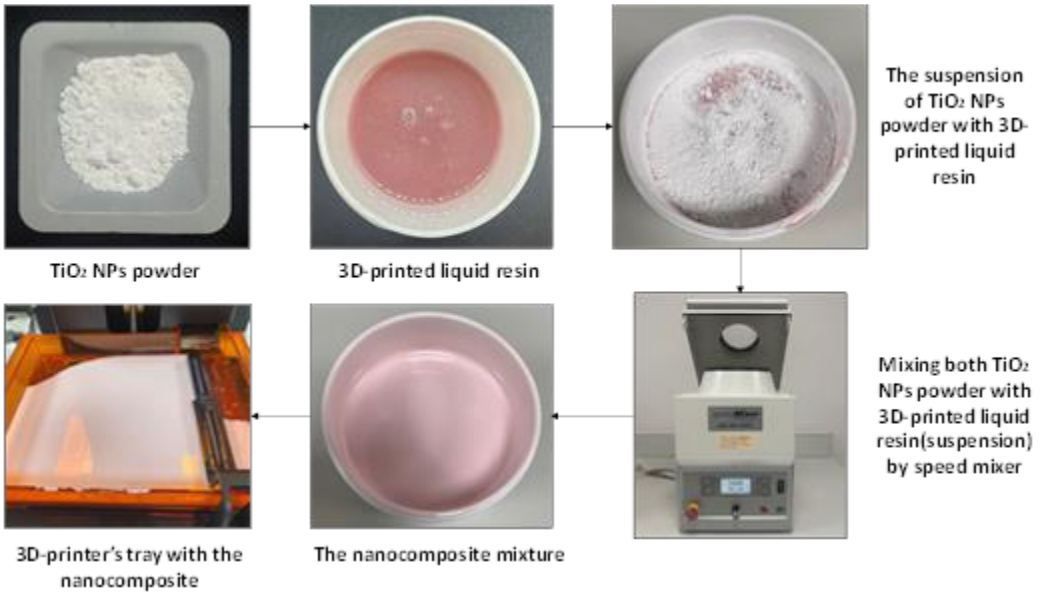

Figure 3.9. Stages of the mixing silanated TiO_2 NPs powder with 3D-printed denture base resin

3.6. ASSESSMENT OF PHYSICAL PROPERTIES

3.6.1. Filler content assessment

The proportions of inorganic elements in each category of resin material utilised in this research were gauged by removing the organic portion of the resin materials. The process was guided by the ISO standard 1172:2022 (BS EN ISO 1172, 2022), involving the application of the ash method. Three specimens (n=3) were subjected to heat in an electric furnace (Programat EP 5000; Ivoclar Vivadent, Liechtenstein, Austria) with temperatures oscillating between 470°C and 500°C over a quarter of an hour, and then left to cool in a desiccator. Subsequently, each specimen was weighed utilising an electronic balance (Ohaus Analytical Plus, Ohaus, USA) to a precision of 0.01 mg (Figure 3.10). The proportion of inorganic fillers was then computed using equation 3.1:

$$\text{Filler weight\%} = \frac{m_3 - m_1}{m_2 - m_1} \times 100 \qquad (3.1)$$

Where m_1 is the initial mass of the dry crucible without the specimen in grams, m_2 is the initial mass of the dry crucible plus the dried specimen in grams, m_3 is the final mass of the crucible plus the residues of the specimen after calcination in grams.

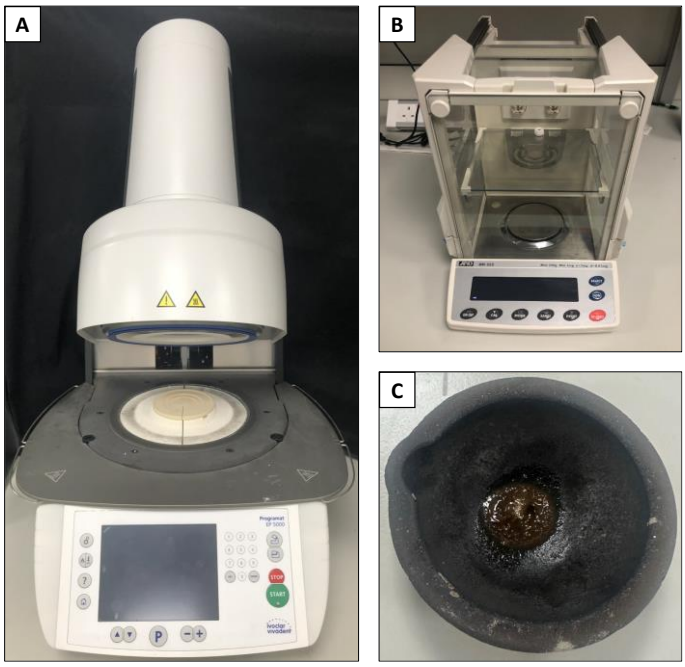

Figure 3.10. A representative figure showing (a) Programat EP 5000 electric furnace used for specimen heating, (b) Electronic balance used to measure the specimen's weight before and after burnout process, (c) 3D-printed denture base specimen after burnout process.

3.6.2. Fourier Transform Infra-red (FTIR) spectroscopy

FTIR spectroscopy was deployed to ascertain the degree of conversion (DC) of the resin materials used. Five specimens (n=5) were created for each group with dimensions of 15.0 ± 0.2 mm in diameter and 2.0 ± 0.2 mm in thickness for the examination. The Spotlight 200i FT-IR Microscope System in conjunction with the Spectrum Two was used to gauge the FTIR spectra, employing a wavelength scope from 4000 to 400 m^{-1} and a resolution of 4 cm^{-1} (Figure 3.11). The evaluation was conducted at ambient temperature (23±1 °C), averaging 32 scans. The apparatus was tuned using a background spectrum. The resin materials were scanned for baseline recording in their pre-polymerised state, and then rescanned following final polymerisation. The degree of conversion was calculated in percentage terms (Equation 3.2), by measuring the ratio of the double carbon bond peaks at two distinct frequencies (stretch of aliphatic frequency at 1637 cm^{-1} versus the reference aromatic frequency at 1608cm^{-1}). For heat-cured resin, the double carbon bond was measured at peak of 1637 cm^{-1}, and the referenced peak was measured at the ester bond (C=O) at 1720 cm^{-1} to calculate the DC (Equation 3.3).

$$\text{DC (\%)} = \left(1 - \left(\frac{\left(\frac{1637^{-1}}{1608^{-1}}\right) peak\ hights\ after\ polymerisation}{\left(\frac{1637^{-1}}{1608^{-1}}\right) peak\ hights\ before\ polymerisation}\right) \times 100 \right) \qquad (3.2)$$

$$DC\ (\%) = \left(1 - \left(\frac{\left(\frac{1637^{-1}}{1720^{-1}}\right) peak\ hights\ after\ polymerisation}{\left(\frac{1637^{-1}}{1720^{-1}}\right) peak\ hights\ before\ polymerisation}\right) \times 100 \right) \quad (3.3)$$

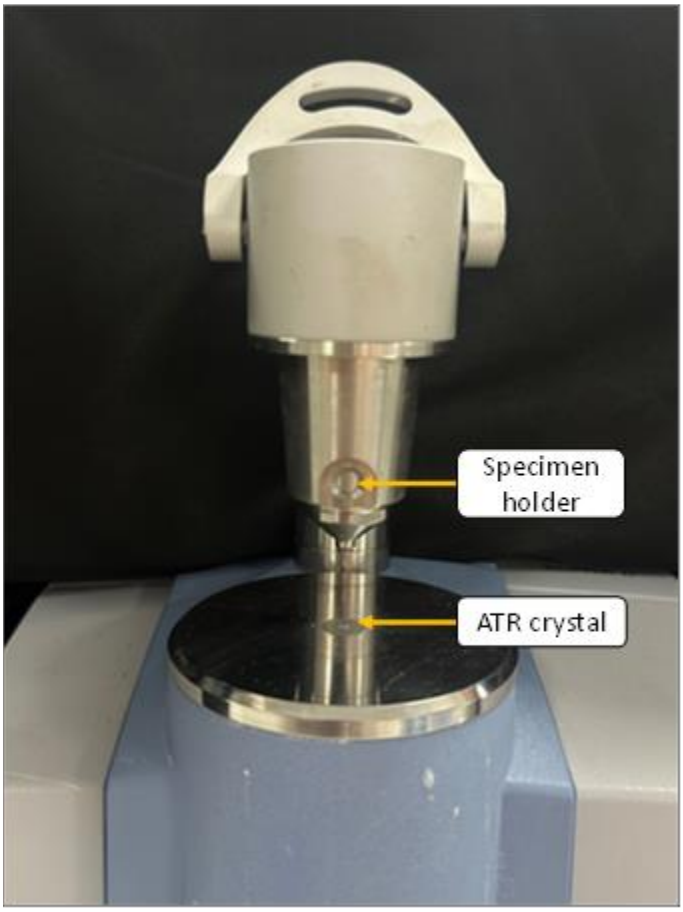

Figure 3.11. FTIR device used for DC measurement

3.6.3. Sorption and solubility

For water sorption and solubility tests, five specimens (n=5) were prepared with dimensions of 50 ± 1.0 mm in diameter and a thickness of 1.0 ± 0.1 mm per group following the EN ISO 20795-1-2013 standards (BS EN ISO 20795-1; 2013). These specimens were kept in a desiccator containing fresh silica gel, placed in an incubator at 37 ± 1 ℃ for 24 ± 1 hours, and then moved to another desiccator maintained at room temperature 23 ± 2 ℃ for 1 hour. Subsequently, the specimens were weighed with a precision of 0.2 mg (0.0002 g) using a calibrated electronic analytical balance (Ohaus Analytical Plus, Ohaus Corporation, USA). The weighing procedure was repeated until the weight loss of each specimen did not exceed 0.0002 g in any 24-hour period, ensuring a constant mass in the specimens. The final weight in grams was documented as m_1. The diameter of each specimen was measured thrice using an electronic digital calliper (Draper, Eastleigh, Hants, UK) to determine the mean values. The thickness measurements was taken at four evenly

spaced points around the circumference. The volume (V) of each specimen was calculated in cm^3 using the mean diameter and thickness. Subsequently, the specimens were immersed in artificial saliva (composition shown in Table 3.3) at a temperature of 37±2°C, with their weight measured daily after being removed from the solution and dried until the difference between consecutive weighings did not exceed 0.2 mg (m_2). The specimens were then reconditioned by storing them in a desiccator filled with freshly dried silica gel for a day at 37 ± 2°C, followed by another hour in a different desiccator at room temperature, also containing freshly dried silica gel. This desorption process was carried out daily until a stable, refurbished weight (m_3) was achieved, ensuring the variance between successive weighings did not surpass 0.2 mg. Figure 3.12 shows specimens immersed in artificial saliva during sorption process, and in silica gel during desorption process.

Utilising Equations (3.4) and (3.5), the sorption and solubility were calculated in g/mm^3. The volume of each specimen was ascertained using Equation (3.6). The percentage variations in weight and weight loss over the course of the sorption and solubility tests were identified using Equation (3.7).

$$\text{Sorption} = \frac{m2-m3}{V} \tag{3.4}$$

$$\text{Solubility} = \frac{m1-m3}{V} \tag{3.5}$$

$$\text{Volume} = 3.14 \text{ x } \left(\left(\frac{mean\ diameter}{2}\right)^2\right) \text{x } mean\ thickness \tag{3.6}$$

$$\text{Change in mass (\%)} = \left(\frac{mt-\ m1}{m1}\right) \text{x } 100 \tag{3.7}$$

Where m^t is the mass of the specimen at a certain time point

Table 3.3. Composition of artificial saliva (Williams et al., 2001)

Compound	**Amount (g/l)**	**Manufacturer**
Sodium chloride (NaCl)	0.400	Acros Organics
Potassium chloride (KCl)	0.400	Fisher Chemical
Calcium chloride (CaCl2)	0.795	Acros Organics
Sodium dihydrogen phosphate (NaH_2PO_4)	0.690	Alfa Aesa
Sodium sulphate hydrate ($Na_2S.9H_2O$)	0.005	Acros Organics

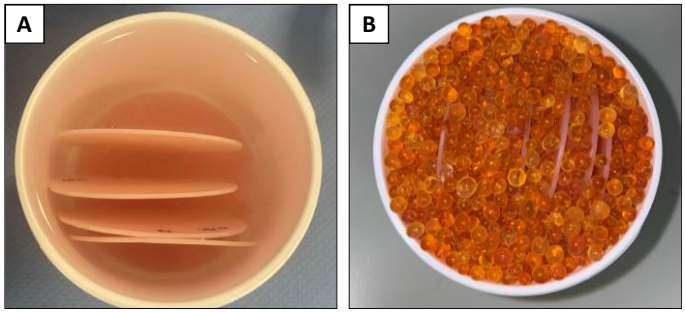

Figure 3.12. Specimens in (a) Artificial saliva during the sorption process, (b) Silica gel during the desorption process

3.6.4. Microscopes imaging

An optical microscope (Echo, Revolve, California, USA), with a ×10 magnification capability, was employed to explore the surface morphology of the polished specimen in greater detail. The fractured surfaces of the specimen, resulting from the flexural strength test, were scrutinised using an Energy Dispersive X-Ray Spectrometer-equipped scanning electron microscope (SEM-EDX, Carl Zeiss Ltd., 40 VP, Smart SEM, Cambridge, UK). The broken specimen was positioned in the SEM chamber after being mounted onto an aluminium stub and lightly overlaid with gold. Images at varying magnifications were created using a secondary electron detector at an acceleration voltage of 10.0 kV.

3.7. ASSESSMENT OF MECHANICAL PROPERTIES

3.7.1. Flexural strength and modulus

The flexural strength of the specimens tested was assessed utilising a three-point bend test on a universal testing machine (Zwick/Roell Z020, Leominster, UK) as exhibited in Figure 3.13.

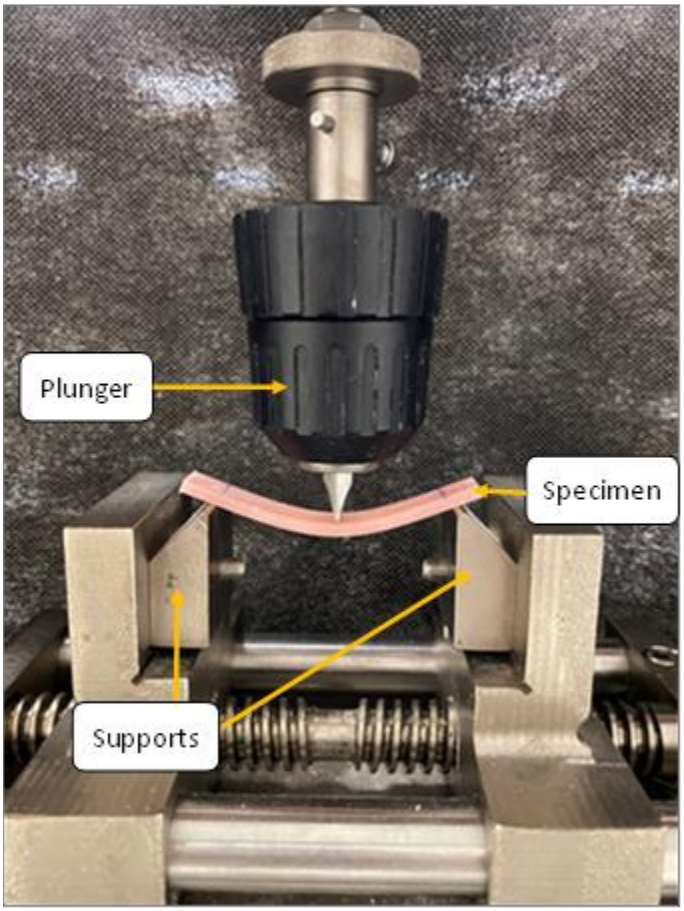

Figure 3.13. Arrangement of the Zwick universal testing apparatus and the specimen (64 mm x 10 mm x 3.3 mm), positioned between bending supports that are spaced 50 mm apart.

In alignment with the British International Standard for Denture Base Polymers (20795-1-2013), ten specimens (n=10) per group were shaped to measurements of 64 ± 1.0 mm length x 10 ± 0.01 mm width x 3.3 ± 0.01 mm thickness. All specimens were kept in distilled water at a temperature of 37 ± 1 °C for a duration of 50 ± 2 hours in an incubator prior to testing as a baseline measure. The specimens were subsequently withdrawn from the distilled water and placed onto a supporting rig. The loading plunger, with a diameter of 7.0 mm, was affixed at the midpoint of the specimen, equidistant between two supports that were parallel and 50 ± 0.1 mm apart. The diameter of the load supports was 3.20 mm. A 500 N load cell was employed to document force, with the load applied at a crosshead speed of 5 mm/minute. The maximum force (F) was recorded in newtons, and flexural strength was determined in MPa for each specimen, utilising Equation 3.8.

$$\sigma = \frac{3Fl}{2bh^2} \tag{3.8}$$

$$E = \frac{F_1 l^3}{4bh^3 d} \quad (3.9)$$

Where, 'F' represents the maximum exerted force in N, 'l' is the gap between the supports in mm, 'b' refers to the specimen's width in mm, and 'h' represents the height of the specimen in mm. To calculate the flexural modulus, Equation 3.9 was employed, in which 'd' is the deflection in mm at the F1 load, while 'F1' is the force in N at the point on the straight line (bearing the steepest slope) of the load/deflection graph.

3.7.2. Impact strength

The Charpy un-notch impact test was carried out utilising a universal pendulum impact testing device (Zwick/Roell Z020 Leominster), in accordance with EN ISO 179-1:2010 standards standards (BS EN ISO, 2010). Ten specimens (n=10) of dimensions 80 mm ± 0.5 in length, 10 mm ± 0.2 in width, and 4 ± 0.2 mm in thickness, were supported horizontally at both extremities (40 ±0.2 mm) and struck at the midpoint by a freely swinging pendulum equipped with a 4.0J load cell, released from a set height (Figure 3.14). The energy absorbed during the impact was documented in joules (J). The Charpy impact strength (a_{cU}) (kJ/m^2) was computed via Equation 3.10.

$$a_{cU} = \frac{W_B}{bh} \times 10^3 \quad (3.10)$$

Where W_B represents the energy at break in joules, and b and h are the specimen's width and thickness in mm, respectively.

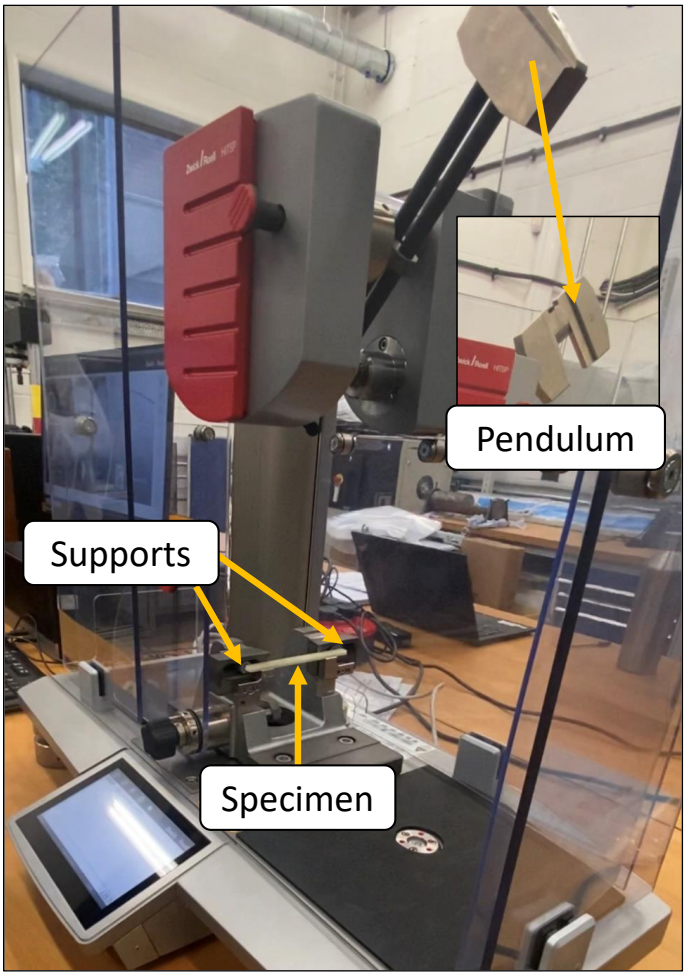

Figure 3.14. Arrangement of universal pendulum impact device and the specimen (80 mm x 10 mm x 4.0 mm) held at its peripheries before releasing the pendulum.

3.7.3. Surface hardness

In order to study the surface properties, two types of surface hardness measures, namely Vickers hardness and Martens hardness, were used. Vickers hardness test entails the use of a diamond indenter with a pyramid shape, which creates an indentation on the material under scrutiny at a designated test force (ranging from 1g to 100kg) for a specific period (referred to as the dwell time) (Figure 3.15). To calculate the Vickers hardness of the specimen, five discs (n=5) per group were prepared with a dimension of 15 mm in diameter and 2 mm in thickness. A Vickers micro-hardness testing machine (FM-700, Future Tech Corp, Tokyo, Japan) was deployed. A test load of 50 g was arranged, and each specimen was polished prior to forming three indentations along a linear path at equidistant points. The mean diagonal length of the indentations was quadrupled to work out the distance between each indentation site. With a dwell time of 30 seconds, the average hardness was established as the initial reading under dry conditions 24-hours after manufacturing.

9

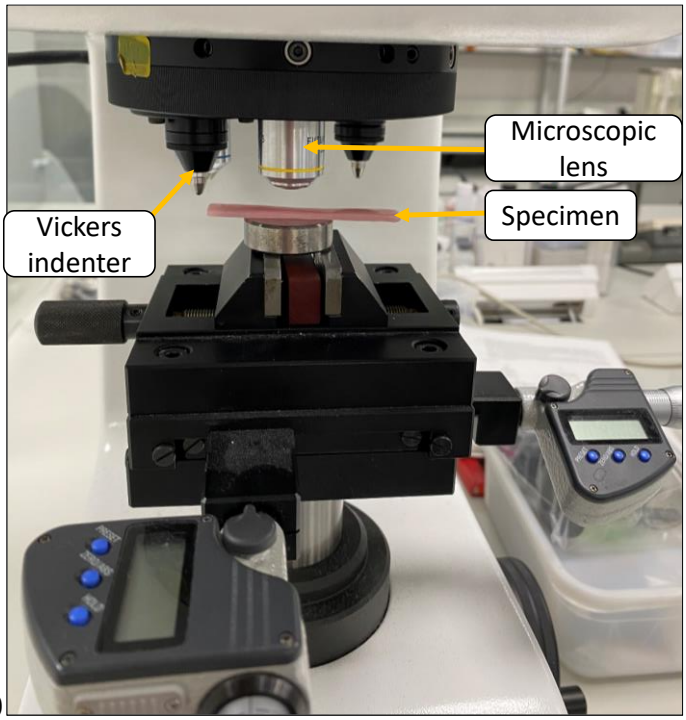

Figure 3.15. Vickers hardness testing device

A Martens Hardness Device (Z2.5, ZwickRoell Ltd., Leominster, UK) equipped with a Vickers hardness measurement indenter was employed to determine Martens hardness (Figure 3.16). Five discs (n=5) per group were prepared, and the dimensions were 15 mm in diameter and 2 mm in thickness. The top surface of the specimen and the hardness measuring head were maintained at a constant 18 mm separation at the commencement of each testing session. A 50 N force was applied at a rate of 5 N/s for 30 seconds prior to release. Before contact, the indenter tip was advancing at 40 mm/min with an initial approach speed of 100 mm/min. The distance between each specimen and the sensor tip was 40 µm. The test load and indentation depth were automatically documented during the loading and unloading of the Vickers indentation tip (136°) and displayed as load-displacement graphs. To prevent repeated measurements at the same location, the indentations were distributed along various lines on the surface of each specimen. The software (TestXpert®, Zwick GmbH & Co, Ulm, Germany) automatically extracted Martens hardness along with other parameters such as indentation modulus and indentation creep. The calculation of Martens hardness was based on Equations (3.11) from ISO 14577-4/2016 (BS EN ISO, 2016).

$$\text{Martens hardness} = \frac{F}{As\ (h)} = \frac{F}{26.43 * h^2} \tag{3.11}$$

Martens hardness was expressed in N/mm^2, where F is the load in N, As (h) is the indenter's surface area at a distance of h from the tip in mm^2, and As is the indenter's surface area in mm^2 (0.3).

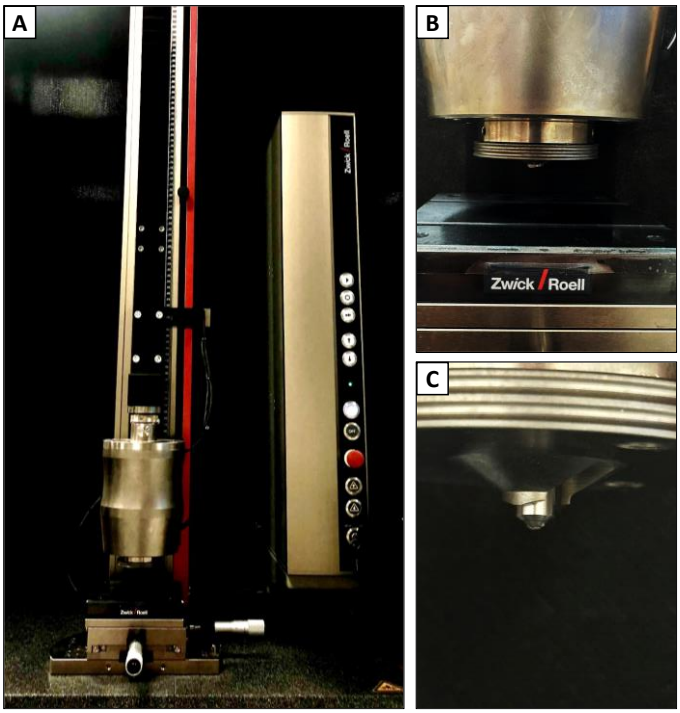

Figure 3.16. A representative figure showing (a) Micro-hardness testing instrument with, (b) Working table, (c) Diamond Vickers indenter.

3.8. ASSESSMENT OF THE BIOLOGICAL PROPERTIES

3.8.1. Specimen sterilisation

After 24 hours following the manufacturing of the specimens, they were individually placed into separate autoclavable bags. It was ensured that adequate space was provided within the bags for steam to circulate around the specimens effectively. Each bag, representing a different group of specimens, was then loaded into the autoclave machine. A sterilisation cycle was programmed to run at a temperature of 120°C and a pressure of 15 psi, and this was maintained for a duration of 30 minutes. After that, specimens were left to cool for 2 hours and stored in sterile glass containers.

3.8.2. Preparation of cell culture

A standard protocol for cell culture, maintenance, freezing, and thawing was adhered to, as per ISO 10993-5 (BS EN ISO, 2009), to culture commercially accessible primary human gingival fibroblast (HGF) cells (LCT-FC-0095, Catlag Medsystems Ltd, Buckingham, UK). HGF cells were cultured using a suitable growth medium (LCT-LL-0001, Catlag Medsystems Ltd, Buckingham, UK). Each component was at the following final concentration: L-glutamine at 7.5 mM, rh FGF basic at 5 ng/mL, rh insulin at 5 µg/mL, rh FGF/TGF beta at 5 ng/mL, ascorbic acid

at 50 µg/mL, and hydrocortisone hemisuccinate at 1 µg/mL. In addition, gentamicin was present at 30 µg/mL and amphotericin B at 15 ng/mL.

The cells were cultivated in a T75 flask and then housed in an incubator at 37°C with a mix of 5% CO_2 and 95% air. After 1 day, the old medium was extracted and the cells were rinsed twice with 5mL Hank's balanced salt solution (HBSS), followed by a medium replenishment. The cells were then passaged at regular intervals three days later, utilising 0.25% trypsin to detach the cells in the T75 flask, in accordance with their growth characteristics. Once the cells had reached confluence in the T75 flask, they were counted using a handheld automated cell counter (Specter 2.0, Merck, Darmstadt, Germany) (Figure 3.19). Then, they were moved and seeded into a 24-well culture plate at a density of 5×10^4 cells per well in 500 µl of complete growth medium. The sterilised specimens were situated in the centre of each well. Once the cells had attached to the base of each well, it indicates the commencement of the test, in line with ISO standard 10993-5. Figures 3.17 and 3.18 illustrate a 24-well plate with the distribution of the specimens.

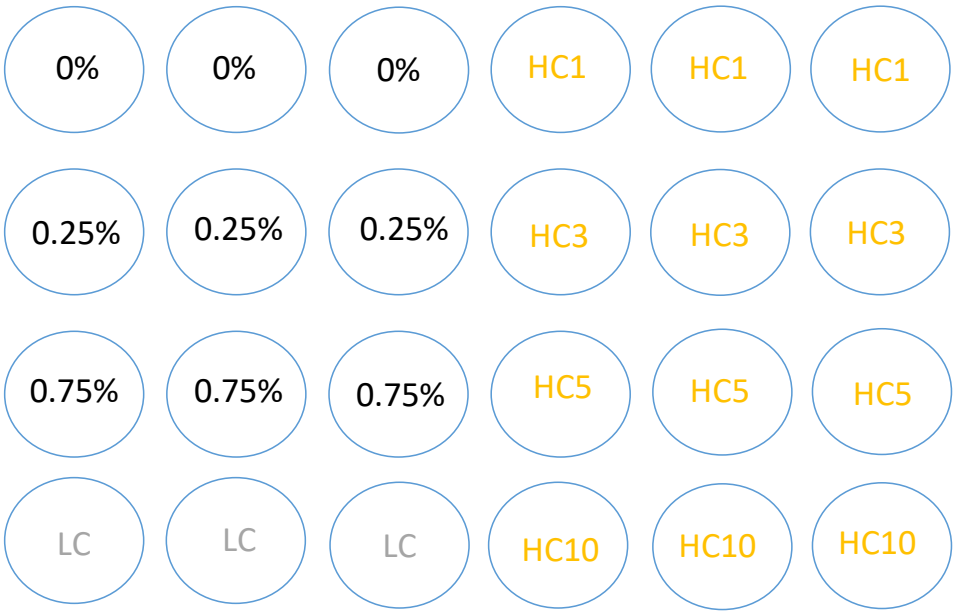

Figure 3.17. Diagram of 24-well plate set up, HC – high control; LC – low control; 0% – material with no TiO_2 NPs (control); 0.25% – nanocomposite material with 0.25 wt.% TiO_2 NPs; 0.75% – nanocomposite material with 0.75 wt.% TiO_2 NPs; BC – background allocated in another 24-well plate (only media and specimen); Nanocomposite material present in 0%, 0.25%, 0.75%, and BG.

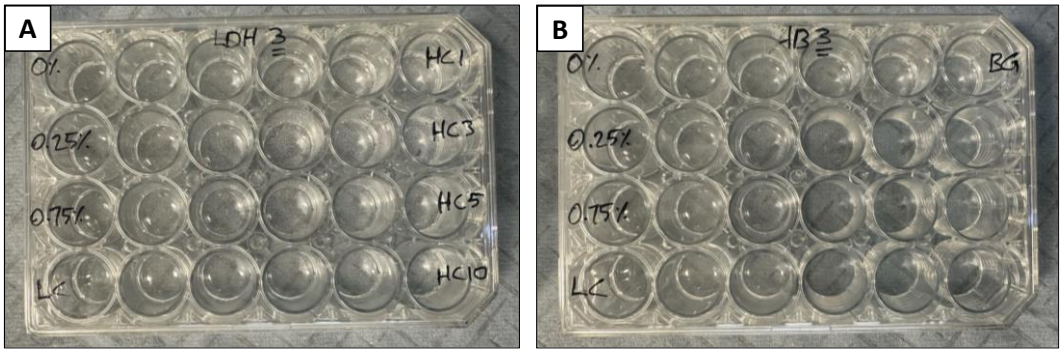

Figure 3.18. 24-well plate set up for (a) LDH experiment, (b) AB experiment

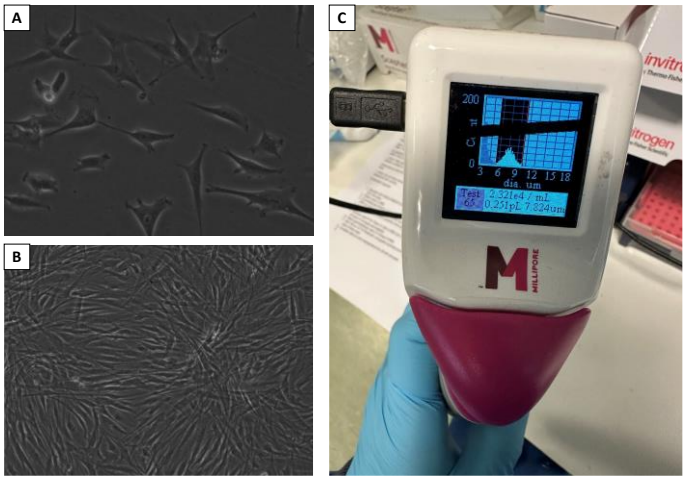

Figure 3.19. HGF at (a) 30% confluence, (b) 100% confluence, and (c) Specter handheld cell counter.

3.8.3. Cell viability

AlamarBlue™ cell viability agent (Thermo Fisher Scientific, IL, USA) was utilised to conduct a colorimetric test to gauge cell viability. For each test at each time point, three biological replica (one 24-well plate per replica) were used at four distinct intervals (1, 3, 5 and 10 days). In the study, three types of control wells were used. The first set, known as "Low Control" wells (LC), contained cells that were allowed to grow without the introduction of any specimen. These LC wells were used as a benchmark for maximum cell viability, and were assigned a value of 100%. The second set, known as "High Control" wells (HC), contained cells that were treated with a 10x lysis solution, causing complete cell destruction. These HC wells represent complete cell death, and were therefore assigned a viability value of 0%. The third set of control wells, referred to as "Background" wells (BG), were set up in a separate 24-well plate due to space constraints on the first plate. These BG wells contained only the media and the specimen but did not contain any cells.

At each interval, HGFs at each well of 0%, 0.25%, 0.75%, BG, and LC were subjected to 500 µL of AB (1:10) for 60 minutes at a temperature of 37°C. Following this, 100 µl of the supernatant was transferred to a 96-well plate in triplicates for evaluation at the time points of 1, 3, 5, and 10 days. A UVM 340 microplate reader (ASYS, scientific laboratory supplies) was used to read the 96-well plate at wavelengths of 570 and 600 nanometres. The morphology and proliferation of cells were captured using a light microscope at a magnification of x10 (Olympus IX51 fluorescence microscope). Cell viability was then calculated using Equation (3.12).

$$\text{Cell viability \%} = \frac{A570-(A600 \text{ x } Ro) for\ test\ well}{A570-(A600 \text{ x } Ro)\ positive\ growth\ control} \times 100 \quad (3.12)$$

Where A_{570} and A_{600} were absorbance at 570 and 600 nm respectively, and R_O was the correction factor calculated from (A_{570}/A_{600}) of the positive growth control.

3.8.4. Cell cytotoxicity

A Pierce™ Lactate dehydrogenase (LDH) cytotoxicity assay kit (Thermo Fisher Scientific, IL, USA) was utilised to test the cytotoxicity potential of the specimens under investigation. Each of the experiments at every time point was carried out with three biological replicas (24-well plate for each replica). For each of the four designated time points, a blend of 50 µl of the supernatant and 50 µl of the LDH cell reaction solutions were combined and left to incubate in a dark environment at room temperature for a duration of 30 minutes to assay HGF. Following this, an LDH stop solution was employed to halt the reaction. The cytotoxicity of the specimen was evaluated at four growth intervals: days 1, 3, 5, and 10. Controls were established following the manufacturer's guidance. The peak LDH release from the cells was assessed by introducing a membranolytic solution and was deemed the positive high control (HC), whilst the spontaneous LDH release (induced by water) was identified as the low control (LC). A UVM 340-microplate reader (ASYS, scientific laboratory supplies) was utilised to read the 96-well plate at 490 nm subtracted from 680 nm, with cytotoxicity then determined in accordance with Equation (3.13):

$$\text{Cytotoxicity \%} = \frac{Specimen\ treated\ LDH\ activity - Spontaneous\ LDH\ activity}{Maximum\ LDH\ activity - Spontaneous\ LDH\ activity} \times 100 \quad (3.13)$$

Where specimen-treated LDH activity is the LDH amount expressed by cells cultured with composite materials; maximum LDH activity is the LDH amount expressed by cells treated with membranolytic-solution; and spontaneous LDH activity is the LDH amount expressed by cells treated with water.

3.8.5. Anti-fungal test

In order to study the antifungal properties of the nanocomposite specimen, Candida albicans (ATCC 10231) was cultivated in Sabouraud dextrose (SD) broth at 37° C over a period of 24 hours. Following incubation, the Candida albicans suspension was regulated using a spectrophotometer at an optical density (OD) of 600 nm to 0.08 nm (according to the McFarland standard), before being diluted by a factor of 100 to ensure the number of microbial cells were calibrated to 1.5 x 10^6 cells per millilitre.

Discs of the nanocomposite material, with dimensions of 15 × 2 mm, were placed at the base of a 6-well plate, with each well representing a distinct group. Each well was then filled with 4 mL of the candidal suspension and left to incubate at 37° C for 24 hours. Post incubation, the specimens were cleansed twice with phosphate buffered saline (PBS) to remove any cells that hadn't adhered.

Next, the specimens in their 6-well plate were sealed and subjected to ultrasonication (USC200T, VWR, Malaysia) at a frequency of 40 kHz for a duration of 5 minutes in order to dislodge the fungal cells from the surface of the specimens (Figure 3.20). Following ultrasonication, the fungal solution underwent dilution in a 96-well plate, repeated six times by the addition of 20 µl of the fungal solution to 180 µl of PBS (a dilution factor of 10 for each repetition).

A quantity of 20 µl of the diluted fungal solution from each well was then sown into an SD agar plate in triplicates and incubated at 37° C for 24 hours. The colonies were subsequently counted and noted as colonies forming unit per millilitre (CFU/mL), using Equation 3.14 for calculation. For the antifungal tests, unlike the cytotoxicity tests, all groups underwent testing.

$$\text{CFU/mL} = \frac{Number\ of\ colonies \times Total\ dilution\ factor}{Volume\ of\ the\ culture\ plated\ in\ mL} \quad (3.14)$$

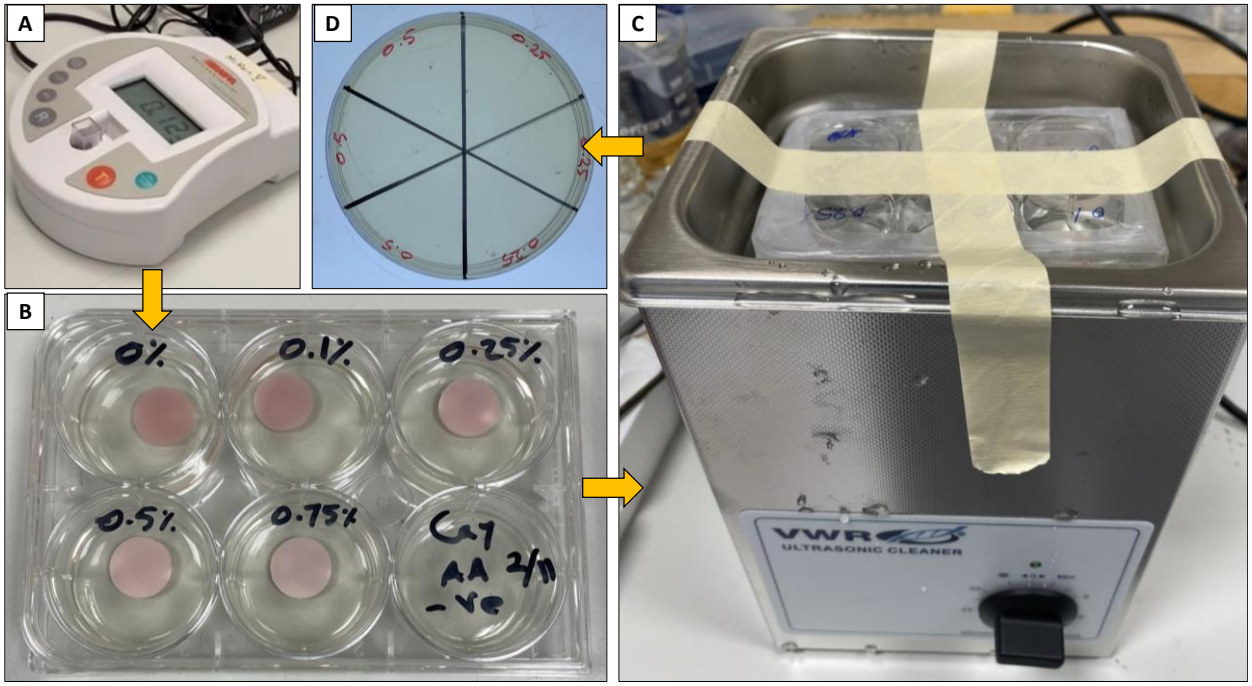

Figure 3.20. Sequence of figures that shows (A) Spectrophotometer to adjust the OD according to the McFarland standard, (B) 6-well plate with different specimens representing different nanocomposite group immersed in fungal suspension, (C) Ultrasonication of the specimens to detach fungal cells from specimens, (D) SDA plate to seed the fungal cells before incubation.

Chapter 4: Assessing the Physical and Mechanical Properties of 3D Printed Acrylic Material for Denture Base Application

Ahmed Altarazi, Julfikar Haider, Abdulaziz Alhotan, Nick Silikas, Hugh Devlin

doi.org/10.1016/j.dental.2022.09.006

4.1. ABSTRACT

Background: Three-dimensional (3D) printing is increasingly being utilised in the dental field because of its time-saving potential and cost effectiveness. It enables dental practitioners to eliminate several fabrication steps, achieve higher precision, and attain consistency in complex prosthetic models. The properties of 3D-printed resin materials can be affected by many factors, including the printing orientation (PO) and insufficient post-curing time (CT).

Purpose: This study aimed to investigate the effect of PO and CT on the mechanical and physical properties of a 3D-printed denture base resin (NextDent).

Materials and Methods: 3D-printed specimens were fabricated in 0°, 45°, and 90° POs, followed by three CTs (20, 30, and 50 min). The microhardness was tested using a Vickers hardness test, while the flexural property was evaluated using a three-point bending test. Sorption and solubility were measured after the specimens had been stored in an artificial saliva for 42 days, and the degree of conversion during polymerisation was analysed using Fourier Transform Infrared (FTIR) spectroscopy.

Results: The flexural strength of the material significantly increased *($p<0.05$)* when the printing orientation was changed from 0° to 90°. A similar increase was observed in the hardness, degree of conversion, and water sorption results. In general, no significant difference *($p>0.05$)* in any of the tested properties was found when the post-curing times were increased from 20 to 50 min.

Significance: The highest physical and mechanical properties of the 3D-printed denture base resin can be obtained by printing vertically (90° angle to the platform base with the denture bases printed on their sides to avoid midline fractures). The minimal post-curing time to achieve ideal results is 30 min, as further curing will have no significant effect on the properties of the material.

Keywords

Polymer resin; PMMA; Denture base; 3D-printing; Stereolithography

4.2. INTRODUCTION

The fabrication of denture was revolutionised by the introduction of clinical acrylic resin (Bilgin et al., 2015), a material based on polymethyl methacrylate (PMMA) that was first developed in 1936 (M. D. Murray and B. W. Darvell, 1993). Since 1948, 98% of the dentures have been fabricated from PMMA and copolymers (Tasaka et al., 2019), and PMMA has become the ideal material for the denture bases due to its good aesthetic characteristics, biocompatibility with oral tissues, light weightiness, low cost, and ease of processing and handling (Bilgin et al., 2015). However, it also poses some disadvantages that need to be addressed, such as dimensional inaccuracy, insufficient mechanical properties, including flexural and impact strength, and polymerisation shrinkage (Gad and Abualsaud, 2019).

Recent advances in technology have shown potential in changing the conventional denture fabrication practice. In particular, three-dimensional (3D) printing, which first appeared in 1983, is advancing rapidly. This is a computer-controlled digital manufacturing technique that employs 3D model data to create both simple and complex objects. Its operating principle can be represented as opposite to subtractive manufacturing and sometimes named as rapid prototyping or additive manufacturing (Bilgin et al., 2016; Ngo et al., 2018). 3D printing technology produces complex models using a layer by layer build-up principle (Palaganas et al., 2017). In addition, 3D printing has the capability to precisely print parts or products in a cost effective manner with less material waste (Berman, 2012).

More recently, several studies have reported 3D printing of photo-polymerised denture base resins with an aim to achieve similar mechanical properties of conventional PMMA (Aati et al., 2021b; Gad et al., 2021; Prpic et al., 2020). Various factors related to resin material composition and chemistry, printer type and its operating principle, and post-curing process can affect the properties of the printed product, and one of the most important factors is printing orientation (Tian et al., 2021b). Among the literature, there are different opinions regarding the effect of layer orientation on the mechanical properties of the printed object, where some authors claimed that the horizontal printing orientation (0°) along the build platform has the highest flexural strength compared to the vertical printing orientation (90°). Weaker bonds between successive layers compared to the bond forces within the layer itself was suggested as the possible cause (Alharbi et al., 2016; Letcher and Waytashek, 2014; Shim et al., 2020). Others claimed (Unkovskiy et al., 2018; Vayrynen et al., 2016) that a vertical layer orientation produced the highest flexural strength compared to the horizontal printing orientation, and they explained that there was no difference between the bond strength between successive layers and the bond within an individual layer itself.

Unlike the conventional heat-cured PMMA used for the denture base fabrication, 3D printed resin is a photo-polymerised material, and post-curing time is an essential process that affects the performance of the material. The curing process occurs partially during the printing via the printer's laser or light projector, and further curing is continued in a light cure unit as a post-curing step to complete the polymerisation process. One study reported that photo polymerised denture base material had superior mechanical properties compared to the conventionally polymerised counterparts (Hashem et al., 2014), but the study did not test any type of 3D printed denture base materials. With the emergence of different 3D printing techniques and photo-polymerised materials, the manufacturers advised varying amount of post-curing times (ranging from 20-60 mins) to complete polymerisation of the materials (FORMLABS, 2021; NextDent, 2022b). Some authors investigated the effect of post-curing times on the 3D printed resins, and they confirmed that it had a significant effect on the properties of the 3D printed resin (Aati et al., 2021b; Bonada et al., 2017; Jindal et al., 2020; Kim et al., 2020). However, the studies on the effect of post-curing time with different denture base resins are limited and hence demand further investigation. To the author's knowledge, no study has shown results on the effect of both printing orientation and post-curing time with 3D printed NextDent denture base resin.

In this study, the aim was to investigate the effect of changing post-curing time and printing orientation on the mechanical and physical properties of 3D printed denture base resin material in term of micro hardness, flexural strength and modulus, sorption and solubility, and the DC. The null hypothesis was that (1) the post-curing time and (2) different printing orientations do not affect the mechanical, chemical and physical properties of the 3D printed denture base resin.

4.3. MATERIALS AND METHODS

4.3.1. Resin material

The material used was commercial NextDent denture 3D+ light cured resin with light pink colour (3D systems, Soesterberg, Netherland) for denture base application. The properties for the NextDent material such as ultimate flexural strength (MPa), flexural modulus (MPa), sorption (µg/mm^3) and solubility (µg/mm^3) suggested by the material's manufacturer are 84, 2383, 28 and 0.1 respectively (NextDent, 2022b). According to the material's safety data sheet, the composition (w/w%) of the resin as follows: Ethoxylated bisphenol A dimethacrylate (=> 75); 7,7,9(or 7,9,9-trimethyl-4,13-dioxo-3,14-dioxa-5,12-diazahexadecane-1,16-diyl bismethacrylate (10-20); 2-hydroxyethyl methacrylate (5-10); Silicon dioxide (5-10); diphenyl(2,4,6-trimethylbenzoyl)phosphine oxide (1-5) and Titanium titanium dioxide (<0.1).

4.3.2. 3D printing and post processing

Liquid resin was poured into the resin tank of the Formlabs Form 2 printer (Formlabs, Somerville, USA), which worked based on uses SLA technology with 405 nm laser wavelength and a layer thickness 50 µm layers. After designing test specimens by using an open source CAD software (Tinkercad) the final design was exported in STL format to be compatible for use with the printer's software. Preform software was used to open the STL file and to manipulate the CAD design with vertical (90^o), horizontal (0^o), or any angular positions. Support structures were printed automatically to support the specimen during printing of the specimens. Once printing was finished, all specimens were removed from the build platform, cleaned by eliminating support structures and submerged in a container (Form Wash) filled with ethanol 99.8% (Formlabs, Somerville, USA) for 5 minutes to get rid of any excess resin without damaging the printed parts. Then, the specimens were left out to dry from any ethanol residues for 10 minutes. After cleaning and drying, specimens were placed in an ultraviolet (UV) light box (Formlabs, Somerville, USA) under at a temperature of 60° C, 405 nm LED wavelength and 39W LED power to complete the polymerisation process.

4.3.3. Specimen grouping

The literature suggested that the properties of the 3D printed resins could vary with the printing orientation (PO) and length of the curing time (CT) after printing (Aati et al., 2021b; Bonada et al., 2017; Jindal et al., 2020; Shim et al., 2020; Unkovskiy et al., 2018). Therefore, in this study, all the specimens were divided into nine groups based on the three POs and three CTs (0^o/20, 45^o/20, 90^o/20, 0^o/30, 45^o/30, 90^o/30, 0^o/50, 45^o/50, 90^o/50). A total of 147 specimens were prepared with different dimensions and group sizes required for testing different physical and mechanical properties (Table 4.1). 0^o/30 was considered as the control group, based on the manufacturer's recommendation of curing time and shortest printing time.

Table 4.1 Determination of sample number with different testing conditions

Tests	Printing Orientations (degree)	Curing time (min)	Total number of specimens	Specimen dimension
Flexural strength/Flexural modulus	0º, 45º and 90º	20, 30 and 50	*3×ǂ3×§10 = 90 (n=10)	65×10×3.3 mm^3
Hardness			3×3×3 = 27 (n=3)	15 mm dia×2 mm thick
Sorption and solubility		30	3×1×5 = 15 (n=5)	50 mm dia×0.5 mm thick
DC			3×1×5 = 15 (n=5)	2 mm dia × 2 mm thick

**3 (number of printing orientations) × ǂ3 (curing times) ×§10 (group size)*

4.3.4. Characterisation of 3D printed specimens

The Vickers hardness of the specimens was measured using a micro hardness testing machine (FM-700, Future Tech Corp, Tokyo, Japan). The test load was set to 50 g with a dwell time of 30 sec. For each specimen, three indentations were made at different equidistant points in a straight line after polishing the surface. The distance between the points was calculated by multiplying the average indentation's diagonal length by four. The mean hardness were recorded under dry conditions (at 23°C) (Alamoush et al., 2018; A. P. Farina et al., 2012) 24 hours after printing.

The flexural strength of the specimens was evaluated using a 3-point bending test in a universal testing machine (Zwick/Roell Z020 Leominster, UK) with a load cell of 500 N (Chhabra et al., 2022; Gad et al., 2021; Prpic et al., 2020). Figure 4.1 shows different layer orientations with respect to the direction of applied load during the testing. According to the BS EN ISO 20795-1:2013 standard for Denture Base Polymers, the dimension of the specimen was 64 mm (length) × 10.0 ± 0.2 mm (width) × 3.3 ± 0.2 mm (thickness). Before testing, the edges and faces of all specimens were ground wet until smooth and flat using silicon carbide polishing papers at a grain size of approximately 30 µm (P500), 18 µm (P1000), and 15 µm (P1200). They were used sequentially resulting in the required width and height of the specimen. A digital calliper (Draper, Eastleigh, Hants, UK) was used to measure the specimens' height and width at the middle and at each end to an accuracy of ±0.01 mm. The specimens were stored in distilled water in an incubator at a temperature of 37 ± 1 °C for 50 ± 2 h. After that, each specimen was placed over a supporting jig separated by 50 ± 0.1 mm. The two polished cylindrical supports were 3.2 mm in diameter, and at least 10.5 mm long. The crosshead preload speed and the test speed were set to 5 mm/min. Equation 4.1 and 4.2 were used to calculate the flexural strength and flexural modulus respectively.

$$\sigma = \frac{3Fl}{2bh^2} \tag{4.1}$$

Where F is the maximum force applied in Newton, l is the distance between the supports in mm, b is the width of the specimen in mm, h is the height of the specimen in mm. The flexural modulus was determined from the slope of the linear portion of the stress strain curve for each test run.

$$E = \frac{F_1 l^3}{4bh^3 d} \tag{4.2}$$

Where F_1 is the load, in newtons, at a point in the straight line (with the maximum slope) of the load/deflection curve, b is the width of the specimen in mm, h is the height of the specimen in mm, d is the deflection in millimetre at load of F_1.

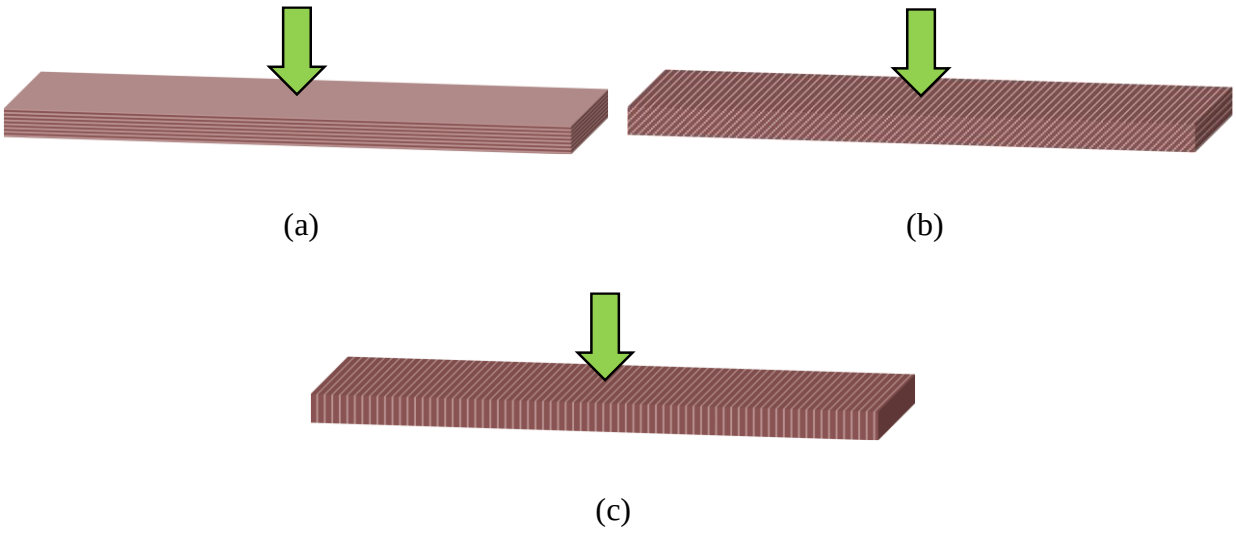

Figure 4.1. Direction of the force on the specimen surface during flexural strength test with respect to the layer orientations: (a) horizontal (0°), (b) angled (45°), and (c) vertical (90°)

Fourier Transform Infrared spectroscopic (FTIR) was used to determine the DC of the 3D printed specimen using a Spotlight 200i FT-IR Microscope System with Spectrum Two (ALPHA II, Bruker, Massachusetts, USA). The parameters used to measure the FTIR spectra were a wavelength ranging from 4000 to 400 cm^{-1}, and a resolution of 4 cm^{-1} with an average of 32 scans at room temperature. A background spectrum was generated to calibrate the instrument. The 3D printed resin material was scanned in its liquid form as a baseline record, and then scanned again after the final polymerisation (after post-curing). To calculate the DC in percentage (Equation 4.3), the difference in the double carbon bond peaks ratio at two frequencies (stretch of aliphatic frequency at 1637cm^{-1} against the reference aromatic frequency at 1608 cm^{-1}) was measured (Algamaiah et al., 2020).

$$DC\ (\%) = \left(1 - \left(\frac{\left(\frac{1637cm^{-1}}{1608cm^{-1}}\right) peak\ hights\ after\ polymerization}{\left(\frac{1637cm^{-1}}{1608cm^{1}}\right) peak\ hights\ before\ polymerization}\right)\right) \times 100 \quad (4.3)$$

Water sorption was carried out according to the BS EN ISO 20795-1:2013 standard for Denture Base Polymers. Five specimens used for each test group. Specimens were placed in a desiccator containing fresh dry silica gel at 37 ± 2°C for 1 day, and then moved to room temperature in a second desiccator containing freshly dried silica gel for 1 h to be weighed. This process was repeated every day until the change between each successive weighing was not greater than 0.2 mg to gain the baseline mass (m_1). The volume (V) of each specimen was calculated by measuring the diameter and thickness using a digital calliper (Draper, Eastleigh, Hants, UK). Then, the specimens were immersed in artificial saliva at 37 ± 2°C. Each specimen was dried after removal from the artificial saliva and continued re-weighing until the change between each successive weighing was not greater than 0.2 mg to achieve a constant mass (m_2). Subsequently, the specimens were reconditioned by placing them in a desiccator containing fresh dry silica gel at 37 ± 2°C for 1 day, and then moved to room temperature in a second desiccator containing freshly dried silica gel for 1 h. The desorption process was carried out by continuing re-weighing until the change between each successive weighing was not greater than 0.2 mg to achieve a constant mass (m_3, reconditioned mass). Finally, the sorption and solubility in µg/mm³ were measured using Equation 4.4 and Equation 4.5 respectively (Akin et al., 2015).

$$Sorption = \frac{m2 - m3}{v} \quad (4.4)$$

$$Solubility = \frac{m1 - m3}{v} \quad (4.5)$$

The volume of each specimen was calculated using Equation 4.6.

$$Volume = 3.14 \times \left(\left(\frac{mean\ diameter}{2}\right)^2\right) \times mean\ thickness \quad (4.6)$$

The percentage of mass change and mass loss during the sorption and solubility test were calculated using Equation 4.7 and Equation 4.8 respectively.

$$Change\ in\ mass, SP(\%) = \left(\frac{m2 - m1}{m1}\right) \times 100 \quad (4.7)$$

$$Mass\ loss, SL(\%) = \left(\frac{m1 - m3}{m1}\right) \times 100 \quad (4.8)$$

The surface morphology of the as printed and polished specimens was studied using an optical microscope (Echo, Revolve, California, USA) with a magnification of ×10. The fractured surfaces of the specimens from the flexural strength test were studied using a scanning electron microscope

equipped with an Energy Dispersive X-Ray Spectrometer (SEM-EDX, Carl Zeiss Ltd., 40 VP, Smart SEM, Cambridge, UK). The fractured specimen was mounted onto an aluminium stub and coated with a thin gold layer before it was loaded into the SEM chamber. The images were created using secondary electron detector at an acceleration voltage of 10.0 kV at various magnifications.

4.3.5. Statistical analysis

All data were statistically analysed using SPSS version 22 (IBM, New York, NY, USA). The normality of data distribution was determined using Shapiro-Wilk test, and the homogeneity of the data was confirmed by Levene test. The data were statistically compared using two-ways ANOVA for the mechanical tests (Vickers hardness, flexural strength and modulus), followed by Tukey's post-hoc statistical analysis according to a significance level set at $p \leq 0.05$. One-way ANOVA was used for the other tests (DC, sorption and solubility) as there was only one variance (layer orientation).

4.4. RESULTS

4.4.1. Mechanical properties

Table 4.2 presents the mean hardness and the standard deviation for all three curing times and printing layer orientations. The results indicated no statistical difference between the mean values ($p>0.05$) of the groups with different POs at a particular CT except for the samples prepared at 0° layer orientation and 20 min curing time (0°/20 min), which showed significantly lower values compared to the other groups ($p<0.001$). On the other hand, the results did not show any statistical difference between the mean values ($p>0.05$) of the groups with different CTs at a particular PO except for the 0°/20 min group, which showed significantly lower values compared to the other groups ($p<0.05$).

Table 4.2 Hardness of 3D printed resin at different curing times and printing orientations

Curing time (CT)	**Printing orientation (PO)**		
	0°(*)	**45°**	**90°**
	Vickers Hardness (VHN)		
20 min	10.74 (0.88) ^{Ab}	13.31 (0.20) ^{Ba}	14.08 (0.41) ^{Ba}
30 min (**)	12.99 (1.13) ^{Aa}	14.10 (0.12) ^{Aa}	14.63 (0.86) ^{Aa}
50 min	12.83 (1.04) ^{Aa}	14.14 (0.43) ^{Aa}	14.04 (0.46) ^{Aa}

**Within a row, cells having similar (upper case) letters are not significantly different from the control (0° layer orientation). **Within a column, cells having similar (lower case) letters are not significantly different from the control (30 min curing time)*

The means and the standard deviations of flexural strength for the groups were recorded and presented in Table 4.3. Two-way ANOVA of the flexural strength results indicated a statistical difference between the mean values ($p<0.001$) of the groups and the Games-Howell's test showed a significant difference between the 0° PO group and the other two PO groups for each particular CTs ($p<0.001$), but no significant difference was found between the 45° and the 90° PO groups. On the other hand, no statistical difference between the mean values ($p>0.05$) of the groups with different CTs at a particular PO was found.

Table 4.3 Flexural strength of 3D printed resin at different curing times and printing orientations

Curing time	Printing orientation		
	0°(*)	45°	90°
	Flexural strength (MPa)		
20 min	55.3 (6.3) ^{Aa}	80.6 (2.8) ^{Ba}	88.9 (2.7) ^{Ba}
30 min (**)	58.9 (6.6) ^{Aa}	86.1 (2.1) ^{Ba}	88.4 (1.6) ^{Ba}
50 min	59.9 (5.5) ^{Aa}	81.5 (3.5) ^{Ba}	88.5 (2.8) ^{Ba}

**Within a row, cells having similar (upper case) letters are not significantly different from the control (0º layer orientation). **Within a column, cells having similar (lower case) letters are not significantly different from the control (30 min curing time)*

The means and the standard deviations of flexural modulus for the groups were recorded and presented in Table 4.4. Two-way ANOVA showed a statistical difference between the groups' mean values ($p<0.001$). Games-Howell's test showed that at 30 min CT, 90° PO group was significantly different from the other two PO groups ($p<0.001$), where there was no statistical difference between the 0° and 45° PO groups. On the other hand, at 50 min CT, 0° PO group was significantly different from the other two PO groups ($p<0.001$), where there was no statistical difference between the 45° and 90° PO groups. At 45º PO, 30 min CT group showed statistically significant difference compared to the other two CT groups ($p<0.001$), with no statistical difference between the 20 min and 50 min CT groups.

Table 4.4. Flexural modulus of 3D printed resin at different curing times and printing orientations

Curing time	Printing orientation		
	0°(*)	45°	90°
	Flexural modulus (MPa)		
20 min	2466.5 (97.8) ^{Aa}	2416.8 (70.6) ^{Ab}	2385.3 (16.5) ^{Aa}
30 min (**)	2571.0 (45.4) ^{Aa}	2610.9 (107.8) ^{Aa}	2380.3 (66.8) ^{Ba}
50 min	2554.3 (97.0) ^{Aa}	2386.3 (110.9) ^{Bb}	2374.2 (88.5) ^{Ba}

**Within a row, cells having similar (upper case) letters are not significantly different from the control (0º layer orientation). **Within a column, cells having similar (lower case) letters are not significantly different from the control (30 min curing time)*

Figure 4.2 shows graphical representations of the results on the mechanical properties at different CTs and POs.

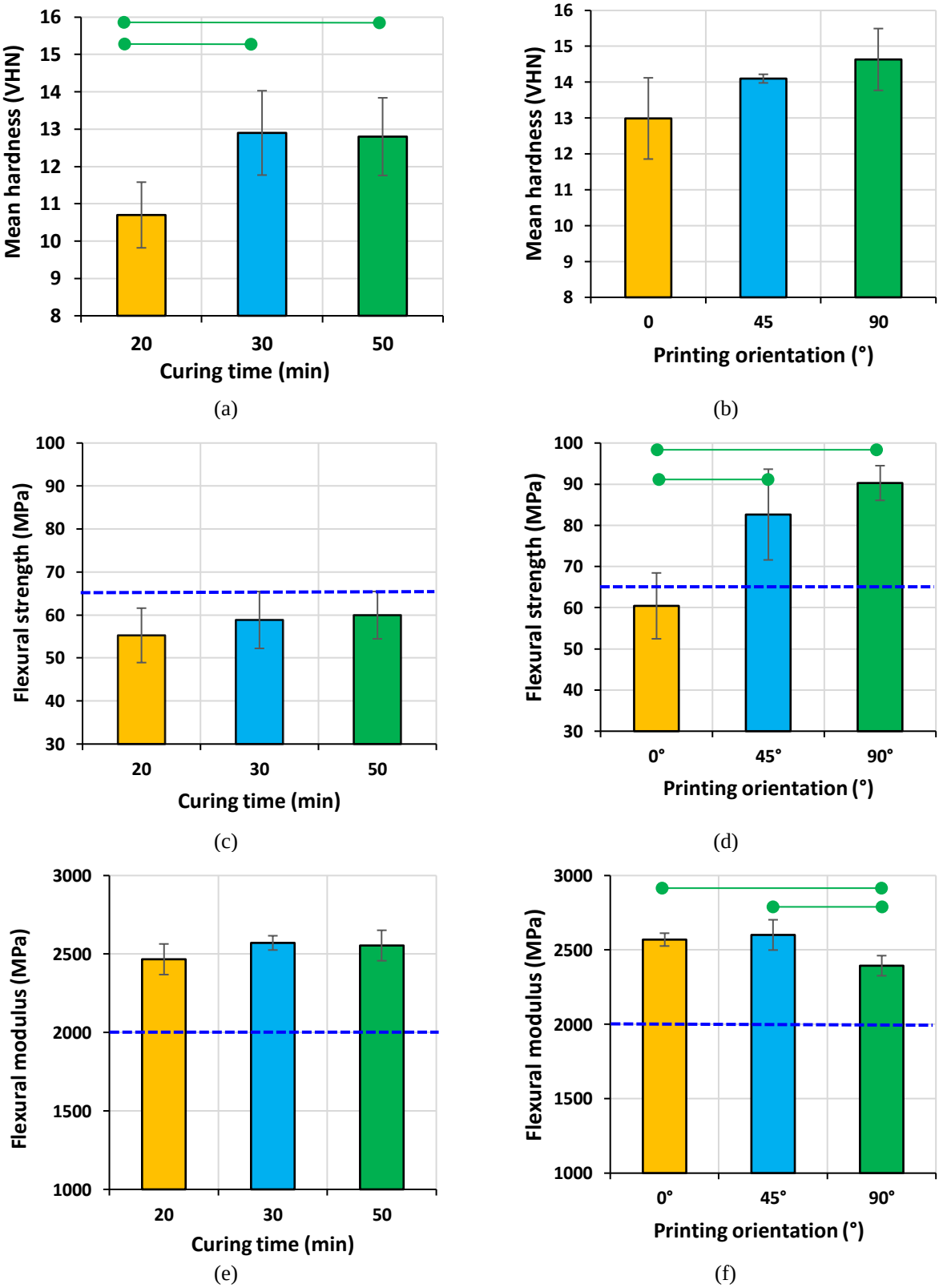

Figure 4.2. The effect of curing times and layer orientations on (a, b) Vickers hardness, (b, c) flexural strength, and (d, e) flexural modulus of 3D printed resin. Horizontal solid lines (green) joining two points indicate statistically significant difference. Horizontal dotted lines (blue) indicate minimum requirements for denture base

Horizontal dotted lines (blue) indicate minimum ISO requirements for denture base applications.

4.4.2. Degree of conversion (DC) analysis

FTIR analysis was performed to assess the DC of the 3D printed resin and to reveal any difference between different the layer orientations and curing times. Figure 4.5 shows a typical FTIR spectra of the specimen and the peak heights at the wave number of 1637 cm^{-1} and 1608 cm^{-1} was used to calculate the DC.

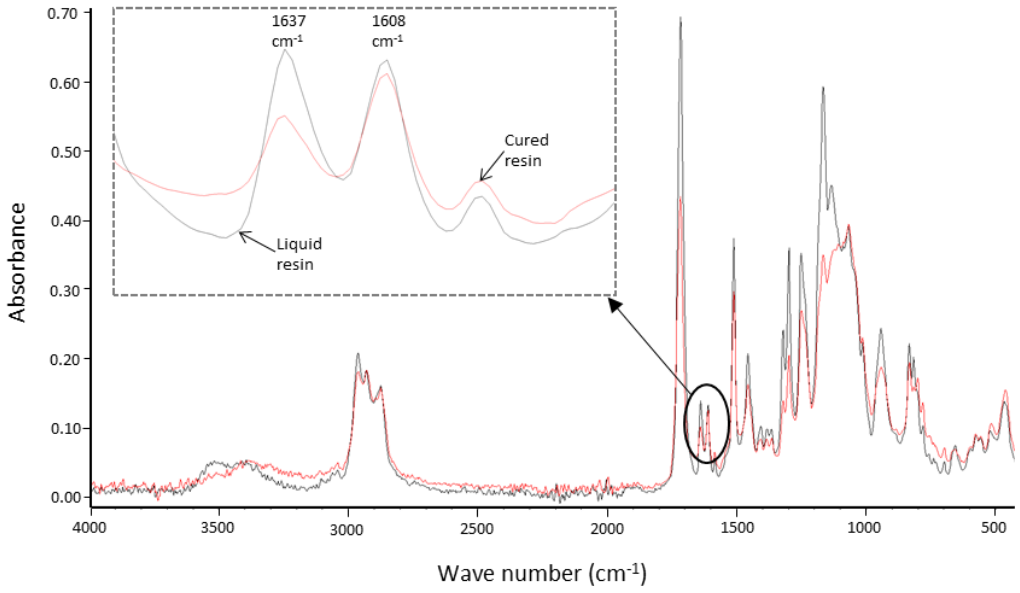

Figure 4.3. FTIR analysis for liquid and fully cured (30 min curing and 90º printing orientation) 3D printed resins.

The mean and the standard deviation of DC were calculated to be 86.28% ± 0.05 %, 83.27% ± 0.02 %, and 87.79% ± 0.06 % for 20, 30, and 50 min respectively (Figure 4.4a). The effect of post-curing time on DC was analysed, and one-way ANOVA indicated no statistical difference between the groups' mean values ($p>0.05$).

DC mean values were recorded as 52.33% ± 0.02 %, 67.88% ± 0.04 %, and 83.02% ± 0.02 % for 0°, 45°, and 90° specimen groups respectively (Figure 4.6b). One-way ANOVA indicated a statistical difference between the groups' mean values ($p<0.001$). Tukey's test showed a significant difference between all the groups with different layer orientations ($p<0.002$).

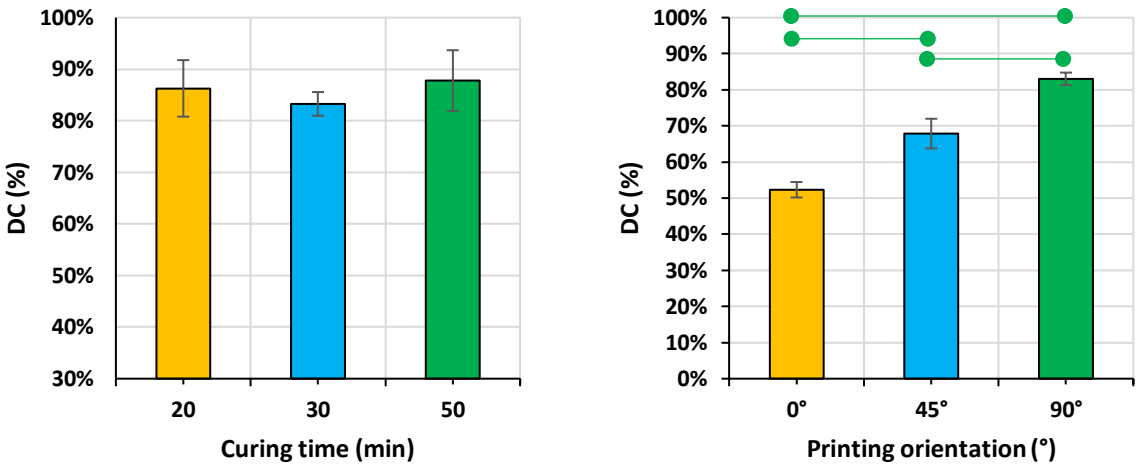

(a) (b)

Figure 4.4. Degree of Conversion (DC) for the 3D printed resins at different (a) curing times and (b) layer orientations. Horizontal solid lines (green) joining two points indicate a statistically significant difference between two groups.

4.4.3. Sorption and solubility analysis

The mechanical and structural test results indicated that 30 min curing could be optimum time as recommended by the manufacturers. Therefore, sorption and solubility analysis were carried out only for 30 min curing time but with different layer orientations.

The mean sorption and the standard deviation were calculated to be 31.2 ± 1.3 µg/mm³, 30.6 ± 0.5 µg/mm³, and 22.8 ± 0.4 µg/mm³ for 0°, 45°, and 90° layer orientations respectively (Figure 4.7a). One-way ANOVA indicated a statistical difference between the groups' mean values ($p<0.001$), and the Tukey's test showed a significant difference between the 0° layer-oriented group and 90° PO group ($p<0.001$). Also, a significant difference was reported between the 90° and the 45° layer orientation group ($p<0.001$).

The mean solubility and the standard deviation for all three layer orientation groups were calculated to be 1.5 ± 0.4 µg/mm³, 1.3 ± 0.3 µg/mm³, and 1.4 ± 0.5 µg/mm³ for 0°, 45°, and 90° layer orientation respectively (Figure 4.5b). One-way ANOVA indicated no statistical difference between the groups' mean values ($p>0.05$).

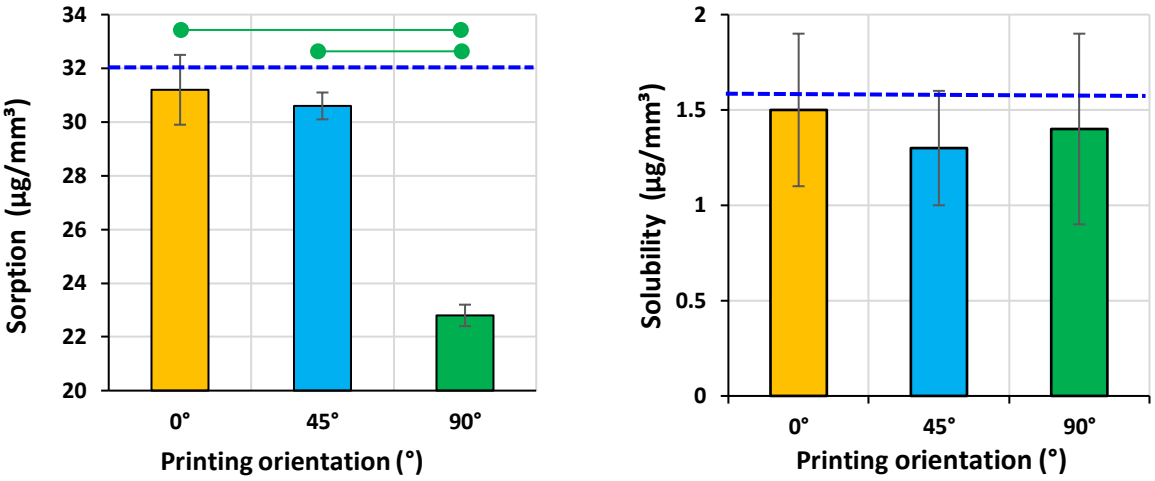

(a) (b)

Figure 4.5. The effect layer orientation on artificial saliva (a) sorption and (b) solubility. Horizontal solid lines joining two points indicate statistically significant difference. Horizontal dotted lines indicate minimum requirements for denture base applications.

All experimental groups underwent mass change with time upon storage in artificial saliva. During the sorption process, the mass rapidly increased in the first 7 days, followed by a reduced rate of increase until the equilibrium was reached at day 42 (Figure 4.6). Then, the mass was decreased with the desorption process steadily in the first 7 days, followed by a slow decrease until equilibrium was reached at day 21of the desorption process. The highest rate of mass change was associated with the 0° orientation group, followed by 45° and 90° groups.

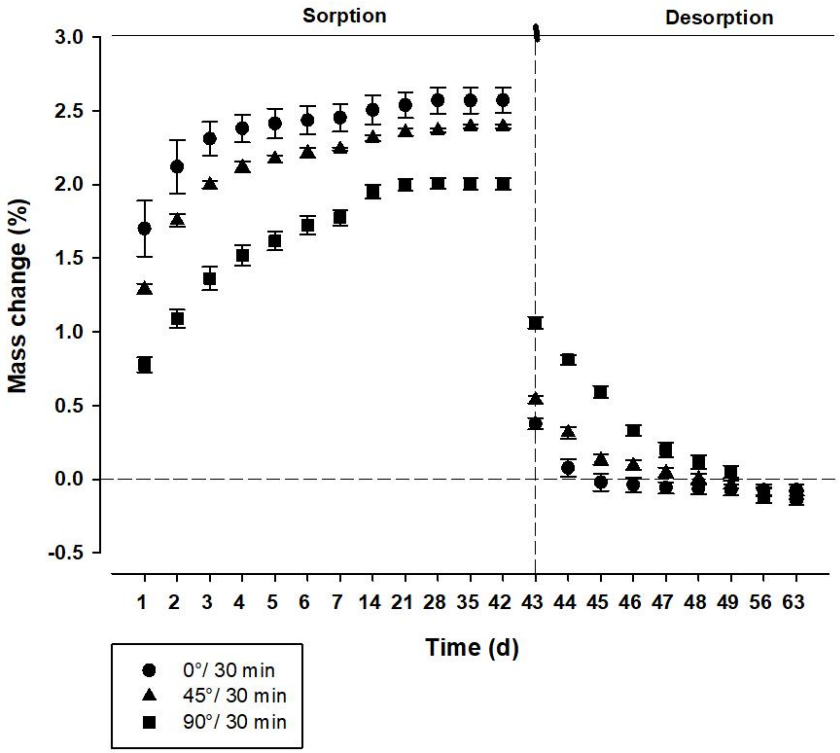

Figure 4.6. A graph illustrating the mass change of specimens immersed in artificial saliva over 63 days.

4.4.4. Morphology of the superficial and fractured surfaces

Layering structure was observed in the specimens prepared with all three orientations and with different curing times as shown in Figure 4.7. However, after polishing to a depth of approximately 0.5 mm into the sample, the layering structure was disappeared in all cases. This indicated that the layering structure was only present at the superficial surface not within the main body of the specimens.

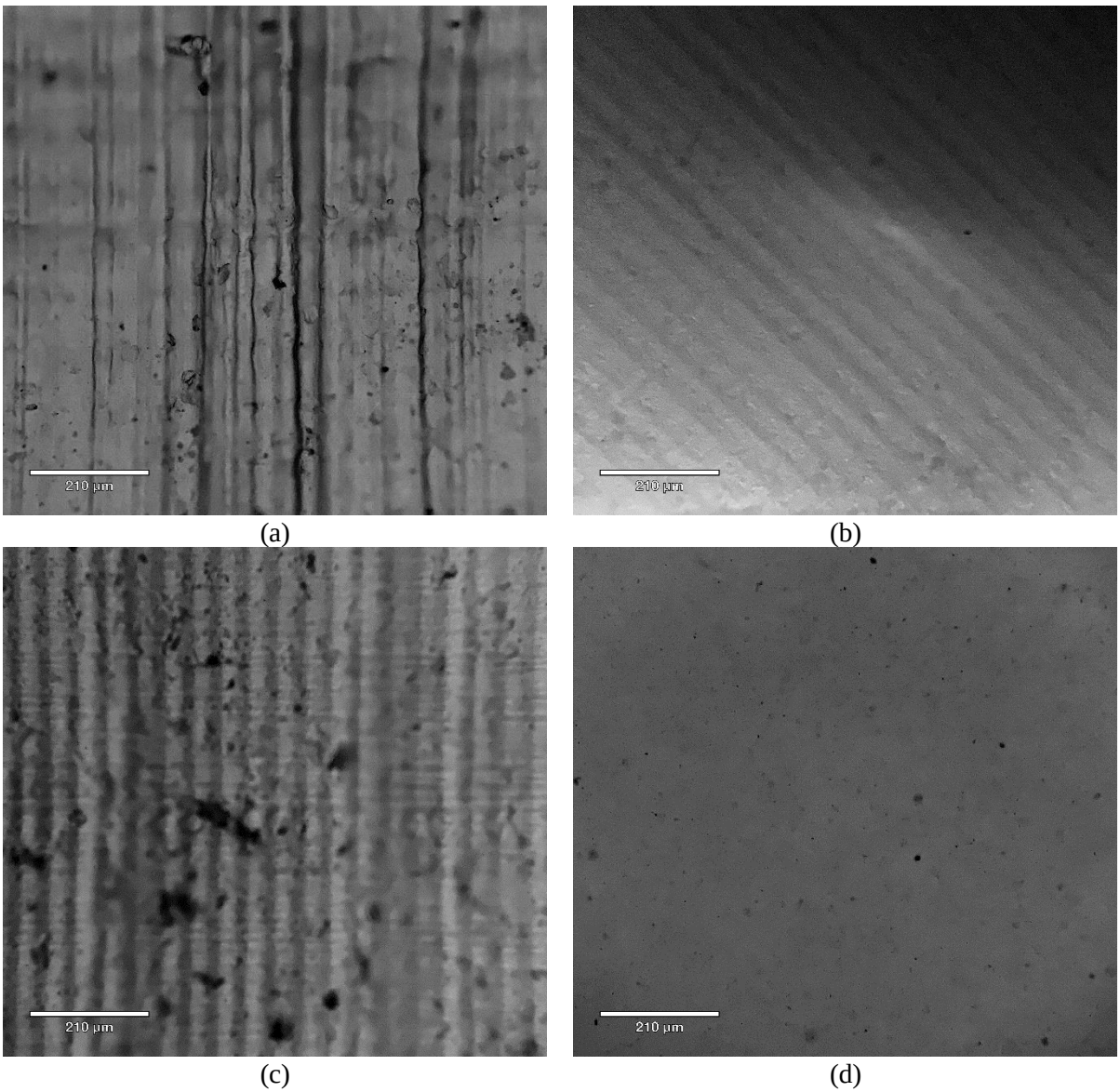

Figure 4.7. Optical microscope images of 3D printed denture base resin material cured for 30 mins showing the surface morphology across the thickness with different layer orientations: (a) 0˚ (b) 45˚ and (c) 90˚. (d) Representative surface for all specimens after mechanical polishing

SEM images of the fractured surface are presented in Figure 4.8 to illustrate the differences between different layer orientations. The microstructures in all the specimens showed globular-flower shaped flower type lamellar structures with clear separation boundaries. Long and narrow structures were also found in some cases. Random voids, white particles and cracks were also visible in the microstructure. However, after careful screening of the images, no clear differences were found among the specimens with respect to cracks direction, crack amount, or volume of voids.

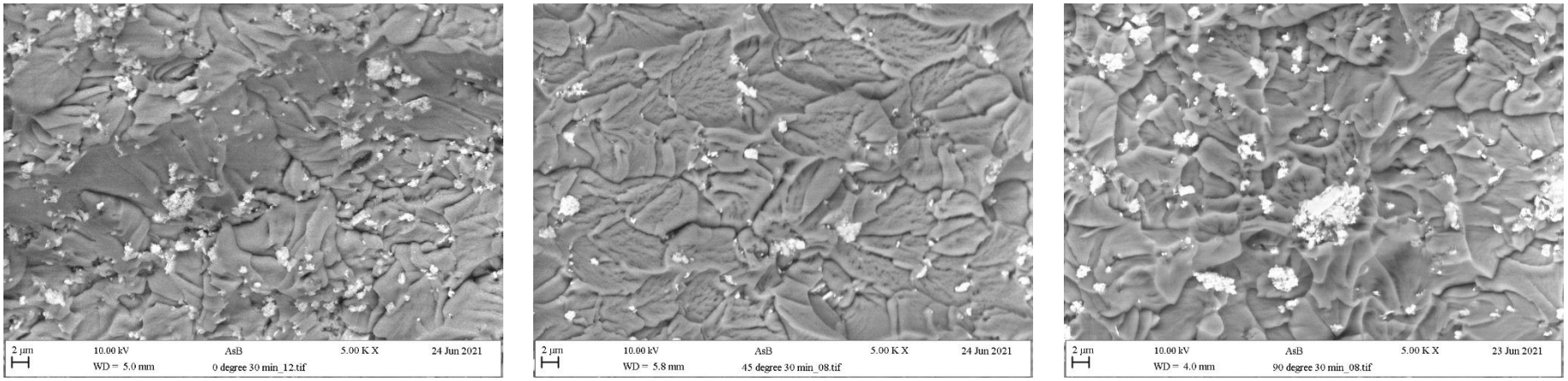

(a) (b) (c)

Figure 4.8. Fractured surface morphology of 3D printed denture base resin material with different layer orientations and 30 min curing times showing no layering at the internal structures: (a) 0° , (b) 45° , (c) 90°

4.5. DISCUSSION

4.5.1. Summary of the study and hypothesis testing

Denture base is a polymeric material that is mainly composed of PMMA. The digital revolution of 3D printing technology introduced many advantages to the current manufacturing methods in dentistry (Hada et al., 2020; Kurzmann et al., 2017). Many factors could affect the properties of the printed resin for denture base application and these factors can be divided into un-controllable factors such as material composition, light wavelength, and light power whereas the controllable factors included printing orientation, post-curing time, and post-curing temperature (Alharbi et al., 2016; Della Bona et al., 2021; Katheng et al., 2021; Kim et al., 2020; Puebla et al., 2012b; Unkovskiy et al., 2018; Z. c. Zhang et al., 2019). The aim of this study was to investigate the effects of printing orientation and post-curing time on the mechanical and physical properties of the 3D printed denture base resin. The results showed that the post-curing times and printing orientations considered in this study did affect properties of the printed NextDent resin. Therefore, the null hypothesis tested here should be rejected. The flexural strength and flexural modulus found in this study were higher than the ISO standard recommendation and the values provided by the manufacturer. On the other hand, the sorption was lower than the manufacturer's value, and the solubility was higher than the manufacturer's value but still within the ISO standard recommended range.

4.5.2. Analysis of the results and comparison with the literature

4.5.2.1. Mechanical properties

During clinical function, a combination of compressive, tensile, and shear stresses are exerted on the denture base which could lead to failure of the prosthesis (Jagger et al., 2002; J. John et al., 2001; Li et al., 2016; Vallittu et al., 1994). Hence, it is important to ensure that the denture base meets certain standards in term of surface and core mechanical strength in order to resist deformation and fracture under the mastication loads. Mechanical and physical properties of 3D printed objects differ from those made by subtractive manufacturing in because the latter are cured at a high temperature and pressure, and their properties are well established before denture fabrication (Duarte et al., 2016). 3D printing technology uses photopolymerised resin materials that are highly dependent on the parameters used during printing and post-curing processes (Dimitrov et al., 2006; Puebla et al., 2012b; Z. c. Zhang et al., 2019).

Vickers hardness represents abrasion and indentation of the prosthesis during function especially when chewing hard food (Prpic et al., 2019). Denture base materials should have high surface hardness in order to resist dimensional changes, surface damages, and scratches after using toothbrushes to clean the prosthesis (Al-Harbi et al., 2019; Kawaguchi et al., 2014). Vickers hardness results showed that the 0^o/30 min group (control) did not show any significant difference compared to the other groups except 0^o/20 min group, which showed significantly lower value. The shorter CT (20 min) at 0° PO could lead to insufficient polymerisation which eventually affected the Vickers hardness negatively. At 0^o PO, an increase in curing time beyond 30 min did not show any further improvement in hardness. One study (Kim et al., 2020) found similar observations to this study as they disclosed an insignificant increase in the surface hardness when increasing CT beyond 15 min. Another study (Aati et al., 2021b) revealed that the increase in CT had significantly improved the surface hardness of the denture base, but the comparison was made between specimens prepared with no post-curing (green state) and 20 min CT. However, generally the surface hardness showed an increasing trend with the POs in this study. The highest hardness was achieved in the 90^o/30 min group, which could be considered as the optimum combination of PO and CT.

Flexural strength and flexural modulus are important mechanical properties that determine the extent to which the denture base can resist plastic deformation under loading (Anusavice and Phillips, 2003). During flexural testing, the applied force was parallel to the layer orientation in a 90° PO specimen (Figure 4.1) compared to the perpendicular to the layer orientation in a 0° PO specimen. Before carrying out the flexural test, it was assumed that the 90° orientation would produce the lowest values based on the data of Shim et al (Shim et al., 2020) and Alharbi et al (Alharbi et al., 2016) that strength between the successive layers was weaker than the strength within individual layers. Surprisingly, the 90° PO group showed higher values compared to the 0° and 45° PO groups. This outcome agreed with studies by Unkovskiy et al (Unkovskiy et al., 2018) and Vayrynen et al (Vayrynen et al., 2016). They hypothesised that there was no difference in strength between and within the resin layers. It should be noted that for all three curing times at 0° PO, the specimens failed to achieve the minimum flexural strength of 65 MPa as recommended by the ISO standard, but the other two PO groups produced much higher flexural strengths than the recommended value, while the 90° PO groups produced the highest value (>88 MPa). One of the observations that could affect the results is the material's shrinkage behaviour, as the 0° PO specimens distorted (bent), unlike the other groups where the specimens were much straighter During the flexural strength tests, the

specimen was oriented in a way that the bent direction was downward facing the same direction as the force was applied. (Appendix: Figure A.1). This could reduce the value of the flexural strength compared to the specimen oriented in the opposite direction. On another note, much longer time required for printing the 90° PO group (~ 8 hrs) compared to the 0° PO group (~ 2 hr) might compromise the fabrication time significantly.

In this study, denture base resin material manufactured via 3D printing was evaluated based on three CTs. In general, the 20 min curing time showed lower mechanical properties in this investigation. However, highest flexural strength and modulus were found with 50 min and 30 min curing times respectively. Bonada et al (Bonada et al., 2017) studied the effect of post-curing time on the flexural strength of a 3D printed resin, and found no significant difference between 20 and 40 min post-curing times (41.72 MPa and 40.36 MPa respectively). Katheng et al (Katheng et al., 2021) also studied the effect of CT and temperature on the printed part accuracy, fit, and DC and they concluded that the results were less likely to be affected by the CT. These two reported studies were in agreement with the current study. On the contrary, Kim et al (Kim et al., 2020) found a significant difference in flexural strength of a 3D printed resin material when post-cured for 60 and 90 min (145.0 MPa and 150.0 MPa) compared to 15 and 30 min (around 121.9 MPa). These differences could be related to the difference in materials, printing technology, and the post-curing devices used. Aati et al (Aati et al., 2021b) found a significant difference when they compared the mechanical and physical properties of 3D printed denture bases of 0 and 5 min post-curing time groups to 20 min post-curing time group. They reported no significant difference between 10 and 20 min post-curing time in term of mechanical properties, DC, and water sorption and solubility, and 20 min was recommended to provide the optimal result. The current study did not include any groups that were cured beyond 50 min, as a prior pilot study found that 70 min post-curing time did not result in any statistical difference in the properties of the material when compared to the 50 min group. The current study found that a curing time of 30 min represented the optimum duration to achieve the highest mechanical properties without wasting curing time.

For any combination of CTs and POs, the flexural modulus was found to be higher than the recommended value of 2000 MPa for the denture base, and the highest value was found for 45^{o}/30 min group. Surprisingly the 0° PO group showed a relatively higher flexural modulus compared to the other PO groups. Unkovskiy et al (Unkovskiy et al., 2018) had similar results and they explained that this could be due to the reduction in the specimen thickness, which was

inversely proportional to the flexural modulus by a power of 3 (in the equation). During printing, the Z axis of the printed object was reduced compared to the original dimension entered in the STL file. Thus, the thickness of the 0° oriented specimen was reduced which subsequently increased the flexural modulus. They also claimed that if the thickness was controlled precisely between all PO groups, the 0° PO group would show the lowest flexural modulus value.

4.5.2.2. Degree of conversion

To investigate the effect of PO on the properties of the specimens, FTIR analysis was conducted to measure the DC. During printing, photo-initiators start to convert monomers into polymer in order to create bonded chains at the molecular level (Andreescu et al., 2018). Increasing the DC could enhance the physical, mechanical, chemical, and biological properties of photopolymerised resin materials (Abed et al., 2015; Calheiros et al., 2008; Galvão et al., 2013; Hague et al., 2004; Steyrer et al., 2017). The layering technique used in additive manufacturing technology could potentially lead to insufficient polymerisation between each added layer which could lower the degree of polymerisation. Hence, the post-curing process was introduced to convert the unreacted monomers into polymers that could increase the DC (Kim et al., 2020). Katheng et al (Katheng et al., 2021) reported a significant effect of curing time and temperature on the DC of 3D printed resin. Also, Lowery et al (Perea-Lowery et al., 2021a) found a similar relationship between the post-curing environment and the DC. On the other hand, in this study, although no significant difference in DC was found with different curing times, the printing orientation was positively related with the DC. FTIR analysis confirmed that at 30 min CT, the DC of 90° PO group demonstrated significantly higher values compared to the other PO groups with 0° PO group showing the lowest DC values. To explain the effect of printing orientation, the number of layers required to form the flexural test specimens at each orientation were counted as an example. For the 0° PO group, 45 layers with a cross section of 65 mm × 10 mm were required to print one specimen, while 1,297 layers per specimen was recorded for the 90° PO group having 10 mm × 3.3 mm cross-section. The extra light exposure and smaller cross-sectional area due to the higher number of layers during printing might have a direct influence on the DC as both groups underwent the same post-curing process to complete the polymerisation process. The DC's results could explain the significant improvement in the mechanical properties of the 90° PO group.

4.5.2.3. Sorption and solubility

Water sorption and solubility are very important factors that could affect the denture durability. Polymeric materials tend to absorb water due to their inherent polarity (Dhir et al., 2007). Water sorption is a process where water molecules are absorbed within the polymeric material due to its small size (Al-Mulla et al., 1989; Polat et al., 2003). Water solubility represents the unreacted monomers and other soluble materials that was dissolved after water (or other solutions) penetrated the resin matrix causing leaching, weakening and plasticisation of the polymeric material (Malacarne et al., 2006b; Rahal et al., 2004a). Artificial saliva was used in this test as a storage medium in order to simulate the effect of oral fluids on the material properties. The sorption results showed that at 30 min CT with different POs most of the mass change of the specimens occurred within the first week, and equilibrium was reached after 2-4 weeks. Sorption progressively decreased with the increasing angles of the PO particularly at 90^{o}. The sorption results were associated with the DC results, as the 90° oriented group showed highest DC compared to other groups, which led to a less AS uptake due to the higher monomer conversion rate. The mean values for sorption test also coincided with the hardness and flexural strength results as the higher values were associated with the 90º PO group. On the other hand, during desorption, the most mass change occurred within the first 4 days, and the equilibrium point was reached after 14 days. 0° PO group showed slightly higher solubility as its DC was lower compared to the other groups. Therefore, more unreacted monomers were leaching out along with other additives (Rahal et al., 2004a).

4.5.2.4. Surface characteristics

Lines representing stacking of successive layers during printing were clearly visible along the width of 90˚ and 45˚ PO specimens and along thickness of 0˚ PO specimens as seen with the optical microscope and in the SEM images. After mechanical polishing, it was noticed that the layered structure disappeared, which indicated their presence was only on the external surfaces of the specimens. SEM images of the fractured surfaces also confirmed this observation, as the layer separating lines could not be observed. This was in agreement with the observations of other studies [23, 24].

4.5.3. Limitations and future studies

The complete specification of the commercial resin was not fully revealed by the material manufacturers due to confidentiality reasons. For instance, unidentified white particles were observed in the SEM images of the cured resin, and it was confirmed by EDX that they were not any organic particles but could be some form of pigment.

In some cases, the samples were printed from two different batches of the same resins due to one litre resin bottle. This could cause some variations in the sample properties.

Curing temperature was set to 60^{o}C as per the recommendations by the manufacturer. In general, the results demonstrated that the curing time did not cause any significant changes in the resin properties. However, variation in the combination of different curing times and curing temperatures could affect the resin properties and this could be a subject of future study. Other mechanical properties such as impact or fracture toughness and physical properties such as colour stability in food simulating fluids could be conducted in future.

4.5.4. Clinical significance

The 3D printed resin materials showed promise with improved mechanical and physical properties suitable for replacing conventional denture base fabrication technique in prosthetic dentistry. The denture base should be printed on their side to avoid the midline fracture.

4.6. CONCLUSIONS

In this study, NextDent resin denture base specimens were prepared using 3D printing at different printing orientations and curing times. Given the limitations of this study discussed previously, the following conclusions can be derived.

(1) The flexural strength of the 3D printed denture base resin was affected by the printing orientation but not the curing time, and the values increased with the increasing angles of the layer orientation from 0^{o} to 90^{o}.

(2) Surface hardness was altered with the printing orientation and curing times, but in all cases the changes were not significant except for the 0^{o}/20 min group which showed the lowest value.

(3) An increasing trend of DC of the 3D printed resin with the printing orientation angles was found and the highest values were associated with 90° layer orientation.

(4) At 30 min curing time, the 90^{o} printed resin displayed significantly lower sorption compared to the other two orientations.

(5) Overall, 90^{o} printing orientations and 30 min curing times produced the highest mechanical and physical properties.

Chapter 5: Effect of Artificial Ageing on the Physical and Mechanical Properties of 3D-printed Denture Base Materials

Ahmed Altarazi, Julfikar Haider, Abdulaziz Alhotan, Nick Silikas, Hugh Devlin

5.1. ABSTRACT

Objective: The aim of this in-vitro study was to assess the physical and mechanical properties of two types of 3D-printed materials after being subjected to artificial ageing.

Methods: A total of 219 acrylic resin specimens were produced with two types of 3D-printed materials, namely NextDent (ND) and Formlabs (FL), and a Scottlander heat-cured (HC) resin material as a control. Sorption and solubility tests (n=5) were conducted in artificial saliva according to the ISO recommendation. Vickers and Martens hardness (n=5) were used to test the surface hardness, while flexural properties (n=10) were evaluated through a three-point bending test, and impact strength (n=10) by a Charpy un-notched test device. Degree of conversion (DC) (n=5), elemental analysis, and filler content (n=3) were also investigated. The specimens were then subjected to hydrolytic ageing in artificial saliva for three months, after which their surface hardness and mechanical properties were re-evaluated.

Results: The results showed that 3D-printed resins had significantly higher sorption values compared to the heat-cured resin controls ($p<0.05$). On the other hand, there was no significant difference ($p>0.05$) in Vickers and Martens hardness as well as impact strength among the tested materials. However, the flexural strength values of the 3D-printed materials were significantly higher ($p<0.05$) compared to the heat-cured material. The DC of 3D-printed resins was lower compared to the control group, but the difference was not significant ($p>0.05$). Additionally, 3D-printed materials contained significantly higher filler content compared to the control ($p<0.05$). Moreover, the ageing process in artificial saliva for three months had a significant effect on the Vickers hardness for all tested groups, and the Martens hardness for the control group only ($p<0.05$), but it had no significant effect on the mechanical properties ($p>0.05$).

Significance: 3D-printed denture base materials demonstrated lower performance compared to heat-cured material in terms of sorption, solubility, and DC. On the other hand, 3D-printed materials exhibited either comparable or superior mechanical properties when compared to the conventional heat-cured material, and while the ageing process influenced the surface properties but not the mechanical properties. The 3D printed materials were compliant with ISO recommendations and could be used alongside conventional heat-cured materials when appropriate clinical trials are successfully completed.

Keywords

Denture base; PMMA; Additive manufacturing; Stereolithography (SLA); 3D-printing; Physical; Mechanical.

5.2. INTRODUCTION

Complete denture treatment remains a viable therapy choice for individuals with missing teeth. Significant efforts have been invested in improving the material properties of polymethylmethacrylate (PMMA) material and, thereby overcoming the known disadvantages associated with the traditional method of denture manufacturing such as human errors and the lengthy procedure (Paulino et al., 2015). The production of digital denture templates has been made possible due to recent advancements in computer-aided design and computer-aided manufacturing (CAD/CAM) technology and its associated software (Al-Dwairi et al., 2019; Infante et al., 2014). A Standard Tessellation Language (STL) file is created once the denture has been digitally designed, and then either a subtractive (computerized numerical controlled milling) or additive (3D-printing) method is used to produce the denture (Alp et al., 2019; Steinmassl et al., 2018).

Several benefits of CAD/CAM-fabricated prostheses include fewer appointments, streamlined denture manufacturing processes, greater tissue adaptability, simple replication of pre-existing dentures, fewer manufacturing errors, and more rapid production, all of which are advantages associated with using digital technologies (Bidra et al., 2016; Bidra et al., 2013; Bilgin et al., 2016; Infante et al., 2014). Although milling is a common method for making dentures, 3D-printing offers important benefits. For instance, it is more cost-effective since it allows for the simultaneous production of several components without wasting raw materials or wearing out rotary tools (Kattadiyil and AlHelal, 2017; Shim et al., 2020).

In order to assess the physical and mechanical qualities of new materials in a representative setting, research in restorative dentistry increasingly uses simulated oral environments. The goals of such studies are to confirm prospective improvements and ensure the high quality and safety of the end products supplied to patients (Babaier et al., 2022). The mechanical properties of the polymer, regardless of its manufacturing technology, could be compromised by oral cavity fluids, due to the absorption of water by the acrylic, which could compromise the physical properties. (Lin et al., 2000). Denture bases produced through 3D-printing must meet stringent criteria for oral stability to ensure their long-term usage. This includes low water absorption and water solubility, high mechanical properties to withstand masticatory forces, and a high degree of conversion to prevent biological effects from residual monomers (Aati et al., 2022a; Zafar, 2020). The interaction of water and the polymer chains can cause internal strains due to swelling, chemical degradation, and leftover monomer elution, making sorption

and solubility crucial indicators for assessing denture resin durability (Gad et al., 2022b; Perea-Lowery et al., 2021b). Additionally, maintaining the lowest possible quantity of unreacted monomers is essential for ensuring excellent biocompatibility in the processed resin. The resin's degree of conversion (DC) can be measured to predict the amount of un-polymerised monomer that can irritate and harm a patient's oral mucosa (Bartoloni et al., 2000).

On the other hand, monitoring variations in hardness after preserving specimens in solvents can be used to indirectly examine polymer degradation. The hardness of a solid material can be measured by assessing its level of resistance to a compressive force applied to its surface by an indenter (Broitman, 2017; Ferracane et al., 2017). Studies of this nature typically assess the hardness after the load has been removed. While this is useful for materials that flex plastically, elastic-plastic materials are less accurately described in this way (Broitman, 2017). The Martens hardness approach was developed to overcome these limitations. This method incorporates sensors that can capture elastic and plastic deformation components during a force- or depth-controlled instrumented indentation while being loaded with a traditional Vickers diamond tip. The indentation modulus, creep, and depth are just a few of the numerical parameters that are automatically captured from the resulting force-displacement plots at each point. While a few studies have determined the Martens hardness for various polymer-based composites and ceramics (Hampe et al., 2018; Liebermann et al., 2016; Shahdad et al., 2007), there is a need to study the surface stability of 3D-printed denture base polymers.

The fabrication of dentures frequently employs 3D-printing technologies and related materials. However, there are few investigations comparing the physical and mechanical characteristics of denture base acrylic resins that have been 3D-printed and aged hydrolytically using artificial saliva. In this study, flexural strength, flexural modulus, impact strength, surface hardness, including Martens hardness and Vickers hardness, sorption and solubility, and degree of polymerisation of 3D-printed denture base resins were compared to those of traditional heat-polymerised acrylic resin both before and after hydrolytic aging in artificial saliva. The first null hypothesis was assumed that the physical and mechanical properties of the 3D-printed resins would not differ significantly compared to the traditional heat-polymerised resin. The second null hypothesis was hydrolytic aging in artificial saliva would not impact the tested properties of the control and 3D-printed resin.

5.3. MATERIALS AND METHODS

5.3.1. Resin material

The first 3D-printed material tested in this study was a commercial NextDent (ND) denture 3D+ light-cured resin with a light pink colour (3D systems, Soesterberg, Netherlands), which was specifically designed for denture base applications. According to the manufacturer, NextDent has the following properties: ultimate flexural strength of 84 MPa, flexural modulus of 2383 MPa, sorption of 28 g/mm^3, and solubility of 0.1 g/mm^3. (NextDent, 2022a).

The second 3D-printed material used in this study was a commercially available Formlabs digital denture (FL) resin in light pink (Formlabs, Somerville, USA). The manufacturer did not disclose the specific properties of the material, as the precise composition is considered proprietary information. However, the resin composition can be found in the safety data sheet, as presented in Table 5.1.

The control material used in this study was a heat-cured PMMA (HC). To create the specimens, powder and liquid monomer of methyl methacrylate (Pegasus Plus, Schottlander, Hertfordshire, UK) were utilised.

Table 5.1. Tested materials and manufacturers information.

Code	Manufacturing technology	Composition (wt.%)	Manufacturer
ND	Additive manufacturing	- Ethoxylated bisphenol A dimethacrylate (≥ 75) - 7,7,9-trimethyl-4,13-dioxo-3,14-diazahexadecane-1,16-diyl bismethacrylate (10-20) - 2-hydroxyethyl methacrylate (5-10) - Silicon dioxide (5-10) - Titanium dioxide (< 0.1)	NextDent
FL	Additive manufacturing	- Methacrylate monomer (40–60) - diurethane dimethacrylate (30–50) - propylidynetrimethyl trimethacrylate (5–10)	Formlabs
HC	Heat-cured manufacturing	- Polymethylmethacrylate (> 98)	Schottlander

5.3.2. Fabrication and ageing of the specimens

A total of 219 specimens (n = 73 per material) were fabricated for this study (Figure 1). The manufacturing procedure of FL material is described previously in chapter 4 (Altarazi et al., 2022), but the key steps are as follows: Formlabs Form 2 printer (Formlabs, Somerville, USA) was deployed. Test specimen designs were created using an open-source CAD software (Tinkercad.com), and then exported in STL format that was compatible with the printer's software. PreForm software was used to edit the CAD design, positioning it vertically (90°). Specimens were cleaned in 99.9% isopropyl alcohol (IPA) for 10 minutes and then left to air dry. Following this, the specimens were dipped in pre-heated glycerine at 80°C and cured at 80°C for 30 minutes in a light chamber box (Form Cure, Formlabs, Somerville, USA). ND specimens were manufactured in a similar way except that the specimens were soaked in 99.8% ethanol (instead of IPA) in a washing box for five minutes to remove any residual resin from the printer's resin pool without damaging the printed pieces. Specimens were then left out to air dry for 10 minutes to clear any alcohol residues. Following cleaning and drying, ND specimens were placed in an ultraviolet (UV) light box at 60°C to complete the polymerisation process.

All specimens had their edges and faces wet ground flat and smooth to the required width and height using silicon carbide grinding papers with grain sizes of approximately 30 µm (P500), 18 µm (P1000), and 15 µm (P1200), in that order. The height and width of the specimens at the centre and the edges were measured using a digital calliper (Draper, Eastleigh, Hants, UK) with an accuracy of 0.01mm.

In accordance with the manufacturer's instructions, the HC material's powder was added to the liquid and mixed until a uniform mixture with a manageable, dough-like consistency was achieved. This mixture was then manually packed into a mould. After closing the mould and placing it in a hydraulic press with a 15 MPa pressure, excess material was removed from the mould’s edges. The mould was then placed in a curing bath for six hours to polymerise at a temperature of 80°C. Following this, it was removed and allowed to cool slowly for 30 minutes at room temperature before opening the mould to retrieve the specimens. A polishing machine (Interlab, Hull, UK) was then used to trim, grind, and polish the specimens, employing pumice powder, emery paper, and a tungsten carbide bur.

The specimens were stored in artificial saliva at a temperature of 37℃ for a period of 3 months (Aati et al., 2022b). After this period, they were assessed for their Vickers hardness, Martens hardness, flexural strength/modulus, and impact strength. The artificial saliva solution was made by dissolving specific components listed in Table 5.2 in 1000 ml of distilled water with a pH of 5.52. The solution was mixed thoroughly using a magnetic stirrer until all components were fully dissolved (Williams et al., 2001). The solution was replenished every 14 days.

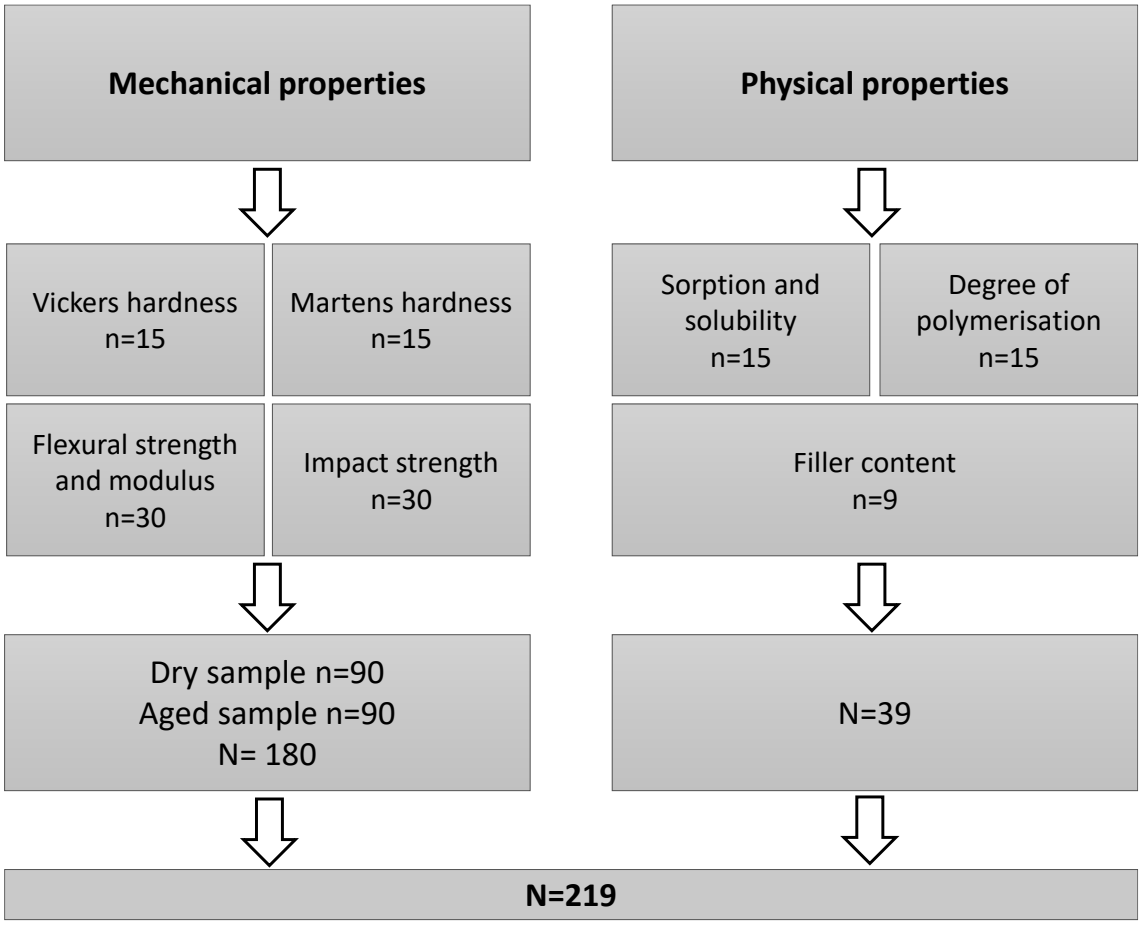

Figure 5.1. Overall plan for characterisation study

Table 5.2. Composition of artificial saliva

Compound	Amount (g/l)	Manufacturer
Sodium chloride (NaCl)	0.400	Acros Organics
Potassium chloride (KCl)	0.400	Fisher Chemical
Calcium chloride ($CaCl_2$)	0.795	Acros Organics
Sodium dihydrogen phosphate (NaH_2PO_4)	0.690	Alfa Aesa
Sodium sulfate hydrate ($Na_2S.9H_2O$)	0.005	Acros Organics

5.3.3. Characterisation of the specimens

5.3.3.1. Analysis of filler content

The percentage of inorganic components in each type of resin material used in this study was measured by eliminating the organic component of the resin materials. Following ISO standard 1172:2022 (BS EN ISO 1172, 2022), the specimens were heated at a constant temperature for a period of time, using the ash technique. Three specimens (n=3) were heated in an electric furnace (Programat EP 5000; Ivoclar Vivadent, Liechtenstein, Austria) at a temperature ranging from 470°C to 500°C for 15 min, and then cooled down in a desiccator. After that, each specimen was weighed using an electronic balance (Ohaus Analytical Plus, Ohaus, USA) to an accuracy of 0.01 mg. The percentage of inorganic fillers was calculated using equation 5.1:

$$\text{Filler weight\%} = \frac{m_3 - m_1}{m_2 - m_1} \times 100 \quad (5.1)$$

Where m_1 is the initial mass of the dry crucible without the specimen in grams, m_2 is the initial mass of the dry crucible plus the dried specimen in grams, m_3 is the final mass of the crucible plus the residues of the specimen after calcination in grams.

5.3.3.2. Fourier Transform Infra-red (FTIR) spectroscopy

Fourier Transform Infra-red (FTIR) spectroscopy was utilised to determine the DC of the 3D-printed specimen. Five specimens (n = 5) were printed in a dimension of 15.0 ± 0.2 mm in diameter and 2.0 ± 0.2 mm in thickness for the test. The Spotlight 200i FT-IR Microscope System with Spectrum Two was employed to measure the FTIR spectra, using a wavelength range of 4000 to 400 m−1 and a resolution of 4 cm−1. The measurement was performed at room temperature, with an average of 32 scans. The instrument was calibrated using a background spectrum. The 3D-printed resin material was scanned as a baseline record while in its liquid state and subsequently scanned again after the final polymerisation (post-curing). To determine the DC in percentage (Equation 5.2), the ratio of the double carbon bond peaks at two frequencies (stretch of aliphatic frequency at 1637 cm−1 against the reference aromatic frequency at 1608cm−1) was measured. For HC specimens, the peaks used were 1637 cm−1 and the C=O bond at 1720 cm−1 as a referenced peak.

$$\text{DC (\%)} = (1 - \left(\frac{\left(\frac{1637^{-1}}{1608^{-1}}\right) peak\ hights\ after\ polymerisation}{\left(\frac{1637^{-1}}{1608^{-1}}\right) peak\ hights\ before\ polymerisation} \right) \times\ 100 \qquad (5.2)$$

5.3.3.3. Assessment of Sorption and solubility

In accordance with the ISO 20795-1:2013 standard for Denture Base Polymers, the sorption and solubility tests were carried out on each test group, utilising five specimens per group (n=5). Each specimen was 50.0 ± 0.5 mm in diameter and 1.0 ± 0.2 mm in thickness. Prior to weighing, the specimens were conditioned to room temperature in a desiccator filled with freshly dried silica gel for an hour. A second desiccator, containing fresh dry silica gel, was used to obtain the baseline mass, which was determined by daily repeated weighing until the difference between subsequent measurements was no greater than 0.2 mg (m1). Using a computerized calliper, the diameter and thickness of each specimen were measured to calculate its volume (V).

Next, the specimens were immersed in synthetic saliva (Table 5.2) at a temperature of 37 ± 2°C, and their mass was determined after each removal from the solution and subsequent drying until the difference between subsequent weighing was no greater than 0.2 mg (m2). The specimens were then reconditioned by storing them in a desiccator with freshly dried silica gel for 1 day at 37°C ± 2, followed by a 1-hour conditioning period at room temperature in another desiccator containing freshly dried silica gel. The desorption procedure was repeated until the difference between subsequent weighing was no greater than 0.2 mg to obtain a constant reconditioned mass (m3).

Using Equations (5.3) and (5.4), the sorption and solubility in g/mm3 were determined, respectively. The volume of each specimen was calculated using Equation (5.5), while Equation (5.6) was used to calculate the percentage of mass change and mass loss during the sorption and solubility tests.

$$\text{Sorption} = \frac{m2-m3}{V} \qquad (5.3)$$

$$\text{Solubility} = \frac{m1-m3}{V} \qquad (5.4)$$

$$\text{Volume} = 3.14 \times \left(\left(\frac{mean\ diameter}{2}\right)^2\right) \times mean\ thickness \quad (5.5)$$

$$\text{Change in mass, SP (\%)} = \left(\frac{m^t - m1}{m1}\right) \times 100 \quad (5.6)$$

Where: m^t: is the mass of the specimen at a specific time point.

5.3.3.4. Hardness measurement procedure

A micro-hardness testing device (FM-700, Future Tech Corp, Tokyo, Japan) was used to determine the HVN of the specimens. The test load was set at 50 g with a 30 s dwell time. Five specimens were printed for this test (n=5) with a dimension of 15.0 ± 0.2 mm in diameter and 2.0 ± 0.2 mm in thickness. After polishing the surface of each specimen, three indentations were made along a straight line at several equally spaced sites. The average indentation's diagonal length was multiplied by four to determine the distance between each location. The mean hardness was measured under dry conditions 24 hours after manufacturing and then again after 3 months of ageing in artificial saliva.

The Martens hardness (Z2.5, ZwickRoell Ltd., Leominster, UK) was measured using a Martens Hardness Instrument with a Vickers hardness measurement tip. Five specimens were printed for this test (n = 5) with a dimension of 15.0 ± 0.2 mm in diameter and 2.0 ± 0.2 mm in thickness At the beginning of each test session, a fixed gap of 18 mm was maintained between the specimen's top surface and the hardness measuring head. A loading speed of 5 N/s was used to apply a force of up to 50 N, which was maintained for 30 s before being removed. The initial approaching rate was 100 mm/min, and the indenter tip's initial approaching speed before making contact was 40 mm/min. After proximity, the sensor tip's distance from each specimen was 40 µm. Each specimen had five indentations with equal spacing 24 h after manufacturing in a dry condition, and after it had been kept in artificial saliva for three months. During the test method of loading and unloading the Vickers indentation tip (136°), the test load and the indentation depth were automatically recorded and displayed as load-displacement curves. To prevent taking duplicate measurements at the same spot on the surface of each specimen, which would invalidate the findings, the indentations were placed along several lines marked on each specimen's surface. Software (TestXpert®, Zwick GmbH & Co, Ulm, Germany) automatically retrieved Martens hardness (HM). Equations (5.7) found in ISO 14577-4/2016 was used as the basis for the HM computations.

$$HM = \frac{F}{As\ (h)} = \frac{F}{26.43 * h^2} \quad (5.7)$$

HM was expressed in N/mm^2, F is the load in N, A_s (h) is the indenter's surface area at a distance of h from the tip in mm^2.

5.3.3.5. Flexural tests

Using a universal testing machine (Zwick/Roell Z020, Leominster, UK) with a 500 N load cell, a three-point bending test was employed to evaluate the flexural strength of the specimens. The specimens met the requirements of ISO 20795-1:2013 standard for denture base polymers, measuring 64 ± 0.5 mm in length, 10.0 ± 0.2 mm in width, and 3.3 ± 0.2 mm in thickness (n=10). The specimens were stored in distilled water in an incubator at a temperature of 37°C for 50 h to obtain baseline values. Each specimen was then set over supporting jigs that were separated by 50 ± 0.1 mm. Polished cylindrical supports of 3.2 mm in diameter and 10.5 mm in length were used. Both the test speed and the cross-head preload speed were set to 5 mm/min. The flexural strength and flexural modulus were determined using equations (5.8) and (5.9), respectively.

$$\sigma = \frac{3Fl}{2bh^2} \quad (5.8)$$

$$E = \frac{F^1 l^3}{4bh^3 d} \quad (5.9)$$

Equation 5.8 was used to calculate the flexural strength, where F is the maximum applied force in N, l is the distance between the supports in mm, b is the specimen's width in mm, and h is the specimen's height in mm.

Equation 5. 9 was used to calculate the flexural modulus, where b is the specimen's breadth in mm, h is its height in mm, and d is the deflection in mm at load of F_1, F_1 is the load in N at a position on the straight line (with the maximum slope) of the load/deflection curve.

5.3.3.6. Impact tests

A universal pendulum impact testing device (Zwick/Roell Z020 Leominster) was used for the Charpy un-notch impact test. The specimen's dimensions were 80 mm ± 0.5 in length, 10 mm ± 0.2 in width, and 4 ± 0.2 mm in thickness following EN ISO 179-1:2010 (n=10). Each

specimen was put into the apparatus and supported horizontally at both ends (40 ± 0.2 mm). The specimen's centre was marked and subsequently struck using a free-swinging pendulum with a 4.0 J load cell that was released from a fixed height. The impact energy absorbed was measured in joules (J). The Charpy impact strength (a_{cU}) (kJ/m^2) was determined per Equation 5.10:

$$a_{cU} = \frac{W_B}{bh} \times 10^3 \quad (5.10)$$

Where W_B is the energy at break in joules, b is the width of the specimen in mm, and h is the thickness of the specimen in mm.

5.3.3.7. Optical microscope and scanning electron microscope (SEM)

Using an optical microscope (Echo, Revolve, California, USA) with a magnification of ×10, it was possible to study the surface morphology of the printed and polished specimens in more depth. An Energy Dispersive X-Ray Spectrometer-equipped scanning electron microscope (SEM-EDX, Carl Zeiss Ltd., 40 VP, Smart SEM, Cambridge, UK) was used to examine the fractured surfaces of the specimens that resulted from the flexural strength test. The shattered specimen was placed into the SEM chamber after being mounted onto an aluminium stub and thinly coated with gold. Using a secondary electron detector at an acceleration voltage of 10.0kV, images at various magnifications were produced.

5.3.4. Statistical analysis

All data were statistically analysed using SPSS version 25 (IBM, New York, NY, USA). Shapiro-Wilk test was used to determine the distribution of the data, and a Levene test was utilised to confirm its homogeneity. Two-ways and one-way ANOVA, followed by Tukey's or Games-Howell post-hoc analysis were conducted depending on the data homogeneity to compare between groups' means according to a significance level set at $p \leq 0.05$.

5.4. RESULTS

5.4.1. Filler content

Table 5.3 represents the amount of filler measured in this study compared with data provided by the manufacturers, where available. The 3D-printed materials had a significantly higher

filler content compared to the HC material ($p<0.001$). No significant difference was reported between ND and FL.

Table 5.3. Filler content in the denture base materials

Resin material	Measured filler content (wt.%)	Manufacturer filler content (wt.%)
HC	Not measurable	< 2
FL	13.0 (2.2)^{A}	Not available
ND	15.2 (2.8)^{A}	6 - 15

**Within a column, cells having similar letters are not significantly different*

EDX analysis was used to identify the elemental composition of the fillers within the 3D-printed resins, as the HC material was almost a 100% PMMA. The results identified the presence of aluminium (Al) within FL, and a very minor trace of cupper (Cu). EDX analysis also revealed the presence of aluminium (Al), silica (Si), titanium (Ti), and iron (Fe) within ND resin material as non-organic fillers. The range of inorganic fillers detected were 1 - 13 wt.% and 1 – 20 wt.% for FL and ND respectively.

5.4.2. Degree of conversion (DC)

DC means and standard deviations of the resin materials are presented in Figure 5.2. HC groups showed the highest DC amongst the tested materials with a value of 97.2%. One-way ANOVA indicated a significant difference between the groups' mean values ($p<0.02$), and Games-Howell post-hoc revealed a significant difference between HC and ND groups ($p<0.02$). FL was also slightly higher compared to ND, but no significant difference was reported (93.7 % and 92.0 % respectively).

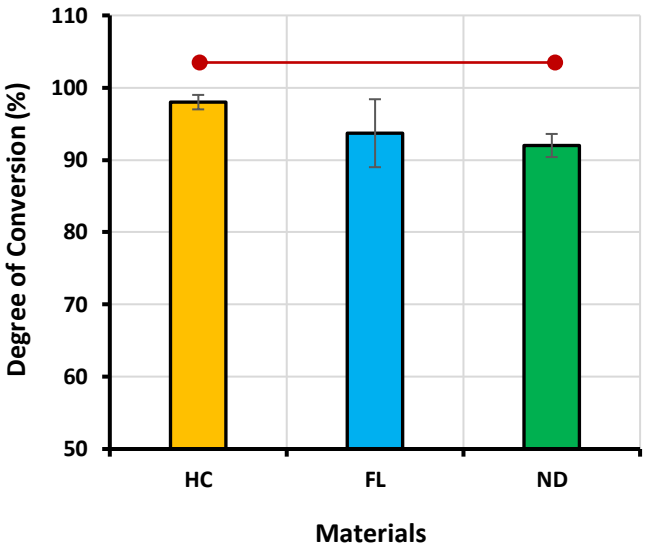

Figure 5.2. Degree of conversion (DC) of the three tested materials. Horizontal red line joining two points indicates statistically significant difference.

5.4.3. Sorption and solubility analysis

The mean sorption values and the standard deviations are presented in Figure 5.3. One-way ANOVA indicated the presence of a statistical differences between the group means ($p<0.001$), and Tukey's post hoc analysis showed a significant difference between HC and the other 3D-printed groups ($p<0.001$), and between ND and FL ($p<0.001$). On the other hand, one-way ANOVA did not show any significant difference between the solubility mean values ($p>0.05$). During the sorption process, HC showed a notable increase in mass within the initial 3 days. Following this, the mass increase plateaued, becoming negligible up until day 42. This plateau indicates that equilibrium had been reached, as shown in Figure 5.4. In a similar fashion, during the desorption process, the change in mass of the specimens was mostly observed within the first 3 days, with negligible changes thereafter. In the case of the 3D-printed groups (ND and FL), a different pattern was observed. The mass change occurred consistently up to 21 days during the sorption process, with small change after this point and remaining so until day 42. In the desorption phase, the mass change was concentrated in the first 7 days, with very slight variations in mass detected thereafter.

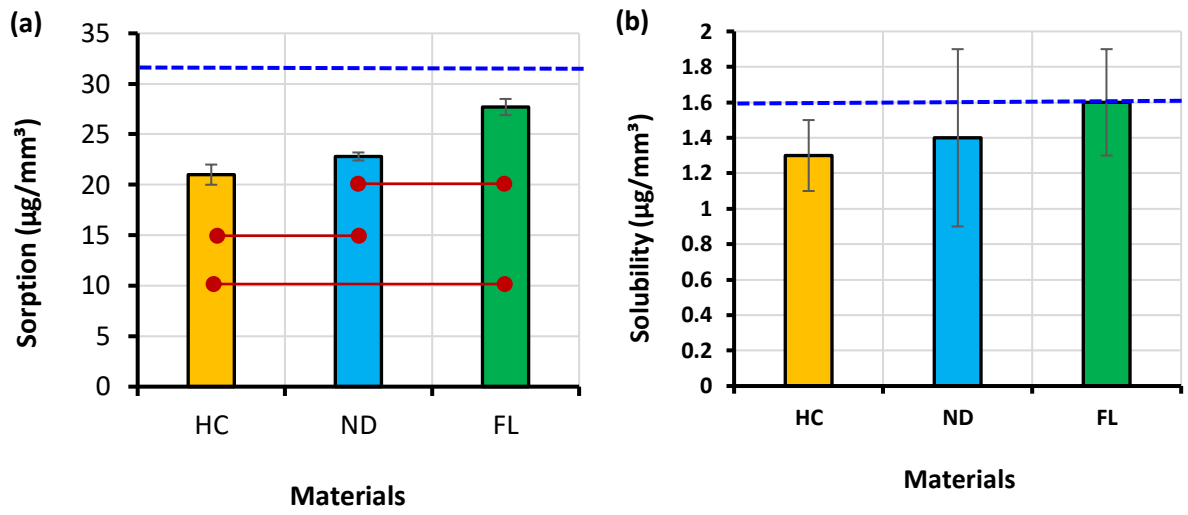

Figure 5.3. (a) Sorption and (b) solubility in artificial saliva for five weeks of the three tested materials. Horizontal red lines joining two points indicate statistically significant difference. Horizontal dotted lines (blue) indicate minimum requirements for denture base

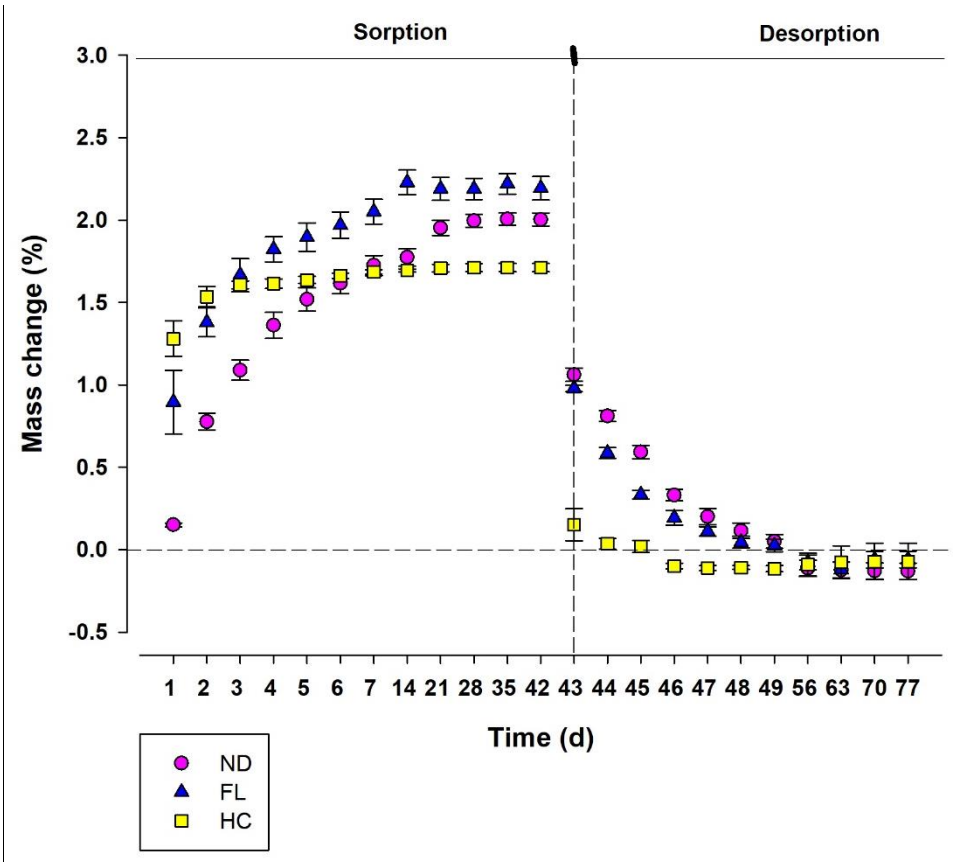

Figure 5.4. A graph illustrating the mass change of specimens immersed in artificial saliva over 77 days.

5.4.4. Vickers and Martens hardness

The means and standard deviations of Vickers hardness are presented in Figure 5.5(a). No significant difference was noticed across different materials when comparing baseline readings, and also after the ageing process. Looking at the same material before and after ageing, the values of Vickers hardness decreased significantly in all the groups ($p<0.001$).

Figure 5.5(b) shows the mean and standard deviation of Martens hardness for different materials before and after ageing. At baseline, no statistical significant difference was reported between all groups. After ageing period, HC group showed significantly lower value compared to FL resin ($p<0.01$). However, no significant difference was reported between 3D-printed resin materials ($p>0.05$). Within the same material, no significant difference was noticed before and after the ageing process for the 3D printed resins, except for the value of the HC group, which decreased significantly ($p<0.001$).

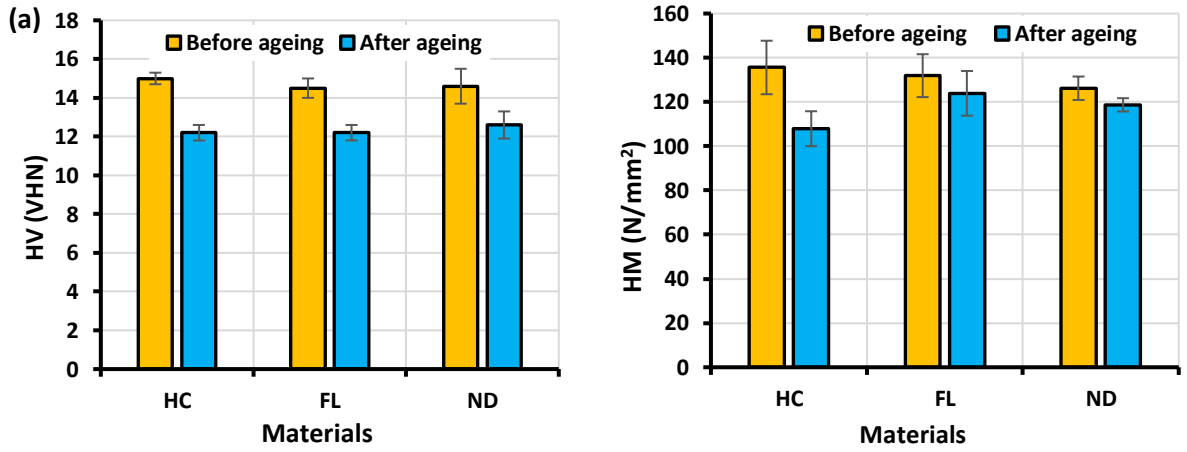

Figure 5.5. (a) Vickers and (b) Marten hardness of the three tested materials before and after ageing in artificial saliva for three months

5.4.5. Flexural strength and modulus

Figure 5.6 represents the means and the standard deviations of flexural strength and flexural modulus. Flexural strength values showed a significant increase associated with 3D-printed resins compared to HC material before ($p<0.02$) and after ageing ($p<0.03$) across different materials. Ageing in artificial saliva for three months decreased the values for all the materials, but the decrease was not significant ($p>0.05$). Flexural modulus analysis showed no significant

difference between the tested groups before ageing ($p>0.05$). However, the ageing process affected the HC resin significantly ($p<0.002$).

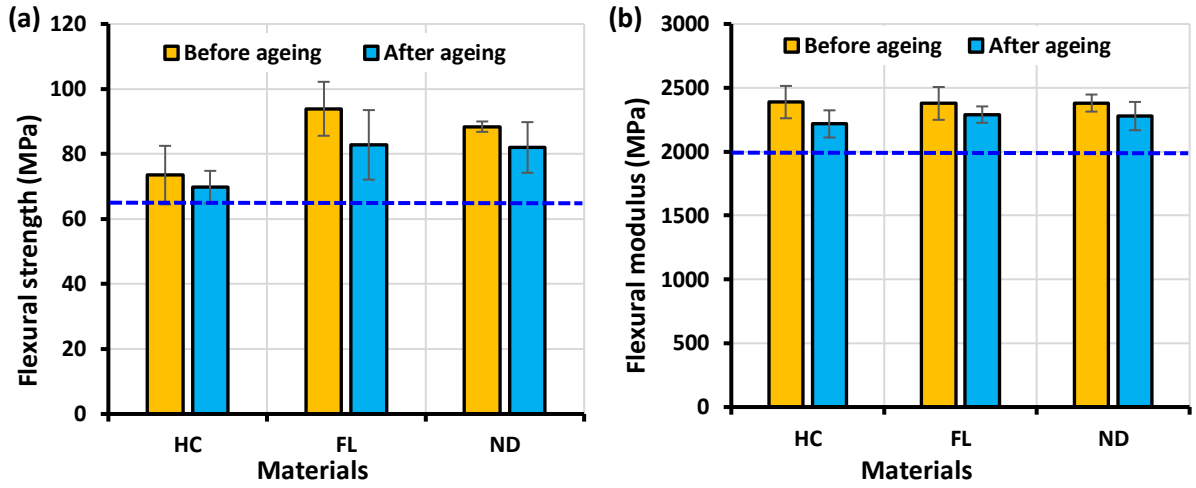

Figure 5.6. Flexural (a) strength and (b) modulus of the three tested materials before and after ageing in artificial saliva for three months. Horizontal dotted lines (blue) indicate minimum requirements for denture base

5.4.6. Impact strength

The mean values for impact strength test are shown in Figure 5.7. Two-ways ANOVA did not show any significant difference between all groups across the materials, and before/after ageing process within the same material ($p>0.05$).

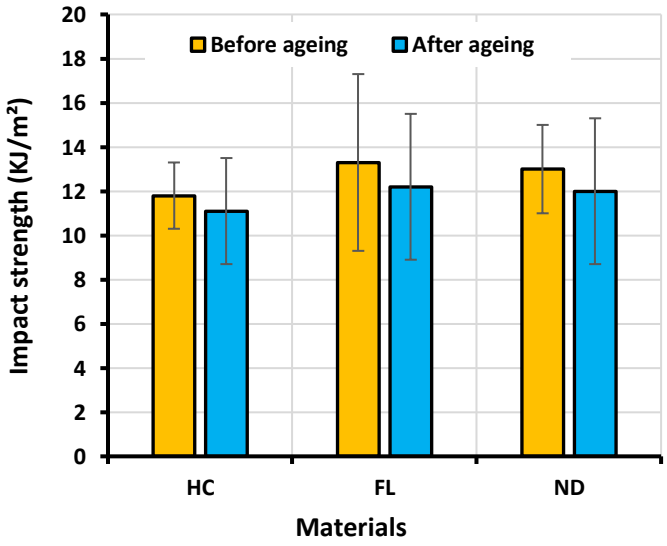

Figure 5.7. Impact strength of the three tested materials before and after ageing in artificial saliva for three months

5.5. DISCUSSION

In this study, the mechanical and physical properties of denture base materials manufactured using different technologies were investigated, with a focus on 3D-printing technology. Both null hypotheses were partially rejected, as the statistical analysis revealed that 3D-printed specimens had significantly higher values in some tests compared to the conventional heat-cured resin. Additionally, the aging process significantly affected the materials in some tests.

Acrylic denture base resins are polar materials that tend to absorb water over time. PMMA, for example, contains functional ester groups that interact with water molecules through hydrogen bonding. This interaction leads to water absorption, which can affect the properties of the material (Barsby, 1992; Saini et al., 2016). Water absorption can cause swelling and plasticisation of the polymer matrix, affecting the mechanical properties and dimensional stability of the material. Additionally, it can impact residual monomers that did not undergo complete polymerisation, which could potentially affect the material's biocompatibility if they leach from the resin. (Barsby, 1992; Iwaki et al., 2020). Therefore, it is important to evaluate the sorption and solubility of denture base materials.

In this study, sorption and solubility were assessed in artificial saliva to mimic the oral environment. The specimens were immersed until all tested groups reached full equilibrium, where the specimens could gain no more weight. This process lasted between 2-3 weeks for sorption, and 1-2 weeks for desorption (solubility). Sorption of 3D-printed denture base materials was higher compared to the control heat-cured material, and this finding is in agreement with other studies (Gad et al., 2022b; Greil et al., 2023; Perea-Lowery et al., 2021b). The increased sorption values associated with 3D-printed materials can be attributed to some factors, including the degree of conversion (Gad et al., 2022c; Perea-Lowery et al., 2021b) and the chemical composition of the materials (Arima et al., 1996; Perea-Lowery et al., 2021b; Pfeiffer and Rosenbauer, 2004).

Based on the results of this study, a negative correlation was found between DC and sorption/ solubility performance. The DC of the tested materials in this study revealed that HC material had a higher value compared to its 3D-printed counterparts. A higher DC generally results in a more densely cross-linked polymeric network that leaves less un-reacted monomers and less spaces for water molecules within the material (Aati et al., 2022a; Ferracane et al., 1998; Ghavami-Lahiji et al., 2018; Imazato et al., 1999). As a result, materials with higher DC

typically have lower sorption rates. One of the possible reasons that can explain the increased DC of HC material compared to the 3D-printed materials is the manufacturing technology. HC material is polymerised under higher temperature and pressure, and for a longer time (cycling six hours in water bath); this could have a positive effect on the DC (Doğan et al., 1995; Garcia et al., 2010; Wong et al., 1999). Another possible reason is the filler content of the material. To calculate the amount of fillers on each type of materials, the ash technique was performed in addition to EDX analysis. It was found that FL and ND had significantly higher amounts of inorganic fillers compared to HC. This finding established a relationship between filler content and DC, as more inorganic fillers within the material resulted in lower DC. Although the relationship between the two is complex, the presence of more inorganic components can hinder the DC in some ways: (1) High filler content may interfere with the polymerisation reaction by physically hindering the movement of reactive sites, making it more difficult for monomers to come into close contact and react with each other. This can result in a lower DC. (2) The presence of certain types of inorganic fillers can scatter or absorb the light, which may potentially reduce the available energy to initiate the polymerisation process (Asmussen and Peutzfeldt, 1998; Ilie and Hickel, 2009; Kim et al., 2002). Based on this, there is a potential effect on the dimensional stability of the final printed denture base, where any ill-fitting denture base could attract the growth. In general, the relationship between inorganic filler content and DC is not directly straightforward, as filler content, morphology, distribution, the quality of the filler-matrix interface, and the matrix composition must be considered.

Another aspect to look at is the interlayering spaces found within FL and ND due to their manufacturing technology. Gad et al. (Gad et al., 2022b) and Greil et al. (Greil et al., 2023) found similar observation to this study in regards to water sorption, as 3D-printed denture material absorbed more water compared to conventional materials. This is due to the presence of voids and interlayer spaces of 3D-printed specimens, due to their manufacturing process, and these can accommodate water molecules. However, this phenomenon has been denied in our previously published study (Altarazi et al., 2022), as the optical microscope and SEM analysis confirmed the absence of any visible interlayering spaces.

Solubility of the material is defined as the amount of components including water-soluble elements, plasticiser, initiators, and un-reacted monomer that leached out of the specimen when immersed in water (or any other solvent) (Cucci et al., 1998). Many studies have found that the solubility of 3D-printed materials was higher in comparison to heat-cured materials or pressed

resin materials (Berli et al., 2020; Gad et al., 2022b; Greil et al., 2023; Perea-Lowery et al., 2021b). In this study, similar observation was found as the 3D-printed materials showed higher solubility compared to the control in the following order: FL > ND > HC. However, the difference between all the tested materials was insignificant. It is worth mentioning that all the tested materials are compliant with the ISO 20795-1-2013 recommendations in terms of sorption and solubility (32 µg/mm³ and 1.6 µg/mm³ respectively).

3D-printed resins are photo-polymerised resin materials, making the DC play a crucial role in determining the overall performance of the denture base. The DC can influence the water absorption behaviour of the material, as the densely cross-linked network is less susceptible to water penetration as previously explained. It is also important to consider the chemical composition of the material along with DC, as it also can play an important role in the water absorption capacity and the durability of the resin material.

Micro-hardness is a non-intrinsic, non-destructive parameter used to characterise materials (Eliades et al., 2003; Szczesio-Wlodarczyk et al., 2020). In this study, Vickers hardness and Martens hardness—two forms of static hardness measurements—were applied. Vickers hardness is calculated from the residual indentation after load removal using optical aids, and it measures the plastic deformation of the material. Meanwhile, Martens hardness is determined via a loading/unloading process that does not require subjective visual measurement of the indentation, and it measures the elastic/plastic deformation (Broitman, 2017; Czichos et al., 2011).

Vickers hardness represents the ability of the denture base to resist abrasion, scratches, and indentation on the surface during function, especially when chewing hard substances or cleaning the denture with a toothbrush after use to prevent plaque accumulation and pigmentation (Al-Harbi et al., 2019; Kawaguchi et al., 2014). In this study, similar patterns were observed between 3D-printed specimens and the HC group at baseline. Vickers hardness of HC specimens was slightly higher, but not significantly different from the 3D-printed materials. Similar to our results, other studies in the literature reported the same observations (Aati et al., 2022a; Prpic et al., 2020).

Martens hardness parameters used in this study were adopted from another study (Shahdad et al., 2007), which was suitable for use with polymer-based materials. At baseline, Martens hardness results were similar to Vickers hardness, and no significant difference was observed

between different groups. Martens hardness results in this study were in agreement with other studies that reported a range of 116-183 N/mm^2 for heat-cured denture base materials (Polychronakis et al., 2020), and 109-142 N/mm^2 for 3D-printed denture based materials (Reymus and Stawarczyk, 2021).

Flexural strength is a critical property for denture base materials, as it reflects their ability to withstand bending and twisting forces in the oral environment generated during normal functioning and natural movements. Conclusions regarding the comparison of flexural strength values between 3D-printed and conventional heat-cured materials varies in the literature. Some studies reported that 3D-printed materials showed lower values compared to the heat-cured materials (Gad et al., 2022c; Prpic et al., 2020). Others found comparable results (Aati et al., 2022a; Di Fiore et al., 2022). In contrast, some studies reported that 3D-printed materials showed higher values compared to the conventional materials (Greil et al., 2023). This variation in the comparison may be related to the settings used during the printing of the 3D-printed specimens, and the composition of the materials used in the comparison. In 3D-printing manufacturing, photopolymerised resin materials are used, and these materials depend on printing parameters and post-curing procedures (Dimitrov et al., 2006; Puebla et al., 2012a; Z.-c. Zhang et al., 2019). In this study, the printing orientation and post-curing process followed another study (Altarazi et al., 2022), where a vertical orientation (90° to the build platform) and 30-minute curing time settings were used to obtain the optimal mechanical and physical properties for the same material. Most studies do not report the printing orientation used; however, Lowery et al. (Perea-Lowery et al., 2021b) reported using a horizontal orientation and indicated a lower flexural strength of the 3D-printed material compared to the conventional one. On the other hand, Greil et al. (Greil et al., 2023) used a vertical printing orientation and claimed that 3D-printed specimens produced had higher flexural strength values compared to the conventional material. This is in line with previous study findings (Altarazi et al., 2022), as vertical orientation produces higher mechanical properties than horizontal printing orientation. Furthermore, some studies have reported that weaknesses associated with 3D-printed materials may be related to the layering structure within the specimens, potentially leading to poor mechanical properties due to internal defects (Gad et al., 2022c). However, the present study results for the optical microscope and SEM analysis of fractured surfaces did not reveal such defects (Appendix: Figure B1 and Figure B2), which aligns with the findings of other researchers. (Altarazi et al., 2022; Unkovskiy et al., 2018; Vayrynen et al., 2016). These findings could explain the variety in the literature regarding different conclusions about

mechanical properties. In this study, it was found that ND and FL with vertical printing settings exhibited higher flexural strength and modulus compared to the conventional HC group. One aspect to consider when explaining the differences between heat-cured resin and 3D-printed resin materials is the filler content. Polymeric materials primarily consist of a polymer matrix (organic component) and reinforcing fillers (inorganic component) (Ferracane, 1995; Junior et al., 2008). The amount of inorganic components directly affects the mechanical properties of the material (Junior et al., 2008). In this study, it was discovered that the amounts of filler particles in ND and FL were greater than those in HC, which could further explain the superior mechanical properties associated with 3D-printed materials. Another aspect of the utmost importance is the chemical composition and structure of the resin materials. The main composition of the HC material used in this study was PMMA, while FL and ND used dimethacrylate-based polymers. Dimethacrylate and PMMA are both acrylic-based polymers, but they have some differences in their chemical structure and properties with PMMA (Anusavice et al., 2012; Ratner et al., 2004). Dimethacrylates are compounds with two methacrylate groups, often connected by a spacer molecule. They are typically formed by the reaction of methacrylic acid with a diol or other di-functional molecule. PMMA is a polymer derived from the polymerisation of methyl methacrylate (MMA) monomers. The chemical structure consists of repeated units of methyl methacrylate linked together to form a linear chain. PMMA can form cross-linked structures, but the degree of cross-linking is generally lower than that of dimethacrylate-based resins. In contrast, dimethacrylate-based resins are specifically designed to create highly cross-linked polymer networks. This is because the presence of two methacrylate groups allows for the formation of multiple covalent bonds between polymer chains. As a result, dimethacrylate-based resins exhibit greater mechanical strength and rigidity compared to PMMA (Anusavice et al., 2012).

Impact strength is an important intrinsic characteristic of denture base materials, representing their resistance to fracture after an accidental drop (da Cruz Perez et al., 2014; Faot et al., 2006). It has been reported that 80% of mandibular denture fractures are caused by impact forces (Sasaki et al., 2016). The impact strength test measures the amount of energy that can be absorbed by the material before rupturing (Abdulwahhab, 2013; Faot et al., 2006). The results of this study showed no significant difference in impact strength between the tested materials, although 3D-printed materials demonstrated a slight superiority. Some studies reported similar observations with no significant difference between 3D-printed and heat-cured materials (Al-Dwairi et al., 2023; Alshaikh et al., 2022; Lee, 2020). Others reported the opposite (Chhabra

et al., 2022; Gad et al., 2022c), and the diversity in conclusions could be attributed to the factors previously explained for the flexural strength test, as many variables could lead to different conclusions, especially with 3D-printed materials.

During their use, denture base materials are exposed to 100% humidity (Reymus and Stawarczyk, 2021). The objective of the artificial aging procedure in this study was to replicate the conditions inside the mouth and evaluate its effect on the materials' characteristics. The aging process had a significant effect on the surface properties of the materials but not on the mechanical ones. The Vickers hardness for all tested groups was lower, and similarly, a significant decrease in Martens hardness was reported for the HC material, while a slight decrease was associated with the ND and FL. This increased decline in Martens hardness for the HC compared to the 3D-printed ones reveals more plastic/elastic deterioration on its surface, which might be related to the filler content of the materials, as HC had fewer fillers compared to the other groups. It is challenging to make additional inferences from these findings, as the exact composition and percentages of the 3D-printed materials is not disclosed by the manufacturers, and for this reason, it would be desirable to determine their composition. Flexural and impact strength decreased slightly with the aging process, but not significantly. It is worth mentioning that the surface and mechanical properties are not correlated, and one cannot replace the other to characterise the materials' properties after aging (Fischer et al., 2010).

3D-printed materials are considered a promising alternative option for conventional materials, and the results of this study support that. However, the results published in this field should be interpreted with care, as the diverse distribution of conclusions may result from different factors, such as differences in resin composition, printing orientations, and post-printing polymerisation procedures, which can have detrimental effects on the objects produced. Using one type of heat-cured material can be considered a limitation of this study. Another limitation is that the specimen dimensions did not simulate a real-time denture base. Further studies can be conducted using the same materials in a real denture base configuration to obtain more clinically relevant results. Furthermore, volumetric changes during sorption and solubility testing should be monitored to examine whether any dimensional changes may occur. Additionally, impact strength of the 3D-printed materials could be compared with high-impact PMMA, a material commonly employed to prevent denture fractures.

5.6. CLINICAL SIGNIFICANCE

3D-printed denture base materials proved to be a considerable alternative to conventional heat-cured materials with an acceptable level of mechanical and surface properties for prosthetic dentistry.

5.7. CONCLUSIONS

1. 3D-printed resin materials (NextDent and Formlab) showed a slightly lower DC compared to its heat-cured counterpart.

2. The investigated 3D-printed denture base materials were compliant with the ISO 20795-1-2013 recommendations in terms of sorption and solubility. However, their performance was lower compared to the heat-cured materials, especially water sorption, as the difference was significant.

3. At baseline, the surface properties including Vickers and Martens hardness, and the impact strength of the 3D-printed materials, were shown to be comparable to those of the conventional heat-cured material. Additionally, the flexural strength of the 3D-printed material was superior to its counterpart.

4. The ageing process in artificial saliva for three months affected the surface properties of the heat-cured material, including Vickers and Martens hardness, and only Vickers hardness for the 3D-printed materials. However, it had only a slight, non-significant effect on mechanical properties such as flexural strength/modulus and impact strength.

Chapter 6: 3D Printed Denture Base Material: Effect of Incorporating TiO_2 Nanoparticles and Artificial Ageing on the Physical and Mechanical Properties

Ahmed Altarazi, Julfikar Haider, Abdulaziz Alhotan, Nick Silikas, Hugh Devlin

doi.org/10.1016/j.dental.2023.10.005

6.1. ABSTRACT

Objectives: To evaluate the physical and mechanical properties of three-dimensional (3D) printed denture base resin incorporated with TiO_2 nanoparticles (NPs), subjected to physical ageing process.

Methods: Acrylic denture base samples were prepared by Stereolithography (SLA) 3D printing technique reinforced with different concentrations (0.10, 0.25, 0.50, and 0.75) of silanated TiO_2 NPs. The resulted nanocomposite materials were characterised in terms of degree of conversion (DC), sorption/solubility flexural strength, impact strength, Vickers hardness, and Martens hardness and compared with unmodified resin and conventional heat-cured (HC) material. The nanocomposites were reassessed after subjecting them to ageing in artificial saliva. The fractured surface was studied under a scanning electron microscope (SEM).

Results: The addition of TiO_2 NPs into 3D-printed resin significantly improved flexural strength/modulus, impact strength, Vickers hardness, and DC, while also slightly enhanced Martens hardness compared to the unmodified resin. Sorption values did not show any improvements, while solubility have improved significantly. The addition of 0.10 wt.% NPs provided the highest performance amongst the other concentrations, and 0.75 wt.% NPs showed the lowest. Although ageing degraded the materials' performance to a certain extent but the trend remained same. SEM images showed a homogenous distribution of the NPs at lower concentrations (0.10 and 0.25 wt.%) but revealed agglomeration of the NPs with the higher concentrations (0.50 and 0.75 wt.%).

Significance: The outcomes of this study suggested that the incorporation of TiO_2 NPs (0.10 wt.%) into 3D-printed denture base material showed superior performance compared to the unmodified 3D-printed resin even after ageing in artificial saliva. The nanocomposite could be considered to extend service life of denture bases in future clinical use.

Keywords

3D printed resin; Titanium dioxide; Nanoparticles; Nanocomposite, Stereolithography (SLA); Additive manufacturing; Denture base;

6.2. INTRODUCTION

The advancement of medical technology and expertise has increased the life expectancy (Slade et al., 2014), leading to a rise in the prevalence of complete edentulism, which is a significant oral health issue among the elderly (Al-Rafee, 2020; Cooper, 2009). Although various treatment options are available, complete removable dentures remain the preferred choice (Anadioti et al., 2020; Lee and Saponaro, 2019). However, the materials used to fabricate dentures must meet specific requirements, including sufficient strength, to comply with the minimum acceptable clinical ISO guideline (Diwan, 2004). Polymethyl methacrylate (PMMA) is the most commonly used denture base material due to its low cost, excellent aesthetics, outstanding stability, biocompatibility, and ease of repair (Zafar, 2020). However, PMMA has several drawbacks, including low strength, polymerisation shrinkage, high susceptibility to microbial colonization, and low wear resistance in an aqueous environment (Alla et al., 2015; Gautam et al., 2012). To address these issues, researchers have attempted various methods to strengthen PMMA, with the use of nanoparticles (NPs) being one of the most promising approaches (Gad et al., 2017; Gad et al., 2016). In dentistry, incorporating nanosized fillers in PMMA has been explored as a means of enhancing properties of the dental materials (Chaijareenont et al., 2012). The resulting composite material's properties are influenced by the type, size, shape and concentration of the additional NPs used in conjunction with the type of polymer matrix (Jordan et al., 2005). One such nanoparticle is TiO_2, which is known for its distinct characteristics, including biocompatibility, chemical stability, non-toxicity, corrosion resistance, and high strength and refractive index. Additionally, TiO_2 NPs have been shown to possess excellent antimicrobial properties (Alwan and Alameer, 2015; Ghahremani et al., 2017; Khaled et al., 2007; Li et al., 2006). Even the smallest addition of TiO_2 NPs such as 0.5 wt.% as a reinforcing agent to a polymeric material can significantly affect the resulting hybrid material's mechanical, physical, optical, and chemical properties (Chatterjee, 2010; Reijnders, 2009).

In recent years, digital manufacturing technologies have been widely adopted in dentistry. Computer-aided design and computer-aided manufacturing (CAD-CAM), encompassing subtractive and additive methods, such as 3D-printing and rapid prototyping, have enabled the production of removable dentures (Dawood et al., 2015; Kessler et al., 2020). 3D-printing is a manufacturing technique that builds products one layer at a time (Dawood et al., 2015; Kessler et al., 2020). It has gained popularity in recent years due to the many advantages it offers over

the traditional approaches for instance this technology reduces the time a dentist needs to create and fit dentures to just 2-3 sessions. It simplifies the process of making replacements by utilising previously stored digital data and also eases the burden on dental technicians. Moreover, it either matches or outperforms the traditional method in terms of the overall accuracy of the produced dentures (Cristache et al., 2020; Lee et al., 2019; Masri et al., 2020). Its fast-evolving nature and wide range of applications makes it an enabling technology in emerging dentistry (Dawood et al., 2015; Kessler et al., 2020).

The use of 3D-printing in creating complete removable denture bases has become increasingly popular both in research and clinical practices. However, this method still has limitations related to its mechanical and physical properties (Alifui-Segbaya et al., 2019; Lee, 2020). Studies have shown that double bond conversion in 3D printing is poorer than in traditional acrylic resins (Alifui-Segbaya et al., 2019). Additionally, 3D-printed resin exhibits inferior flexural strength, elastic modulus, impact strength, and surface hardness when compared to the heat-polymerised resin (Gad et al., 2022c; Perea-Lowery et al., 2021b). Nevertheless, research has demonstrated that incorporating various additives can enhance the properties of 3D-printed materials. Aati et al. found that adding ZrO_2 to 3D-printed resin improved the quality of the temporary restoration over time (Aati et al., 2021a). Similarly, Mubarak et al. found that adding 1 wt.% silver-titanium dioxide nanofiller improved the tensile and flexural strength of the 3D-printed material (Mubarak et al., 2020). Chen et al. also demonstrated that the addition of cellulose nanocrystals and silver NPs to a 3D-printed resin improved its flexural and impact strength (S. Chen et al., 2018). Finally, a recent study investigating the effects of SiO_2 NPs on 3D-printed denture base resin found improvements in impact strength, flexural strength, and hardness (Gad et al., 2022a). Considering these findings, the addition of NPs appears to be a promising reinforcing strategy for 3D-printable materials.

To the best of the author's knowledge, previous studies have neither investigated the effect of incorporating TiO_2 NPs on the mechanical, physical, surface properties, and DC of 3D-printed resins for denture-base fabrication, nor have they examined the impact of aging on the resulting composite material's physio-mechanical properties. Thus, the aims of this study were to assess i) the flexural strength, ii) flexural modulus, iii) impact strength, iv) surface hardness (including Vickers and Martens hardness), v) DC, and vi) sorption and solubility of a series of 3D-printed denture-base resins containing increasing amounts of TiO_2 NPs after setting and after storage. The null hypotheses were that (1) adding TiO_2 NPs to the 3D-printed denture base material

would have no influence on the properties of 3D-printed denture base resin, and (2) the aging process in artificial saliva (AS) would not show any effect on the physical and mechanical properties.

6.3. MATERIALS AND METHODS

6.3.1. Resin and filler materials

The denture bases examined were manufactured using a commercial NextDent denture 3D+ light-cured resin (3D systems, Soesterberg, Netherland) in a light pink hue (LOT: WW251N04). The manufacturer indicated that it has an ultimate flexural strength of 84 MPa, a flexural modulus of 2382 MPa, a sorption of 28 $\mu g/mm^3$, and a solubility of 0.1 g/mm^3. The safety data sheet for the product shows that the resin contains Ethoxylated bisphenol A dimethacrylate (75%), 7,7,9-trimethyl-4,13,14,dioxo-3,14,diazahexadecane-1,16-diyl bismethacrylate (10–20%), 2-hydroxyethyl methacrylate (5–10%), Silicon dioxide (5–10%), diphenyl (2,4,6–trimethylbenzoyl) phosphine oxide (1–5%), and titanium dioxide (<0.1%).

Silane (KH-550) coated titanium dioxide NPs in the rutile form (LOT: 7920-111419) with a size of 10-30 nm (99.5%) was bought and added (Skyspring nanomaterials, Texas, USA).

6.3.2. Fabrication and ageing of the specimens

TiO_2 powder was a weighed using an electronic scale with a precision of 0.01 mg, and the compositions are shown in Table 6.1. To ensure a uniform mixture without any powder particle agglomeration, the TiO_2 powder was progressively added to the liquid resin before being mixed with a speed mixer at 2000 rpm for five min. Due to the higher concentration of NPs, the 0.50 wt.% and 0.75wt.% groups required two mixing stages: first, half the amount of powder was mixed with the liquid resin and then the other half was added. The composite material was then poured into the tray of the 3D printer to initiate the printing process.

Table 6.1. Weight percent of TiO_2 in combination with 3D acrylic resin content of the specimen groups

Groups	Composite material (3D printed liquid resin + TiO_2)	3D printed liquid resin (g)	Added TiO_2 NPs (g)
A (control)	0%	100.0	0.0
B	0.1 wt.%	99.9	0.10
C	0.25 wt.%	99.75	0.25
D	0.5 wt.%	99.50	0.50
E	0.75 wt.%	99.25	0.75

A total of 420 specimens were manufactured including 3D-printed and HC materials (Figure 6.1). A Formlabs Form 2 printer (Formlabs, Somerville, USA), utilising SLA technology with a 405 nm laser wavelength and a 50 µm layer thickness, was used to manufacture 3D-printed specimens in a vertical orientation, which was previously shown to optimise mechanical properties (Altarazi et al., 2022). Preform software (Formlabs, Somerville, USA) was used to prepare the digital specimens before the printing process (Figure 6.2). After printing, all specimens were immersed in 99.8% ethanol for five minutes in a Form Wash container (Formlabs, Somerville, USA). After that, specimens were exposed to air for ten minutes to eliminate any residual ethanol traces according to the manufacturer's instructions. Subsequently, the specimens were cured in an ultraviolet (UV) light curing box with a 405 nm LED wavelength and 39W power at 60°C (Formlabs, Somerville, USA). The cured specimens were ground using a water lubricant, polished with silicon carbide papers with grain sizes of 400 (P600), 600 (P1200), and 1200 (P2500), and finally polished with 0.05 µm MasterPrep Alumina discs. Figure 6.3 represents a schematic stepwise fabrication for the 3D-printed specimens.

In line with the manufacturer's guidelines, the heat-cured material (HC) powder was blended into the liquid until a uniform mixture exhibiting a pliable, dough-like texture was achieved. This blend was then hand-loaded into a mould. Upon sealing the mould and placing it in a hydraulic press exerting a pressure of 15 MPa, surplus material was scraped off from the mould periphery. The mould was subsequently submerged in a curing bath for a span of six h. to initiate polymerisation at a temperature of 80°C. It was then taken out and permitted to gradually cool down for 30 min to ambient temperature prior to unsealing the mould to extract the specimens. A polishing machine (Interlab, Hull, UK) was thereafter utilised to trim, grind, and buff the specimens, employing pumice powder, emery paper and a tungsten carbide bur.

The artificial saliva solution was prepared by dissolving the specific ingredients listed in Table 6.2 in 1000 ml of distilled water with a pH of 5.52. After being stored in artificial saliva for three months at 37°C, the specimens were evaluated for mechanical properties. A new solution was added every 14 days to maintain the solution's freshness.

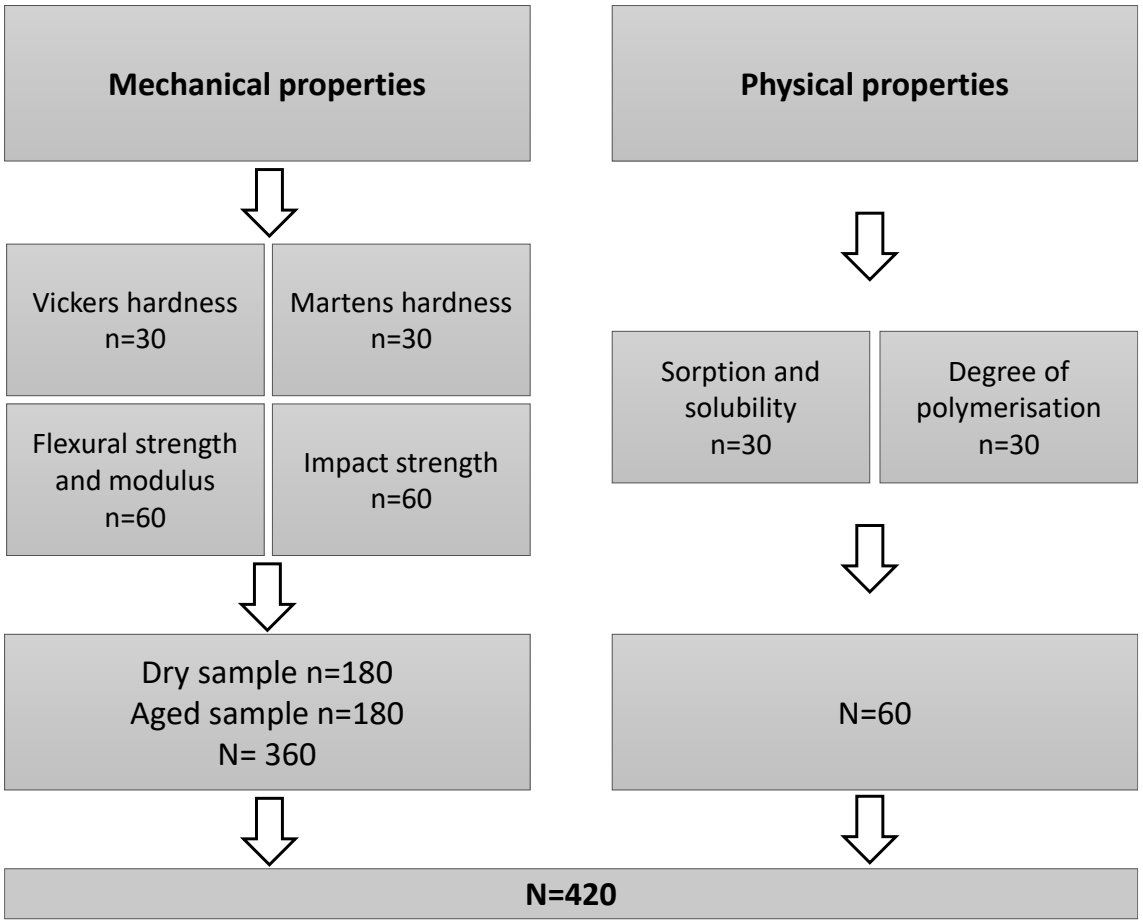

Figure 6.1. Overall plan for characterisation study

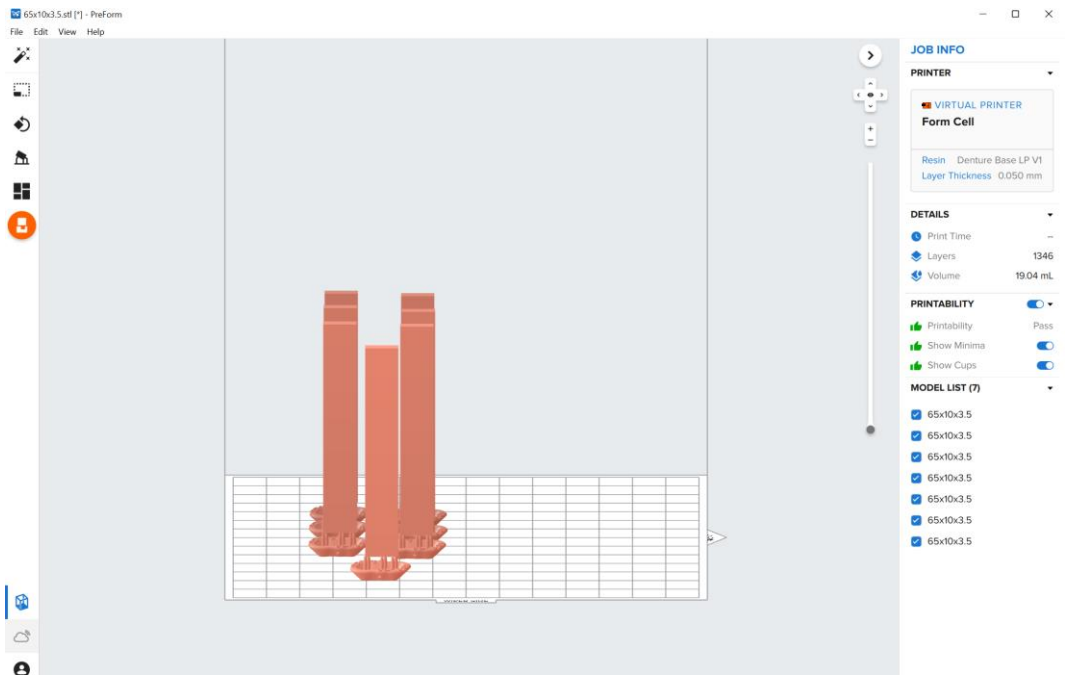

Figure 6.2. Preparing the digital specimens via Preform software before printing

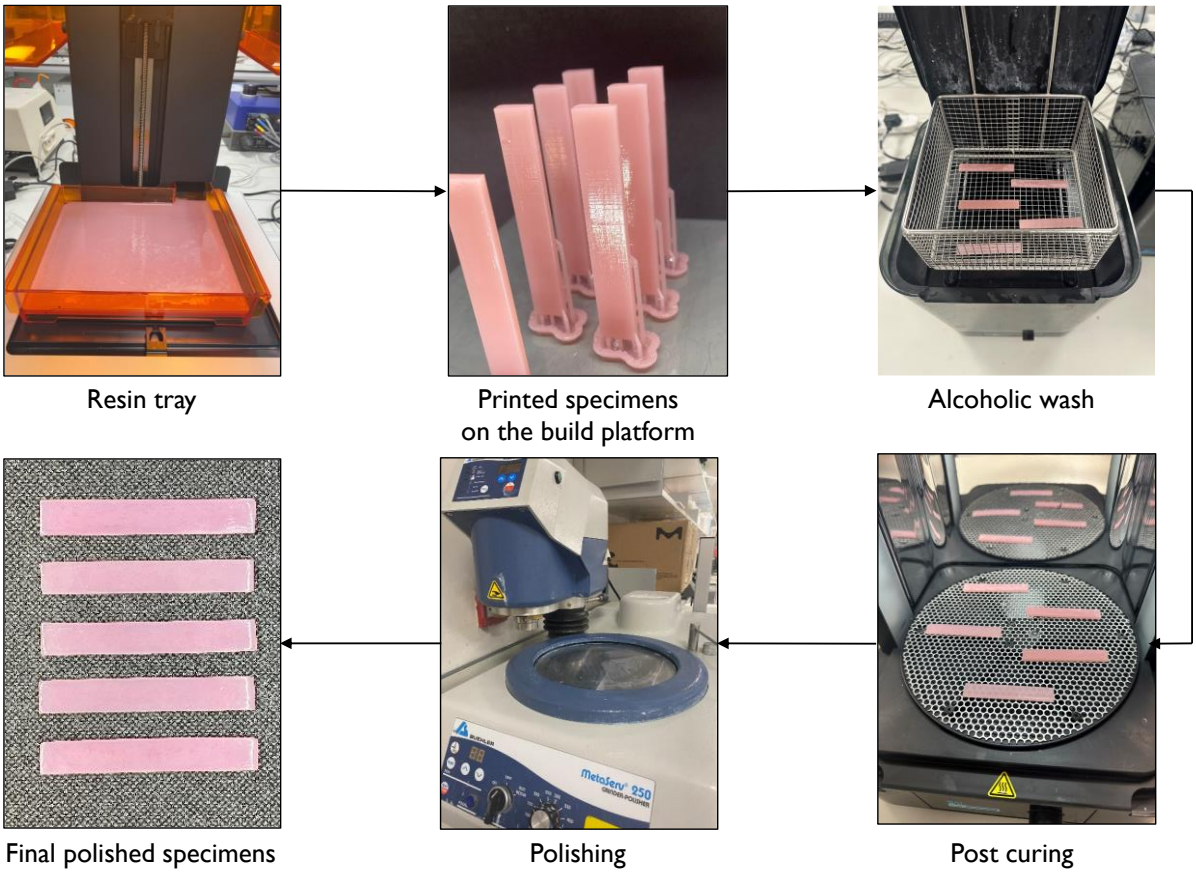

Figure 6.3. 3D-printed specimens' stepwise fabrication

Table 6.2. Composition of artificial saliva

Compound	Amount (g/l)	Manufacturer
Sodium chloride (NaCl)	0.400	Acros Organics
Potassium chloride (KCl)	0.400	Fisher Chemical
Calcium chloride ($CaCl_2$)	0.795	Acros Organics
Sodium dihydrogen phosphate (NaH_2PO_4)	0.690	Alfa Aesa
Sodium sulphate hydrate ($Na_2S.9H_2O$)	0.005	Acros Organics

6.3.3. Characterisation of the specimens

6.3.3.1. FTIR study

Spectra were collected in the 4000-400 cm^{-1} wavelength range at a resolution of 4 cm^{-1}, with an average of 32 scans measured using the Spotlight 200i FT-IR Microscope System at a temperature of 23 ±1 ^{o}C (Figure C.1). To calibrate the equipment, a background spectrum was used.

To determine the DC of the 3D-printed specimens (n=5), Fourier Transform Infrared (FTIR) spectroscopy was utilised with a single reflection ATR accessory. The resin substance used in 3D printing was scanned once while still in liquid form to provide a baseline record and once again after the final polymerisation (15×2 disc-shaped specimens). The DC for the 3D-printed material in percentage was determined by evaluating the ratio of the double carbon bond peaks at two frequencies: the stretch of the aliphatic frequency at 1637cm^{-1} against the reference aromatic frequency at 1608 cm^{-1} (Equation 6.1). For the HC specimens, the referenced peak used was the ester group (C=O) at 1720 cm^{-1} (Equation 6.2). Regarding the preparation to prevent the oxygen noise effect, it was self-resolved with the liquid resin form as it covers the crystal properly. The peaks produced appeared with no air noises.

$$\text{DC (\%)} = (1 - \left(\frac{\left(\frac{1637^{-1}}{1608^{-1}}\right) peak\ hights\ after\ polymerisation}{\left(\frac{1637^{-1}}{1608^{-1}}\right) peak\ hights\ before\ polymerisation} \right) \times 100 \quad (6.1)$$

$$\text{DC (\%)} = (1 - \left(\frac{\left(\frac{1637^{-1}}{1720^{-1}}\right) peak\ hights\ after\ polymerisation}{\left(\frac{1637^{-1}}{1720^{-1}}\right) peak\ hights\ before\ polymerisation} \right) \times 100 \quad (6.2)$$

6.3.3.2. Sorption and solubility

To conduct sorption and solubility tests per the ISO 20795-1:2013 standard for Denture Base Polymers, each test group (n=5) with a disc dimensions of 50 × 1 mm underwent the following procedures. First, the specimens were conditioned to room temperature in a desiccator with newly dried silica gel for 60 min before being weighed to acquire the baseline mass (m_1). The baseline mass was established by daily repeated weighing until the variation between consecutive measurements was no higher than 0.2 mg. Then, the diameter and thickness of each specimen were measured using a digital calliper to determine its volume.

Following that, the specimens were submerged in artificial saliva at 37±2°C, and their mass was measured daily after each withdrawal from the solution and subsequent drying until the difference between subsequent weighing was no higher than 0.2 mg (m_2). The specimens were then reconditioned by placing them in a desiccator with freshly dried silica gel for a day at 37±2°C, followed by another desiccator for an hour at ambient temperature with freshly dried silica gel. The desorption technique was repeated daily until a constant refurbished mass (m_3) was acquired, with the discrepancy between subsequent weighing was no larger than 0.2 mg.

Using Equations (6.3) and (6.4), the sorption and solubility in g/mm^3 were calculated. The percentage of mass change and mass loss throughout the sorption and solubility tests were determined using Equations (6.5).

$$\text{Sorption} = \frac{m2-m3}{V} \tag{6.3}$$

$$\text{Solubility} = \frac{m1-m3}{V} \tag{6.4}$$

$$\text{Change in mass (\%)} = \left(\frac{m^t - m1}{m1}\right) \text{x } 100 \tag{6.5}$$

Where m^t is the mass of the specimen at a certain time point

6.3.3.3. Vickers and Martens hardness

A Vickers micro-hardness instrument (FM-700, Future Tech Corp, Tokyo, Japan) was utilised to determine the HV of the specimens. A test load of 50 g was set with a dwell time of 30 s, and each disc (n=5) with a dimension of 15 × 2 mm was polished as described in section 6.3.2 before creating three indentations along a straight line at evenly spaced spots.

A Martens Hardness Instrument (Z2.5, ZwickRoell Ltd., Leominster, UK) with a Vickers hardness measurement tip was utilised to determine Martens hardness. The specimen's top surface and the hardness measuring head were kept at a fixed distance of 18 mm at the start of each test session. A force of 50 N was applied at a rate of 5 N/s for 30s before release. Before contact, the indenter tip was moving at 40 mm/min with an initial approaching rate of 100 mm/min. The proximity between each specimen and the sensor tip was 40 µm. Five controlled indentations were made at baseline with identical spacing on each specimen (n=5 for each ageing condition). The test load and indentation depth were automatically recorded during the loading and unloading the Vickers indentation tip (136°) and presented as load-displacement curves. To avoid obtaining duplicate measurements at the same location, the indentations were placed along several lines marked on the surface of each specimen. The software (TestXpert®, Zwick GmbH & Co, Ulm, Germany) automatically extracted Martens hardness (HM) as well as other parameters including indentation modulus (E_{IT}) and indentation creep (C_{IT}). The calculations of HM was based on Equations (6.6) from ISO 14577-4/2016.

$$HM = \frac{F}{As\ (h)} = \frac{F}{26.43 * h^2} \quad (6.6)$$

HM was expressed in N/mm^2, where F is the load in N, As (h) is the indenter's surface area at a distance of h from the tip in mm^2, and As is the indenter's surface area in mm^2 (0.3). Each specimen underwent five indentations 24 h after dry manufacture and again after being stored in artificial saliva for three months.

6.3.3.4. Flexural strength and modulus

The flexural strength of the specimens was determined through a three-point bending test conducted on a universal testing machine (Zwick/Roell Z020, Leominster, UK) equipped with a 500N load cell, following ISO 20795-1:2013 standards for denture base polymers. Specimens (n=10 with 64 x10 x 3.3), were first immersed in distilled water at 37°C for 50 h. to establish baseline values. The specimens were then positioned onto a supporting jig, with a distance of 50±0.1 mm between the supports. These were polished cylinders: 3.2 mm in diameter and 10.5 mm in length. The tests were carried out at a preload and test speed of 5 mm/min. This measurement was considered as a baseline measurement. Another set of specimens were kept in artificial saliva for three months, and then tested to measure the effect of ageing on the flexural strength and modulus.

Flexural strength was determined using Equation (6.7), where F is the maximum applied force in N, l is the distance between the supports in mm, b is the specimen s width in mm, and h is the specimen height in mm. To calculate the flexural modulus, Equation (6.8) was used, where d is the deflection in mm at the load of F1, F1 is the load in N at the point on the straight line (with the highest slope) of the load/deflection curve.

$$\sigma = \frac{3Fl}{2bh^2} \tag{6.7}$$

$$E = \frac{F_1 l^3}{4bh^3 d} \tag{6.8}$$

6.3.3.5. Impact test

The Charpy un-notched impact test was conducted using a universal pendulum impact testing device (Zwick/Roell Z020 Leominster), following EN ISO 179-1:2010 standards (n=10 for each ageing condition). The specimens, with dimensions of 80 mm ±0.5 in length, 10 mm ±0.2 in width, and 4±0.2 mm in thickness, were horizontally supported at both ends (40±0.2 mm) and struck at the centre using a free-swinging pendulum with a 4.0J load cell released from a fixed height. The amount of energy absorbed during impact was recorded in joules (J). The Charpy impact strength (a_{cU}) (kJ/m^2) was calculated using Equation 6.9. This measurement was regarded as the baseline reading. A separate collection of specimens were stored in artificial saliva for a duration of three months to determine the impact strength of the aged specimens.

$$a_{cU} = \frac{W_B}{bh} \times 10^3 \tag{6.9}$$

Where W_B represents the energy at break in joules, and b and h are the specimen's width and thickness in mm, respectively.

6.3.3.6. SEM and EDX analysis

Specimens were mounted on an aluminium stub, and a thin layer of gold was deposited before placing it in the scanning electron microscope (SEM) chamber. Images were captured at different magnifications ranging from ×1000 to ×100000 using a secondary electron detector with an acceleration voltage of 10.0kV.

6.3.4. Statistical analysis

All data were statistically analysed using SPSS version 25 (IBM, New York, NY, USA). The Shapiro-Wilk test was used to determine the distribution of the data, and the Levene test was utilised to confirm its homogeneity. The data were statistically analysed using one-way ANOVA, followed by Tukey's/Games-Howell post-hoc analysis according to data homogeneity, to compare the means between groups with a significance level set at $p \leq 0.05$.

6.4. RESULTS

6.4.1. Fractured surface analysis

SEM images at a magnification of ×100k revealed the presence of two types of fillers within the tested 3D-printed specimens. Silicon dioxide (SiO_2), as reported by the manufacturer to make up 5-10 % by weight, appeared as shapeless crystal (Appendix: Figure C.2), and TiO_2 NPs that were added to the resin material in this study at different weight percentages, and they appeared as smaller spherical clusters. The smaller spherical particles were not found within the unmodified NextDent resin. To further investigate the distribution and quantity of TiO_2 NPs present within the specimens, EDX mapping and analysis were performed. EDX mapping at many sites confirmed the distribution of TiO_2 NPs, showing that as the amount of NPs increased, so did their agglomeration (Appendix: Figure C.3 and Figure C.4). Furthermore, EDX quantitative spectral analysis confirmed the presence of TiO_2 NPs and verified the variation in the amount of NPs corresponding to each group (Table 6.1). On group A, although there were minor traces of TiO_2 NPs (<0.1 wt.%), it was not shown on the SEM and EDX analysis, as a minimal amount of the NPs are needed before it to be possible to be detected.

6.4.2. Degree of conversion

Figure 6.4 presents the means and standard deviations of DC for the examined materials. One-way ANOVA indicated a significant differences between groups mean values ($p<0.001$), and Tukey's post hoc showed that Group A had the lowest DC, showing a significant difference in comparison to HC group ($p<0.001$). For the nanocomposite groups, the DC rose significantly compared to Group A, and the results became not significantly different compared to HC, except for Group E, at which point the value declined and became significantly lower than HC

($p<0.002$). The remaining TiO_2 NPs groups had lower values compared to HC, but these differences were not statistically significant ($p>0.05$).

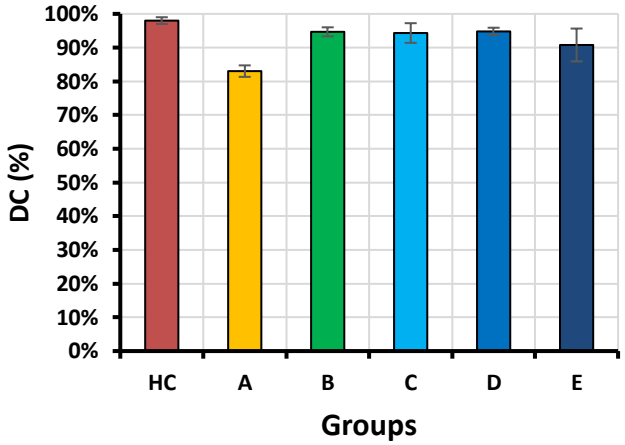

Figure 6.4. Mean values of DC of the tested materials. (HC: heat-cured;A: unmodified NextDent; B: 0.10; C: 0.25; D: 0.50; E: 0.75 TiO_2 NP wt.%)

6.4.3. Sorption and solubility

The means and standard deviations for sorption and solubility are provided in Figures 6.5 and 6.6 respectively. One-way ANOVA exhibited a significant difference between groups' mean values ($p<0.001$). The lowest sorption value was observed for the HC group, which was significantly lower than the other groups ($p<0.03$). This was followed by 3D-printed/ TiO_2 NPs groups (except Group E), where they displayed non-significantly different values compared to Group A ($p>0.05$). Group E showed the highest sorption value with a significant difference compared to the other tested groups ($p<0.001$).

In contrast, solubility exhibited a different pattern. The highest solubility value was associated with the Group A, followed by the HC and they were not significantly different from each other ($p>0.05$). Both groups had significantly higher solubility values compared to the 3D-ptinted/ TiO_2 NPs groups ($p<0.001$), with the exception of Group E, which showed the highest solubility amongst the 3D-ptinted TiO_2 NPs groups and became not significantly different compared to Group A and HC ($p>0.05$).

All study groups observed changes in mass over time when stored in artificial saliva. Throughout the sorption process, there was a rapid mass increase in the initial 14 days, which then slowed until equilibrium was achieved on day 42, as depicted in Figure 6.7. Subsequently,

during the desorption process, the mass consistently reduced in the first 7 days and then continued to decrease slowly until a state of balance was reached on the 28th day of the desorption process.

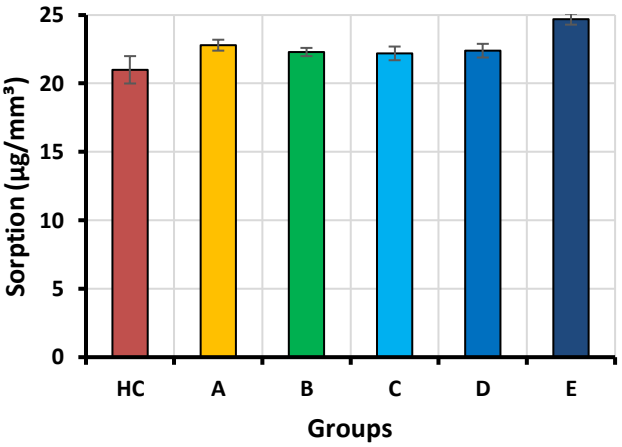

Figure 6.5. Sorption values of the tested materials in artificial saliva for six weeks (HC: heat-cured;A: un-modified NextDent; B: 0.10; C: 0.25; D: 0.50; E: 0.75 TiO_2 NP wt.%)

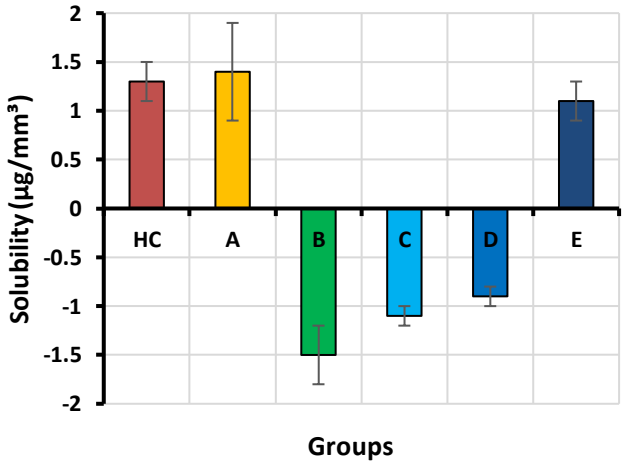

Figure 6.6. Solubility values of the tested materials in artificial saliva for five weeks. (HC: heat-cured;A: un-modified NextDent; B: 0.10; C: 0.25; D: 0.50; E: 0.75 TiO_2 NP wt.%)

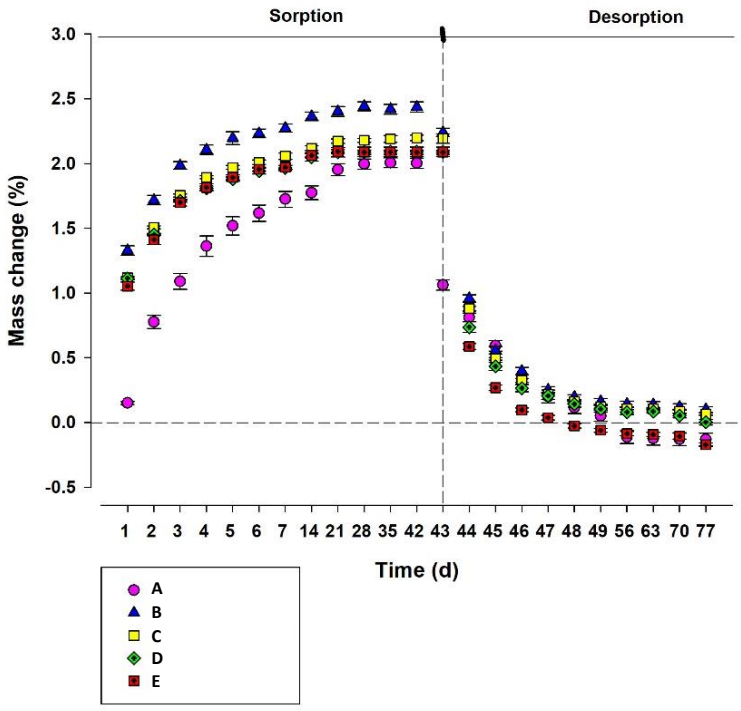

Figure 6.7. A graph illustrating the mass change of specimens immersed in AS over 77 days. (HC: heat-cured;A: un-modified NextDent; B: 0.10; C: 0.25; D: 0.50; E: 0.75 TiO_2 NP wt.%)

6.4.4. Vickers and Martens hardness

The mean and standard deviation of Vickers hardness are displayed in Figure 6.8. One-way ANOVA indicated a significant difference between the groups' mean values ($p<0.001$). Before aging, no significant difference was observed among the groups except for Group A, which had significantly lower value compared to others ($p<0.04$). After aging, Group B showed the highest value, while HC showed the lowest. Vickers hardness decreased in value with the increase in TiO_2 NPs to be significantly lower with Group D and E compared to other 3D-printed/TiO_2 NPs groups ($p<0.001$). When comparing the same group before and after aging, Vickers hardness decreased significantly in the HC, D, and E groups ($p<0.001$). However, this observation was not seen with the other 3D-printed/TiO_2 NPs groups, where the decrease was not significant ($p>0.05$).

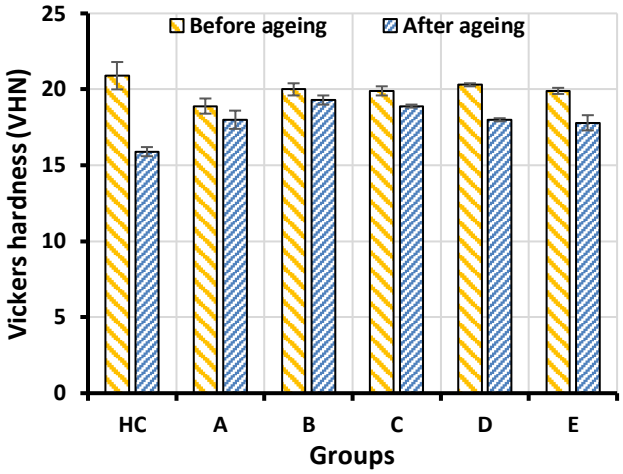

Figure 6.8. Vickers hardness of the tested materials before and after ageing in artificial saliva for three months. (HC: heat-cured;A: un-modified NextDent; B: 0.10; C: 0.25; D: 0.50; E: 0.75 TiO_2 NP wt.%)

Figure 6.9 present the mean and standard deviation of Martens hardness for all groups before and after aging. One-way ANOVA indicated a significant difference between groups' mean values ($p<0.005$). Before aging, no statistically significant differences were observed between the groups (column wise Table C2 Appendix C). On the other hand, the aged HC group exhibited a significantly lower value compared to the other aged groups ($p<0.05$), except for the Group E ($p>0.05$). However, when compared between before and after ageing within each group (row wise Table C2 Appendix C), all values decreased after the aging process without significant differences, except for the HC group, where the value decreased significantly ($p<0.001$). The indentation modulus (Table C2 Appendix C) demonstrated a trend similar to that of Martens hardness, with the notable exception of the Group A, which exhibited a significantly lower value before the ageing process compared to other groups ($p<0.03$). Within each group, the ageing process did not induce any significant impact, except for the Group A, where the result significantly increased ($p<0.001$). The indentation creep (Table C2 Appendix C) was significantly greater with HC compared to the other groups before ageing ($p<0.001$), and the ageing process significantly affected only Group D and E ($p<0.002$).

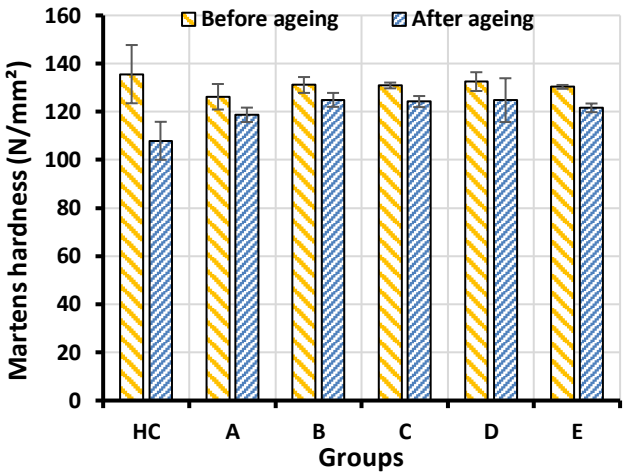

Figure 6.9. Martens hardness of the three tested materials before and after ageing in artificial saliva for three months. (HC: heat-cured;A: un-modified NextDent; B: 0.10; C: 0.25; D: 0.50; E: 0.75 TiO_2 NP wt.%)

6.4.5. Flexural strength and modulus

Figure 6.10 and Figure 6.11 display the means and standard deviations of flexural strength and modulus for the control and tested materials before and after the aging process. In terms of flexural strength, one-way ANOVA showed a significant difference between groups' mean values ($p<0.001$), and the post hoc analysis registered that the HC group had the lowest value, showing a significant difference compared to the other groups ($p<0.001$). Conversely, Group B exhibited the highest value with a significant difference compared to the other groups ($p<0.001$). The flexural strength of the materials decreased as the amount of TiO_2 NPs increased beyond 0.10 wt.% (Group B), with the lowest value associated with group E compared to the other nanocomposite groups. The aging process significantly and negatively impacted all groups containing TiO_2 NPs ($p<0.001$) except for Group C ($p>0.05$). Although the values for the HC and Group A also decreased after the aging process, the decline was not significant ($p>0.05$).

The flexural modulus exhibited a pattern nearly similar to the flexural strength, where one-way ANOVA registered a significant difference between groups' mean values ($p<0.001$). The HC group had the lowest value, but no significant difference was observed compared to Group A and E ($p>0.05$). Groups B and C demonstrated the highest value, with a significant difference compared to all other tested groups ($p<0.001$). The aging process significantly affected some of the groups containing TiO_2 NPs (Group B and D) and the HC group ($p < 0.001$).

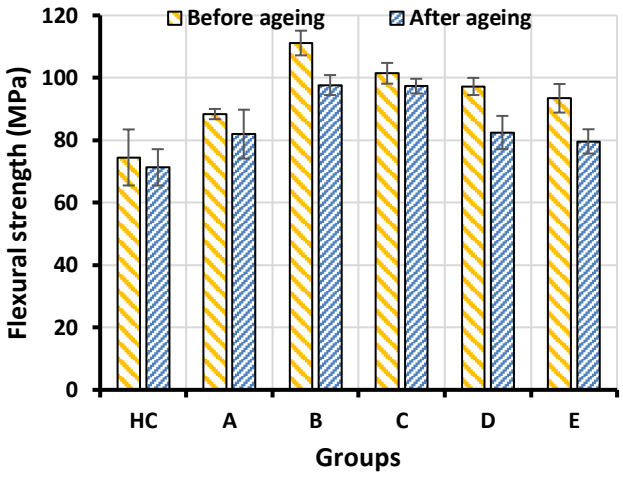

Figure 6.10. Flexural strength of the tested materials before and after ageing in artificial saliva for three months. (HC: heat-cured;A: un-modified NextDent; B: 0.10; C: 0.25; D: 0.50; E: 0.75 TiO_2 NP wt.%)

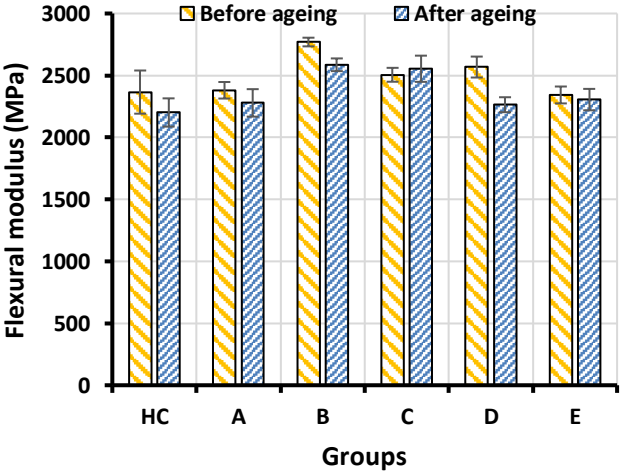

Figure 6.11. Flexural modulus of the tested materials before and after ageing in artificial saliva for three months. (HC: heat-cured;A: un-modified NextDent; B: 0.10; C: 0.25; D: 0.50; E: 0.75 wt. TiO_2 NP %)

6.4.6. Impact test

The means and standard deviations of the impact strength test are displayed in Figure 6.12. One-way ANOVA indicated a significant difference between groups' mean values ($p<0.001$). Before aging, no statistically significant difference was observed between the HC and Group A ($p>0.05$). However, a significant difference was noted between these groups and Group B ($p<0.005$). The impact strength values of Groups D and E decreased slightly compared to

Group B, and became not significantly different from the other groups, including Group A and HC ($p>0.05$).

After aging, the results were similar, except for Group E, which exhibited a significantly lower value compared to Groups B and C ($p<0.05$). Furthermore, ageing process did not show any significant difference on the impact strength ($p>0.05$).

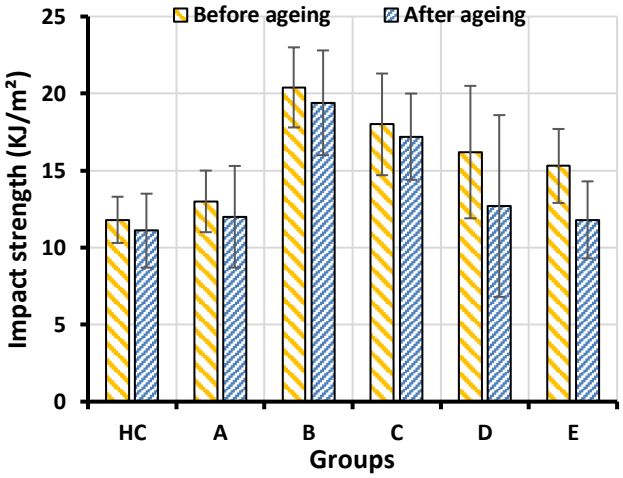

Figure 6.12. Impact strength of the tested materials before and after ageing in artificial saliva for three months. (HC: heat-cured;A: un-modified NextDent; B: 0.10; C: 0.25; D: 0.50; E: 0.75 wt. TiO_2 NP %)

6.5. DISCUSSION

The effect of adding TiO_2 NPs into the 3D-printed denture base resin was investigated in this study. According to the results, the first null hypothesis was rejected, as the addition of TiO_2 NPs altered the properties of the 3D-printed denture base resin. Furthermore, the second null hypothesis was also rejected, as the ageing process in artificial saliva adversely affected some of the properties of the 3D-printed nanocomposites.

TiO_2 NPs remained a preferred additive metal oxide to be added to denture base resin due to their advantages, including cost-effectiveness, ease of availability, biocompatibility, chemical stability, solid physical properties, and antimicrobial properties (Bangera et al., 2020). Numerous researchers have incorporated metal oxide NPs into dental resin materials, and treated their surfaces to prevent agglomeration, which arises from the repulsive interaction between PMMA and the NPs (Hamming et al., 2009). Moreover, achieving a uniform dispersion was difficult due to the Van der Waals forces between the NPs, which may further

cause agglomeration and hence adversely affect the composite material (Gad and Abualsaud, 2019). The goal was to achieve a homogeneous dispersion and interaction of the NPs within the matrix of material. To accomplish this, researchers have altered the surfaces of the NPs with modifiers, such as proteins and acids (Alshaikh et al., 2022; De Palma et al., 2007; Frankamp et al., 2006; Gad et al., 2022a). In this study, TiO_2 NPs with silanated surfaces were used in conjunction with a speed mixing technique to minimise agglomeration and achieve as uniform a dispersion of the NPs as possible. It is worth noting that even minor discrepancies in the manufacturing process of 3D-printed materials can significantly impact the properties of the resultant object.

The amount of TiO_2 NPs incorporated in this study was based on two factors. First, two previous studies used TiO_2 NPs with 3D-printed denture base resins (Chen et al., 2019; Totu et al., 2017), where they used a range of 0.10 – 2.5 wt.% TiO_2 NPs. Second, in a pilot run in this study aimed to check the printability of the composite material with difference percentages of TiO_2 NPs. It was found that the addition of 2.0 wt.% of TiO_2 NPs increased the viscosity of the liquid resin and led to failure in printing, so a range of TiO_2 NPs between 0.10 – 1.0 wt.%. was used After initial testing, it was found that the tested properties significantly decreased after adding 0.75 wt.% TiO_2 NPs, hence a range between 0.10 - 0.75 wt.% TiO_2 NPs was considered for this work.

Flexural strength is a critical property for denture bases to be tested, as it is considered the primary mode of clinical failure (Alshaikh et al., 2022). The results in this study indicated a higher flexural strength of Group A (89.2 MPa) compared to HC (74.5 MPa), which was opposite to the findings in other studies (Al-Dwairi et al., 2023; Alshaikh et al., 2022; Gad et al., 2022a). The reason behind this could be related to the HC control material used in other studies with differences in their compositions compared to the HC material used in this study, as well as the printing settings and the chemical composition of the 3D-printed materials used. Lowery et al. (Perea-Lowery et al., 2021b) reported a value of 90 MPa for their tested material, and Aati et al. recorded 134 MPa when testing the flexural strength of 3D-printed denture base material (Aati et al., 2022a). All the previous values recorded revealed a similar or higher flexural strength compared to the current results, which confirm that the various conclusions between 3D-printed and heat-cured materials mainly depended on the materials used in different studies. Also, the printing parameters could have a direct effect on the mechanical properties of the 3D-printed material; for example, one study used a horizontal printing

orientation and reported a lower flexural strength of 3D-printed denture base material compared to the conventional material (Perea-Lowery et al., 2021b), while a different study used a vertical printing orientation, and indicated a higher flexural strength of the 3D-printed material compared to the conventional one (Greil et al., 2023).

The integration of TiO_2 NPs into 3D-printed resin significantly increased both flexural strength and modulus. Group B exhibited the highest readings in comparison to the Group A and HC. However, the flexural strength reduced as the concentration of NPs increased beyond this point, with group E showing no significant difference compared to Group A. The enhancement in flexural strength and modulus after the addition of TiO_2 NPs is a concentration-dependent process. TiO_2 NPs are physically rigid particles that can fill voids within the material's matrix. With proper distribution, they can absorb energy and stresses before failure (Gad and Abualsaud, 2019; Mangal et al., 2020b). TiO_2 nanoparticles, being physically rigid, can play a significant role in absorbing energy within the material. When external forces or stresses are applied to the material, these nanoparticles can help distribute the stress more evenly throughout the matrix. As a result, they act as stress absorbers, reducing the concentration of stress at specific points (Bangera et al., 2020; Gad and Abualsaud, 2019; Mangal et al., 2020b). Lower concentrations of TiO_2 NPs (Groups B and C) yielded the highest flexural strength and modulus, consistent with other studies involving different types of NPs with 3D-printed dental resins (such as SiO_2, ZrO_2, and TiO_2 NPs) (Aati et al., 2021a; Chen et al., 2019; Gad et al., 2022a). As the NPs concentration increased, the properties began to decrease. This was confirmed by previous studies and attributed to NPs agglomeration within the matrix that can create stress concentration areas, thus weakening the material's internal structure (Ahmed et al., 2016; Sodagar et al., 2013).

The main reason for denture failure after an accidental fall is the lower impact strength associated with denture base materials (Faot et al., 2006; Gad et al., 2022c). Hence, adequate impact strength is required to protect the denture base from this type of failure. Impact strength showed a similar behaviour to flexural strength and modulus, as impact strength of Group A was slightly higher compared to the HC. Group B showed a significantly increased impact strength compared to the Groups A and HC, and the value decreased with higher concentrations of filler until Group E, where the value was slightly higher but not significantly different compared to Group A and HC. Other studies reported the same observation after incorporating different types of NPs into 3D-printed and heat-cured denture base resins (Alshaikh et al., 2022;

Alwan and Alameer, 2015; Gad et al., 2022a; Ghahremani et al., 2017; Mosalman et al., 2017). The interpretation of this observation is aligned to the analysis with the flexural strength and modulus mentioned above.

Group A had a lower Vickers hardness compared to that of the HC, in line with other studies reporting similar observations (Gad et al., 2022c; Prpic et al., 2020). This could be related to the difference in DC between the materials, as HC had a significantly higher DC compared to Group A. After adding TiO_2 NPs, Vickers hardness increased significantly, and this increase was directly proportional with the increase in DC. Aati et al. (Aati et al., 2021a) studied the effect of adding ZrO_2 NPs to 3D-printed denture bases and noticed that Vickers hardness values increased until a certain point, where the composite material became saturated. Similarly, Gad et al. investigated the effect of adding SiO_2 NPs and found a significant increase in Vickers hardness values compared to the unmodified material. Both aforementioned studies' findings agreed with the findings in this study. Although the increase in the Vickers hardness was statistically significant, the clinical value of that increase might be irrelevant.

Martens hardness exhibited behaviour similar to the Vickers hardness. Group A displayed a lower value compared to HC, and as TiO_2 NPs were added, Martens hardness increased, which was also correlated to DC for each group. This can be attributed to the enhancement of material stiffness and the reduction of matrix mobility due to the addition of rigid particles that may be present on the surface of the specimen, which decreases the elastic-plastic deformation. Similar observations were found in other studies, indicating an increase in surface hardness for heat-cured denture base materials after adding TiO_2 NPs (Alwan and Alameer, 2015; Harini et al., 2014; Hashem et al., 2017; Mosalman et al., 2017).

To further explain the change in surface hardness, DC for each group was investigated. As shown in Figure 6.4, DC of the HC sample was highest. A potential explanation for the enhanced DC of the HC material in comparison to the 3D-printed materials could be the manufacturing process. The HC material is polymerised under more extreme conditions of temperature and pressure, and for a prolonged period (cycled for six hours in a water bath); this could potentially contribute positively to the DC (Doğan et al., 1995; Garcia et al., 2010; Wong et al., 1999). Another possibility is the filler content of the materials, as a higher DC could be attributed to the absence of fillers within the matrix of HC material. The addition of filler particles, such as silicon dioxide found within 3D-printed resin to increase the viscosity of the material, can affect the polymerisation process of the resin matrix by reducing the mobility of

the unreacted monomers (Aati et al., 2021a). This may lead to a change in the DC, which is a measure of the extent to which monomers are converted into polymers during the polymerisation process (Bartoloni et al., 2000). On the other hand, the results of this study indicated that the addition of TiO_2 NPs increased the DC of the resultant composite material. In some cases, certain types of fillers with specific shape, size, concentration, and distribution within the resin matrix can increase DC. In this case, TiO_2 NPs might have helped scatter curing light energy within the 3D-printed material and increased the rate of DC, which may explain the increase in surface hardness and the mechanical properties of the composite material compared to the unmodified one (Asmussen and Peutzfeldt, 1998; Ilie and Hickel, 2009).

Water sorption and solubility of the denture base are important properties that can indirectly measure denture durability within the oral cavity. The polar nature of the polymeric material, due to the presence of the ester group, can interact with water molecules through hydrogen bonding, which could lead to water absorption and consequently affect the properties of the material (Polat et al., 2003; Saini et al., 2016). Sorption and solubility tests in this study were conducted in artificial saliva until equilibrium was reached, at which point the specimen could no longer gain any weight. The sorption process lasted about 2-4 weeks, while the solubility test (desorption) lasted around 1-2 weeks for all the tested groups. Based on the results of this study, the sorption increased in the following order: HC < C < B < D < A < E. A relationship between sorption and DC can be established here, as HC showed the highest DC, followed by 3D-printed/ TiO_2 NPs groups and finally Group A. A higher rate of DC is an indication of a more condensed and cross-linked polymeric matrix, which has fewer unreacted monomers and fewer spaces for water molecules. As a result, the material with a higher DC will typically have lower water sorption (Aati et al., 2022a; Ferracane et al., 1998; Ghavami-Lahiji et al., 2018; Imazato et al., 1999). HC sample showed the lowest saliva sorption compared to other groups, which might be related to the higher DC that resulted from a long polymerisation cycle (6 hours in a water bath) to achieve full polymerisation and the lowest amount of void formation (Garcia et al., 2010). With the addition of TiO_2 NPs, DC was enhanced compared to the unmodified resin as explained earlier. Additionally, the addition of TiO_2 NPs could fill the pores within the material, decreasing the uptake of water molecules. The type of silane used is KH-550, which is characterised by having an epoxy (oxirane) functional group, a methoxy group, and a propyl chain attached to the silicon atom. The epoxy group is reactive and can form chemical bonds with a variety of dental resins. This makes KH-550 suitable for promoting adhesion between polymers and inorganic surfaces by facilitating covalent bonding between the two.

Furthermore, the hydrophobic nature of silane coated TiO_2 NPs could aid in decreasing the water uptake (Pazokifard et al., 2015). It is worth mentioning that Group E had the highest sorption value compared to other 3D-printed/ TiO_2 NPs groups, and the lowest DC, which may have resulted from the agglomeration of particles that adversely affected various properties of the material. The observation in this study was in agreement with a study that used ZrO_2 NPs with 3D-printed provisional dental restorations (Aati et al., 2021a), and other studies which investigated the addition of TiO_2 NPs to heat-cured denture base materials (Alwan and Alameer, 2015; Tuna et al., 2008). On the other hand, saliva solubility showed different behaviour. Solubility depends mainly on the leached-out materials such as unreacted monomers, plasticisers, and initiators (Cucci et al., 1998). The addition of TiO_2 NPs decreased solubility significantly, and the values of solubility from lowest to highest were as follows: B < C < D < E < HC < A. Two possible explanations can be drawn for this observation: (1) the increased DC with the 3D-printed/ TiO_2 NPs groups, which decreases the amount of unreacted monomers, and (2) the interaction between TiO_2 NPs and saturated remaining monomers (Doğan et al., 1995).

Clinically, denture bases are exposed to a process of sorption/desorption frequently. Along with the dynamic intraoral environment, both apply significant stresses to the brittle nature of the prosthesis, which can greatly affect its properties. The aim of our aging assessment of the tested materials in artificial saliva was to mimic the oral environment and then evaluate the effect of aging on the materials' properties. In general, the aging process in artificial saliva adversely affected all the mechanical and surface properties of the tested materials, with some differences among the tested groups. For example, Vickers hardness and Martens hardness of the HC group were significantly affected by the aging process, while only Vickers hardness of Groups E and D were significantly affected, which showed that the elastic/plastic behaviour of the 3D-printed material acted differently. This could be explained by the different composition of the two tested materials, and as the composition of the 3D-printed material was not clearly illustrated by the manufacturer, a definite conclusion cannot be reached on that. On the other hand, flexural strength and impact strength of the HC samples and the Group A were not affected significantly by the aging process. However, the 3D-printed/TiO_2 NPs groups showed a significant reduction in the properties, especially with higher concentrations of TiO_2 NPs, where the concentration of the NPs at higher levels can agglomerate within the material and act as local stress areas where cracks can initiate and negatively affect the properties of the

material. SEM images approved the presence of agglomeration within the groups with higher concentrations of TiO_2 NPs.

The results of all the tested properties for all tested groups were compatible with the ISO recommendations, even after exerting artificial ageing process to the tested material. Further studies on colour stability and accuracy are suggested, as the TiO_2 NPs are whitish in colour, and the change in colour with higher concentrations is very noticeable (Appendix: Figure C.5). Also, concentrations between 0.0-0.10 wt.% of TiO_2 NPs are recommended for future studies to determine the optimal concentration. Additionally, exploring the biological properties is worthwhile, since TiO_2 NPs have antibacterial capabilities which could benefit denture wearers by protecting against bacterial/fungal growth.

6.6. CLINICAL SIGNIFICANCE

Clinically, 3D-printed denture base material has proven to be a promising alternative to conventional heat-cured materials. Combining this with nanotechnology could further improve the current denture properties leading longer service life and patient satisfaction and address the drawbacks of existing conventional materials.

6.7. CONCLUSIONS

1. Incorporating TiO_2 NPs into 3D-printed NextDent denture base resin significantly increased the properties such as flexural strength/modulus and impact strength, Vickers hardness, as well as DC and solubility compared to the unmodified material. The highest values were associated with the addition of 0.1 wt.% TiO_2 NPs. However, the effect on saliva sorption and Martens hardness, was not significant.

2. An increased concentration of TiO_2 NPs of 0.5 wt.% and higher showed agglomeration of the NPs under the microscope, which lowered the material properties compared to those with lower concentrations of TiO_2 NPs.

3. The aging process in artificial saliva negatively affected both the heat-cured and the modified 3D-printed materials, particularly with respect to flexural strength, where the effect was significant.

Chapter 7: 3D-Printed Nanocomposite Denture Base Resin: The Effect of incorporating TiO_2 Nanoparticles on the Growth of Candida albicans

Ahmed Altarazi, Layali Jadaan, Andrew J McBain, Julfikar Haider, Evgeny Kushnerev, Julian M Yates, Abdulaziz Alhotan, Nick Silikas, Hugh Devlin

doi.org/10.1111/jopr.13784

7.1. ABSTRACT

Aim: To develop a biocompatible denture base resin/ TiO_2 nanocomposite material with antifungal characteristics that is suitable for 3D-printing denture bases.

Methods: TiO_2 nanoparticles (NPs) with a 0.10, 0.25, 0.50, and 0.75 weight percent (wt.%) were incorporated into a commercially available 3D-printed resin material. The resulting nanocomposite material was analysed and compared to the control (0% added NPs) using Lactate dehydrogenase (LDH) and AlamarBlue (AB) assays for the biocompatibility testing with human gingival fibroblasts (HGF). The composite material was also tested for its antifungal efficacy against *Candida albicans.* Fourier transform infrared (FTIR) and Energy Dispersive X-ray Spectroscopy (EDX) mapping were conducted to assess the surface silane coating and the dispersion of the NPs.

Results: LDH and AB assays confirmed the biocompatibility of the material showing cells proliferation at a rate of nearly 100% at day 10, with a cytotoxicity of less than 13% of the cells at day 10. The concentrations of 0.10, 0.25, and 0.50 wt.% caused a significant reduction of the candida cells attached to the surface of the specimens ($p<0.05$), while 0.75 wt% did not show any significant difference compared to the control (no TiO_2 NPs) ($p>0.05$). FTIR and EDX analysis confirmed the presence of TiO_2 NPs within the nanocomposite material with a homogenous dispersion for 0.10 and 0.25 wt.% groups, and an aggregation of the NPs within the material as the concentrations went higher.

Significance: The addition of TiO_2 NPs into 3D-printed denture base resin proved to have an antifungal effect against *Candida albicans*, and the optimal concentration was 0.25 wt.% The resultant nanocomposite material was a biocompatible material with HGFs, and was successfully used for 3D-printing.

Keywords

Denture base resin; titanium dioxide; additive manufacturing; cytotoxicity; antifungal; Candida albicans.

7.2. INTRODUCTION

The introduction of CAD–CAM systems using additive manufacturing or three-dimensional (3D) printing has led to myriad novel modalities of restorative dentistry (J. W. Stansbury and M. J. Idacavage, 2016). Fabricating removable dentures using 3D-printing compared to the conventional methods introduced several advantages such as the simplicity in the laboratory construction, cost-effective fabrication, and enabling complicated structure creation, leading to individualized prosthetic therapies in the clinical settings (Berman, 2012; Beuer et al., 2008; Osman et al., 2017; J. W. Stansbury and M. J. Idacavage, 2016).

Many patients can experience fungal infection or denture stomatitis due to wearing poorly fitted prostheses and failing to maintain good oral hygiene (Pereira et al., 2013). Denture related oral candidiasis is considered to be the most prevalent fungal infection in the mouth. Risk of oral candidiasis can be as high as 65% (Akpan and Morgan, 2002; Gendreau and Loewy, 2011). Researchers identified several risk factors associated with oral candidiasis in previous studies, including immune suppression, diabetes, extended use of antibiotics, hyposalivation, and inhaled corticosteroids (Lockhart et al., 1999; Pereira et al., 2013). The antibacterial/antifungal properties of removable dentures have been the subject of numerous studies (Monteiro et al., 2012; Totu et al., 2017), including research on surface modification, the addition of functional nanoparticles, and antibiotic compounds.

Natural compounds exhibit antifungal properties as a therapeutic method for treating fungal infection. This method is gaining popularity due to the safety and efficacy of this approach (Dalben-Dota et al., 2010). Titanium dioxide nanoparticles (TiO_2 NPs), for instance, have demonstrated effective antifungal properties. In addition, TiO_2 with NPs is an inexpensive biocompatible material with good chemical stability, low toxicity, great strength, and a high refractive index (Alwan and Alameer, 2015; Ghahremani et al., 2017; Li et al., 2006). Moreover, research has shown that even a small amount of TiO_2 NPs reinforcing agent added to a polymeric material can change the hybrid material's chemical, electrical, physical, and optical properties (Chatterjee, 2010; Reijnders, 2009). Because of its photocatalytic property, TiO_2 NPs can produce reactive oxygen species (ROS) that can oxidize and decompose microorganisms. Now, researchers have recognised TiO_2 as an antifungal agent that can be incorporated within biomaterials to constrain the microbial activities of many microorganisms. These including gram-positive and gram-negative bacteria, fungi, and viruses (Anehosur et al., 2012; Aziz, 2018; Ghahremani et al., 2017) due to its capability to produce ROS (Tsuji et al.,

2016). They also possess some antifungal properties that can break down and oxidise other organic and inorganic compounds when exposed to UV radiation in the presence of oxygen and water. As such, it can be regarded as a useful antifungal addition to dental materials (L. S. Acosta-Torres et al., 2011).

Researchers reported that TiO_2 NPs embedded in heat-cured PMMA denture base material could reduce the microbial numbers. Anehosur et al. (Anehosur et al., 2012) concluded that adding 3.0 wt.% TiO_2 NPs to PMMA had a beneficial antibacterial impact. Totu et al. (Totu et al., 2017) demonstrated that incorporating 0.4% TiO_2 NPs into a 3D-printed denture base resin resulted in a notable antifungal effect, particularly when exposed to UV light. Also, Chen et al. (Chen et al., 2017) showed that adding 3 wt.% TiO_2 NPs to PMMA-based resin had an antibacterial/fungal impact. Plaque development on the surface of PMMA/TiO_2 nanocomposite materials was prevented by its ability to reduce the microbial population, which also prevents quorum sensing (Anehosur et al., 2012). By exposing their dentures to solar energy or other light sources to activate the TiO_2 NPs, patients can conveniently maintain the hygiene of their dentures due to the material's photocatalytic capability to reduce the number of micro-organisms. This capability offers broad spectrum antimicrobial action, targeting gram-positive, gram negative bacteria, and fungi. More importantly, TiO_2 NPs-polymer nanocomposite has a natural affinity for the environment and operates as a non-contact biocide (Hashem et al., 2017). As a result, TiO_2 NPs have been proposed as a top candidate for polymeric fillers with antibacterial/ antifungal actions.

The objectives of this study were: (1) to develop a TiO_2 NP incorporated resin composite material suitable for fabricating dental prosthetics via 3D-printing, (2) to evaluate its antifungal properties against *Candida albicans*, and (3) to assess the biocompatibility of the resultant composite material. The first null hypothesis stated that the nanocomposite material would not have any adverse biological effects, while the second null hypothesis was the resultant composite material would not exhibit antifungal properties.

7.3. MATERIALS AND METHODS

7.3.1. Resin material and TiO_2 NPs

The material used for the denture base manufacturing in the current study was commercial NextDent denture 3D+ light-cured resin in a light pink colour (3D systems, Soesterberg, Netherlands).. The safety data sheet for the product states that the resin has the following composition (w/w%): Ethoxylated bisphenol A dimethacrylate (75%), 7,7,9-trimethyl-4,13,14,dioxo-3,14,diazahexadecane-1,16-diyl bismethacrylate (10–20%), 2-hydroxyethyl methacrylate (5–10%), Silicon dioxide (5–10%), diphenyl (2,4,6–trimethylbenzoyl) phosphine oxide (1–5%), and titanium dioxide (<0.1%).

Silane-coated titanium dioxide NPs (Skyspring nanomaterials, Texas, USA) in a size of 10-30 nm (99.5%, rutile form) was used, as silane coupling agent can bond organic materials to inorganic surfaces, and helps with the homogenous distribution of the nano-particles. FTIR (Perkin-Elmer, Ohio, USA) analysis was conducted to determine the functional groups within the TiO_2 powder to predict the resulted type of the bond after mixing the powder with 3D-printed resin. Spectra were measured in a 4000-400 cm^{-1} wavelength range at a resolution of 4 cm^{-1}. The average number of scans was 32 using Spotlight 200i FT-IR Microscope System (FTIR, Perkin-Elmer, Ohio, USA) at room temperature.

7.3.2. Preparation and characterisation of the specimens

An electronic balance (Ohaus Analytical plus, Ohaus Corporation, USA) with an accuracy of 0.001 g was used to weigh TiO_2 powder according to Table 7.1. The TiO_2 powder was added gradually to the liquid resin and mixed with a speed mixer (DAC 150.1 FVZK, High Wycombe) for 5 min at a speed of 2000 rpm to ensure a homogeneous mixture with no aggregated granules of powder. 0.50 wt.% and 0.75 wt.% groups needed to be mixed at two stages due to the higher concentration of NPs. The resultant composite material was poured into the 3D printer's tray to proceed with the printing procedure.

Table 7.1. Weight percent of TiO_2 in combination with 3D acrylic resin content of the specimen groups

Groups	Composite material (3D-printed liquid resin + TiO_2)	3D-printed liquid resin (g)	Added TiO_2 NPs (g)
A (control)	0%	100	0
B	0.10 wt.%	99.9	0.10
C	0.25 wt.%	99.75	0.25
D	0.50 wt.%	99.5	0.50
E	0.75 wt.%	99.25	0.75

A total of 69 specimens were printed using Formlabs Form 2 printer (Formlabs, Somerville, USA), which employs SLA technology with a 405 nm laser wavelength and a layer thickness of 50 µm layers. The proposed test specimens were designed in a disc shape (15 mm x 2 mm) using an open-source CAD program (Tinkercad.com), and the design was subsequently uploaded to the printer's software in STL format. Preform software was used to manipulate the CAD design to print in a vertical (90^o) orientation. Support structures were automatically produced to support the specimen during printing. Figure 7.1 presents a schematic diagram showing the study groups the corresponding sample allocations.

After printing, all specimens were taken off the printer, removed the support structures, and submerged in a Form Wash container (Formlabs, Somerville, USA) for five minutes in ethanol 99.8% to remove any uncured resin stuck with the printed specimens from the liquid resin pool, as per the manufacturer recommendation. The specimens were then exposed to air for ten minutes to remove any traces of ethanol and placed in an ultraviolet (UV) light curing box (Formlabs, Somerville, USA) with a 405 nm LED wavelength and 39 W power at 60^oC to complete the process of polymerisation. The cured specimens were ground with a water lubricant and polished using silicon carbide papers with the following abrasive SiC grain sizes: 400 (P600), 600 (P1200), 1200 (P2500), and then polished using 0.05 µm MasterPrep Alumina disc (MetaServ 250, Buehler, IL, USA).

The dispersion of the TiO_2 NPs was studied using a scanning electron microscope equipped with an Energy Dispersive X-Ray Spectrometer (SEM-EDX, Carl Zeiss Ltd., 40 VP, Smart SEM, Cambridge, UK). The specimens were coated with a thin gold layer and mounted on an aluminium stub, and then placed into the SEM chamber. A secondary electron detector with a voltage of 10.0 kV was used to create the images at a magnification of x5000.

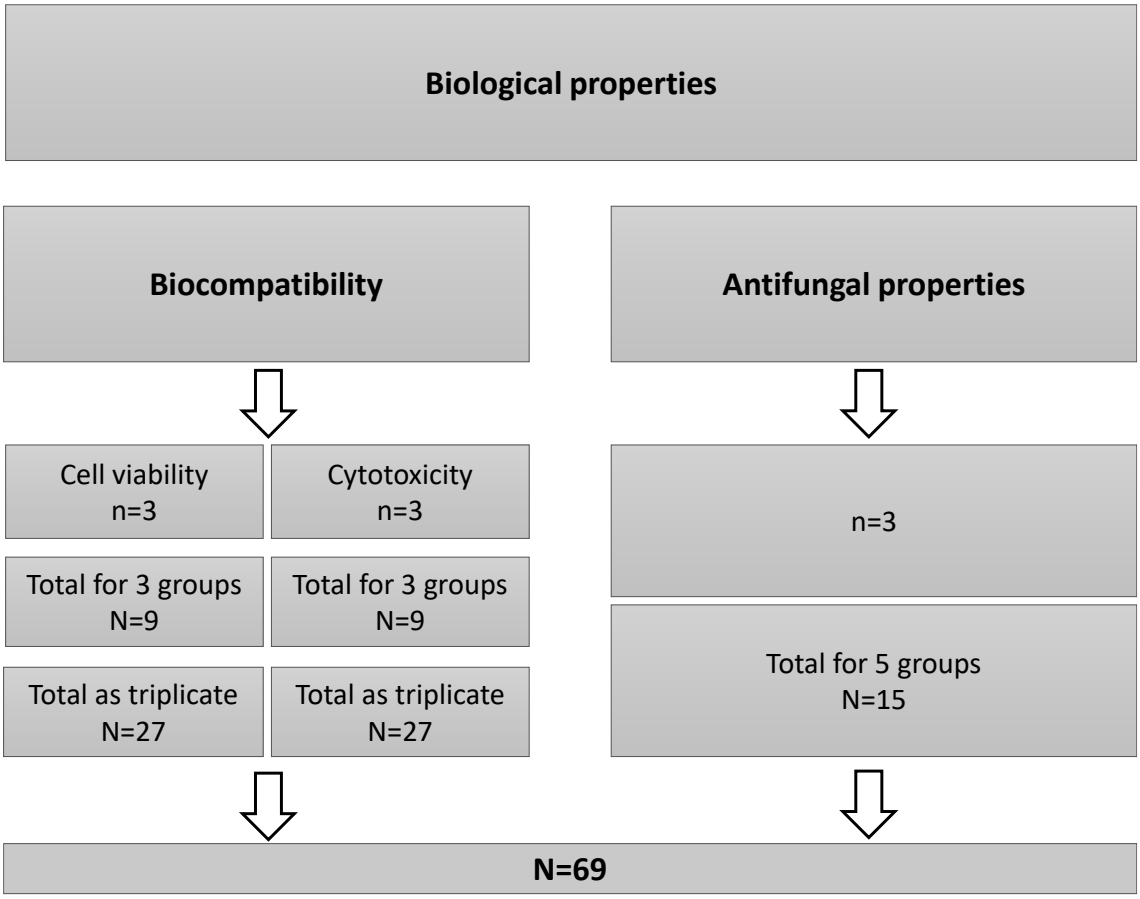

Figure 7.1. ***Overall plan for the study groups***

7.3.3. Preparation of cell culture

Standard cell culture, maintenance, freezing, and thawing protocol was employed following ISO 10993-5 (BS EN ISO, 2009) to culture commercially available primary human gingival fibroblast (HGF) cells (LCT-FC-0095, Catlag Medsystems Ltd, Buckingham, UK). HGF cells were cultured in growth medium provided by the manufacturer (LCT-LL-0001, Catlag medsystems Ltd, Buckingham, UK). The following was the final concentration for each component: L-glutamine 7.5 mM, rh FGF basic 5 ng/mL, rh insulin 5 µg/mL, rh FGF/TGF beta 5 ng/mL, ascorbic acid 50 µg/mL, and hydrocortisone hemisuccinate 1 µg/mL. Also, 30 µg/mL of gentamicin and 15 ng/mL of amphotericin B.

The cells were cultivated in a T75 flask and subsequently stored in an incubator at 37^{o} C with 5% CO_2 and 95% air. After 1 day, the cells were washed twice with Hank's balanced salt solution (HBSS) and the medium was replenished. Three days later using 0.25% trypsin, the

cells were passaged at regular intervals according to their growth properties. The cells were taken from the T75 flask once they had reached confluence and seeded into a 24-well culture plate at a density of 5×10^4 cells per well in 500 µl of a complete growth media. According to ISO standard 10993-5, the sterilised composite specimens were placed in the centre of each well once the cells had attached to the bottom of each well, signalling the start of the test (day 0).

7.3.4. Cell viability

AlamarBlue™ cell viability reagent (Thermo Fisher Scientific, IL, USA) was used to conduct a colourimetric experiment to measure cell viability. For each test at each time point, three biological replicas (24-well plate per one biological replica) were utilised at four time points (1, 3, 5 and 10 days) (n=3). The control wells, where the cells were cultivated without any composite specimen, were credited with 100% cellular viability (low control or LC).

At each time point, HGFs were exposed to alamarBlue (1:10) for 60 min at 37 °C. A 96-well plate was subsequently used to transfer 100 µl of the supernatant for examination at the time points of 1, 3, 5, and 10 days. A UVM 340 microplate reader (ASYS, scientific laboratory supplies) read the 96-well plate at 570 and 600 nanometres. Cells morphology and proliferation images were taken using a light microscope at a magnification of x10 (Olympus IX51 fluorescence microscope). Equation (7.1) was used to calculate cell viability:

$$\text{Cell viability \%} = \frac{A570 - (A600 \text{ x } Ro) \, for \; test \; well}{A570 - (A600 \text{ x } Ro) \; positive \; growth \; control} \times 100 \qquad (7.1)$$

A_{570} and A_{600} were absorbances at 570 and 600 nm respectively, and R_O was the correction factor calculated from (A_{570}/A_{600}) of the positive growth control.

7.3.5. Cytotoxicity

A Pierce™ Lactate dehydrogenase (LDH) cytotoxicity assay kit (Thermo Fisher Scientific, IL, USA) was used to examine the tested materials' potential for cytotoxicity. Each experiment at each time point involved using three biological replicas (24-well plate per biological replica) (n=3).

For each of the four-time points, 50 µl of the supernatant and 50 µl of the LDH cell reaction solutions were mixed and incubated for 30 min at room temperature and in the dark to assay HGF. After 30 min, a LDH stop solution was used to stop the reaction.

Cytotoxicity was assessed at four growth time points: 1, 3, 5, and 10 days. Controls were applied in line with the manufacturer's instructions. The maximum LDH release from the cells was determined by adding membranolytic solution and was regarded as the high control (HC), while the spontaneous LDH release (water-treated) was regarded as the low control (LC). A UVM 340-microplate reader (ASYS, scientific laboratory supplies) was employed to read the 96-well plate at 490 nm subtracted from 680 nm, and cytotoxicity was determined according to Equation (7.2):

$$\text{Cytotoxicity \%} = \frac{Specimen\ treated\ LDH\ activity - Spontaneous\ LDH\ activity}{Maximum\ LDH\ activity - Spontaneous\ LDH\ activity} \times 100 \qquad (7.2)$$

Where specimen-treated LDH activity is the LDH amount expressed by cells cultured with composite materials; maximum LDH activity is the LDH amount expressed by cells treated with membranolytic-solution; and spontaneous LDH activity is the LDH amount expressed by cells treated with water.

To assess cell viability and cytotoxicity, only the groups containing 0.25 wt.% and 0.75 wt.% TiO_2 NPs, as well as the control group (0 wt.%), were tested to represent the lowest, medium and highest particle concentrations.

7.3.6. Anti-fungal test

To test the antifungal activity of the nanocomposite material, *Candida albicans* (ATCC 10231) was cultured in Sabouraud dextrose (SD) broth at 37° C for 24 h. After incubation, the *Candida albicans* suspension was adjusted using a spectrophotometer at an optical density (OD) of 600 nm to 0.08 nm (McFarland standard), and then diluted 100 times in order to adjust the microbial cells to 1.5 x 10^6 cells per millilitre. The composite material discs were printed with a dimension of 15 × 2 mm (n=3) and placed at the bottom of a 6-well plate, where each well represented a different group. Each well was filled with 4 mL of candidal suspension and incubated at 37° C for 24 h. Following that, the specimens were washed with phosphate-buffered saline (PBS) twice to remove non-attached cells. Subsequently, the specimens in their 6-well plate were sealed and ultrasonicated at 40 kHz for 5 min to detach the fungal cells from

the surface of the specimens (USC200T, VWR, Malaysia). After ultrasonication, the fungal solution was diluted using a 96-well plate 6 times by adding 20 µl of the fungal solution into 180 µl of PBS (10 times per dilution). Subsequently, a 20 µl of the diluted fungal solution from each well was seeded into an SD agar plate in triplicates and incubated at 37° C for 24 h. The colonies were then counted and reported as colonies forming unit per millilitre (CFU/mL) (Jeon et al., 2022) using Equation 7.3. In antifungal tests, all groups were tested unlike the cytotoxicity tests.

$$\text{CFU/mL} = \frac{Number\ of\ colonies \times Total\ dilution\ factor}{Volume\ of\ the\ culture\ plated\ in\ mL} \quad (7.3)$$

7.3.7. Statistical analysis

SPSS software (SPSS ver. 25, IBM, IL, USA) was used to analyse the data. Shapiro-Wilk and Levene's tests were used to test the normal distribution and the homogeneity of variance, and two-way ANOVA was performed to analyse the effects of materials and time followed by Tukey's multiple comparison test to compare the cell cytotoxicity and viability for all the materials at different time points (α=0.05). One way ANOVA and Tukey's tests were performed to compare different CFUs/mL groups' results.

7.4. RESULTS

7.4.1. Cell viability of the nanocomposites

Three of the five groups (A, C, E) were tested for cell viability and cytotoxicity tests because the minimal and highest concentration groups should represent the effect of TiO_2 NPs well. HGF showed a high proliferation rate for all the nanocomposite groups (>70%) at day 1, with the highest proliferation rate of 95.9% (±7.6) when cultured with group C, followed by group E and group A (Table 7.2 and Figure 7.2). No significant differences were reported between the groups ($p>0.05$). At day 3, it was noted that all the proliferation percentages were decreased slightly as a normal reaction of the cells to a new object in their environment, with the lowest proliferation rate of 90.4% (±3.6) for group E, followed by group C and A. The proliferation rate at day 5 showed an increasing trend with the highest proliferation rate of 97.1% (±4.5) for group C, followed by group A and E. Similarly, an increase in the proliferation continued at day 10 for all groups with the highest proliferation rates amongst all the other days, and the

highest rate was exhibited by group C with a proliferation rate of 99.6% (±2.6), followed by group A and E. Figure 7.3 also shows the cell proliferation images for different groups at different days. Two-way ANOVA showed no significant difference between any of the TiO_2 concentration groups at any time points ($p>0.05$).

Table 7.2. Mean and standard deviation of HGF proliferation for 3D-printed resin mixed with different concentrations of TiO_2 NPs at days 1, 3, 5, and 10

Time (days)	HGF proliferation with TiO_2 Concentrations (wt.%) (SD)		
	A	C	E
1	94.0 (13.1)^{A,1*}	95.9 (7.6)^{A,1}	95.7 (1.5)^{A,1}
3	92.9 (3.8)^{A,1}	92.5 (11.8)^{A,1}	90.4 (3.6)^{A,1}
5	95.6 (10.4)^{A,1}	97.1 (4.5)^{A,1}	94.1 (12.4)^{A,1}
10	99.1 (2.5)^{A,1}	99.6 (2.6)^{A,1}	97.0 (5.1)^{A,1}

**Within a column, cells having similar letters are not significantly different from the control (day 1), and within a row, cells having similar numbers are not significantly different from the control (A).*

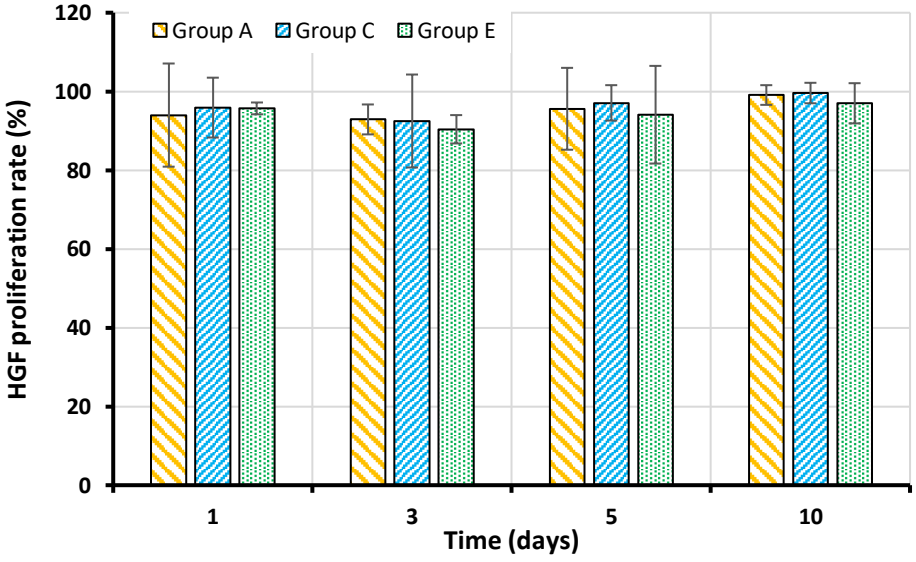

Figure 7.2. A bar chart representing the mean values of HGF proliferation in percentage at days 1, 3, 5, and 10 with different concentrations of TiO_2 NPs (wt.%) in 3D-printed resin

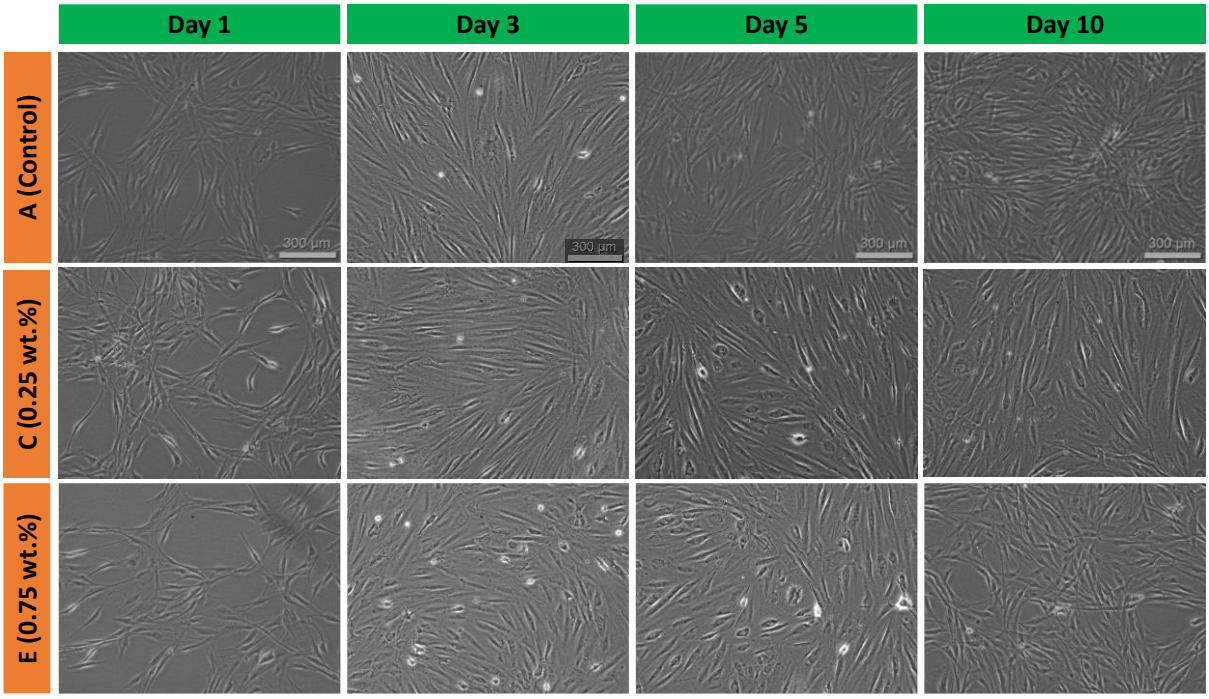

Figure 7.3. Cells morphology of HGF at days 1, 3, 5, and 10 for the control and the tested materials. The scale bar at the right bottom corner of the control material is 300µm.

7.4.2. Cytotoxicity of the nanocomposites

Cytotoxicity was lowest at day 1, with no significant differences between different groups, and the highest cytotoxicity of 5.8% (0.3) was associated with group C followed by group E and A (Table 7.3 and Figure 7.4). The cytotoxicity increased at day 3 for all groups, but with no significant differences compared to the values on day 1 and amongst all different concentrations. The order of the cytotoxicity from lowest to highest was as follows: C < E < A. At day 5, the cytotoxicity further increased and kept gradually increasing until day 10, where it showed the highest rate of cytotoxicity, with the highest value of 10.8% (1.4) associated with group C, followed by group A and E with no significant differences between different groups. Two-way ANOVA indicated a statistical difference ($p<0.002$) at 0 wt.% between day 1 and both day 5 and day 10. On the other hand, no significant difference was revealed between different time points at the other TiO_2 concentration groups ($p>0.05$).

Microscopic imaging of the cells provided a visualisation of the cell count and shape on days 1, 3, 5, and 10. HGF maintained their standard shape during the test period, and showed an increase in the proliferation rate with time in the control and the tested materials (Figure 7.3).

Table 7.3. Mean and standard deviation of HGF cytotoxicity percentage in 3D-printed resin mixed with different concentration of TiO_2 at days 1, 3, 5, and 10

Time (days)	Cytotoxicity at TiO_2 concentrations (wt.%) (SD)		
	A	C	E
1	2.6 (0.2)^{A,1}	5.8 (0.3)^{A,1}	5.8 (1.7)^{A,1}
3	7.5 (1.4)^{B,1}	7.3 (1.4)^{A,1}	7.5 (1.2)^{AB,1}
5	9.5 (1.5)^{B,1}	9.5 (1.5)^{AB,1}	10.9 (1.9)^{B,1}
10	10.8 (1.4)^{B,1}	10.8 (1.4)^{B,1}	10.4 (1.1)^{B,1}

**Within a column, cells having similar letters are not significantly different from the control (day 1), and within a row, cells having similar numbers are not significantly different from the control (A).*

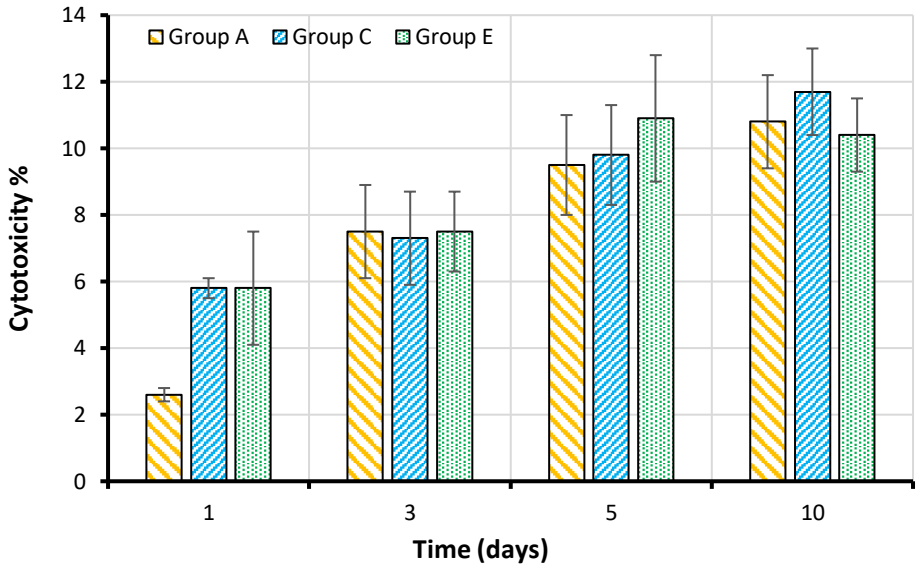

Figure 7.4. A bar chart representing the mean values of cytotoxicity in percentage at days 1, 3, 5, and 10 with different concentrations of TiO_2 NPs (wt.%) in 3D-printed resin.

7.4.3. Antifungal activity of the nanocomposites

The number of fungal colonies grown at the surfaces of 3D-printed nanocomposite specimens with different TiO_2 concentrations differs from the control discs that had no added TiO_2 NPs. The colony count decreased with an increase in TiO_2 NPs concentration (groups B, C, and D), where they showed the lowest colonies count, while Group E showed an increased colony count compared to the aforementioned groups. One-way ANOVA indicated a statistical significant increase in the colonies count in Groups A and E compared to Groups B, C, and D ($p<0.001$) (Figure 7.5). Figure D.1 at Appendix D presents *Candida albicans* colonies that was seeded in SD agars.

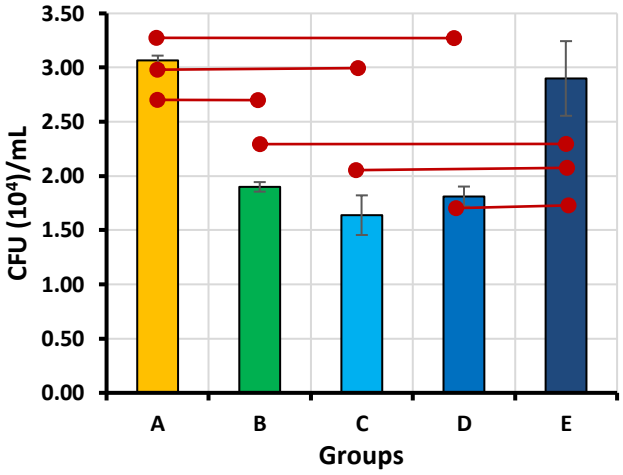

Figure 7.5. Colonies forming units per millilitre (CFU/mL) of detached cells of Candida albicans from the surfaces of 3D-printed denture base resin discs with different amounts of TiO_2 NPs in the nanocomposite groups. Horizontal red lines connecting two columns indicate significant differences

7.5. DISCUSSION

Dental practitioners have been using acrylic-based resin materials for many years in the manufacture of denture bases to restore aesthetic and masticatory functions and improve the quality of life for edentulous patients. The incorporation of 3D-printing in prosthetic manufacturing has led to a significant reduction in the burden on dental practitioners and patients by eliminating some steps in the manufacturing process, improving denture base quality, and reducing the number of patient visits (Kurzmann et al., 2017). However, 3D-printed photo-cured resin is not as strong as conventionally heat-cured PMMA (Gad et al., 2022c). To address this issue, the addition of TiO_2 to denture base resin in the form of NPs has been proposed, although the effects on human cell viability, cytotoxicity, and microorganism-killing have not been fully explored. This study confirmed the first null hypothesis, as the addition of TiO_2 NPs showed no cytotoxic effect. However, the second null hypothesis was rejected, as the composite material exhibited antifungal properties against *Candida albicans*.

To assess the nanocomposite material's biocompatibility in vitro, HGF cells were chosen due to their ease of cultivation, favourable multiplying time (doubling in 24 h), status as one of the predominant cell types in the body, and recommendation by many standard institutions (Akin et al., 2015). HGF plays a crucial role in regeneration processes and in maintaining the integrity of oral soft tissue. Denture bases come into close contact with oral soft tissue, and any adverse effect will impact the cells near the denture base, including allergic reactions, cell cytotoxicity,

and inflammation (Jerg et al., 2018; Nicholson and Czarnecka, 2008; Schulz et al., 2012; Urcan et al., 2010). Cell cytotoxicity and viability assays are considered effective indicators to evaluate the interaction of cells with different types of materials and the compounds that may release from them. Cytotoxicity assays can detect damage that may lead to cell death, while cell viability assays can quantify the number of living cells and their growth (42-44). Both tests can be conducted either by direct contact of the cells with the material, indirect contact using a barrier between the cells and the material, or by exposing the material's extracts to the cells (Sjögren et al., 2000; Thangaraju and Varthya, 2022; Wataha, 2012).

Due to an incomplete conversion of the methacrylate (MA), one of the primary components of 3D-printed denture base resin, elution of residual monomers can result in unfavourable reactions on the surrounding cells in the oral cavity (Ausiello et al., 2013; Gautam et al., 2012; R. D. Singh et al., 2013; Treglia et al., 2012). In the literature, TiO_2 NPs have proven to be chemically stable and non-toxic materials. These particles are commonly added to removable appliances because of their biocompatibility and antifungal properties (Laura S Acosta-Torres et al., 2011; Gad and Abualsaud, 2019; Trapalis et al., 2003; Tsuji et al., 2016). All of the 3D-printed nanocomposite specimens in this study with different concentrations of TiO_2 NPs showed cell viability of more than 70% when tested with the alamarBlue assay, which is the recommended reference point for cytotoxicity according to ISO 10993-5 (Thangaraju and Varthya, 2022). In fact, all tested groups with TiO_2 NPs showed nearly 100% viability at day 10, and group C showed slightly more cellular viability compared to the control group at different time points. Furthermore, none of the tested groups showed more than 12% cytotoxic activities when tested using the LDH assay at different time points (based on ISO 10993-5, ISO recommendation, below 12% would be considered biocompatible). Tsuji et al. (Tsuji et al., 2016) conducted a study of coating denture base acrylic resin with TiO_2, and they found no adverse reaction or irritation occurred in the oral mucosa, hence they concluded that TiO_2 was biocompatible. Similarly, Raj et al. (Raj et al., 2021) made a similar observation when they modified heat-cured denture base resin with different concentrations of TiO_2 NPs ranging from 3.0% – 7.0%. They stated that denture base resin with TiO_2 showed comparable or even greater cellular viability when compared to the unmodified counterpart, emphasising the biocompatibility of TiO_2 NPs.

Epidemiological studies have found that a range of 15 - 65% of patients with complete dentures have suffered from fungal infections, especially denture stomatitis, which is mainly caused by

Candida albicans (Gendreau and Loewy, 2011). The exact dominance of different fungal microorganisms varied between different studies, but it has been reported that 65 – 90 % of the denture stomatitis is caused by *Candida albicans*, in addition to other less common species of candida including *Candida glabrata*, *Candida krusei*, *Candida parapsilosis*, and *Candida tropicalis* (Coco et al., 2008; Gendreau and Loewy, 2011; Pereira-Cenci et al., 2008). Hence, the effect of the nanocomposite material against *Candida albicans* was studied specifically. The high prevalence of oral stomatitis encouraged researchers to look into solutions, e.g., by adding antifungal agents to the currently used denture materials (Bajunaid, 2022). In light of this, TiO_2 NPs are considered one of the nano-sized metal oxides, in addition to silver oxide, zinc oxide, and zirconia oxide, that has a fungicidal and/or fungistatic effect against fungal biofilm colonization and could be considered to reduce the prevalence of oral candidiasis (Gad et al., 2017; Siedenbiedel and Tiller, 2012). Totu et al. (Totu et al., 2017) discussed the advantages of adding TiO_2 NPs into 3D-printed denture base resin, and to their knowledge, they were the first to investigate this nanocomposite material. They succeeded in developing a composite material that can be printed and showed antifungal properties by adding 0.4 wt.% to the 3D-printed material. Chen et al. (30) found a similar observation of antifungal properties on *Candida albicans* after adding 3.0 wt.% TiO_2 NPs into denture base resin material. The study of Totu et al. (Totu et al., 2017) and the pilot study previously described, demonstrated that adding more than 0.75 wt.% TiO_2 NPs into the 3D-printed denture base resin caused a deterioration of the mechanical properties and the 2.0 wt.% TiO_2 NPs led to a failure in printing. Therefore, the amount of TiO_2 NPs ranging from 0.10 – 0.75 wt.% was considered in this study.

EDX mapping of the specimens with different amounts of TiO_2 NPs up to group C showed a homogeneous dispersion, and as the concentration increased as with group E and D, an agglomeration of the particles was noticed (Appendix: Figure C.3). In agreement with this, Chen et al. reported adding up to 2 wt.% of TiO_2 NPs to 3D-printed denture base resin showed aggregation at the SEM mapping analysis, which affected the composite material negatively (Chen et al., 2019). The results of the antifungal properties in this study revealed that 3D-printed denture base resin with TiO_2 NPs at different concentrations significantly suppressed the growth of *Candida albicans* on their surfaces, especially groups B and C. This finding agrees with the report of Totu et al. as they noted that adding 0.4 wt.% TiO_2 NPs showed the most effective antifungal property compared to other concentrations in the range 0.2 – 2.5 wt.%. Moreover, adding 0.75 wt.% of TiO_2 NPs (group E) in this study showed a slight but not significant reduction in antifungal action compared to the control group. This is in line with

other findings that adding TiO_2 NPs at more than a certain limit had a deleterious effect on some of the mechanical properties (Karci et al., 2019). This can be explained as above a certain level, more NPs could affect the intrinsic molecular structure of the polymerised nanocomposite material. The presence of TiO_2 NPs could act as an impurity within the nanocomposite material that could affect the polymerisation reaction, acting as a plasticiser. This can cause an increase in the unreacted monomers which led to more material leaching out (including TiO_2 NPs) and resulted in instability of the printed specimen with unfavourable properties (Elsaka et al., 2011; Raj et al., 2021).

In this study, the results demonstrated the possibility of printing TiO_2/3D-printed denture base composite material that showed an antifungal ability against *Candida albicans* using the stereolithography printing technique. Furthermore, the tested composite material with different TiO_2 concentrations showed no cytotoxicity, with cellular viability against HGF near 100% after 10 days, confirming the material's biocompatibility.

Further studies should be conducted at prolonged time points to assess the anti-fungal properties of the composite material over a longer period. Furthermore, extensive clinical trial should be carried out to ensure the stability and suitability of the 3D-printed nanocomposite in clinical practice, as excessive dimensional changes resulting from a humid environment could create a reservoir for microorganisms, potentially negating the antifungal effect of the resultant nanocomposite material.

This experimental approach shows that TiO_2 NPs reinforced dentures with antifungal activity can be 3D-printed for edentulous patients to help maintain the prosthesis cleanliness due to the antifungal characteristics of TiO_2 NPs, and to decrease the likelihood of denture-related oral stomatitis. Although the statistical analysis confirmed the significant effect of TiO_2 NPs on the fungal growth, the clinical effect might be irrelevant on the long term.

7.6. CONCLUSION

Within the limitations of this study, 3D-printed TiO_2 NPs incorporated denture base with TiO_2 NPs up to 0.50 wt.% showed statistically significant antifungal properties against *Candida albicans*, compared to the unmodified denture base resin, with no cytotoxic effect against human gingival fibroblast (HGF). However, 0.75 wt.% showed a slight but insignificant reduction in the antifungal action against the fungal colonies, and the optimal concentration of TiO_2 NPs was determined as 0.25 wt.%.

Chapter 8: Summary, Conclusions and Future Work

8.1. INTRODUCTION

Complete denture prostheses continue to serve as a practical treatment option for those who have lost teeth. A considerable amount of effort has been dedicated to enhancing the attributes of polymethylmethacrylate (PMMA) materials to counter the inherent limitations of traditional denture production methods (Paulino et al., 2015). Computer-aided design and manufacturing (CAD/CAM) has offered numerous advantages in prosthesis creation, including a reduced number of dental visits, a more efficient manufacturing process, improved tissue adaptability, effortless duplication of existing dentures, a decrease in production errors, and expedited manufacturing, all of which are benefits derived from digital technology utilisation (Bidra et al., 2016; Bidra et al., 2013; Bilgin et al., 2016; Infante et al., 2014).

While milling is a standard procedure for denture fabrication, 3D-printing presents notable benefits. For example, it is more cost-effective as it permits the concurrent production of multiple components without unnecessary consumption of raw materials or the degradation of rotary tools (Kattadiyil and AlHelal, 2017; Shim et al., 2020). However, research has indicated that 3D-printed denture bases have relatively lower physical and mechanical properties compared to their PMMA counterparts (Alshaikh et al., 2022; Gad et al., 2022a; Gad et al., 2022c).

A further issue confronting the denture base is the build-up of fungi, which can lead to denture stomatitis, affecting 15-70% of those wearing dentures (Akpan and Morgan, 2002; Gendreau and Loewy, 2011). In an attempt to counter these problems, investigators have explored various techniques to fortify the resin material. The employment of nanoparticles (NPs) is emerging as one of the most significant promising strategies.

One such nanoparticle, TiO_2, is recognised for its unique properties, such as biocompatibility, chemical stability, non-toxicity, corrosion resistance, and high strength and refractive index. Furthermore, TiO_2 NPs are proven to possess antimicrobial properties. TiO_2 NPs have been successfully combined with heat-cured PMMA, demonstrating encouraging outcomes (Gad and Abualsaud, 2019).

The materials, techniques, and equipment utilised in the present investigation for specimen preparation and materials property testing adhered to established ISO standards, the manufacturer's guidelines, and methodologies presented in earlier research (Aati et al., 2022a;

Gad et al., 2022a; Gad et al., 2022b; Gad et al., 2022c; Thangaraju and Varthya, 2022; Totu et al., 2017).

A preliminary aim of this study was to evaluate the relevant physical and mechanical properties of filler-reinforced 3D-printed denture base resin. This component of the investigation focussed on the initial phase of nanocomposite material development. If the material does not meet the strength benchmarks stipulated by the relevant ISO specifications, it negates the need for assessing the biological facets of such dentures. As such, the initial phase of the experiment aimed to confirm the degree of compliance of the materials under scrutiny with the necessary standards for denture base material usage. However, before subjecting the printed specimens to testing, it was critical to establish optimal printing parameters to ensure the best possible settings were employed for specimen printing.

8.2. PRINTING PARAMETERS OPTIMISATION

Before initiating the printing process, there exist both uncontrollable and controllable parameters, the latter of which can be adjusted according to the practitioner's preference. Variables such as printing orientation, post-curing time, and post-curing temperature can significantly influence the properties of the resulting printed specimen. Chapter 4 explored the impact of various printing orientations (0°, 45°, 90°) and post-curing times (20, 30, 50 minutes) on the physical and mechanical properties of NextDent 3D-printed resin. The results showed that a printing orientation of 90° significantly improved flexural strength, degree of polymerisation, and water absorption in comparison to a 0° orientation, and yielded slightly, though not significantly, better results than a 45° orientation. However, surface hardness and water solubility did not differ significantly between any of the orientations. Regarding post-curing time, an increase to 30 min led to slight, but not statistically significant, improvements over 20 min in the properties tested, with no observable changes when compared to a 50 min post-curing time. Optical and scanning electron microscopes revealed that there was no separation within the internal structure between different printed layers as suggested by other studies.

Overall, 90° printing orientation (denture base printed vertically and oriented sideways to avoid midline fractures) and 30 min curing time provided the highest results.

8.3. MECHANICAL AND PHYSICAL PROPERTIES OF THE UN-MODIFIED MATERIAL

Upon determining the optimal printing parameters (90° printing orientation and 30 min post-curing time), Chapter 5 turned its attention towards the use of these optimal settings for printing two variants of 3D-printed denture base materials, namely NextDent (ND) and Formlabs (FL). These were then compared with the conventional heat-cured PMMA (HC) as a control regarding physical and mechanical properties. These included filler content, degree of polymerisation, sorption/solubility, surface hardness, flexural strength/modulus, and impact strength.

Preliminary test findings indicated that FL and ND materials contained a significantly higher quantity of fillers compared to HC. This could potentially account for the later discussed enhanced mechanical properties. Conversely, the degree of polymerisation of the HC was significantly higher compared to the FL and ND materials, and this might be related to the polymerisation environment during manufacturing, with HC cured at a higher temperature and for a longer duration compared to the light-cured 3D-printed material.

Sorption values for the HC material in artificial saliva were significantly lower than those for FL and ND. This could be ascribed to the degree of polymerisation of the materials tested. In contrast, the solubility test did not unveil any significant differences between the 3D-printed materials and HC.

Surface hardness measurements, encompassing Vickers and Martens hardness, did not show any significant differences between the tested 3D-printed materials and the control, although the values were slightly superior with the control. By contrast, flexural strength of the FL and ND material was significantly greater compared to HC. This could be related to the filler content within the material as previously stated. Impact strength did not show any significant discrepancies between the materials tested, although 3D-printed materials values were slightly higher.

Additionally, Chapter 5 explored the impact of hydrolytic ageing in artificial saliva over a period of three months. This duration was selected because it allowed the specimen to reach a saturated state, where it no longer gains weight, providing a stable point of observation. The

aim of this approach was to replicate, to an extent, the conditions of the oral environment. Data gathered from this examination is more clinically relevant compared to the dry state. The results demonstrated that ageing in artificial saliva affected the surface properties of the control material, including Vickers and Martens hardness, and only Vickers hardness for the 3D-printed materials. However, it only had a slight, non-significant impact on mechanical properties, such as flexural strength/modulus and impact strength.

8.4. ADDITION OF NANOPARTICLES

8.4.1. Mechanical and physical properties of the nanocomposite material

Chapter 6 embarked on a study into the effects of integrating varying concentrations of TiO_2 NPs (0.0, 0.10, 0.25, 0.50, and 0.75 wt.%) into the NextDent 3D-printed material. This was with a view to forming a new nanocomposite material and examining its physical and mechanical properties. The NPs concentration did not exceed 0.75 wt.% as an addition of 1.0 wt.% did not demonstrate any enhancements when compared to 0.75 wt.%, and a 2.0 wt.% addition resulted in a failure in the printing process.

Initial test outcomes signalled a significant increase in the degree of polymerisation across all the NPs concentration groups compared to the unmodified material (Control 1), putting them on a par with HC (control 2), except the 0.75 wt.% group. Sorption values of the nanocomposite material did not alter when compared to the unmodified 3D-printed material, but solubility values showed a significant improvement across all NPs groups, except the 0.75 wt% group again, where the change was insignificant relative to the unmodified 3D-printed material. This has an important clinical significance as the release of the un-polymerised monomers and the other components into the surrounding tissues may show an unfavourable reaction to the denture wearers. Similarly, Vickers hardness exhibited a significant improvement in all NPs groups compared to the un-modified material. However, this increase would not be considered clinically relevant. Martens hardness remained unchanged, suggesting that the elastic-plastic deformation during the Martens hardness test was not affected unlike the plastic deformation evident with the Vickers hardness test.

The flexural strength and modulus saw a significant increase compared to the un-modified material, particularly with the addition of 0.10 wt.%. A decline in flexural strength and modulus values was noticed when the concentration of NPs surpassed 0.25 wt.%, and this could perhaps

be attributed to the agglomerations of particles observed on the SEM images of the fractured surface of the specimens, notably in the 0.50 and 0.75 wt.% groups. Impact strength followed a similar trend to flexural properties, with the addition of NPs up to 0.25 wt.% significantly enhancing the impact strength value compared to the unmodified material. The 0.50 and 0.75 wt.% delivered an insignificant increase in the impact strength value for the same reason mentioned in relation to the flexural strength.

The effect of hydrolytic ageing in artificial saliva on the nanocomposite material was discussed as well on Chapter 6. The nanocomposite material groups displayed a significant reduction in some of the values of the materials being tested such as flexural strength and modulus, and Vickers hardness particularly with elevated concentrations of TiO_2 NPs. Here, a high concentration of NPs can lead to agglomeration within the material, serving as local stress points where cracks can start, and adversely impact the properties of the material. Impact strength and Martens hardness shown a slight drop on their results after the ageing process. However, none of the tested properties went below the ISO standard for denture base materials after hydrolytic ageing.

8.4.2. Biological properties of the nanocomposite material

Chapter 7 examined the biological behaviour of the new nanocomposite material. Assessments of cell cytotoxicity and viability are deemed potent measures for examining how cells interact with various types of materials and any substances they might potentially release. An incomplete transformation of methyl methacrylate (MMA), a core ingredient in the resin used for 3D-printed denture base resin, can lead to the leakage of residual monomers. This can subsequently cause adverse reactions in the cells located within the mouth. Results from the cytotoxicity and biocompatibility tests have proven the biocompatibility of the nanocomposite material, as it exhibited no detrimental impact on human gingival fibroblasts. All the examined 3D-printed nanocomposite specimens, featuring varying amounts of TiO_2 nanoparticles, demonstrated a cell survival rate above 70% in the alamarBlue assay tests. This rate surpasses the recommended cytotoxicity threshold set by ISO 10993-5. In addition, when specimens assessed using the LDH assay at various intervals, none of the examined groups exhibited cytotoxic activities exceeding 12%.

Epidemiological studies have found that denture stomatitis, one of the most common diseases affecting denture wearers, is primarily caused by *Candida albicans*. In this study, anti-fungal

test results demonstrated that the addition of TiO_2 NPs up to 0.50 wt.% led to a statistically significant decrease in the number of *Candida albicans* colonies adhering to the specimen surface. However, 0.75 wt.% showed no significant differences compared to the un-modified material. This discrepancy might be attributed to the agglomeration of the nanoparticles, which negatively impacted the properties of the resulting nanocomposite material. Yet, from a biological perspective, this decrease in colony count may not hold clinical relevance, necessitating further efforts to significantly reduce the formation of these colonies.

8.5. SUMMARY

In conclusion, 3D-printed materials displayed comparable or superior physical and mechanical properties relative to conventional heat-cured PMMA. The integration of TiO_2 NPs further enhanced these properties, and also conferred the ability to resist fungal growth without showing any unwanted effects on human gingival fibroblasts. To get the optimal physical and mechanical properties of 3D-printed denture base, 90° printing orientation and 30 min post-curing time should be used. On the other hand, the ideal amount of NPs to augment the properties was found to be 0.10 and 0.25 wt.%, while the 0.75 wt.% tend to show agglomeration of the NPs within the material that explained the lower properties compared to other concentrations. Tables 8.1 - 8.3 provide a brief summary of the test results and aspects for improvement. These findings hold promise for the future of 3D-printing in prosthetic dentistry.

Table 8.1. Summary table of varying PO and CT on the physical and mechanical properties

Chapter no.	Quality tested	Control (0° PO/ 30 min CT)	Best PO/ CT	Improvement over control	Significant difference over the control
4	Degree of polymerisation*	86.3%	87.8% (90°/ 50 min)	Yes	No
	Sorption*	22.8 µg/mm³	22.7 µg/mm³ (90°/ 20 min)	Yes	No
	Solubility*	1.4 µg/mm³	1.4 µg/mm³ (90°/ 30 min)	No	No
	Vickers hardness	13.0 VHN	14.6 VHN (90°/ 30 min)	Yes	No
	Flexural strength	58.9 MPa	88.9 MPa (90°/ 20 min)	Yes	Yes
	Flexural modulus	2571.0 MPa	2610.9 MPa (45°/ 30 min)	Yes	Yes

**Control is 90° PO/ 30 min CT*

Table 8.2. Summary table of varying manufacturing technology and denture base resin materials on the physical and mechanical properties

Chapter no.	Quality tested	Control (HC)	Best denture base resin	Improvement over control	Significant difference over the control
5	Filler weight	> 2 wt.%	15.2 wt.% (ND)	Yes	Yes
	Degree of polymerisation	98.1%	98.1% (HC)	No	No
	Sorption	21.1 µg/mm³	21.1 µg/mm³ (HC)	No	No
	Solubility	1.3 µg/mm³	1.3 µg/mm³ (HC)	No	No
	Vickers hardness	15.0 VHN	15.0 VHN (HC)	No	No
	Martens hardness	135.6 N/mm²	135.6 N/mm² (HC)	No	No
	Flexural strength	73.5 MPa	93.9 MPa (FL)	Yes	Yes
	Flexural modulus	2388.0 MPa	2388 MPa (HC)	No	No
	Impact strength	11.8 KJ/m²	13.3 KJ/m² (FL)	Yes	No

Note: ND: NextDent; FL: Formlab ; HC: Heat Cure.

Table 8.3. Summary table of varying TiO_2 NPs on the physical, mechanical, and biological properties of 3D-printed resin

Chapter no.	Quality tested	Control (un-modified 3D-printed resin)	Best TiO_2 nanocomposite percentage wt.%	Improvement over control	Significant difference over the control
6	Degree of polymerisation	84.0%	94.7% (0.10)	Yes	Yes
	Sorption	22.8 µg/mm³	22.2 µg/mm³ (0.25)	Yes	No
	Solubility	1.4 µg/mm³	-1.5 µg/mm³ (0.10)	Yes	Yes
	Vickers hardness	18.9 VHN	20.3 VHN (0.50)	Yes	Yes
	Martens hardness	126.2 N/mm^2	132.5 N/mm^2 (0.50)	Yes	No
	Flexural strength	89.2 MPa	111.2 MPa (0.10)	Yes	Yes
	Flexural modulus	2391.4 MPa	2769.6 MPa (0.10)	Yes	Yes
	Impact strength	13.0 KJ/m²	20.4 KJ/m² (0.10)	Yes	Yes
7	Antifungal	3.1 CFU/mL	1.64 CFU/mL	Yes	Yes
	Cytotoxicity (day 10)	10.8%	10.4% (0.75)	Yes	No
	Cytocompatibility (day 10)	99.1%	99.6% (0.25)	Yes	No

8.6. CONCLUSIONS

1. Optimal mechanical and physical properties for 3D-printed denture base resin (NextDent) were obtained with a 90° printing orientation and a post-curing time of 30 minutes.

2. 3D-printed denture base material exhibited less desirable properties in terms of DC and solubility when compared to conventional heat-cured material, but it displayed significantly higher sorption.

3. When compared to the heat-cured material, 3D-printed materials showed similar mechanical properties such as surface hardness and impact strength, but demonstrated significantly greater flexural strength.

4. Three-month immersion of 3D-printed material to artificial saliva had a slight negative impact on the mechanical properties. This effect was not significant except for Vickers hardness.

5. The integration of TiO_2 NPs resulted in an enhanced nanocomposite material with superior physical and mechanical properties, including DC, saliva solubility, flexural strength, and modulus. The ideal percentage for this was found to be 0.10 wt.%.

6. The inclusion of 0.50 wt.% or more of TiO_2 NPs led to particles aggregation which negatively impacted the resulting composite material.

7. Subjecting the nanocomposite material to hydrolytic ageing in artificial saliva for a three-month period adversely affected the material, particularly its flexural strength and modulus.

8. The incorporation of TiO_2 NPs into the 3D-printed resin did not adversely affect HGF, affirming the material's biocompatibility.

9. The addition of TiO_2 to 3D-printed denture base material was found to diminish the number of fungal colonies on the denture surface, thereby reducing the incidence of denture stomatitis.

8.7. RECOMMENDATION FOR FUTURE WORK

- Further studies can be conducted focusing on potential changes in colour of the 3D printed materials, particularly after the addition of nanoparticles, fracture toughness, and fatigue resistance.

- Incorporation of TiO_2 NPs at less than 0.10 wt.% into the 3D-printed material is recommended, as this range, although currently unknown, is likely to be optimal for enhancing the properties of the composite material.

- By incorporating more samples in each group, it may be feasible to identify statistical significance with greater ease during the mechanical properties experiments and achieve a Weibull analysis.

- Future research should be carried out over extended time frames (1-3 months) to assess the anti-fungal property of the nanocomposite material over a longer duration. *Candida albicans* isolated from patients can be used for testing as well.

- The accuracy of 3D-printed denture bases fabricated utilising various printing orientations can be determined, and the dimensional changes can be compared with the original design, and with a conventional heat-cured denture base, especially before and after the effect of water sorption.

- Additional research can be conducted using the same materials after printing a complete denture to obtain more trustworthy results (3-point bending test evaluating the possibility of resisting midline fractures with vertical orientation (denture base printed sideways) compared to any other orientations, mechanical fatigue test, tensile bond strength between denture base and artificial teeth).

- The impact of slight deviations from the manufacturer's recommendations during the manufacturing of 3D-printed specimens/objects should be studied, as 3D-printing is a technique-sensitive technology. It has been observed that even minor adjustments, such as extending the alcoholic wash by two extra minutes, can lead to a significant deterioration in the material's properties.

References

Aati, S., Akram, Z., Ngo, H. & Fawzy, A. S. (2021a). 'Development of 3D printed resin reinforced with modified ZrO2 nanoparticles for long-term provisional dental restorations', *Dental Materials,* 37(6), pp. e360-e374.

Aati, S., Akram, Z., Shrestha, B., Patel, J., Shih, B., Shearston, K., Ngo, H. & Fawzy, A. (2021b). 'Effect of post-curing light exposure time on the physico–mechanical properties and cytotoxicity of 3D-printed denture base material', *Dental Materials*.

Aati, S., Akram, Z., Shrestha, B., Patel, J., Shih, B., Shearston, K., Ngo, H. & Fawzy, A. (2022a). 'Effect of post-curing light exposure time on the physico–mechanical properties and cytotoxicity of 3D-printed denture base material', *Dental Materials,* 38(1), pp. 57-67.

Aati, S., Aneja, S., Kassar, M., Leung, R., Nguyen, A., Tran, S., Shrestha, B. & Fawzy, A. (2022b). 'Silver-loaded mesoporous silica nanoparticles enhanced the mechanical and antimicrobial properties of 3D printed denture base resin', *Journal of the mechanical behavior of biomedical materials,* 134, p. 105421.

Abdulwahhab, S. S. (2013). 'High-impact strength acrylic denture base material processed by autoclave', *Journal of prosthodontic research,* 57(4), pp. 288-293.

Abduo, J., Lyons, K. & Bennamoun, M. (2014). 'Trends in computer-aided manufacturing in prosthodontics: a review of the available streams', *Int J Dent,* 2014, p. 783948.

Abed, Y., Sabry, H. & Alrobeigy, N. (2015). 'Degree of conversion and surface hardness of bulk-fill composite versus incremental-fill composite', *Egypt Dent J,* 12(2), pp. 71-80.

Abou Tara, M., Eschbach, S., Bohlsen, F. & Kern, M. (2011). 'Clinical outcome of metal-ceramic crowns fabricated with laser-sintering technology', *International Journal of Prosthodontics,* 24(1), p. 46.

Acosta-Torres, L. S., Lopez-Marin, L. M., Nunez-Anita, R. E., Hernandez-Padron, G. & Castano, V. M. (2011). 'Biocompatible Metal-Oxide Nanoparticles: Nanotechnology Improvement of Conventional Prosthetic Acrylic Resins', *Journal of Nanomaterials*.

Acosta-Torres, L. S., López-Marín, L. M., Nunez-Anita, R. E., Hernández-Padrón, G. & Castaño, V. M. (2011). 'Biocompatible metal-oxide nanoparticles: nanotechnology improvement of conventional prosthetic acrylic resins', *Journal of Nanomaterials,* 2011, pp. 1-8.

Ahmed, M. A. & Ebrahim, M. I. (2014). 'Effect of zirconium oxide nano-fillers addition on the flexural strength, fracture toughness, and hardness of heat-polymerized acrylic resin', *World journal of nano science and engineering,* 2014.

Ahmed, M. A., El-Shennawy, M., Althomali, Y. M. & Omar, A. A. (2016). 'Effect of titanium dioxide nano particles incorporation on mechanical and physical properties on two different types of acrylic resin denture base', *World Journal of Nano Science and Engineering,* 6(3), pp. 111-119.

Akin, H., Tugut, F. & Polat, Z. A. (2015). 'In vitro comparison of the cytotoxicity and water sorption of two different denture base systems', *J Prosthodont,* 24(2), pp. 152-5.

Akpan, A. & Morgan, R. (2002). 'Oral candidiasis', *Postgraduate medical journal,* 78(922), pp. 455-459.

Al-Ahdal, K., Silikas, N. & Watts, D. C. (2015). 'Development of viscoelastic stability of resin-composites incorporating novel matrices', *Dental Materials,* 31(12), pp. 1561-1566.

Al-Douri, M. E. & Sadoon, M. M. (2023). 'Flexural Strength, Hardness and Surface Roughness of 3D Printed Denture Base Resin Reinforced by Zinc Oxide Nanoparticles', *Journal of Research in Medical and Dental Science,* 11(01), pp. 194-200.

Al-Dulaijan, Y. A., Alsulaimi, L., Alotaibi, R., Alboainain, A., Alalawi, H., Alshehri, S., Khan, S. Q., Alsaloum, M., AlRumaih, H. S. & Alhumaidan, A. A. (2022). 'Comparative Evaluation of Surface Roughness and Hardness of 3D Printed Resins', *Materials,* 15(19), p. 6822.

Al-Haddad, A., Roudsari, R. V. & Satterthwaite, J. D. (2014). 'Fracture toughness of heat cured denture base acrylic resin modified with Chlorhexidine and Fluconazole as bioactive compounds', *Journal of dentistry,* 42(2), pp. 180-184.

Al-Harbi, F. A., Abdel-Halim, M. S., Gad, M. M., Fouda, S. M., Baba, N. Z., AlRumaih, H. S. & Akhtar, S. (2019). 'Effect of Nanodiamond Addition on Flexural Strength, Impact Strength, and Surface Roughness of PMMA Denture Base', *J Prosthodont,* 28(1), pp. e417-e425.

Al-Mulla, M., Murphy, W., Huggett, R. & Brooks, S. (1989). 'Effect of water and artificial saliva on mechanical properties of some denture-base materials', *Dental Materials,* 5(6), pp. 399-402.

Al-Rafee, M. A. (2020). 'The epidemiology of edentulism and the associated factors: A literature Review', *Journal of family medicine and primary care,* 9(4), p. 1841.

Al-Dwairi, Z. N., Al Haj Ebrahim, A. A. & Baba, N. Z. (2023). 'A Comparison of the Surface and Mechanical Properties of 3D Printable Denture-Base Resin Material and Conventional Polymethylmethacrylate (PMMA)', *Journal of Prosthodontics,* 32(1), pp. 40-48.

Al-Dwairi, Z. N., Tahboub, K. Y., Baba, N. Z., Goodacre, C. J. & Özcan, M. (2019). 'A comparison of the surface properties of CAD/CAM and conventional polymethylmethacrylate (PMMA)', *Journal of Prosthodontics,* 28(4), pp. 452-457.

Alamoush, R. A., Silikas, N., Salim, N. A., Al-Nasrawi, S. & Satterthwaite, J. D. (2018). 'Effect of the Composition of CAD/CAM Composite Blocks on Mechanical Properties', *Biomed Res Int,* 2018, p. 4893143.

Algamaiah, H., Silikas, N. & Watts, D. C. (2020). 'Conversion kinetics of rapid photo-polymerized resin composites', *Dental Materials,* 36(10), pp. 1266-1274.

Alghazzawi, T. F. (2016). 'Advancements in CAD/CAM technology: Options for practical implementation', *J Prosthodont Res,* 60(2), pp. 72-84.

Alharbi, N., Osman, R. & Wismeijer, D. (2016). 'Effects of build direction on the mechanical properties of 3D-printed complete coverage interim dental restorations', *Journal of Prosthetic Dentistry,* 115(6), pp. 760-767.

Alhareb, A. O. & Ahmad, Z. A. (2011). 'Effect of Al2O3/ZrO2 reinforcement on the mechanical properties of PMMA denture base', *Journal of Reinforced Plastics and Composites,* 30(1), pp. 86-93.

Ali, I. L., Yunus, N. & Abu-Hassan, M. I. (2008). 'Hardness, flexural strength, and flexural modulus comparisons of three differently cured denture base systems', *Journal of Prosthodontics: Implant, Esthetic and Reconstructive Dentistry,* 17(7), pp. 545-549.

Alifui-Segbaya, F., Bowman, J., White, A. R., George, R. & Fidan, I. (2019). 'Characterization of the Double Bond Conversion of Acrylic Resins for 3D Printing of Dental Prostheses', *Compendium,* 40(10).

Alla, R., Raghavendra, K., Vyas, R. & Konakanchi, A. (2015). 'Conventional and contemporary polymers for the fabrication of denture prosthesis: part I–overview, composition and properties', *Int J Appl Dent Sci,* 1(4), pp. 82-89.

Alp, G., Murat, S. & Yilmaz, B. (2019). 'Comparison of flexural strength of different CAD/CAM PMMA-based polymers', *Journal of Prosthodontics,* 28(2), pp. e491-e495.

Alrahlah, A., Khan, R., Alotaibi, K., Almutawa, Z., Fouad, H., Elsharawy, M. & Silikas, N. (2018). 'Simultaneous evaluation of creep deformation and recovery of bulk-fill dental composites immersed in food-simulating liquids', *Materials,* 11(7), p. 1180.

Alshaikh, A. A., Khattar, A., Almindil, I. A., Alsaif, M. H., Akhtar, S., Khan, S. Q. & Gad, M. M. (2022). '3D-Printed Nanocomposite Denture-Base Resins: Effect of ZrO2 Nanoparticles on the Mechanical and Surface Properties In Vitro', *Nanomaterials,* 12(14), p. 2451.

Alshamrani, A. A., Raju, R. & Ellakwa, A. (2022). 'Effect of printing layer thickness and postprinting conditions on the flexural strength and hardness of a 3D-printed resin', *BioMed Research International,* 2022.

Altarazi, A., Haider, J., Alhotan, A., Silikas, N. & Devlin, H. (2022). 'Assessing the physical and mechanical properties of 3D printed acrylic material for denture base application', *Dental Materials,* 38(12), pp. 1841-1854.

Altıncı, P. & Durkaya, P. (2016). 'Effects of thermocycling and various drinks on color stability of heat-polymerized acrylic resin', *Journal of Istanbul University Faculty of Dentistry,* 50(3), pp. 15-20.

Alwan, S. A. & Alameer, S. S. (2015). 'The effect of the addition of silanized Nano titania fillers on some physical and mechanical properties of heat cured acrylic denture base materials', *Journal of baghdad college of dentistry,* 325(2218), pp. 1-12.

Anadioti, E., Musharbash, L., Blatz, M. B., Papavasiliou, G. & Kamposiora, P. (2020). '3D printed complete removable dental prostheses: a narrative review', *BMC Oral Health,* 20(1), p. 343.

Andreescu, C. F., Ghergic, D. L., Botoaca, O., Hancu, V., Banateanu, A. M. & Patroi, D. N. (2018). 'Evaluation of different materials used for fabrication of complete digital denture', *Mater. Plast.,* 55(1), p. 124.

Anehosur, G. V., Kulkarni, R., Naik, M. & Nadiger, R. (2012). 'Synthesis and determination of antimicrobial activity of visible light activated TiO2 nanoparticles with polymethyl methacrylate denture base resin against Staphylococcus aureus', *J. Gerontol. Geriat. Res,* 1, pp. 103-111.

Anusavice, K. J. & Phillips, R. W. (2003). *Phillips' science of dental materials*. St. Louis, Mo.: Saunders.

Anusavice, K. J., Shen, C. & Rawls, H. R. (2012). *Phillips' science of dental materials*: Elsevier Health Sciences.

Arima, T., Murata, H. & Hamad, T. (1996). 'The effects of cross-linking agents on the water sorption and solubility characteristics of denture base resin', *Journal of oral rehabilitation,* 23(7), pp. 476-480.

Asmussen, E. & Peutzfeldt, A. (1998). 'Influence of UEDMA, BisGMA and TEGDMA on selected mechanical properties of experimental resin composites', *Dental Materials,* 14(1), pp. 51-56.

Ausiello, P., Cassese, A., Miele, C., Beguinot, F., Garcia-Godoy, F., Di Jeso, B. & Ulianich, L. (2013). 'Cytotoxicity of dental resin composites: an in vitro evaluation', *Journal of Applied Toxicology,* 33(6), pp. 451-457.

Averyanova, M. (2012). 'Quality control of dental bridges and removable prostheses manufactured using Phenix systems equipment', *Proceedings of AEPR'12*.

Ayad, N. M., Badawi, M. F. & Fatah, A. A. (2008). 'Effect of reinforcement of high-impact acrylic resin with zirconia on some physical and mechanical properties', *Archives of Oral Research,* 4(3).

Aziz, H. K. (2018). 'TiO2-nanofillers effects on some properties of highly-impact resin using different processing techniques', *The open dentistry journal,* 12, p. 202.

Babaier, R., Watts, D. C. & Silikas, N. (2022). 'Effects of three food-simulating liquids on the roughness and hardness of CAD/CAM polymer composites', *Dental Materials,* 38(5), pp. 874-885.

Bacali, C., Badea, M., Moldovan, M., Sarosi, C., Nastase, V., Baldea, I., Chiorean, R. S. & Constantiniuc, M. (2019). 'The Influence of Graphene in Improvement of Physico-Mechanical Properties in PMMA Denture Base Resins', *Materials (Basel),* 12(14).

Bajunaid, S. O. (2022). 'How effective are antimicrobial agents on preventing the adhesion of candida albicans to denture base acrylic resin materials? A systematic review', *Polymers,* 14(5), p. 908.

Bangera, M. K., Kotian, R. & Ravishankar, N. (2020). 'Effect of titanium dioxide nanoparticle reinforcement on flexural strength of denture base resin: A systematic review and meta-analysis', *Japanese Dental Science Review,* 56(1), pp. 68-76.

Barsby, M. (1992). 'A denture base resin with low water absorption', *Journal of Dentistry,* 20(4), pp. 240-244.

Bartoloni, J., Murchison, D., Wofford, D. & Sarkar, N. (2000). 'Degree of conversion in denture base materials for varied polymerization techniques 1', *Journal of oral rehabilitation,* 27(6), pp. 488-493.

Batisse, C. & Nicolas, E. (2021). 'Comparison of CAD/CAM and Conventional Denture Base Resins: A Systematic Review', *Applied Sciences,* 11(13), p. 5990.

Bencharit, S., Staffen, A., Yeung, M., Whitley, D., Laskin, D. M. & Deeb, G. R. (2018). 'In Vivo Tooth-Supported Implant Surgical Guides Fabricated With Desktop Stereolithographic Printers: Fully Guided Surgery Is More Accurate Than Partially Guided Surgery', *Journal of Oral and Maxillofacial Surgery,* 76(7), pp. 1431-1439.

Berli, C., Thieringer, F. M., Sharma, N., Müller, J. A., Dedem, P., Fischer, J. & Rohr, N. (2020). 'Comparing the mechanical properties of pressed, milled, and 3D-printed resins for occlusal devices', *The Journal of prosthetic dentistry,* 124(6), pp. 780-786.

Berman, B. (2012). '3-D printing: The new industrial revolution', *Business horizons,* 55(2), pp. 155-162.

Beuer, F., Schweiger, J. & Edelhoff, D. (2008). 'Digital dentistry: an overview of recent developments for CAD/CAM generated restorations', *Br Dent J,* 204(9), pp. 505-11.

Bidra, A. S., Farrell, K., Burnham, D., Dhingra, A., Taylor, T. D. & Kuo, C.-L. (2016). 'Prospective cohort pilot study of 2-visit CAD/CAM monolithic complete dentures and implant-retained overdentures: Clinical and patient-centered outcomes', *The Journal of prosthetic dentistry,* 115(5), pp. 578-586. e1.

Bidra, A. S., Taylor, T. D. & Agar, J. R. (2013). 'Computer-aided technology for fabricating complete dentures: systematic review of historical background, current status, and future perspectives', *The Journal of prosthetic dentistry,* 109(6), pp. 361-366.

Bilgin, M. S., Baytaroglu, E. N., Erdem, A. & Dilber, E. (2016). 'A review of computer-aided design/computer-aided manufacture techniques for removable denture fabrication', *Eur J Dent,* 10(2), pp. 286-291.

Bilgin, M. S., Erdem, A., Aglarci, O. S. & Dilber, E. (2015). 'Fabricating Complete Dentures with CAD/CAM and RP Technologies', *Journal of Prosthodontics-Implant Esthetic and Reconstructive Dentistry,* 24(7), pp. 576-579.

Bonada, J., Muguruza, A., Fernández-Francos, X. & Ramis, X. (2017). 'Influence of exposure time on mechanical properties and photocuring conversion ratios for photosensitive materials used in additive manufacturing', *Procedia Manuf,* 13, pp. 762-769.

Bonsor, S. J. & Pearson, G. (2012). *A clinical guide to applied dental materials*: Elsevier Health Sciences.

Bowen, R. (1979). 'Compatibility of various materials with oral tissues. I: The components in composite restorations', *Journal of Dental Research,* 58(5), pp. 1493-1503.

Bremer-Hoffmann, S., Halamoda-Kenzaoui, B. & Borgos, S. E. (2018). 'Identification of regulatory needs for nanomedicines', *Journal of Interdisciplinary Nanomedicine,* 3(1), pp. 4-15.

Broitman, E. (2017). 'Indentation hardness measurements at macro-, micro-, and nanoscale: a critical overview', *Tribology Letters,* 65(1), p. 23.

BS EN ISO, -. (2009). 'BS, EN, ISO 10993–5: 2009 Biological evaluation of medical devices—part 5: tests for in vitro cytotoxicity', *International Organization for Standardization, Geneva*, p. 34.

BS EN ISO, -. (2010). 'ISO 179–1: 2010, Plastics—Determination of Charpy Impact Properties, Part 1: Non-Instrumented Impact Test', *ISO: Geneva, Switzerland*.

BS EN ISO, -. (2013). 'Dentistry-Base Polymers–Part 1: Denture Base Polymers'.

BS EN ISO, -. (2016). Metallic Materials—Instrumented Indentation Test for Hardness and Materials Parameters—Part 4: Test Method for Metallic and Non-Metallic Coatings. ISO Geneva, Switzerland.

Bural, C., AktaŞ, E., Deniz, G., Ünlüçerçi, Y. & Bayraktar, G. (2011). 'Effect of leaching residual methyl methacrylate concentrations on in vitro cytotoxicity of heat polymerized denture base acrylic resin processed with different polymerization cycles', *Journal of applied oral science,* 19, pp. 306-312.

Calheiros, F. C., Daronch, M., Rueggeberg, F. A. & Braga, R. R. (2008). 'Degree of conversion and mechanical properties of a BisGMA: TEGDMA composite as a function of the applied radiant exposure', *J Biomed Mater Res B Appl Biomater,* 84(2), pp. 503-509.

Cavalcante, L. M., Schneider, L. F. J., Silikas, N. & Watts, D. C. (2011). 'Surface integrity of solvent-challenged ormocer-matrix composite', *Dental Materials,* 27(2), pp. 173-179.

Chaijareenont, P., Takahashi, H., Nishiyama, N. & Arksornnukit, M. (2012). 'Effect of different amounts of 3-methacryloxypropyltrimethoxysilane on the flexural properties and wear resistance of alumina reinforced PMMA', *Dent Mater J,* 31(4), pp. 623-8.

Chatterjee, A. (2010). 'Properties improvement of PMMA using nano TiO2', *Journal of applied polymer science,* 118(5), pp. 2890-2897.

Chebib, N., Imamura, Y., El Osta, N., Srinivasan, M., Müller, F. & Maniewicz, S. (2022). 'Fit and retention of complete denture bases: Part II–conventional impressions versus digital scans: A clinical controlled crossover study', *The Journal of Prosthetic Dentistry*.

Chen, J., Liu, X., Tian, Y., Zhu, W., Yan, C., Shi, Y., Kong, L. B., Qi, H. J. & Zhou, K. (2022). '3D-Printed anisotropic polymer materials for functional applications', *Advanced Materials,* 34(5), p. 2102877.

Chen, R., Han, Z., Huang, Z., Karki, J., Wang, C., Zhu, B. & Zhang, X. (2017). 'Antibacterial activity, cytotoxicity and mechanical behavior of nano-enhanced denture base resin with different kinds of inorganic antibacterial agents', *Dental materials journal,* 36(6), pp. 693-699.

Chen, S., Yang, J., Jia, Y. G., Lu, B. & Ren, L. (2018). 'A Study of 3D-Printable Reinforced Composite Resin: PMMA Modified with Silver Nanoparticles Loaded Cellulose Nanocrystal', *Materials (Basel),* 11(12).

Chen, S., Yang, J., Li, K., Lu, B. & Ren, L. (2018). 'Carboxylic acid-functionalized TiO2 nanoparticle-loaded PMMA/PEEK copolymer matrix as a dental resin for 3D complete denture manufacturing by stereolitographic technique', *International Journal of Food Properties,* 21(1), pp. 2557-2565.

Chen, S. G., Yang, J. Z., Jia, Y. G., Lu, B. H. & Ren, L. (2019). 'TiO2 and PEEK Reinforced 3D Printing PMMA Composite Resin for Dental Denture Base Applications', *Nanomaterials,* 9(7).

Chhabra, M., Kumar, M. N., RaghavendraSwamy, K. & Thippeswamy, H. (2022). 'Flexural strength and impact strength of heat-cured acrylic and 3D printed denture base resins-A comparative in vitro study', *Journal of Oral Biology and Craniofacial Research,* 12(1), pp. 1-3.

Chia, H. N. & Wu, B. M. (2015). 'Recent advances in 3D printing of biomaterials', *J Biol Eng,* 9, p. 4.

Chockalingam, K., Jawahar, N. & Chandrasekhar, U. (2006). 'Influence of layer thickness on mechanical properties in stereolithography', *Rapid Prototyping Journal,* 12(2), pp. 106-113.

Chua, C. K., Leong, K. F. & Lim, C. S. (2010). *Rapid prototyping: principles and applications (with companion CD-ROM)*: World Scientific Publishing Company.

CHUNG, K. H. & Greener, E. (1990). 'Correlation between degree of conversion, filler concentration and mechanical properties of posterior composite resins', *Journal of oral rehabilitation,* 17(5), pp. 487-494.

Cierech, M., Osica, I., Kolenda, A., Wojnarowicz, J., Szmigiel, D., Lojkowski, W., Kurzydlowski, K., Ariga, K. & Mierzwinska-Nastalska, E. (2018). 'Mechanical and Physicochemical Properties of Newly Formed ZnO-PMMA Nanocomposites for Denture Bases', *Nanomaterials (Basel),* 8(5).

Coco, B., Bagg, J., Cross, L., Jose, A., Cross, J. & Ramage, G. (2008). 'Mixed Candida albicans and Candida glabrata populations associated with the pathogenesis of denture stomatitis', *Oral microbiology and immunology,* 23(5), pp. 377-383.

Combe, E. C., Burke, F. T. & Douglas, W. H. (1999). *Dental biomaterials*: Springer.

Cooper, L. F. (2009). 'The current and future treatment of edentulism', *Journal of Prosthodontics: Implant, Esthetic and Reconstructive Dentistry,* 18(2), pp. 116-122.

Cristache, C. M., Totu, E. E., Iorgulescu, G., Pantazi, A., Dorobantu, D., Nechifor, A. C., Isildak, I., Burlibasa, M., Nechifor, G. & Enachescu, M. (2020). 'Eighteen Months Follow-Up with Patient-Centered Outcomes Assessment of Complete Dentures Manufactured Using a Hybrid Nanocomposite and Additive CAD/CAM Protocol', *J Clin Med,* 9(2).

Cucci, A. L. M., Vergani, C. E., Giampaolo, E. T. & Afonso, M. C. d. S. F. (1998). 'Water sorption, solubility, and bond strength of two autopolymerizing acrylic resins and one heat-polymerizing acrylic resin', *The Journal of prosthetic dentistry,* 80(4), pp. 434-438.

Czichos, H., Saito, T. & Smith, L. E. (2011). *Springer handbook of metrology and testing*: Springer Science & Business Media.

da Cruz Perez, L. E., Machado, A. L., Vergani, C. E., Zamperini, C. A., Pavarina, A. C. & Canevarolo Jr, S. V. (2014). 'Resistance to impact of cross-linked denture base biopolymer materials: Effect of relining, glass flakes reinforcement and cyclic loading', *Journal of The Mechanical Behavior of Biomedical Materials,* 37, pp. 33-41.

Dalben-Dota, K. F., Faria, M. G., Bruschi, M. L., Pelloso, S. M., Lopes-Consolaro, M. E. & Svidzinski, T. I. (2010). 'Antifungal activity of propolis extract against yeasts isolated from vaginal exudates', *The Journal of Alternative and Complementary Medicine,* 16(3), pp. 285-290.

Davidowitz, G. & Kotick, P. G. (2011). 'The use of CAD/CAM in dentistry', *Dent Clin North Am,* 55(3), pp. 559-70, ix.

Dawood, A., Marti Marti, B., Sauret-Jackson, V. & Darwood, A. (2015). '3D printing in dentistry', *Br Dent J,* 219(11), pp. 521-9.

De Palma, R., Peeters, S., Van Bael, M. J., Van den Rul, H., Bonroy, K., Laureyn, W., Mullens, J., Borghs, G. & Maes, G. (2007). 'Silane ligand exchange to make hydrophobic

superparamagnetic nanoparticles water-dispersible', *Chemistry of Materials,* 19(7), pp. 1821-1831.

Dean, J. A. (2021). *McDonald and Avery's dentistry for the child and adolescent-E-book*: Elsevier Health Sciences.

Deeb, G. R., Allen, R. K., Hall, V. P., Whitley, D., Laskin, D. M. & Bencharit, S. (2017). 'How Accurate Are Implant Surgical Guides Produced With Desktop Stereolithographic 3-Dimentional Printers?', *Journal of Oral and Maxillofacial Surgery,* 75(12).

Della Bona, A., Cantelli, V., Britto, V. T., Collares, K. F. & Stansbury, J. W. (2021). '3D printing restorative materials using a stereolithographic technique: A systematic review', *Dental Materials,* 37(2), pp. 336-350.

Devlin, H. & Watts, D. C. (1984). 'Acrylic 'allergy'?', *Br Dent J,* 157(8), pp. 272-5.

Dhir, G., Berzins, D. W., Dhuru, V. B., Periathamby, A. R. & Dentino, A. (2007). 'Physical properties of denture base resins potentially resistant to Candida adhesion', *J Prosthodont,* 16(6), pp. 465-472.

Di Fiore, A., Meneghello, R., Brun, P., Rosso, S., Gattazzo, A., Stellini, E. & Yilmaz, B. (2022). 'Comparison of the flexural and surface properties of milled, 3D-printed, and heat polymerized PMMA resins for denture bases: An in vitro study', *Journal of prosthodontic research,* 66(3), pp. 502-508.

Dimitrov, D., Schreve, K. & de Beer, N. (2006). 'Advances in three dimensional printing–state of the art and future perspectives', *Rapid Prototyping Journal*.

Diwan, R. (2004). 'Materials prescribed in the management of edentulous patients', *Prosthodontic Treatment for Edentulous Patients. ed,* 12, pp. 190-207.

Doğan, A., Bek, B., Cevik, N. & Usanmaz, A. (1995). 'The effect of preparation conditions of acrylic denture base materials on the level of residual monomer, mechanical properties and water absorption', *Journal of dentistry,* 23(5), pp. 313-318.

Druck, C. C., Pozzobon, J. L., Callegari, G. L., Dorneles, L. S. & Valandro, L. F. (2015). 'Adhesion to Y-TZP ceramic: Study of silica nanofilm coating on the surface of Y-TZP', *Journal of Biomedical Materials Research Part B: Applied Biomaterials,* 103(1), pp. 143-150.

Duan, A., Li, Y., Li, B. & Zhu, P. (2020). '3D-printable thermochromic acrylic resin with excellent mechanical performance', *Journal of Applied Polymer Science,* 137(2).

Duarte, S., Sartori, N. & Phark, J. H. (2016). 'Ceramic-reinforced polymers: CAD/CAM hybrid restorative materials', *Curr Oral Health Rep,* 3(3), pp. 198-202.

Eakle, W. S. & Bastin, K. G. (2019). *Dental materials: clinical applications for dental assistants and dental hygienists*: Elsevier Health Sciences.

El Hejazi, A. & Watts, D. (1999). 'Creep and visco-elastic recovery of cured and secondary-cured composites and resin-modified glass-ionomers', *Dental Materials,* 15(2), pp. 138-143.

Eliades, G., Eliades, T., Brantley, W. A. & Watts, D. C. (2003). *Dental materials in vivo: aging and related phenomena*: Quintessence Chicago.

Elsaka, S. E., Hamouda, I. M. & Swain, M. V. (2011). 'Titanium dioxide nanoparticles addition to a conventional glass-ionomer restorative: influence on physical and antibacterial properties', *Journal of dentistry,* 39(9), pp. 589-598.

Elshereksi, N. W., Ghazali, M. J., Muchtar, A. & Azhari, C. H. (2014). 'Perspectives for titanium-derived fillers usage on denture base composite construction: A review article', *Advances in Materials Science and Engineering,* 2014.

Fahad, M., Dickens, P. & Gilbert, M. (2013). 'Novel polymeric support materials for jetting based additive manufacturing processes', *Rapid Prototyping Journal,* 19(4), pp. 230-239.

Faot, F., Costa, M. A., Cury, A. A. D. B. & Garcia, R. C. R. (2006). 'Impact strength and fracture morphology of denture acrylic resins', *The Journal of prosthetic dentistry,* 96(5), pp. 367-373.

Farina, A. P., Cecchin, D., Soares, R. G., Botelho, A. L., Takahashi, J. M., Mazzetto, M. O. & Mesquita, M. F. (2012). 'Evaluation of Vickers hardness of different types of acrylic denture base resins with and without glass fibre reinforcement', *Gerodontology,* 29(2), pp. e155-60.

Farina, A. P., Cecchin, D., Soares, R. G., Botelho, A. L., Takahashi, J. M. F. K., Mazzetto, M. O. & Mesquita, M. F. (2012). 'Evaluation of Vickers hardness of different types of acrylic denture base resins with and without glass fibre reinforcement', *Gerodontology,* 29(2), pp. e155-e160.

Ferracane, J., Berge, H. & Condon, J. (1998). 'In vitro aging of dental composites in water—effect of degree of conversion, filler volume, and filler/matrix coupling', *Journal of Biomedical Materials Research: An Official Journal of The Society for Biomaterials, The Japanese Society for Biomaterials, and the Australian Society for Biomaterials,* 42(3), pp. 465-472.

Ferracane, J., Hilton, T., Stansbury, J., Watts, D., Silikas, N., Ilie, N., Heintze, S., Cadenaro, M. & Hickel, R. (2017). 'Academy of Dental Materials guidance—Resin composites: Part II—Technique sensitivity (handling, polymerization, dimensional changes)', *Dental materials,* 33(11), pp. 1171-1191.

Ferracane, J. L. (1995). 'Current trends in dental composites', *Critical Reviews in Oral Biology & Medicine,* 6(4), pp. 302-318.

Ferracane, J. L. (2001). *Materials in dentistry: principles and applications*: Lippincott Williams & Wilkins.

Fischer, J., Roeske, S., Stawarczyk, B. & Haemmerle, C. H. (2010). 'Investigations in the correlation between Martens hardness and flexural strength of composite resin restorative materials', *Dental materials journal,* 29(2), pp. 188-192.

FORMLABS (2021). *Form Cure time and temperature settings*. Available at: https://support.formlabs.com/s/article/Form-Cure-Time-and-Temperature-Settings?language=en_US.

Frankamp, B. L., Fischer, N. O., Hong, R., Srivastava, S. & Rotello, V. M. (2006). 'Surface modification using cubic silsesquioxane ligands. Facile synthesis of water-soluble metal oxide nanoparticles', *Chemistry of Materials,* 18(4), pp. 956-959.

Fugolin, A. & Pfeifer, C. (2017). 'New resins for dental composites', *Journal of dental research,* 96(10), pp. 1085-1091.

Gad, M. M. & Abualsaud, R. (2019). 'Behavior of PMMA Denture Base Materials Containing Titanium Dioxide Nanoparticles: A Literature Review', *International Journal of Biomaterials*.

Gad, M. M., Al-Thobity, A. M., Fouda, S. M., Napankangas, R. & Raustia, A. (2020). 'Flexural and Surface Properties of PMMA Denture Base Material Modified with Thymoquinone as an Antifungal Agent', *J Prosthodont,* 29(3), pp. 243-250.

Gad, M. M., Al-Harbi, F. A., Akhtar, S. & Fouda, S. M. (2022a). '3D-Printable Denture Base Resin Containing SiO2 Nanoparticles: An In Vitro Analysis of Mechanical and Surface Properties', *Journal of Prosthodontics*.

Gad, M. M., Alshehri, S. Z., Alhamid, S. A., Albarrak, A., Khan, S. Q., Alshahrani, F. A. & Alqarawi, F. K. (2022b). 'Water sorption, solubility, and translucency of 3D-printed denture base resins', *Dentistry Journal,* 10(3), p. 42.

Gad, M. M., Fouda, S. M., Abualsaud, R., Alshahrani, F. A., Al-Thobity, A. M., Khan, S. Q., Akhtar, S., Ateeq, I. S., Helal, M. A. & Al-Harbi, F. A. (2021). 'Strength and Surface Properties of a 3D-Printed Denture Base Polymer', *J Prosthodont*.

Gad, M. M., Fouda, S. M., Abualsaud, R., Alshahrani, F. A., Al-Thobity, A. M., Khan, S. Q., Akhtar, S., Ateeq, I. S., Helal, M. A. & Al-Harbi, F. A. (2022c). 'Strength and surface properties of a 3D-printed denture base polymer', *Journal of Prosthodontics,* 31(5), pp. 412-418.

Gad, M. M., Fouda, S. M., Al-Harbi, F. A., Napankangas, R. & Raustia, A. (2017). 'PMMA denture base material enhancement: a review of fiber, filler, and nanofiller addition', *Int J Nanomedicine,* 12, pp. 3801-3812.

Gad, M. M., Rahoma, A., Al-Thobity, A. M. & ArRejaie, A. S. (2016). 'Influence of incorporation of ZrO2 nanoparticles on the repair strength of polymethyl methacrylate denture bases', *International journal of nanomedicine,* 11, p. 5633.

Galvão, M. R., Caldas, S. G. F. R., Bagnato, V. S., de Souza Rastelli, A. N. & de Andrade, M. F. (2013). 'Evaluation of degree of conversion and hardness of dental composites photo-activated with different light guide tips', *Eur J Dent,* 7(1), p. 86.

Garcia, L. d. F. R., Roselino, L. d. M. R., Mundim, F. M., Pires-de-Souza, F. d. C. P. & Consani, S. (2010). 'Influence of artificial accelerated aging on dimensional stability of acrylic resins submitted to different storage protocols', *Journal of Prosthodontics: Implant, Esthetic and Reconstructive Dentistry,* 19(6), pp. 432-437.

Gautam, R., Singh, R. D., Sharma, V. P., Siddhartha, R., Chand, P. & Kumar, R. (2012). 'Biocompatibility of polymethylmethacrylate resins used in dentistry', *Journal of Biomedical Materials Research Part B: Applied Biomaterials,* 100(5), pp. 1444-1450.

Gendreau, L. & Loewy, Z. G. (2011). 'Epidemiology and etiology of denture stomatitis', *J Prosthodont,* 20(4), pp. 251-60.

Ghahremani, L., Shirkavand, S., Akbari, F. & Sabzikari, N. (2017). 'Tensile strength and impact strength of color modified acrylic resin reinforced with titanium dioxide nanoparticles', *J Clin Exp Dent,* 9(5), pp. e661-e665.

Ghavami-Lahiji, M., Firouzmanesh, M., Bagheri, H., Kashi, T. S. J., Razazpour, F. & Behroozibakhsh, M. (2018). 'The effect of thermocycling on the degree of conversion and mechanical properties of a microhybrid dental resin composite', *Restorative dentistry & endodontics,* 43(2).

Gibson, I., Rosen, D. & Stucker, B. (2014). 'Additive Manufacturing Technologies: Rapid Prototyping to Direct Digital Manufacturing, 498 Springer', *New York,* 2.

Goiato, M. C., Nóbrega, A. S., Santos, D. M. d., Andreotti, A. M. & Moreno, A. (2013). 'Effect of different solutions on color stability of acrylic resin-based dentures', *Brazilian Oral Research,* 28, pp. 1-7.

Goodacre, B. J., Goodacre, C. J., Baba, N. Z. & Kattadiyil, M. T. (2016). 'Comparison of denture base adaptation between CAD-CAM and conventional fabrication techniques', *The Journal of prosthetic dentistry,* 116(2), pp. 249-256.

Grande, F., Tesini, F., Pozzan, M. C., Zamperoli, E. M., Carossa, M. & Catapano, S. (2022). 'Comparison of the accuracy between denture bases produced by subtractive and additive manufacturing methods: a pilot study', *Prosthesis,* 4(2), pp. 151-159.

Greil, V., Mayinger, F., Reymus, M. & Stawarczyk, B. (2023). 'Water sorption, water solubility, degree of conversion, elastic indentation modulus, edge chipping resistance and flexural strength of 3D-printed denture base resins', *Journal of the Mechanical Behavior of Biomedical Materials,* 137, p. 105565.

Gungor, H., Gundogdu, M., Alkurt, M. & Duymus, Z. Y. (2017). 'Effect of polymerization cycles on flexural strengths and microhardness of different denture base materials', *Dental Materials Journal,* 36(2), pp. 168-173.

Gungor, H., Gundogdu, M. & Duymus, Z. Y. (2014). 'Investigation of the effect of different polishing techniques on the surface roughness of denture base and repair materials', *The Journal of prosthetic dentistry,* 112(5), pp. 1271-1277.

Hada, T., Kanazawa, M., Iwaki, M., Arakida, T. & Minakuchi, S. (2020). 'Effect of printing direction on stress distortion of three-dimensional printed dentures using stereolithography technology', *Journal of the Mechanical Behavior of Biomedical Materials,* 110, p. 103949.

Hague, R., Mansour, S., Saleh, N. & Harris, R. (2004). 'Materials analysis of stereolithography resins for use in rapid manufacturing', *J Mater Sci Mater Med,* 39(7), pp. 2457-2464.

Hamming, L. M., Qiao, R., Messersmith, P. B. & Brinson, L. C. (2009). 'Effects of dispersion and interfacial modification on the macroscale properties of TiO2 polymer–matrix nanocomposites', *Composites science and technology,* 69(11-12), pp. 1880-1886.

Hampe, R., Lümkemann, N., Sener, B. & Stawarczyk, B. (2018). 'The effect of artificial aging on Martens hardness and indentation modulus of different dental CAD/CAM restorative materials', *Journal of the Mechanical Behavior of Biomedical Materials,* 86, pp. 191-198.

Hamza, T. A., Rosenstiel, S. F., Elhosary, M. M. & Ibraheem, R. M. (2004). 'The effect of fiber reinforcement on the fracture toughness and flexural strength of provisional restorative resins', *The Journal of prosthetic dentistry,* 91(3), pp. 258-264.

Harini, P., Mohamed, K. & Padmanabhan, T. V. (2014). 'Effect of Titanium dioxide nanoparticles on the flexural strength of polymethylmethacrylate: an in vitro study', *Indian J Dent Res,* 25(4), pp. 459-63.

Hashem, M., Alsaleem, S. O., Assery, M. K., Abdeslam, E. B., Vellappally, S. & Anil, S. (2014). 'A comparative study of the mechanical properties of the light-cure and conventional denture base resins', *Oral Health Dent Manag,* 13(2), pp. 311-5.

Hashem, M., Rez, M. F. A., Fouad, H., Elsarnagawy, T., Elsharawy, M. A., Umar, A., Assery, M. & Ansari, S. (2017). 'Influence of titanium oxide nanoparticles on the physical and thermomechanical behavior of poly methyl methacrylate (PMMA): a denture base resin', *Science of Advanced Materials,* 9(6), pp. 938-944.

Honorez, P., Catalan, A., Angnes, U. & Grimonster, J. (1989). 'The effect of three processing cycles on some physical and chemical properties of a heat-cured acrylic resin', *The Journal of prosthetic dentistry,* 61(4), pp. 510-517.

Hull, C. W. (1984). 'Apparatus for production of three-dimensional objects by stereolithography', *United States Patent, Appl., No. 638905, Filed*.

Ilie, N. & Hickel, R. (2009). 'Investigations on mechanical behaviour of dental composites', *Clinical oral investigations,* 13, pp. 427-438.

Ilie, N. & Hickel, R. (2011). 'Resin composite restorative materials', *Australian dental journal,* 56, pp. 59-66.

Ilie, N., Hilton, T., Heintze, S., Hickel, R., Watts, D., Silikas, N., Stansbury, J., Cadenaro, M. & Ferracane, J. (2017). 'Academy of dental materials guidance—Resin composites: Part I—Mechanical properties', *Dental materials,* 33(8), pp. 880-894.

Imazato, S., TARUMI, H., KATO, S., EBI, N., EHARA, A. & EBISU, S. (1999). 'Water sorption, degree of conversion, and hydrophobicity of resins containing Bis-GMA and TEGDMA', *Dental Materials Journal,* 18(1), pp. 124-132.

Infante, L., Yilmaz, B., McGlumphy, E. & Finger, I. (2014). 'Fabricating complete dentures with CAD/CAM technology', *The Journal of prosthetic dentistry,* 111(5), pp. 351-355.

Infuehr, R., Pucher, N., Heller, C., Lichtenegger, H., Liska, R., Schmidt, V., Kuna, L., Haase, A. & Stampfl, J. (2007). 'Functional polymers by two-photon 3D lithography', *Applied Surface Science,* 254(4), pp. 836-840.

Iwaki, M., Kanazawa, M., Arakida, T. & Minakuchi, S. (2020). 'Mechanical properties of a polymethyl methacrylate block for CAD/CAM dentures', *Journal of Oral Science,* 62(4), pp. 420-422.

Jagger, D., Jagger, R., Allen, S. & Harrison, A. (2002). 'An investigation into the transverse and impact strength ofhigh strength'denture base acrylic resins', *Journal of oral rehabilitation,* 29(3), pp. 263-267.

Jeon, S., Jo, Y.-H., Yoon, H.-I. & Han, J.-S. (2022). 'Antifungal effect, surface roughness, and cytotoxicity of three-dimensionally printed denture base with phytoncide-filled microcapsules: an in-vitro study', *Journal of Dentistry,* 120, p. 104098.

Jerg, A., Schulz, S., Tomakidi, P., Hellwig, E. & Polydorou, O. (2018). 'Modulation of gingival cell response towards dental composites', *Dental Materials,* 34(3), pp. 412-426.

Jindal, P., Juneja, M., Bajaj, D., Siena, F. L. & Breedon, P. (2020). 'Effects of post-curing conditions on mechanical properties of 3D printed clear dental aligners', *Rapid Prototyp J*.

John, J., Gangadhar, S. A. & Shah, I. (2001). 'Flexural strength of heat-polymerized polymethyl methacrylate denture resin reinforced with glass, aramid, or nylon fibers', *The Journal of prosthetic dentistry,* 86(4), pp. 424-427.

John, J., Gangadhar, S. A. & Shah, I. (2001). 'Flexural strength of heat-polymerized polymethyl methacrylate denture resin reinforced with glass, aramid, or nylon fibers', *J Prosthet Dent,* 86(4), pp. 424-7.

Johnson, W. W. (1959). 'The history of prosthetic dentistry', *The Journal of Prosthetic Dentistry,* 9(5), pp. 841-846.

Jordan, J., Jacob, K. I., Tannenbaum, R., Sharaf, M. A. & Jasiuk, I. (2005). 'Experimental trends in polymer nanocomposites—a review', *Materials science and engineering: A,* 393(1-2), pp. 1-11.

Jorge, J. H., Giampaolo, E. T., Vergani, C. E., Machado, A. L., Pavarina, A. C. & Carlos, I. Z. (2007). 'Biocompatibility of denture base acrylic resins evaluated in culture of L929 cells. Effect of polymerisation cycle and post-polymerisation treatments', *Gerodontology,* 24(1), pp. 52-57.

Juneja, M., Thakur, N., Kumar, D., Gupta, A., Bajwa, B. & Jindal, P. (2018). 'Accuracy in dental surgical guide fabrication using different 3-D printing techniques', *Additive Manufacturing,* 22, pp. 243-255.

Junior, S. A. R., Scherrer, S. S., Ferracane, J. L. & Della Bona, A. (2008). 'Microstructural characterization and fracture behavior of a microhybrid and a nanofill composite', *Dental materials,* 24(9), pp. 1281-1288.

Karami, P., Salkhi Khasraghi, S., Hashemi, M., Rabiei, S. & Shojaei, A. (2019). 'Polymer/nanodiamond composites - a comprehensive review from synthesis and fabrication to properties and applications', *Adv Colloid Interface Sci,* 269, pp. 122-151.

Karci, M., Demir, N. & Yazman, S. (2019). 'Evaluation of Flexural Strength of Different Denture Base Materials Reinforced with Different Nanoparticles', *J Prosthodont,* 28(5), pp. 572-579.

Katheng, A., Kanazawa, M., Iwaki, M. & Minakuchi, S. (2021). 'Evaluation of dimensional accuracy and degree of polymerization of stereolithography photopolymer resin under different postpolymerization conditions: an in vitro study', *J. Prosthet. Dent.,* 125(4), pp. 695-702.

Kattadiyil, M. T. & AlHelal, A. (2017). 'An update on computer-engineered complete dentures: A systematic review on clinical outcomes', *The Journal of prosthetic dentistry,* 117(4), pp. 478-485.

Kawaguchi, T., Lassila, L. V., Sasaki, H., Takahashi, Y. & Vallittu, P. K. (2014). 'Effect of heat treatment of polymethyl methacrylate powder on mechanical properties of denture base resin', *Journal of the mechanical behavior of biomedical materials,* 39, pp. 73-78.

Kessler, A., Hickel, R. & Reymus, M. (2020). '3D printing in dentistry—State of the art', *Operative dentistry,* 45(1), pp. 30-40.

Khaled, S., Sui, R., Charpentier, P. A. & Rizkalla, A. S. (2007). 'Synthesis of TiO2− PMMA nanocomposite: Using methacrylic acid as a coupling agent', *Langmuir,* 23(7), pp. 3988-3995.

Khattar, A., Alsaif, M. H., Alghafli, J. A., Alshaikh, A. A., Alsalem, A. M., Almindil, I. A., Alsalman, A. M., Alboori, A. J., Al-Ajwad, A. M. & Almuhanna, H. M. (2022). 'Influence of ZrO2 Nanoparticle Addition on the Optical Properties of Denture Base Materials Fabricated Using Additive Technologies', *Nanomaterials,* 12(23), p. 4190.

Kim, D., Shim, J. S., Lee, D., Shin, S. H., Nam, N. E., Park, K. H., Shim, J. S. & Kim, J. E. (2020). 'Effects of post-curing time on the mechanical and color properties of three-dimensional printed crown and bridge materials', *Polymers (Basel),* 12(11), p. 2762.

Kim, K.-H., Ong, J. L. & Okuno, O. (2002). 'The effect of filler loading and morphology on the mechanical properties of contemporary composites', *The Journal of prosthetic dentistry,* 87(6), pp. 642-649.

Klapdohr, S. & Moszner, N. (2005). 'New inorganic components for dental filling composites', *Monatshefte für Chemie/Chemical Monthly,* 136, pp. 21-45.

Kruth, J. P., Mercelis, P., Van Vaerenbergh, J., Froyen, L. & Rombouts, M. (2005). 'Binding mechanisms in selective laser sintering and selective laser melting', *Rapid prototyping journal*.

Kurzmann, C., Janjić, K., Shokoohi-Tabrizi, H., Edelmayer, M., Pensch, M., Moritz, A. & Agis, H. (2017). 'Evaluation of resins for stereolithographic 3D-printed surgical guides: the response of L929 cells and human gingival fibroblasts', *BioMed research international,* 2017.

Kwon, T. Y., Bagheri, R., Kim, Y. K., Kim, K. H. & Burrow, M. F. (2012). 'Cure mechanisms in materials for use in esthetic dentistry', *Journal of investigative and clinical dentistry,* 3(1), pp. 3-16.

Lee, D. J. & Saponaro, P. C. (2019). 'Management of edentulous patients', *Dental Clinics,* 63(2), pp. 249-261.

Lee, J. (2020). *Impact strength of 3D printed and conventional heat-cured and cold-cured denture base acrylics.* The University of Texas School of Dentistry at Houston

Lee, S., Hong, S. J., Paek, J., Pae, A., Kwon, K. R. & Noh, K. (2019). 'Comparing accuracy of denture bases fabricated by injection molding, CAD/CAM milling, and rapid prototyping method', *J Adv Prosthodont,* 11(1), pp. 55-64.

Letcher, T. & Waytashek, M. (2014). Material property testing of 3D-printed specimen in PLA on an entry-level 3D printer. *In:* ASME International Mechanical Engineering Congress and Exposition, 2014. American Society of Mechanical Engineers. p. V02AT02A014.

Li, B. B., Xu, J. B., Cui, H. Y., Lin, Y. & Di, P. (2016). 'In vitro evaluation of the flexural properties of All-on-Four provisional fixed denture base resin partially reinforced with fibers', *Dent Mater J,* 35(2), pp. 264-9.

Li, F., Zhou, S., You, B. & Wu, L. (2006). 'Kinetic study on the UV-induced photopolymerization of epoxy acrylate/TiO2 nanocomposites by FTIR spectroscopy', *Journal of applied polymer science,* 99(6), pp. 3281-3287.

Liao, W., Zheng, S., Chen, S., Zhao, L., Huang, X., Huang, L. & Kang, S. (2020). 'Surface silanization and grafting reaction of nano-silver loaded zirconium phosphate and properties strengthen in 3D-printable dental base composites', *J Mech Behav Biomed Mater,* 110, p. 103864.

Liebermann, A., Wimmer, T., Schmidlin, P. R., Scherer, H., Löffler, P., Roos, M. & Stawarczyk, B. (2016). 'Physicomechanical characterization of polyetheretherketone and current esthetic dental CAD/CAM polymers after aging in different storage media', *The Journal of prosthetic dentistry,* 115(3), pp. 321-328. e2.

Lin, C. H., Lin, Y. M., Lai, Y. L. & Lee, S. Y. (2019). 'Mechanical properties, accuracy, and cytotoxicity of UV-polymerized 3D printing resins composed of BisEMA, UDMA, and TEGDMA', *J Prosthet Dent*.

Lin, C. T., Lee, S. Y., Tsai, T. Y., Dong, D. R. & Shih, Y. H. (2000). 'Degradation of repaired denture base materials in simulated oral fluid', *Journal of Oral Rehabilitation,* 27(3), pp. 190-198.

Lockhart, S., Joly, S., Vargas, K., Swails-Wenger, J., Enger, L. & Soll, D. (1999). 'Natural defenses against Candida colonization breakdown in the oral cavities of the elderly', *Journal of dental research,* 78(4), pp. 857-868.

Machado, A. L., Bochio, B. C., Wady, A. F., Jorge, J. H., Canevarolo, S. V. & Vergani, C. E. (2012). 'Impact strength of denture base and reline acrylic resins: An in vitro study', *Journal of Dental Biomechanics,* 3.

Malacarne, J., Carvalho, R. M., de Goes, M. F., Svizero, N., Pashley, D. H., Tay, F. R., Yiu, C. K. & de Oliveira Carrilho, M. R. (2006a). 'Water sorption/solubility of dental adhesive resins', *Dental materials,* 22(10), pp. 973-980.

Malacarne, J., Carvalho, R. M., Mario, F., Svizero, N., Pashley, D. H., Tay, F. R., Yiu, C. K. & de Oliveira Carrilho, M. R. (2006b). 'Water sorption/solubility of dental adhesive resins', *Dental materials,* 22(10), pp. 973-980.

Mangal, U., Kim, J.-Y., Seo, J.-Y., Kwon, J.-S. & Choi, S.-H. (2019). 'Novel poly (methyl methacrylate) containing nanodiamond to improve the mechanical properties and fungal resistance', *Materials,* 12(20), p. 3438.

Mangal, U., Min, Y. J., Seo, J. Y., Kim, D. E., Cha, J. Y., Lee, K. J., Kwon, J. S. & Choi, S. H. (2020a). 'Changes in tribological and antibacterial properties of poly(methyl methacrylate)-based 3D-printed intra-oral appliances by incorporating nanodiamonds', *J Mech Behav Biomed Mater,* 110, p. 103992.

Mangal, U., Seo, J. Y., Yu, J., Kwon, J. S. & Choi, S. H. (2020b). 'Incorporating Aminated Nanodiamonds to Improve the Mechanical Properties of 3D-Printed Resin-Based Biomedical Appliances', *Nanomaterials (Basel),* 10(5).

Masri, G., Mortada, R., Ounsi, H., Alharbi, N., Boulos, P. & Salameh, Z. (2020). 'Adaptation of Complete Denture Base Fabricated by Conventional, Milling, and 3-D Printing Techniques: An In Vitro Study', *J Contemp Dent Pract,* 21(4), pp. 367-371.

Matos, A. O., Costa, J. O., Beline, T., Ogawa, E. S., Assunção, W. G., Mesquita, M. F., Consani, R. X. & Barão, V. A. (2018). 'Effect of disinfection on the bond strength between denture teeth and microwave-cured acrylic resin denture base', *Journal of Prosthodontics,* 27(2), pp. 169-176.

Matta, R. E., Bergauer, B., Adler, W., Wichmann, M. & Nickenig, H. J. (2017). 'The impact of the fabrication method on the three-dimensional accuracy of an implant surgery template', *Journal of Cranio-Maxillofacial Surgery,* 45(6), pp. 804-808.

McCabe, J. F. & Walls, A. W. (2013). *Applied dental materials*: John Wiley & Sons.

McLaughlin, J. B., Ramos, V., Jr. & Dickinson, D. P. (2019). 'Comparison of Fit of Dentures Fabricated by Traditional Techniques Versus CAD/CAM Technology', *J Prosthodont,* 28(4), pp. 428-435.

Miller, F. P., Vandome, A. F. & McBrewster, J. (2010). Fused deposition modeling. VDM Publishing.

Miyazaki, T. & Hotta, Y. (2011). 'CAD/CAM systems available for the fabrication of crown and bridge restorations', *Aust Dent J,* 56 Suppl 1, pp. 97-106.

Mohsen, N. & Craig, R. (1995). 'Effect of silanation of fillers on their dispersability by monomer systems', *Journal of oral rehabilitation,* 22(3), pp. 183-189.

Monteiro, D. R., Gorup, L. F., Takamiya, A. S., de Camargo, E. R., Filho, A. C. R. & Barbosa, D. B. (2012). 'Silver distribution and release from an antimicrobial denture base resin containing silver colloidal nanoparticles', *Journal of Prosthodontics: Implant, Esthetic and Reconstructive Dentistry,* 21(1), pp. 7-15.

Mosalman, S., Rashahmadi, S. & Hasanzadeh, R. (2017). 'The Effect of TiO2 Nanoparticles on Mechanical Properties of Poly Methyl Methacrylate Nanocomposites', *International Journal of Engineering,* 30(5), pp. 807-813.

Moszner, N., Fischer, U. K., Ganster, B., Liska, R. & Rheinberger, V. (2008). 'Benzoyl germanium derivatives as novel visible light photoinitiators for dental materials', *Dental Materials,* 24(7), pp. 901-907.

Moszner, N. & Salz, U. (2001). 'New developments of polymeric dental composites', *Progress in polymer science,* 26(4), pp. 535-576.

Mubarak, S., Dhamodharan, D., B. Kale, M., Divakaran, N., Senthil, T., Wu, L. & Wang, J. (2020). 'A novel approach to enhance mechanical and thermal properties of SLA 3D printed structure by incorporation of metal–metal oxide nanoparticles', *Nanomaterials,* 10(2), p. 217.

Mubaraki, M. Q., Moaleem, M. M. A., Alzahrani, A. H., Shariff, M., Alqahtani, S. M., Porwal, A., Al-Sanabani, F. A., Bhandi, S., Tribst, J. P. M. & Heboyan, A. (2022). 'Assessment of Conventionally and Digitally Fabricated Complete Dentures: A Comprehensive Review', *Materials,* 15(11), p. 3868.

Murray, M. D. & Darvell, B. W. (1993). 'The Evolution of the Complete Denture Base - Theories of Complete Denture Retention - a Review .1.', *Australian Dental Journal,* 38(3), pp. 216-219.

Murray, M. D. & Darvell, B. W. (1993). 'The evolution of the complete denture base. Theories of complete denture retention—a review. Part 1', *Australian dental journal,* 38(3), pp. 216-219.

Navidfar, A., Azdast, T. & Karimzad Ghavidel, A. (2016). 'Influence of processing condition and carbon nanotube on mechanical properties of injection molded multi-walled carbon nanotube/poly (methyl methacrylate) nanocomposites', *Journal of Applied Polymer Science,* 133(31).

NextDent (2022a). *3D systems*. Available at: https:// nextdent.com/products/denture-3dplus/.

NextDent (2022b). *3D systems*. Available at: https://nextdent.com/products/denture-3dplus/.

Ngo, T. D., Kashani, A., Imbalzano, G., Nguyen, K. T. & Hui, D. (2018). 'Additive manufacturing (3D printing): A review of materials, methods, applications and challenges', *Composites Part B: Engineering,* 143, pp. 172-196.

Nicholson, J. W. & Czarnecka, B. (2008). 'The biocompatibility of resin-modified glass-ionomer cements for dentistry', *dental materials,* 24(12), pp. 1702-1708.

Noort, R. v. & Barbour, M. E. (2013). *Introduction to dental materials* (4th edition. ed.). Edinburgh ; New York: Mosby Elsevier.

Oliveira, L. V., Mesquita, M. F., Henriques, G. E. P., Consani, R. L. X. & Fragoso, W. S. (2008). 'Effect of polishing technique and brushing on surface roughness of acrylic resins', *Journal of Prosthodontics,* 17(4), pp. 308-311.

Onwubu, S. C., Mdluli, P. S. & Singh, S. (2018). 'The effect of colloidal silica and diamond suspensions on the surface roughness of automatically finished heat-polymerized acrylic resin', *The Journal of prosthetic dentistry,* 120(3), pp. 485. e1-485. e5.

Osman, R. B., Alharbi, N. & Wismeijer, D. (2017). 'Build angle: does it influence the accuracy of 3D-printed dental restorations using digital light-processing technology?', *International Journal of Prosthodontics,* 30(2).

Ozyilmaz, O. Y. & Akin, C. (2019). 'Effect of cleansers on denture base resins' structural properties', *Journal of applied biomaterials & functional materials,* 17(1), p. 2280800019827797.

Palaganas, N. B., Mangadlao, J. D., de Leon, A. C. C., Palaganas, J. O., Pangilinan, K. D., Lee, Y. J. & Advincula, R. C. (2017). '3D printing of photocurable cellulose nanocrystal composite for fabrication of complex architectures via stereolithography', *ACS Appl Mater Interfaces,* 9(39), pp. 34314-34324.

Park, J. M., Ahn, J. S., Cha, H. S. & Lee, J. H. (2018). 'Wear Resistance of 3D Printing Resin Material Opposing Zirconia and Metal Antagonists', *Materials,* 11(6).

Paulino, M. R., Alves, L. R., Gurgel, B. C. & Calderon, P. S. (2015). 'Simplified versus traditional techniques for complete denture fabrication: a systematic review', *The Journal of prosthetic dentistry,* 113(1), pp. 12-16.

Pazokifard, S., Farrokhpay, S., Mirabedini, M. & Esfandeh, M. (2015). 'Surface treatment of TiO2 nanoparticles via sol–gel method: effect of silane type on hydrophobicity of the nanoparticles', *Progress in Organic Coatings,* 87, pp. 36-44.

Peltzer, K., Hewlett, S., Yawson, A. E., Moynihan, P., Preet, R., Wu, F., Guo, G., Arokiasamy, P., Snodgrass, J. J. & Chatterji, S. (2014). 'Prevalence of loss of all teeth (edentulism) and

associated factors in older adults in China, Ghana, India, Mexico, Russia and South Africa', *International journal of environmental research and public health,* 11(11), pp. 11308-11324.

Pengpid, S. & Peltzer, K. (2018). 'The prevalence of edentulism and their related factors in Indonesia, 2014/15', *BMC oral health,* 18, pp. 1-9.

Perea-Lowery, L., Gibreel, M., Vallittu, P. K. & Lassila, L. (2021a). 'Evaluation of the mechanical properties and degree of conversion of 3D printed splint material', *Journal of the Mechanical Behavior of Biomedical Materials,* 115, p. 104254.

Perea-Lowery, L., Gibreel, M., Vallittu, P. K. & Lassila, L. V. (2021b). '3D-printed vs. heat-polymerizing and autopolymerizing denture base acrylic resins', *Materials,* 14(19), p. 5781.

Pereira-Cenci, T., Del Bel Cury, A. A., Crielaard, W. & Ten Cate, J. M. (2008). 'Development of Candida-associated denture stomatitis: new insights', *Journal of applied oral science,* 16, pp. 86-94.

Pereira, C. A., Toledo, B. C., Santos, C. T., Costa, A. C. B. P., Back-Brito, G. N., Kaminagakura, E. & Jorge, A. O. C. (2013). 'Opportunistic microorganisms in individuals with lesions of denture stomatitis', *Diagnostic microbiology and infectious disease,* 76(4), pp. 419-424.

Petrovic, V., Vicente Haro Gonzalez, J., Jordá Ferrando, O., Delgado Gordillo, J., Ramón Blasco Puchades, J. & Portolés Griñan, L. (2011). 'Additive layered manufacturing: sectors of industrial application shown through case studies', *International Journal of Production Research,* 49(4), pp. 1061-1079.

Pfeiffer, P. & Rosenbauer, E.-U. (2004). 'Residual methyl methacrylate monomer, water sorption, and water solubility of hypoallergenic denture base materials', *The Journal of prosthetic dentistry,* 92(1), pp. 72-78.

Polat, T. N., Karacaer, Ö., Tezvergil, A., Lassila, L. V. & Vallittu, P. K. (2003). 'Water sorption, solubility and dimensional changes of denture base polymers reinforced with short glass fibers', *Journal of biomaterials applications,* 17(4), pp. 321-335.

Polychronakis, N., Dimitriadi, M., Ioannidis, A. & Papadopoulos, T. (2020). 'The effect of different cooling procedures on mechanical properties of denture base materials measured by instrumented indentation testing', *Journal of prosthodontic research,* 64(3), pp. 326-331.

Powers, J. M. & Sakaguchi, R. L. (2006). *Craig's restorative dental materials*: Mosby Elsevier.

Prpic, V., Schauperl, Z., Catic, A., Dulcic, N. & Cimic, S. (2020). 'Comparison of Mechanical Properties of 3D-Printed, CAD/CAM, and Conventional Denture Base Materials', *J Prosthodont,* 29(6), pp. 524-528.

Prpic, V., Slacanin, I., Schauperl, Z., Catic, A., Dulcic, N. & Cimic, S. (2019). 'A study of the flexural strength and surface hardness of different materials and technologies for occlusal device fabrication', *J Prosthet Dent,* 121(6), pp. 955-959.

Puebla, K., Arcaute, K., Quintana, R. & Wicker, R. B. (2012a). 'Effects of environmental conditions, aging, and build orientations on the mechanical properties of ASTM type I specimens manufactured via stereolithography', *Rapid Prototyping Journal*.

Puebla, K., Arcaute, K., Quintana, R. & Wicker, R. B. (2012b). 'Effects of environmental conditions, aging, and build orientations on the mechanical properties of ASTM type I specimens manufactured via stereolithography', *Rapid Prototyp J*.

Rahal, J. S., Mesquita, M. F., Henriques, G. E. P. & Nóbilo, M. A. A. (2004a). 'Influence of chemical and mechanical polishing on water sorption and solubility of denture base acrylic resins', *Braz Oral Res,* 15(3), pp. 225-230.

Rahal, J. S., Mesquita, M. F., Henriques, G. E. P. & Nóbilo, M. A. A. (2004b). 'Influence of chemical and mechanical polishing on water sorption and solubility of denture base acrylic resins', *Brazilian Dental Journal,* 15, pp. 225-230.

Raj, V., Bhat, V., John, N., Shetty, A., Joseph, S., Kuriakose, R. & Hameed, S. (2021). 'Assessment of flexural strength and cytotoxicity of heat cure denture base resin modified with titanium dioxide nanoparticles: an in vitro study', *The Journal of Contemporary Dental Practice,* 22(9), pp. 1025-1029.

Ratner, B. D., Hoffman, A. S., Schoen, F. J. & Lemons, J. E. (2004). *Biomaterials science: an introduction to materials in medicine*: Elsevier.

Reijnders, L. (2009). 'The release of TiO2 and SiO2 nanoparticles from nanocomposites', *Polymer degradation and stability,* 94(5), pp. 873-876.

Rekow, E. D., Erdman, A. G., Riley, D. R. & Klamecki, B. (1991). 'CAD/CAM for dental restorations--some of the curious challenges', *IEEE Trans Biomed Eng,* 38(4), pp. 314-8.

Revilla-León, M. & Özcan, M. (2019). 'Additive manufacturing technologies used for processing polymers: current status and potential application in prosthetic dentistry', *Journal of Prosthodontics,* 28(2), pp. 146-158.

Reymus, M. & Stawarczyk, B. (2021). 'In vitro study on the influence of postpolymerization and aging on the Martens parameters of 3D-printed occlusal devices', *The Journal of Prosthetic Dentistry,* 125(5), pp. 817-823.

Ring, M. E. (1985). *Dentistry : an illustrated history*. New York: Abrams.

Rueggeberg, F. A. (2002). 'From vulcanite to vinyl, a history of resins in restorative dentistry', *J Prosthet Dent,* 87(4), pp. 364-79.

Rupf, S., Berger, H., Buchter, A., Harth, V., Ong, M. F. & Hannig, M. (2015). 'Exposure of patient and dental staff to fine and ultrafine particles from scanning spray', *Clinical oral investigations,* 19, pp. 823-830.

Ruyter, I. E. & Øysæd, H. (1987). 'Composites for use in posterior teeth: composition and conversion', *Journal of biomedical materials research,* 21(1), pp. 11-23.

Saini, R., Kotian, R., Madhyastha, P. & Srikant, N. (2016). 'Comparative study of sorption and solubility of heat-cure and self-cure acrylic resins in different solutions', *Indian Journal of Dental Research,* 27(3), p. 288.

Salim, S., Sadamori, S. & Hamada, T. (1992). 'The dimensional accuracy of rectangular acrylic resin specimens cured by three denture base processing method', *The Journal of prosthetic dentistry,* 67(6), pp. 879-881.

Sasaki, H., Hamanaka, I., Takahashi, Y. & Kawaguchi, T. (2016). 'Effect of long-term water immersion or thermal shock on mechanical properties of high-impact acrylic denture base resins', *Dent Mater J,* 35(2), pp. 204-9.

Schneider, L. F. J., Cavalcante, L. M. & Silikas, N. (2010). 'Shrinkage stresses generated during resin-composite applications: a review', *Journal of dental biomechanics,* 2010.

Schulz, S. D., König, A., Steinberg, T., Tomakidi, P., Hellwig, E. & Polydorou, O. (2012). 'Human gingival keratinocyte response to substances eluted from Silorane composite material reveal impact on cell behavior reflected by RNA levels and induction of apoptosis', *Dental Materials,* 28(8), pp. e135-e142.

Schweiger, J., Bomze, D. & Schwentenwein, M. (2019). '3D printing of zirconia–what is the future?', *Current Oral Health Reports,* 6, pp. 339-343.

Shah, M., Ullah, A., Azher, K., Rehman, A. U., Juan, W., Aktürk, N., Tüfekci, C. S. & Salamci, M. U. (2023). 'Vat photopolymerization-based 3D printing of polymer nanocomposites: current trends and applications', *RSC Advances,* 13(2), pp. 1456-1496.

Shahdad, S. A., McCabe, J. F., Bull, S., Rusby, S. & Wassell, R. W. (2007). 'Hardness measured with traditional Vickers and Martens hardness methods', *Dental Materials,* 23(9), pp. 1079-1085.

Shim, J. S., Kim, J. E., Jeong, S. H., Choi, Y. J. & Ryu, J. J. (2020). 'Printing accuracy, mechanical properties, surface characteristics, and microbial adhesion of 3D-printed resins with various printing orientations', *J Prosthet Dent,* 124(4), pp. 468-475.

Siedenbiedel, F. & Tiller, J. C. (2012). 'Antimicrobial polymers in solution and on surfaces: overview and functional principles', *Polymers,* 4(1), pp. 46-71.

Singh, R. D., Gautam, R., Siddhartha, R., Singh, B. P., Chand, P., Sharma, V. P. & Jurel, S. K. (2013). 'High performance liquid chromatographic determination of residual monomer released from heat-cured acrylic resin. An in vivo study', *Journal of Prosthodontics,* 22(5), pp. 358-361.

Singh, S., Palaskar, J. N. & Mittal, S. (2013). 'Comparative evaluation of surface porosities in conventional heat polymerized acrylic resin cured by water bath and microwave energy with microwavable acrylic resin cured by microwave energy', *Contemporary clinical dentistry,* 4(2), p. 147.

Singh, V. (2013). 'Rapid prototyping, materials for RP and applications of RP', *Int J Eng Res Sci,* 4(7), pp. 473-80.

Sjögren, G., Sletten, G. & Dahl, J. E. (2000). 'Cytotoxicity of dental alloys, metals, and ceramics assessed by millipore filter, agar overlay, and MTT tests', *The Journal of prosthetic dentistry,* 84(2), pp. 229-236.

Skordou, T., Kebi, L., Osnes, C. & Keeling, A. (2021). 'The effect of two different milling instrument sets on CAD proposed cement thickness and fit surface of chairside CAD crowns', *Journal of Osseointegration*, pp. S271-S278.

Slade, G., Akinkugbe, A. & Sanders, A. (2014). 'Projections of US edentulism prevalence following 5 decades of decline', *Journal of dental research,* 93(10), pp. 959-965.

Sodagar, A., Bahador, A., Khalil, S., Shahroudi, A. S. & Kassaee, M. Z. (2013). 'The effect of TiO2 and SiO2 nanoparticles on flexural strength of poly (methyl methacrylate) acrylic resins', *J Prosthodont Res,* 57(1), pp. 15-9.

Spartalis, G. K., Cappelletti, L. K., Schoeffel, A. C., Michél, M. D., Pegoraro, T. A., Arrais, C. A. G., Neppelenbroek, K. H. & Urban, V. M. (2015). 'Effect of conventional water-bath and experimental microwave polymerization cycles on the flexural properties of denture base acrylic resins', *Dental materials journal,* 34(5), pp. 623-628.

Stansbury, J. W. (2000). 'Curing dental resins and composites by photopolymerization', *Journal of esthetic and restorative dentistry,* 12(6), pp. 300-308.

Stansbury, J. W. & Idacavage, M. J. (2016). '3D printing with polymers: Challenges among expanding options and opportunities', *Dental materials,* 32(1), pp. 54-64.

Stansbury, J. W. & Idacavage, M. J. (2016). '3D printing with polymers: Challenges among expanding options and opportunities', *Dent Mater,* 32(1), pp. 54-64.

Steinmassl, O., Offermanns, V., Stöckl, W., Dumfahrt, H., Grunert, I. & Steinmassl, P.-A. (2018). 'In vitro analysis of the fracture resistance of CAD/CAM denture base resins', *Materials,* 11(3), p. 401.

Steyrer, B., Neubauer, P., Liska, R. & Stampfl, J. (2017). 'Visible light photoinitiator for 3D-printing of tough methacrylate resins', *Materials (Basel),* 10(12), p. 1445.

Szczesio-Wlodarczyk, A., Sokolowski, J., Kleczewska, J. & Bociong, K. (2020). 'Ageing of dental composites based on methacrylate resins—A critical review of the causes and method of assessment', *Polymers,* 12(4), p. 882.

Tahayeri, A., Morgan, M., Fugolin, A. P., Bompolaki, D., Athirasala, A., Pfeifer, C. S., Ferracane, J. L. & Bertassoni, L. E. (2018). '3D printed versus conventionally cured provisional crown and bridge dental materials', *Dental Materials,* 34(2), pp. 192-200.

Tasaka, A., Matsunaga, S., Odaka, K., Ishizaki, K., Ueda, T., Abe, S., Yoshinari, M., Yamashita, S. & Sakurai, K. (2019). 'Accuracy and retention of denture base fabricated by heat curing and additive manufacturing', *Journal of Prosthodontic Research,* 63(1), pp. 85-89.

Thangaraju, P. & Varthya, S. B. (2022). 'ISO 10993: Biological Evaluation of Medical Devices', *Medical Device Guidelines and Regulations Handbook*: Springerpp. 163-187.

Thomas, T. C., Mohamed, S., Krishnan, V., Mathew, A. & Manju, V. (2015). 'The effect on the flexural strength, flexural modulus and compressive strength of fibre reinforced acrylic with that of plain unfilled acrylic resin–an in vitro study', *Journal of Clinical and Diagnostic Research: JCDR,* 9(3), p. ZC12.

Tian, Y., Chen, C., Xu, X., Wang, J., Hou, X., Li, K., Lu, X., Shi, H., Lee, E.-S. & Jiang, H. B. (2021a). 'A review of 3D printing in dentistry: Technologies, affecting factors, and applications', *Scanning,* 2021.

Tian, Y., Chen, C., Xu, X., Wang, J., Hou, X., Li, K., Lu, X., Shi, H., Lee, E.-S. & Jiang, H. B. (2021b). 'A review of 3D printing in dentistry: Technologies, affecting factors, and applications', *Scanning Microsc,* 2021.

Torabi, K., Farjood, E. & Hamedani, S. (2015). 'Rapid prototyping technologies and their applications in prosthodontics, a review of literature', *Journal of Dentistry,* 16(1), p. 1.

TOTU, E., CRISTACHE, C., IŞILDAK, İ., YILDIRIM, R., Burlibasa, M., NİĞDE, M. & Burlibasa, L. (2018). 'Preliminary studies on citotoxicity and genotoxicity assessment of the PMMA-TiO2 nanocompozites for stereolithographic complete dentures manufacturing'.

Totu, E. E., Nechifor, A. C., Nechifor, G., Aboul-Enein, H. Y. & Cristache, C. M. (2017). 'Poly(methyl methacrylate) with TiO2 nanoparticles inclusion for stereolitographic complete denture manufacturing - the fututre in dental care for elderly edentulous patients?', *J Dent,* 59, pp. 68-77.

Traini, T., Mangano, C., Sammons, R., Mangano, F., Macchi, A. & Piattelli, A. (2008). 'Direct laser metal sintering as a new approach to fabrication of an isoelastic functionally graded material for manufacture of porous titanium dental implants', *Dental materials,* 24(11), pp. 1525-1533.

Trapalis, C. C., Keivanidis, P., Kordas, G., Zaharescu, M., Crisan, M., Szatvanyi, A. & Gartner, M. (2003). 'TiO2 (Fe3+) nanostructured thin films with antibacterial properties', *Thin Solid Films,* 433(1-2), pp. 186-190.

Treglia, A. S., Turco, S., Ulianich, L., Ausiello, P., Lofrumento, D. D., Nicolardi, G., Miele, C., Garbi, C., Beguinot, F. & Di Jeso, B. (2012). 'Cell fate following ER stress: just a matter of "quo ante" recovery or death?'.

Tsuji, M., Ueda, T., Sawaki, K., Kawaguchi, M. & Sakurai, K. (2016). 'Biocompatibility of a titanium dioxide-coating method for denture base acrylic resin', *Gerodontology,* 33(4), pp. 539-544.

Tuna, S. H., Keyf, F., Gumus, H. O. & Uzun, C. (2008). 'The evaluation of water sorption/solubility on various acrylic resins', *European journal of dentistry,* 2(03), pp. 191-197.

UMEMOTO, K. & KURATA, S. (1997). 'Basic study of a new denture base resin applying hydrophobic methacrylate monomer', *Dental Materials Journal,* 16(1), pp. 21-30,109.

Unkovskiy, A., Bui, P. H. B., Schille, C., Geis-Gerstorfer, J., Huettig, F. & Spintzyk, S. (2018). 'Objects build orientation, positioning, and curing influence dimensional accuracy and flexural properties of stereolithographically printed resin', *Dental Materials,* 34(12), pp. E324-E333.

Urcan, E., Scherthan, H., Styllou, M., Haertel, U., Hickel, R. & Reichl, F.-X. (2010). 'Induction of DNA double-strand breaks in primary gingival fibroblasts by exposure to dental resin composites', *Biomaterials,* 31(8).

Vaidyanathan, J. & Vaidyanathan, T. (2001). 'Flexural creep deformation and recovery in dental composites', *Journal of dentistry,* 29(8), pp. 545-551.

Vallittu, P. K., Lassila, V. P. & Lappalainen, R. (1994). 'Transverse strength and fatigue of denture acrylic-glass fiber composite', *Dent Mater,* 10(2), pp. 116-21.

Vallittu, P. K., Miettinen, V. & Alakuijala, P. (1995). 'Residual monomer content and its release into water from denture base materials', *Dental Materials,* 11(5-6), pp. 338-342.

van Noort, R. (2012). 'The future of dental devices is digital', *Dent Mater,* 28(1), pp. 3-12.

Vasiliu, M. P., Sachelarie, L., Tomita, D. I., Folescu, E. & Stadoleanu, C. (2016). Experimental evaluation of biocompatibility in case of acrylic materials by bio-testing on lab animals. *In:* Key Engineering Materials, 2016. Trans Tech Publ. pp. 231-235.

Vayrynen, V. O. E., Tanner, J. & Vallittu, P. K. (2016). 'The anisotropicity of the flexural properties of an occlusal device material processed by stereolithography', *Journal of Prosthetic Dentistry,* 116(5), pp. 811-817.

Wataha, J. C. (2012). 'Predicting clinical biological responses to dental materials', *Dental Materials,* 28(1), pp. 23-40.

Williams, J. & Cawood, M. (1990). 'European group on fracture: Kc and Gc methods for polymers', *Polymer testing,* 9(1), pp. 15-26.

Williams, J. A., Billington, R. W. & Pearson, G. J. (2001). 'A long term study of fluoride release from metal-containing conventional and resin-modified glass-ionomer cements', *J Oral Rehabil,* 28(1), pp. 41-7.

Wong, D. M., Cheng, L. Y., Chow, T. & Clark, R. K. (1999). 'Effect of processing method on the dimensional accuracy and water sorption of acrylic resin dentures', *The Journal of prosthetic dentistry,* 81(3), pp. 300-304.

Zafar, M. S. (2020). 'Prosthodontic applications of polymethyl methacrylate (PMMA): An update', *Polymers,* 12(10), p. 2299.

Zhang, Z.-c., Li, P.-l., Chu, F.-t. & Shen, G. (2019). 'Influence of the three-dimensional printing technique and printing layer thickness on model accuracy', *Journal of Orofacial Orthopedics/Fortschritte der Kieferorthopädie,* 80(4), pp. 194-204.

Zhang, Z. c., Li, P. l., Chu, F. t. & Shen, G. (2019). 'Influence of the three-dimensional printing technique and printing layer thickness on model accuracy', *J Orofac Orthop,* 80(4), pp. 194-204.

Zitzmann, N., Marinello, C., Zemp, E. & Kessler, P. (2001). 'Zahnverlust, prothetische Versorgung und zahnarztliche Inanspruchnahme in der Schweiz', *Schweizer Monatsschrift fur Zahnmedizin,* 111(11), pp. 1288-1302.

Appendix A

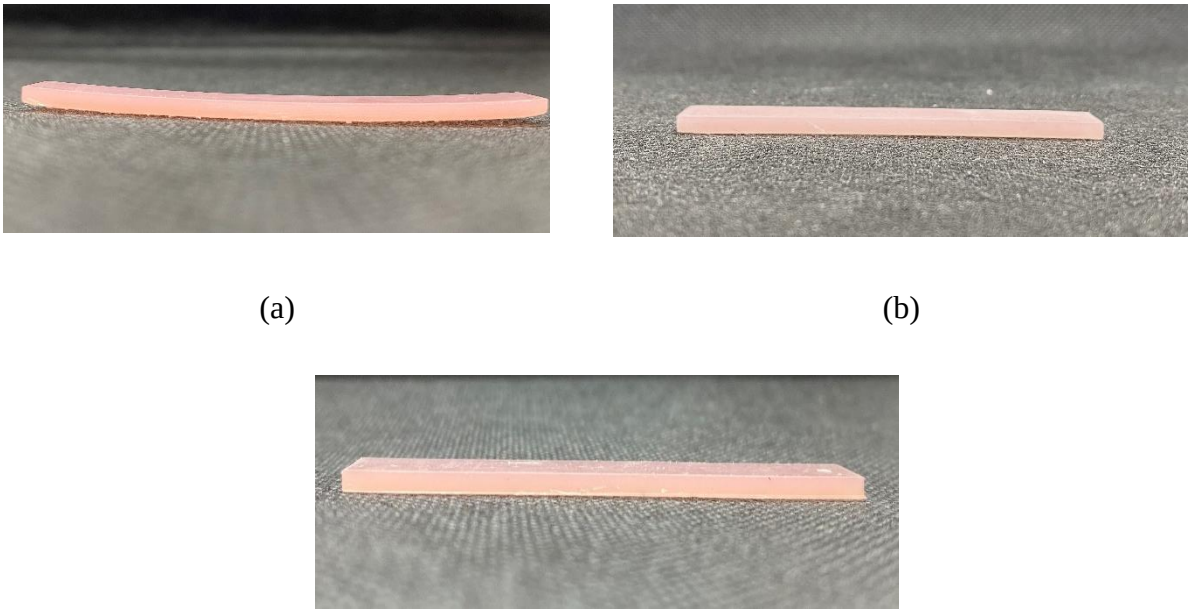

(a) (b)

(c)

Figure A.1. Images of 3D printed denture base resin material cured for 30 mins showing the shrinkage behaviour among: (a) 0˚ (b) 45˚ and (c) 90˚.

Appendix B

Table 0.1. Mean and standard deviation (SD) of sorption, solubility, and degree of conversion, for all test groups

Resin material	Sorption (µg/mm^3)	Solubility (µg/mm^3)	DC (%)
HC	19.9 (1.6)^{A}	1.3 (0.3)^{A}	97.2 (0.5)^{A}
FL	27.7 (0.8)^{B}	1.6 (0.3)^{A}	93.7 (4.7)^{AB}
ND	22.9 (0.4)^{C}	1.5 (0.4)^{A}	92.0 (1.6)^{B}

Table 0.2. Mean and standard deviation (SD) of Vickers and Martens hardness for the control and test groups before and after ageing process in artificial saliva for three months

Resin material	Vickers hardness (VHN)		Martens hardness (N/mm^2)	
	Before ageing	After ageing	Before ageing	After ageing
HC	15.0 (0.3)^{A,1*}	12.2 (0.4)^{A,2}	135.9 (6.1)^{A,1*}	107.0 (5.9)^{A,2}
FL	14.5 (0.5)^{A,1}	12.2 (0.4)^{A,2}	131.9 (9.7)^{A,1}	123.9 (10.1)^{B,1}
ND	14.7 (0.8)^{A,1}	12.6 (0.7)^{A,2}	125.5 (3.7)^{A,1}	119.1 (6.2)^{AB,1}

**Within a column, cells having similar letters are not significantly different from the control (HC), and within a row, cells having similar numbers are not significantly different (before and after ageing for the same material).*

Table 0.3. Mean and standard deviation (SD) of Flexural strength and modulus for the control and test groups before and after ageing process in artificial saliva for three months

Resin material	Flexural strength (MPa)		Flexural modulus (MPa)	
	Before ageing	After ageing	Before ageing	After ageing
HC	73.5 (9.0)^{A,1*}	69.8 (5.0)^{A,1}	2388.0 (126.7)^{A,1*}	2217.1 (106.4)^{A,2}
FL	93.9 (8.3)^{B,1}	82.8 (10.7)^{B,1}	2377.7 (128.4)^{A,1}	2390.0 (64.2)^{A,1}
ND	88.2 (1.5)^{B,1}	80.3 (6.1)^{B,1}	2384.7 (64.5)^{A,1}	2259.9 (120.9)^{A,1}

*Within a column, cells having similar letters are not significantly different from the control (HC), and within a row, cells having similar numbers are not significantly different (before and after ageing for the same material).

Table 0.4. Mean and standard deviation (SD) of impact strength for the control and test groups before and after ageing process in artificial saliva for three months

Resin material	Impact strength (KJ/m²)	
	Before ageing	After ageing
HC	12.0 (1.3)^{A,1*}	11.4 (1.3)^{A,1}
FL	13.3 (4.0)^{A,1}	12.2 (3.3)^{A,1}
ND	13.4 (3.3)^{A,1}	12.2 (4.0)^{A,1}

**Within a column, cells having similar letters are not significantly different from the control (HC), and within a row, cells having similar numbers are not significantly different (before and after ageing for the same material).*

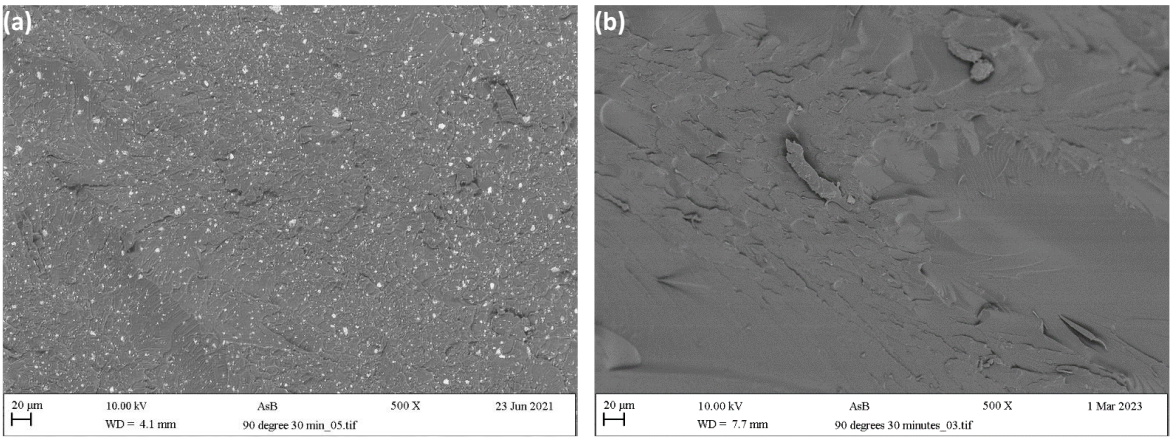

Figure 0.2. SEM images of the fractured surface of 3D printed denture base resin materials with a x500 magnification showing the surface morphology across the thickness: (a) ND, (b) FL

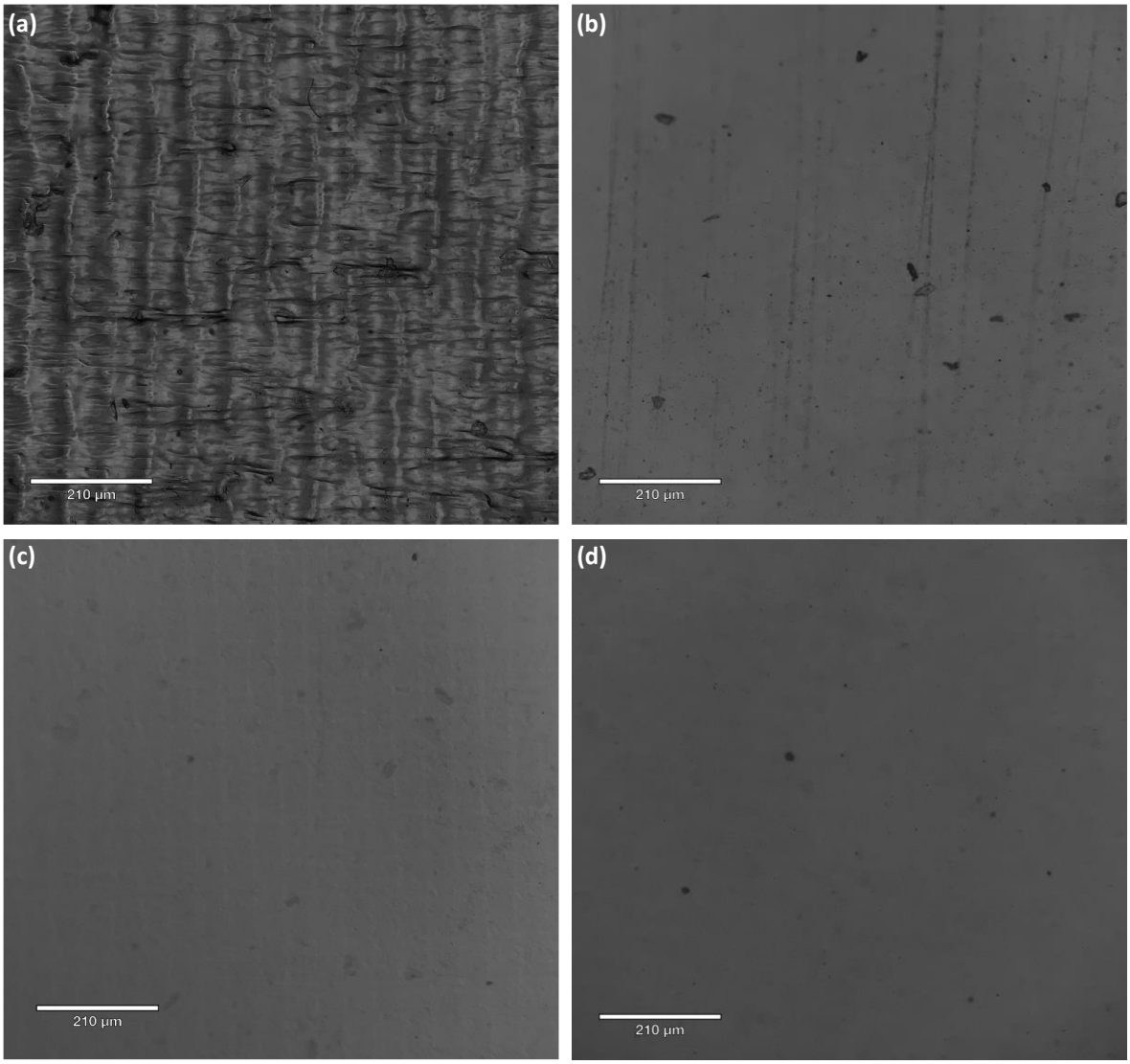

Figure 0.3. Optical microscope images of 3D printed denture base resin materials showing the surface morphology across the thickness: (a) FL before polishing, (b) FL after polishing, (c) ND before polishing, (d) ND after polishing

Appendix C

Table 0.5. Mean and standard deviation (SD) of DC, sorption, and solubility for the control and the nanocomposite test groups

Groups	DC (%)	Sorption (µg/mm³)	Solubility (µg/mm³)
HC	98.0 (1.0)^{A}	21.0 (1.0)^{A}	1.3 (0.2)^{A}
A	84.0 (1.7)^{B}	22.8 (0.4)^{B}	1.4 (0.4)^{A}
B	94.7 (1.3)^{AC}	22.3 (0.3)^{B}	-1.5 (0.3)^{B}
C	94.3 (2.9)^{AC}	22.2 (0.5)^{B}	-1.1 (0.1)^{BC}
D	94.8 (1.1)^{AC}	22.4 (0.5)^{B}	-0.9 (0.1)^{C}
E	90.8 (4.9)^{C}	24.7 (0.4)^{C}	1.1 (0.2)^{A}

**Within a column, cells having similar letters are not significantly different from the control (HC), and within a row, cells having similar numbers are not significantly different (before and after ageing for the same material).*

Table 0.6. Mean and standard deviation (SD) of Martens hardness, Vickers hardness, Indentation modulus, and Indentation creep for the control and the nanocomposite test groups before and after ageing process in artificial saliva

Groups	**Martens hardness (N/mm^2)**		**Indentation modulus (kN/mm^2)**		**Indentation creep (%)**		**Vickers hardness (VHN)**	
	Before ageing	After ageing	Before ageing	After ageing	Before ageing	After ageing	Before ageing	After ageing
HC	135.6 (12.1)^{A,1*}	107.9 (7.9)^{A,2}	3.3 (0.3)^{A,1}	2.8 (0.4)^{A,1}	12.0 (0.9)^{A,1}	11.6 (0.2)^{A,1}	20.9 (0.9)^{A,1*}	15.9 (0.3)^{A,2}
A	126.2 (5.3)^{A,1}	118.7 (3.0)^{AB,1}	2.3 (0.2)^{B,1}	3.0 (0.3)^{A,2}	6.8 (0.1)^{B,1}	6.7 (0.2)^{B,1}	18.9 (0.5)^{B,1}	18.0 (0.6) ^{BC,1}
B	131.1 (3.3)^{A,1}	124.9 (2.9)^{B,1}	2.9 (0.1)^{A,1}	3.0 (0.2)^{A,1}	7.4 (0.1)^{B,1}	6.9 (0.1)^{B,1}	20.0 (0.4)^{A,1}	19.3 (0.3)^{B,1}
C	130.9 (1.2)^{A,1}	124.2 (2.3)^{B,1}	2.8 (0.1)^{A,1}	2.8 (0.1)^{A,1}	7.4 (0.3)^{B,1}	7.4 (0.1)^{B,1}	19.9 (0.3)^{A,1}	18.9 (0.1)^{BC,1}
D	132.5 (3.9)^{A,1}	124.8 (9.1)^{B,1}	2.9 (0.2)^{A,1}	2.9 (0.4)^{A,1}	7.0 (0.1)^{B,1}	8.6 (0.5)^{C,2}	20.3 (0.1)^{A,1}	18.0 (0.1)^{C,2}
E	130.3 (0.8)^{A,1}	121.6 (1.8)^{AB,1}	2.9 (0.04)^{A,1}	2.7 (0.2)^{A,1}	7.3 (0.1)^{B,1}	8.5 (0.1)^{C,2}	19.9 (0.2)^{A,1}	17.8 (0.5)^{C,2}

**Within a column, cells having similar letters are not significantly different from the control (HC), and within a row, cells having similar numbers are not significantly different (before and after ageing for the same material)*

Table 0.7. Mean and standard deviation (SD) of flexural strength and modulus for the control and the nanocomposite test groups before and after ageing process in artificial saliva

Groups	Flexural strength (MPa)		Flexural modulus (MPa)		Impact strength (KJ/m^2)	
	Before ageing	After ageing	Before ageing	After ageing	Before ageing	After ageing
HC	74.5 (8.5)^{A,1*}	71.2 (6.1)^{A,1}	2377.6 (122.4)$^{A.1*}$	2181.1 (31.1)^{A,2}	11.8 (1.5)^{A,1*}	11.1 (2.4)^{A,1}
A	89.2 (1.7)^{B,1}	82.0 (7.8)^{B,1}	2391.4 (70.1)^{A,1}	2278.6 (111.0)^{A,1}	13.0 (2.0)^{AC,1}	12.0 (3.3)^{AC,1}
B	111.2 (4.0)^{C,1}	97.7 (3.2)^{C,2}	2769.6 (35.0)^{B,1}	2586.0 (51.4)^{B,2}	20.4 (2.6)^{B,1}	19.4 (3.4)^{B,1}
C	101.5 (3.3)^{D,1}	97.3 (2.4)^{C,1}	2575.3 (58.6)^{C,1}	2554.1 (105.7)^{B,1}	18.0 (3.3)^{BC,1}	17.2 (2.8)^{BCD,1}
D	97.2 (2.8)^{DE,1}	82.5 (5.3)^{B,2}	2567.7 (84.5)^{C,1}	2263.8 (60.3)^{A,2}	16.2 (4.3)^{AB,1}	12.7 (5.9)^{AD,1}
E	93.4 (4.6)^{BE,1}	79.6 (3.9)^{B,2}	2342.5 (68.2)^{A,1}	2305.1 (86.4)^{A,1}	15.3 (2.4)^{AB,1}	11.8 (2.5)^{A,1}

**Within a column, cells having similar letters are not significantly different from the control (HC), and within a row, cells having similar numbers are not significantly different (before and after ageing for the same material).*

Table 0.8. EDX analysis showing the amount of TiO_2 NPs by weight within each group before and after ageing in artificial saliva for 3 months

Groups	TiO_2 (wt.%) before ageing	TiO_2 (wt.%) after ageing
A	0.04	N/A
B	0.11	0.06
C	0.25	0.20
D	0.43	0.36
E	0.96	0.40

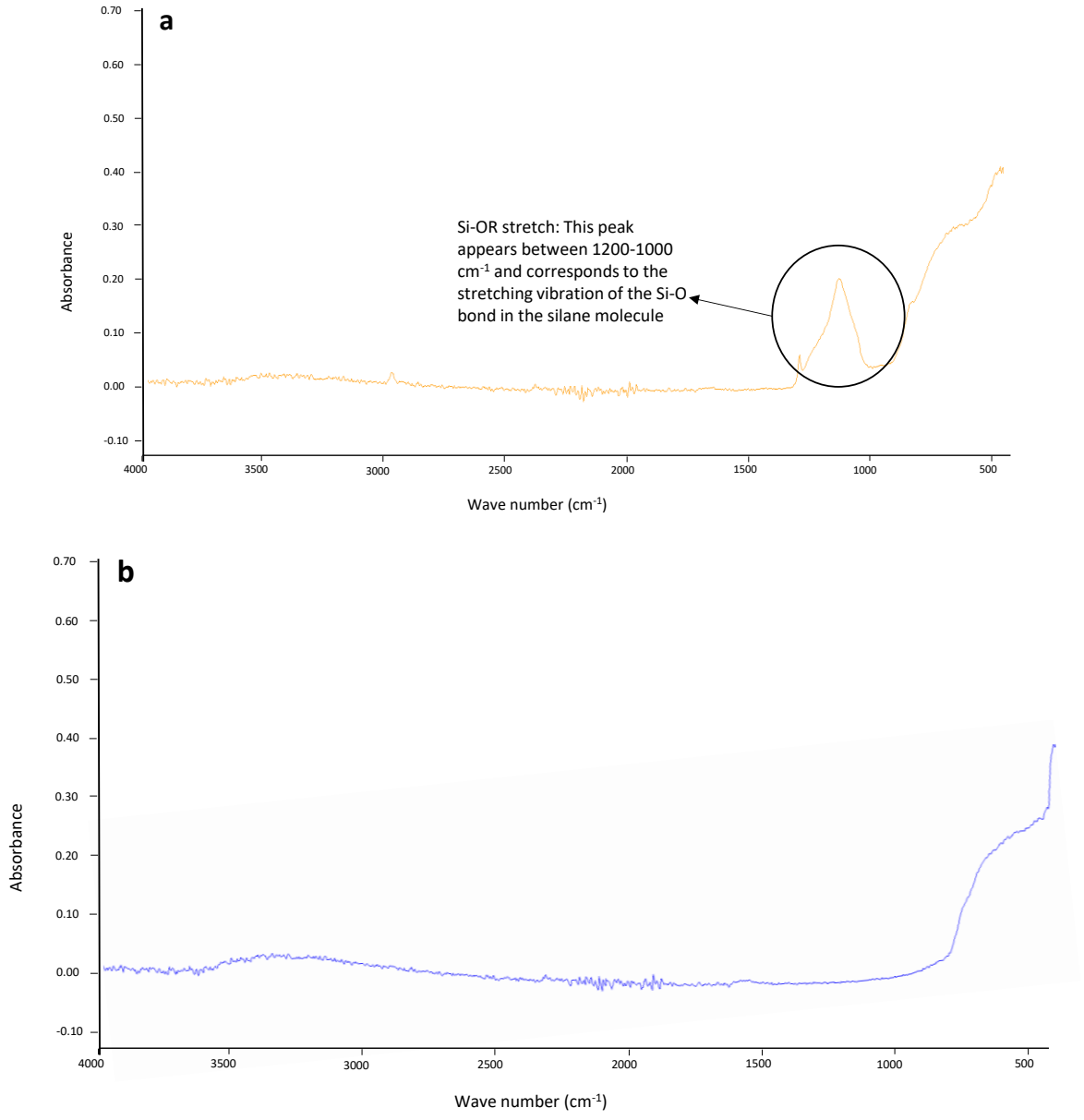

Figure 0.4. FTIR analysis for: (a) silane coated vs. (b) non-silane coated TiO_2 NPs

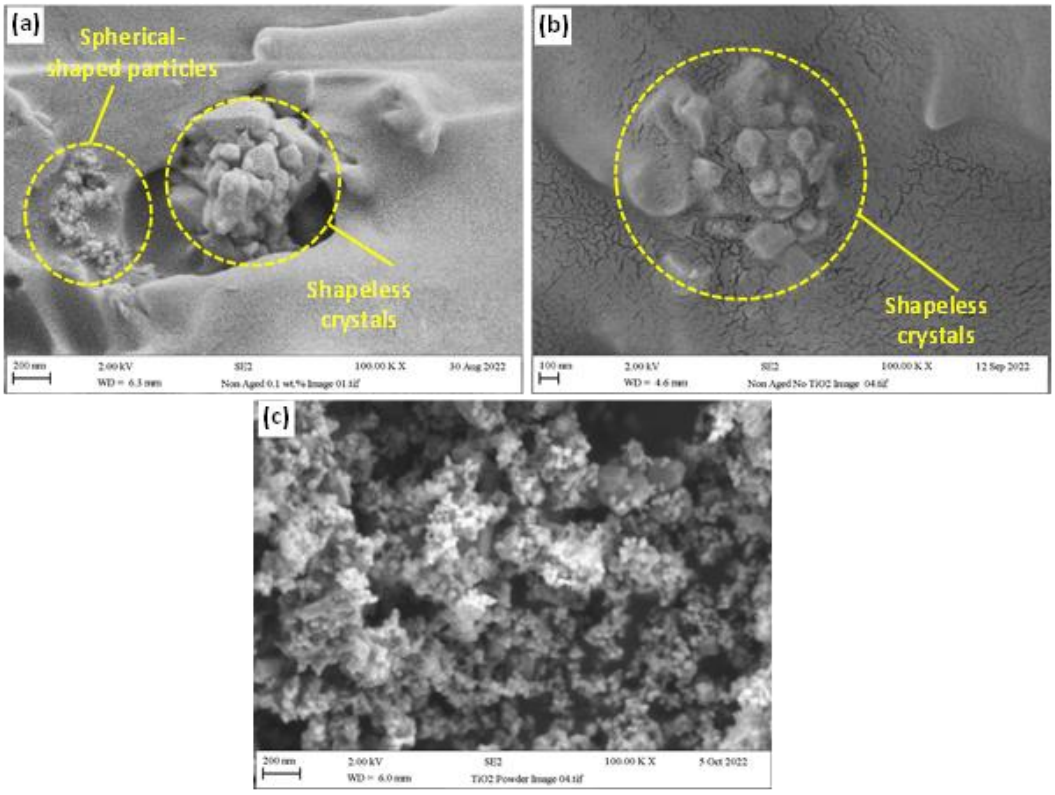

Figure 0.5. Fractured surface morphology of 3D printed denture base resin materials with a magnification of ×100k times showing different types of filler in: (a) 3D-printed TiO_2 reinforced composite material, (b) unmodified 3D-printed material, (c) TiO_2 NPs powder only

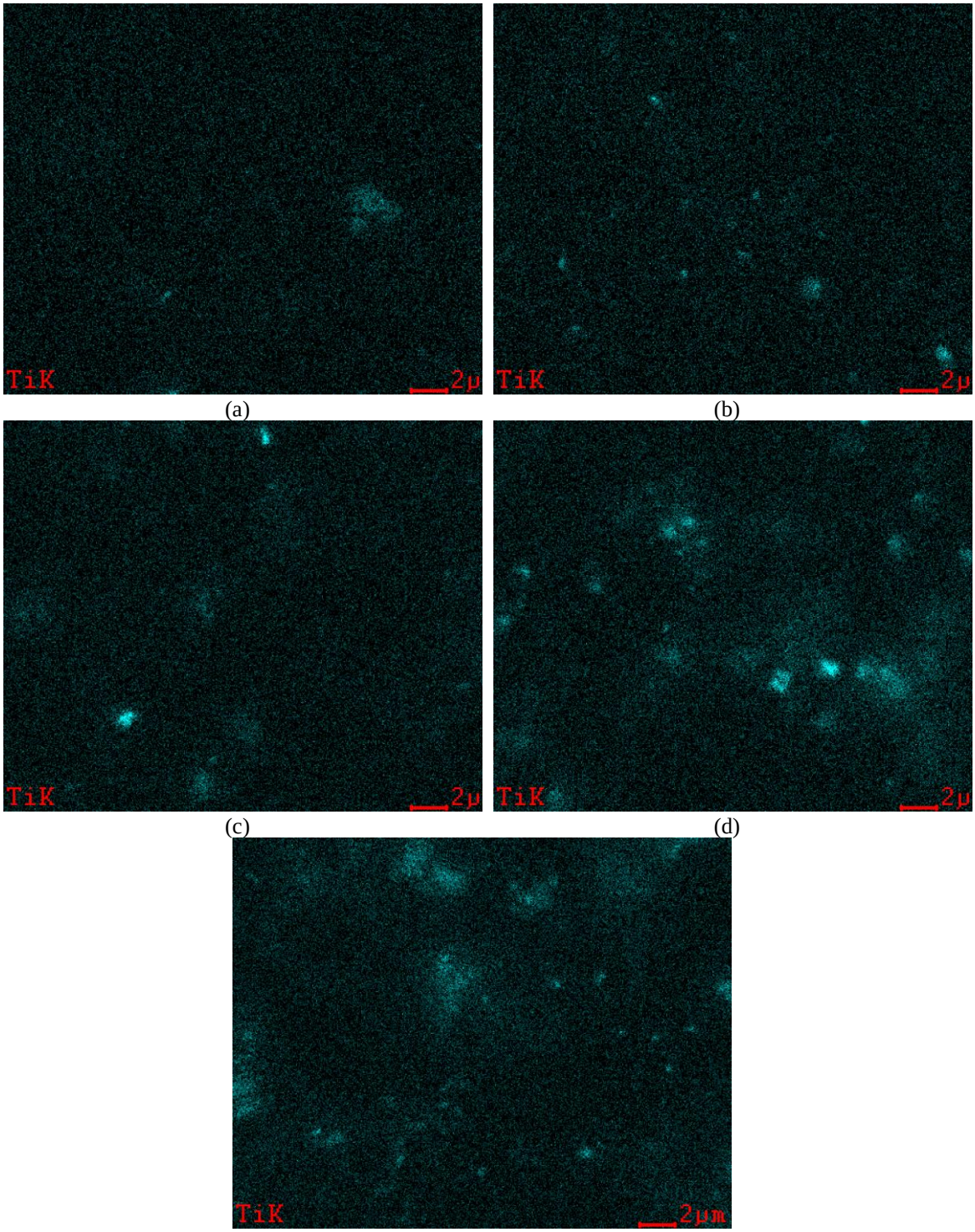

Figure 0.6. EDX mapping images for 3D-printed resin with TiO_2 NPs of: (a) 0 wt.% (b) 0.10 wt.% (c) 0.25 wt.% (d) 0.50 wt.% (e) 0.75 wt.% TiO_2.

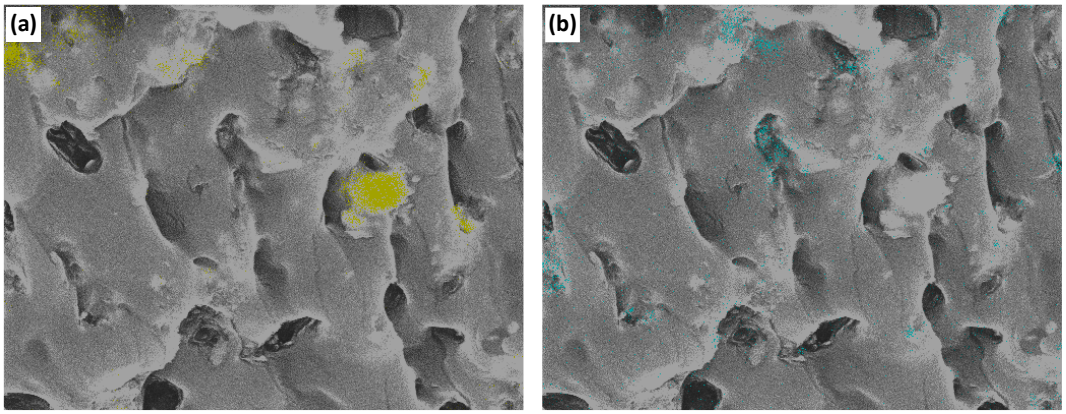

Figure 0.7. EDX analysis of 3D printed/TiO_2 nanocomposite with a concentration of 0.75 wt.% TiO_2 NPs showing: (a) SiO_2 fillers (yellow), (b) TiO_2 fillers (cyan)

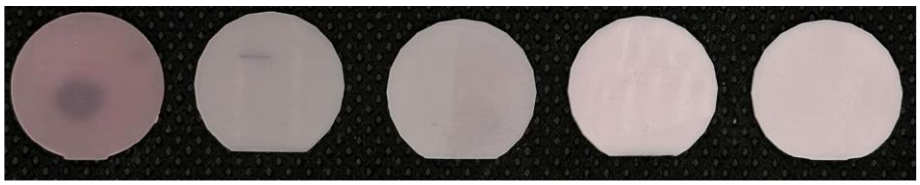

Figure 0.8. Colours of specimens of 3D-printed/ TiO_2 NPs composite material with concentration of 0.0, 0.10, 0.25, 0.50, and 0.75 wt.% from left to right

Appendix D

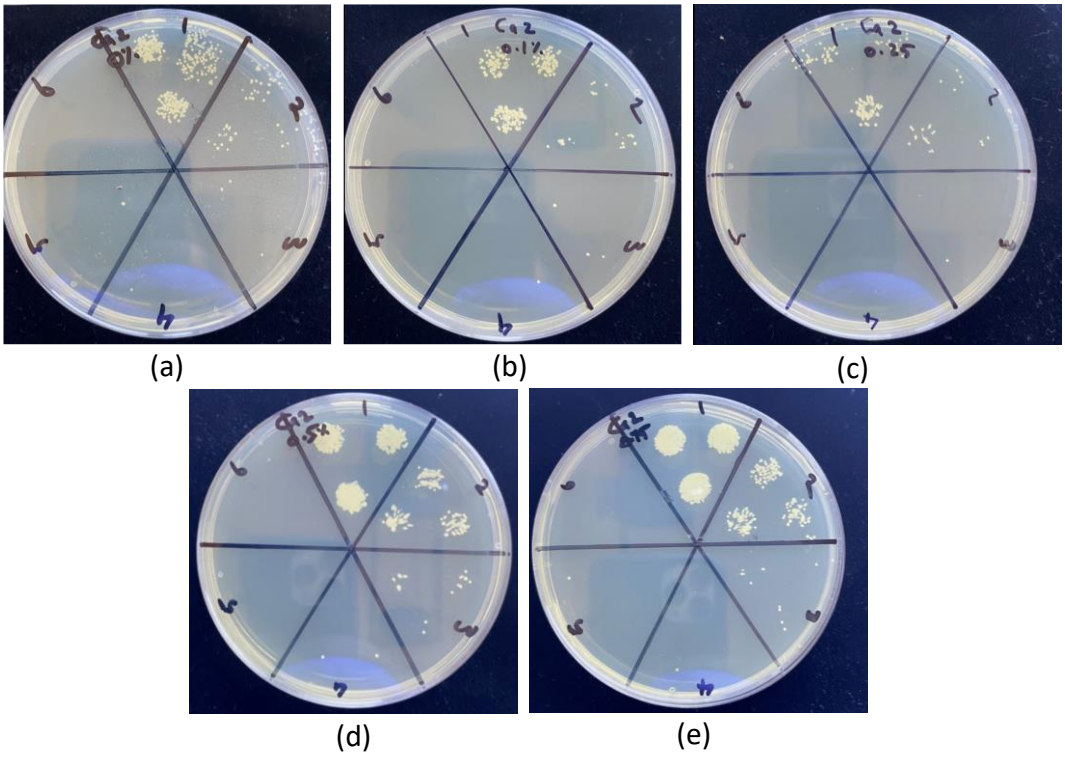

Figure 0.9. Candida albicans colonies that were seeded in SD agars at a dilution range of $10^1 – 10^6$ formed from detached cells from the nanocomposite discs with group: (a) A (control), (b) B, (c) C (d) D, (e) E